ARTIFICIAL SCAFFOLDS FOR NEURAL TISSUE ENGINEERING

by

SURADIP DAS

In Partial Fulfilment of the

Requirements for the Degree of

DOCTOR OF PHILOSOPHY

DEPARTMENT OF BIOSCIENCES AND BIOENGINEERING

INDIAN INSTITUTE OF TECHNOLOGY GUWAHATI

GUWAHATI – 781039, ASSAM, INDIA

JULY, 2015

INDIAN INSTITUTE OF TECHNOLOGY GUWAHATI

Department of Biosciences and Bioengineering

Guwahati – 781 039

DECLARATION

This is to declare that the matter embodied in this thesis entitled "***Artificial Scaffolds for Neural Tissue Engineering***" is the result of investigations carried out by me under the supervision of **Prof. Utpal Bora**, and is submitted to the Indian Institute of Technology Guwahati, Guwahati-781039, Assam, India for the award of degree of *Doctor of Philosophy in Biosciences and Bioengineering*. This work has not been submitted elsewhere for any degree or diploma of any institute or university to the best of my knowledge and belief.

In keeping with the general practice of reporting scientific observations, due acknowledgements have been made wherever the work of other investigators are referred, and copyright licenses have been taken from respective publishers.

Guwahati
July, 2015

Suradip Das
Roll - 10610612

INDIAN INSTITUTE OF TECHNOLOGY GUWAHATI

Department of Biosciences and Bioengineering

Guwahati – 781 039

CERTIFICATE

This is to certify that the matter embodied in this thesis entitled "***Artificial Scaffolds for Neural Tissue Engineering***" is the result of investigations carried out by **Mr. Suradip Das** (Roll No.: 10610612) under my supervision, and is submitted to the Indian Institute of Technology Guwahati Guwahati-781039, Assam, India for the award of degree of *Doctor of Philosophy in Biosciences and Bioengineering*. This work has not been submitted elsewhere for a degree.

Utpal Bora

Guwahati
July, 2015

Professor
Department of Biosciences and Bioengineering
IIT Guwahati

DEDICATION

Dedicated

to

Ma, Baba, my entire Family

and all my Teachers

....Suradip

ACKNOWLEDGEMENT

At the outset, I would like to express my deep sense of gratitude to my thesis supervisor *Prof. Utpal Bora* for his guidance, support and direction. He has been the leading light in my endeavour for translational research in the fast growing field of Biotechnology. He has not only been my thesis supervisor but a philosopher and guide whose teachings have made me approach challenges and failures with optimism and confidence. I must acknowledge the freedom that I was given in every step of my research work. I am grateful to the chairman of the Doctoral Committee *Dr. Ranjan Tamuli* and members *Dr. A.B.Kunnumakkara,* and *Prof. G. Krishnamoorthy* for their valuable suggestions and advices which enabled me to improve my work.

I would like to take this opportunity to thank the present and past Heads of the Department of Biosciences and Bioengineering, IITG for providing all the necessary facilities and a favourable academic environment. I sincerely acknowledge the financial support from *Ministry of Human Resource Development* (Govt. of India) for providing me fellowship, and *Department of Biotechnology* (Govt. of India) and *Central Silk Board* (Govt. of India) for research grants to my supervisor.

I owe my gratitude to the *Central Instruments Facility, IITG* and *Sophisticated Analytical Instrumentation Facility, NEHU, Shillong* for providing me all the support and necessary facilities with sophisticated equipments. Also, I would like to thank all the scientific staff of the *Dept. of Physics* (for Electrical resistance) and *Centre for Nanotechnology* (for XRD) for helping me with various experiments. My special thanks to the *technical staff of the Department of Biosciences and Bioengineering* for their kind co-operation throughout my tenure.

A substantial portion of my thesis work involved extensive animal experimentation. I am grateful to *Prof. Kushal Konwar Sarma*, *Head, Department of Surgery and Radiology, College of Veterinary Sciences (CVSc), Khanapara* for providing all the necessary facilities and his expert guidance in the *in vivo* studies. I also thank the Institutional Animal Ethics Committee of CVSc Khanapara and IIT Guwahati for providing necessary approval for carrying out animal experimentations.

My sincere thanks and gratitude goes *to Dr. Dhiren Saharia, Saharia's Path Lab and Blood Bank, Guwahati* and *Dr. Monalisa Goswami Sarma, Nemcare Hospital, Guwahati* for taking time out of their busy schedule and helping me with the histological and electrophysiological studies respectively. My heartiest thanks to *Dr. Elizabeth Muir, University of Cambridge* for gifting us the rat Schwann cell line (SCTM41) which has been an important component of all my experiments. I would also like to thank *Dr. Bibhuti Bhusan Borthakur, BBCI, Guwahati* for the MRI studies as well as for his constant support, encouragement and guidance in designing and executing the animal experiments.

I take this opportunity to thank all the publishers like *Elsevier, Springer, Nature Publishing Group, Wiley* and others for providing me copyright clearance and license to reuse figures/tables from their publications in the present thesis.

My heartiest thanks to my lab members, *Mr. Arghya, Mr. Manoj, Mr. Disco, Ms. Deepika, Ms. Sambhavi, Ms. Papori, Ms. Sunita, Ms. Swagata* and past members *Mr. Shamim*, *Dr. Ajoy, Dr. Sudipta* for providing a healthy and enjoyable environment in the laboratory. I am immensely pleased to express my heartiest thanks to my seniors *Dr. Naresh, Dr. Punuri, Dr. Anil, Dr. Nayanmoni, Mr. Ratul* and friends *Mr. Nand Kishor*, *Ms. Tulsi, Dr. Soumyadeep, Ms. Darilang, Ms. Ankita, Dr. Himangshu* and others from all departments, centres and hostel, for their moral support. Their presence made my five years stay at IITG memorable. Special thanks to *Dr. Manav Sharma* who has been an integral part of our team and made significant contribution in the animal studies especially in performing the neurosurgeries. His friendship has been a huge support for me and I will cherish it forever.

I would like express my sincere gratitude and regards to my uncle *Dr Pradip Nandi* who has played a major role in encouraging me to follow the path of science. My heartiest thanks to *Dr. V. Prakash*, who inspite of his tremendously hectic schedule always found time for me, provided moral support, encouragement and valuable guidance throughout my career.

Last but not the least; I would like to thank my parents, family members, relatives, well-wishers and my teachers for their endless love, unlimited support and motivation.

July, 2015 *Suradip Das*

TABLE OF CONTENTS

Synopsis **i**

List of Figures **vii**

List of Tables **xiv**

List of abbreviations **xv**

Chapter 1 : Introduction **1-15**

Chapter 2: Review of Literature **16-103**

2.1: Introduction 16

2.2: Scaffolds in Neural Tissue Engineering 20

2.3: Support cells in Neural Tissue Engineering 39

2.4: Growth factors in Neural Tissue Engineering 43

2.5: Silk based scaffolds in Tissue Engineering 46

2.6: Application of Nanotechnology in Neuroscience 64

2.7: Nanotechnology in Neuroregeneration 80

2.8: Sciatic Nerve Injury Model in Neuro-regenerative Research 87

2.9: Commercially available artificial nerve conduits 93

Chapter 3: Silk-Gold nanocomposite based scaffolds for neural tissue engineering **104-131**

3.1: Introduction 104

3.2: Materials and Methods 106

3.3: Results 115

3.4: Discussions 120

3.5: Conclusions 130

Chapter 4: Silk-Polyaniline nanocomposite based scaffolds for neural tissue engineering **132-164**

4.1: Introduction 132

4.2: Materials and Methods 135

4.3: Results 142

4.4: Discussions 152

4.5: Conclusions 164

Chapter 5: Summary and future prospects **165-168**

Bibliography **169-216**

List of Publications **217**

Copyright permissions **218**

Biography **219**

Synopsis

Tissue damage to peripheral nerves results from traumatic injuries caused by accidents, physical conflict as well as during surgical intervention. Peripheral nerve injuries are primarily characterized by flaccid atrophy of surrounding muscles leading to partial or complete paralysis. Seddon had classified neurotmesis as the most severe form of peripheral nerve injury where the nerve is completely severed with limited chance of axon re-growth making surgical intervention essential. Neurotmesis grade injuries with a gap larger than 5 mm rarely show complete axonal reconnection and functional regeneration. Surgical intervention in large nerve gaps generally involves grafting a part of nerve harvested from a healthy area into the damaged area. Although autografts remain the clinical gold standard for repairing large nerve gaps, the technique is largely fraught with donor site morbidity in the secondary surgical site and inefficient functional regeneration. While many studies have shown autografts to be superior to the available conduits there have been reports indicating an increased growth of nociceptive fibers along autografts which result in high autotomy among animals. An alternative approach to nerve autograft is entubulation of nerve gaps using nerve conduits or nerve guides made of synthetic or natural polymers.

In the present study, silk fibroin nanofibers mats have been used to fabricate functional nerve conduits, exploiting the biocompatibility and bio-mimetic properties of silk fibroin protein. Silk fibroin films functionalized with nerve growth factor (NGF) promotes neurite outgrowth and modulates functional properties of dorsal root ganglion (DRG) neurons. Functionalization of silk fibroin based nerve guidance conduits with NGF and glial-derived nerve factor (GDNF) has been reported to enhance functional recovery of injured peripheral nerves. Moreover, the incorporation of electrospun silk fibroin nanofibers within the lumen of the conduit was found to provide topographical guidance to the regenerating axons by directing neurite outgrowth and Schwann cell migration. However, the poor electrical conductivity of the silk polymer has to be improved in order to achieve better results in regeneration of electrically active tissues like cardiac muscles and nerve fibers. Hence to address the loss of nerve impulse transmission following nerve injury it is imperative that the artificial nerve grafts favour electrical conduction.

Electrically active silk scaffolds based on carbon nanotube (CNT) have been explored to facilitate signal transmission across a nerve gap through the conduit. Such conduits can easily interface with neuronal circuits, synapses and facilitate conduction of nerve impulse thereby promoting neural regeneration. These studies indicate that the efficacy of silk fibroin as a biomaterial for facilitating nerve regeneration can be increased by incorporation of electrical cues in the nerve conduits.

Although many advances have been made in the field of neural tissue engineering there are some unmet needs that limit the translation of laboratory materials to clinical products. Lack of long duration *in vivo* studies as well as evaluation of complete neuromuscular regeneration post implantation remains a major challenge. Further there is much scope for innovation in fabrication methods to develop high-throughput techniques aimed at manufacturing nerve conduits of varying diameter from a single process. The fabrication of novel electro-active composite scaffolds using nanoparticles and conducting polymers for developing nerve conduits and subsequent *in vivo* evaluation of neuro-regeneration is also highly desirable.

Objectives – To address these gaps in knowledge the following objectives were formulated to fabricate artificial nerve conduits with the aim to simulate the native neural architecture and to provide a conducive environment for neural regeneration -

i) Fabrication of nerve conduits based on silk fibroin and *in vivo* evaluation of neuro-regeneration.

ii) Functionalization of nerve conduits with metallic nanoparticles and evaluation of neuro-regeneration in a rat sciatic nerve injury model

iii) Functionalization of nerve conduits with synthetic conducting polymers and evaluation of neuro-regeneration in a rat sciatic nerve injury model

iv) Formulation studies of cell-seeded nerve conduits and their *in vivo* evaluation and comparison with un-seeded nerve conduits.

The thesis is organized into various chapters as described herein.

Chapter 1: Introduction

The chapter describes the physiological response to peripheral nerve injury and the available strategies for repair of peripheral nerve. The challenges of neurotmesis grade nerve injury repair and the potential of neural tissue engineering strategies in treating the same are discussed. The chapter is aimed at explaining the target problem, evolving the rationale behind the thesis and formulation of objectives for the study to address some of the existing lacunae in the field.

Chapter 2: Review of Literature

A systematic review of literature was conducted to understand the various existing technological advances in order to devise an effective plan of work to accomplish the chosen objectives of the research work. The chapter discusses in detail the role of scaffolds, support cells and growth factors in neural tissue engineering with a special focus on the tissue engineering applications of silk based biomaterials. The chapter goes on to describe the applications of nanotechnology in neuroscience focussing on the role of nano-dimensional scaffolds in neuro-regeneration. The significance of sciatic injury model in peripheral nerve regeneration studies along with a brief review of commercially available neural implants is also presented to obtain a holistic picture of existing knowledge in the field.

Chapter 3: Silk-Gold nanocomposite based scaffolds for neural tissue engineering

The chapter describes the fabrication of a novel silk-gold nanocomposite based nerve conduit successfully tested in a neurotmesis grade sciatic nerve injury model in rats over a period of eighteen months. The conduit was fabricated by adsorbing gold nanoparticles onto silk fibers and transforming them into a nanocomposite sheet by electrospinning which is finally given a tubular structure by rolling on a stainless steel mandrel of chosen diameter. The nerve conduits were tested for their biocompatibility in vitro and in vivo, pre-seeded with rat Schwann cell line SCTM41 cells and implanted in a 10mm rat sciatic nerve injury model. Upon implantation, the conduits were evaluated for their neuro-regenerative potential through extensive electrophysiological studies and monitoring of gait pattern over a course of 18 months. Gross examination, histological and ultra-structure analyses of the conduits and the regenerated nerve were also performed to evaluate morphological

regeneration of transected nerve. The study was aimed to understand the long term safety of gold nanoparticle based implants as well as the neuroregenerative potential of such nanocomposite based scaffolds.

The chapter is further subdivided into separate sections detailing introduction, materials and methods, results, discussions and conclusions.

Chapter 4: Silk-Polyaniline nanocomposite based scaffolds for neural tissue engineering

In the present study we have fabricated nerve conduits based on polyaniline-silk fibroin nanocomposite (PASF). The nanocomposite was synthesised by single nozzle electrospinning of a mixture of silk fibroin protein and polyaniline wherein the silk nanofibers were observed to be uniformly coated with polyaniline nanoparticles. Tubular shaped nerve conduits were subsequently formed by multiple rolling of the electrospun sheet over a stainless steel mandrel. The nerve conduits were tested for their biocompatibility in vitro and in vivo, pre-seeded with rat Schwann cell line SCTM41 cells and implanted in a 10mm sciatic nerve gap. Upon implantation, the conduits were evaluated for their neuro-regenerative potential through extensive electrophysiological studies and monitoring of gait pattern over a course of 12 months. Gross examination, histological and ultra-structure analyses of the conduits and the regenerated nerve were also performed to evaluate morphological regeneration of transected nerve. The electrophysiological and histomorphometric outcomes of the nanocomposite group was compared with those of animals with pure silk fibroin nanofibers based conduits in order to understand the long term safety of such synthetic polymers as well as their effect on nerve regeneration *in vivo*.

The chapter is further subdivided into separate sub-sections detailing introduction, materials and methods, results, discussions and conclusions.

Chapter 5: Summary and Future prospects

The present study demonstrates the utility of nanocomposite based scaffolds as potential biomaterials for fabricating nerve conduits. Although silk fibroin is one of the most used biomaterial as an implant (sutures), its highly insulating properties render it unsuitable for fabricating scaffolds for mimicking the electrically conductive tissues of the body like nerve and cardiac muscles. We hereby demonstrate how silk based

nanocomposites consisting of metallic nanoparticles and conducting polymer enhances functional and morphological regeneration of nerve in a rat sciatic nerve injury model. The novel sheet rolling method utilised for fabricating conduits from nanofibers enables multiple conduit development of varied dimensions from a single electrospun sheet. Pre-seeding the conduits with Schwann cells also enhanced and accelerated neural regeneration through the nerve gap as evident from the extensive electrophysiological and histological studies. Further the long duration studies undertaken by us establish the safety and neuro-regenerative potential of such nanocomposite conduits.

The work presented in the thesis has been peer reviewed and resulted in the following international journal publications:

Publications

1. Das S, Borthakur BB, Bora U, Applications of silk biomaterials in tissue engineering and regenerative medicine, *Silk biomaterials for tissue engineering and regenerative medicine*, Woodhead Publishing House, UK, ISBN0857096990 ISBN-13: 9780857096999, March, 2014.(***Part of Chapter 2***)
2. Das S, Sharma M, Saharia D, Sarma KK, Sarma MG, Borthakur BB, Bora U, In vivo studies of Silk based Gold Nano-Composite Conduits for Functional Peripheral Nerve Regeneration, Biomaterials, 2015, 62: 66-75. (***Part of Chapter 3***)
3. Das S, Sharma M, Saharia D, Sarma KK, Sarma MG, Borthakur BB, Bora U, Data in Support of In vivo studies of Silk based Gold Nano-Composite Conduits for Functional Peripheral Nerve Regeneration, Data in Brief, 2015 (Available online 16.06.2015). doi:10.1016/j.dib.2015.05.020. (***Part of Chapter 3***)

Other publications (from collaboration)

1. Sett, A. Das, S. Sharma, P. and Bora, U. (2012) Aptasensors in Health, Environment and Food Safety Monitoring. *Open Journal of Applied Biosensor*, 1, 9-19. doi: 10.4236/ojab.2012.12002.
2. Sett A, Das S, Bora U. (2014) Functional nucleic-acid-based sensors for environmental monitoring. *Appl Biochem Biotechnol*.; 174 (3):1073-91. doi: 10.1007/s12010-014-0990-3.

Patents filed

1. Bora U and Das S, Silk Based electrically conductive nerve conduit and the method for preparing the same, 721/KOL/2015 (***Part of Chapter 4***)

Conference proceedings

1. Das S, Sharma M, Saharia D, Sarma KK, Sarma MG, Borthakur BB, Bora U, Nanotechnology in Neuroscience, 16th Network meeting, International Spinal Research Trust, London, UK during 3-5th September, 2014.
2. Das S, Sharma S, Gadewar M, Bora U, Silk in Biomedical Applications, International Sericulture Conference, Bangalore, 2014.

Manuscripts under review

1. Das S, Bora U. Applications of Nanomaterials in Neuroscience, (Manuscript under review). (***Part of Chapter 2***)
2. Das S, Sharma M, Saharia D, Sarma KK, Sarma MG, Borthakur BB, Bora U, Silk-Polyaniline based Nano-Composite Conduits preseeded with Schwann cells for Functional Peripheral Nerve Regeneration**,** (Manuscript under review) (***Part of Chapter 4***)

List of Figures

Figure 1.1: Progressive degeneration and regeneration of nerve post injury **(***Adapted with permission from* Grinsell *et al*, 2014**).**

Figure 1.2: Surgical algorithm of peripheral nerve repair **(***Adapted with permission from Grinsell et al, 2014**).***

Figure 1.3: Properties of an ideal nerve conduit **(***Reprinted with permission from Arslantunali et al, 2014***)**

Figure 1.4: Progression of events upon implantation of nerve conduit ***(****Reprinted with permission from* Heath *et al,* 1998**)**

Figure 1.5: Schematic of thesis work

Figure 2.1: Changes in CNS environments after maturation and injury**.** The figure describes the formation of glial scar inhibiting regeneration in the CNS. (*Adapted with permission from Yiu et al, 2006*)

Figure 2.2: Overview of the experimental protocol used to study neuroregeneration through RevolNerve tube, an EU-approved semipermeable and bioresorbable porcine collagen type I + III nerve conduit as compared to autografts. (*Adapted with permission from Alluin et al, 2009*)

Figure 2.3: Genipin-cross-linked gelatin conduit (GGC). A) SEM micrographs of the GGC in longitudinal section (panel i) and cross section (panel ii). B) Macrographs of the GGCs at different implantation periods: intact (panel i), 1 week (panel ii), 4 weeks (panel iii), and 8 weeks (panel iv). Scale bars=5mm. (*Adapted with permission from Chen et al, 2005*).

Figure 2.4: Representative SEM micrographs of tubes synthesized by SpinFXs technology: (**A**) corrugated tube, (**B**) coil-reinforced tube, (**C**) 130x magnification of the corrugated tube wall, and (**D**) 130x magnification of the coil-reinforced tube wall (arrow indicates coil). Cross section of the mid section of grafts at 16 weeks (**E**) 40x magnification of the regenerating cable (RC) within the tube (**F**) 40x magnification of

the autograft. '*' indicates the tube wall. F is the fascicle of the autograft. (*Adapted with permission from Katayama et al, 2006*).

Figure 2.5: Photo-crosslinked poly(e-caprolactone fumarate) based nerve conduits and neuroregeneration upto 17 weeks post implantation. (*Adapted with permission from Wang et al, 2009*).

Figure 2.6: Electrically Mediated Regeneration Mammalian Spinal Axons Into Polymeric Channels. The figure depicts effect of electrical stimulation on axonal regeneration. (*Adapted with permission from Borgens, 1999)*.

Figure 2.7: Chemical structure of conducting polymers. **(i)** Chemical structure of PPy: (A) before doping; (B) after doping, (**ii**) Polyaniline (PANI): (A) reduced; (B) oxidized; and (C) half-oxidized forms, (**iii**) The structure of PEDOT. (i) and (ii) *Adapted with permission from Ghasemi-Mobarakeh et al, 2011*, (iii) *Adapted with permission from Balint et al, 2014*).

Figure 2.8: Effect of Olfactory Ensheathing Glial (OEG) cells in Functional and morphological regeneration of axons**.** The figure depicts functional recovery of rats with completely transected spinal cords after OEG transplantation. Further, macroscopic repair and motor axon regeneration through the lesioned region of OEG-Transplanted Spinal Cords, 8 months Post Surgery is also represented (*Adapted with permission from Ramon-Cueto et al, 2000*).

Figure 2.9: Silk in engineering various forms of tissues (Reprinted with permission from *Das et al, Elsevier, 2014*)

Figure 2.10: Effect of Silk implants for the healing of critical size bone defects. X-ray analysis of mouse calvarial bone defects 5 weeks after surgery. Defects were treated with tissue-engineered bone on silk scaffolds (silk-TE bone cultured for 5 weeks; column 1), silk scaffolds seeded with mesenchymal stem cells (silk-MSC; column 2), plain silk (silk; column 3), or left unfilled (empty; column 4). (**A–D**) Two defects per group as seen by X-rays. Microcomputer tomography (μCT) images of cranial defects taken 5 weeks after implantation (**E-H**). (*Adapted with permission from Meinel et al, 2005*).

Figure 2.11: Regenerated silk scaffolds for functional meniscus engineering. (*Adapted with permission from Mandal et al, 2011*).

Figure 2.12: Evaluation of gel spun silk-based biomaterials in a murine model of bladder augmentation. *(Adapted with permission from Mauney et al, 2011*).

Figure 2.13: Silk fibroin based composite scaffold in neural tissue engineering**.** A) Surgically implanted aligned NGC to bridge a 10mm rat sciatic nerve defect (10x magnification), (B, C) Contour of the NGC 8 weeks after implantation. *(Adapted with permission from Wang et al, 2011)*

Figure 2.14: Schematic description of the evolution of silk based scaffolds. (*Reprinted with permission from Das et al, Elsevier, 2014*)

Figure 2.15: Lipoproteins as contrast agents. **A**) Schematic depiction of lipoprotein structure. **B**) The ways in which lipoproteins may be modified to act as contrast agents. *(Adapted with permission from Cormode et al, 2010*).

Figure 2.16: Gold nanoparticle imaging and radiotherapy of brain tumors in mice (**i**) *(Adapted with permission from Hainfield et al, 2013*).

Figure 2.17: ZnO nanowires on 3D grapheme foam for detection of Parkinson's disease. *(Adapted with permission from Yue et al, 2014*).

Figure 2.18: Poly(*ε*-caprolactone-*co*-ethyl ethylene phosphate) (PCLEEP) and aligned GDNF-PCLEEP electrospun fiber based conduits.
(Adapted with permission from Chew et al, 2007).

Figure 2.19: Self-Assembling Peptide Nanofiber Scaffold (SAPNS) mediated repair for the animal brain. (*Adapted with permission from Ellis-Behnke et al, 2006*).

Figure 2.20: Promoting Optic Nerve Regeneration through sustained delivery of EGFR TKI AG1478 by nanospheres**.** .(*Adapted with permission from Robinson et al, 2011)*

Figure 2.21. Procedure for performing an axonotomesis of the sciatic nerve at mid-leg level. (*Adapted with permission from Savastano et al, 2014)*

Figure 3.1: Cytotoxicity of GNPs. **(***Reprinted with permission from Das et al, Data in Brief, 2015*)

Figure 3.2: Fabrication and characterization of pre-seeded nanocomposite conduits. (*Reprinted with permission from Das et al, Biomaterials, 2015*)

Figure 3.3: Architecture of nanofibers and culture of Schwann cells over nanofibrous scaffolds.(*Reprinted with permission from Das et al, Data in Brief, 2015*)

Figure 3.4: Swelling ratio of conduits**.** The dynamic swelling ratio of the conduits were calculated periodically every hour upto 24 hours. (*Reprinted with permission from Das et al, Data in Brief, 2015*)

Figure 3.5: In vivo intra cutaneous irritation test**.** The animals observed after 72 hours of injecting saline extract of **A**, GNP-SF conduit and **B**, SF conduit. **C**, In the control group only saline was injected. (*Reprinted with permission from Das et al, Data in Brief, 2015*)

Figure 3.6: Electrical property of GNP-SF nanocomposite scaffold. The figure shows the ohmic nature of the I-V characteristic of the GNP-SF nanocomposite scaffold with the experimental setup in inset.(*Reprinted with permission from Das et al, Data in Brief, 2015*)

Figure 3.7: Magnetic resonance imaging of animals**.** The implanted conduit could be visualized (encircled area) by MRI after a week of implantation.(*Reprinted with permission from Das et al, Data in Brief, 2015*)

Figure 3.8: Surgical implantation and electrophysiological study. **A,** Rat sciatic injury model having a 10mm gap was created. **B,** The fabricated nerve conduits were implanted within the gap and sutured to the proximal and distal ends of the nerve stump. **C**, Experimental setup for conducting NCV and CMAP studies with the nerve stimulator (white) and recording electrode (black). The nerve stimulator is placed once at the distal end (**i**) and again at the proximal end (**ii**) of the implanted conduit (apparent position shown in red) to record NCV through the conduit. The recording

electrode is kept fixed near the ankle of the animal.(*Reprinted with permission from Das et al, Data in Brief, 2015*)

Figure 3.9: Functional analysis of regenerated nerve. A, Nerve conduction velocity **(**NCV) recorded after 9 months and 18 months (n=8). **B**, Compound muscle action potential (CMAP) values recorded after 9 months and 18 months (n=8). **C**, Mean Motor unit potential (MUP) recorded from the gastrocnemius muscle after 9 months and 18 months. **D**, Sciatic function index (SFI) calculated by walking track analysis at 2 week interval for 18 months (n=8). The hind limbs of the animals were stained with methylene blue for obtaining footprints (inset). (*Reprinted with permission from Das et al, Biomaterials, 2015*)

Figure 3.10: Motor unit potential wave patterns**.** (*Reprinted with permission from Das et al, Biomaterials, 2015*)

Figure 3.11: Gait analysis and neural regeneration. A-D, The animals implanted with GNP-SF cell conduits exhibited improved gait and could stand, stretch and jump by the end of 10 months. Black arrows indicate the operated leg. E-H, The implanted conduits were slit open after 18 months to monitor tissue regeneration. Growth of tissue was observed in GNP-SF (E), GNP-SF cell (F), SF (G) and SF cell (H) groups. (*Reprinted with permission from Das et al, Biomaterials, 2015*).

Figure 3.12: Gross examination and histology of harvested conduits**.** (*Reprinted with permission from Das et al, Biomaterials, 2015*)

Figure 3.13: Ultra structure of regenerated tissue**,** across GNP-SF and GNP-SF as compared to the ones implanted with cell SF and SF cell**.** (*Reprinted with permission from Das et al, Biomaterials, 2015*)

Figure 4.1: Fabrication and cytotoxicity of polyaniline powder. A) Scanning electron microscope (SEM) image of polyaniline (PA) powder, B) Viability of rat Schwann cells (SCTM41) against PA measured by MTT assay. (C-E) Live-dead staining assay of untreated SCTM41 under normal light (C), green fluorescence (AO stained) (D) and red fluorescence (EB stained) (E). (F-H) Live-dead staining assay of SCTM41 cells treated with 1000µg/ml under normal light (F), green fluorescence (AO stained) (G) and red fluorescence (EB stained) (H).

Figure 4.2: Molecular mass distribution of synthesised polyaniline (PA). A) PA in Acetonitrile; B) PA in THF; C-D) Solvent-less MALDI showing low molecular weight oligomers (C) and higher molecular weight oligomers of PA (D).

Figure 4.3: Fabrication of electrospun scaffolds and cellular proliferation.

Figure 4.4: Characterization of electrospun scaffolds. A) FTIR spectrum of PA, PASF and SF scaffolds, (B-D) XRD spectrum of B) PASF nanocomposite, C) SF nanofibers and D) PA powder samples.

Figure 4.5: Thermo-gravimetric analysis of scaffolds. Thermal curves of polyaniline (PA), composite (PASF) nanofibers and silk fibroin (SF) nanofibers.

Figure 4.6: Morphology of nerve conduit and cellular growth on conduits

Figure 4.7: Dynamic swelling ratio of PASF and SF conduits over 24 hours.

Figure 4.8: Intracutaneous skin irritation test and surgical implantation of conduit. A) (i) Intra-cutaneuous skin irritation test by administration of compounds through intradermal injection, Nature of skin 72 hours after administration of (ii) Saline extract of PASF conduits, (iii) Saline extract of SF conduits and (iv) Normal saline. B-E) Surgical procedure followed for implantation of conduit.

Figure 4.9: Representative structures of different types of aniline oligomers. (i) Aniline oligomers terminated by phenyl group on both ends (lowest molecular weight species), (ii) Oligomers having an amine in one terminal and equal number of six-carbon rings and nitrogen atoms, (iii) Oligomers having amine group in both terminals

Figure 4.10: Wave pattern of compound muscle action potential.

Figure 4.11: Morphological and electrophysiological assessment in control group.

Figure 4.12: Sciatic Function Index (SFI) calculated through walking track analysis

Figure 4.13: Gross and histological examination. Nerve conduits were harvested for gross observation and histological examination by hematoxylin-eosin staining after (i) 6months and (ii) 12 months of implantation.

Figure 4.14: Ultra structure of regenerated tissue under TEM.

List of Tables

Table 1.1: Grading of nerve injury **(***Adapted with permission from* Grinsell *et al*, 2014**)**

Table 2.1: Overview of scaffold material and fabrication methods employed for fabricating nerve conduits (*Adapted with permission from Wang S e al, 2010*)

Table 2.2: Nanomaterials used in Neuroregeneration

Table 2.3. FDA approved nerve guidance devices (*Adapted with permission from* Kehoe et al, 2012)

Table 2.4. Brief Clinical Trial Data of commercially available nerve conduits (*Adapted with permission from Kehoe et al, 2012**).***

Table 3.1: Outline of animal groups maintained (*Reprinted with permission from Das et al, Biomaterials, 2015*)

Table 4.1: Electrophysiological parameters obtained in different groups

List of Abbreviations

CMAP	:	Compound Muscle Action Potential
DMEM	:	Dulbecco's Modified Eagle Medium
ECM	:	Extracellular Matrix
EDX	:	Energy-dispersive X-ray spectroscopy
EMG	:	Electromyogram
FBS	:	Fetal Bovine Serum
FESEM	:	Field Emission Scanning Electron Microscopy
FTIR	:	Fourier Transform Infrared Spectroscopy
GNP-SF	:	Gold nanoparticle- Silk fibroin composite
MTT	:	3-(4,5-Dimethylthiazol-2-Yl)-2,5-Diphenyltetrazolium Bromide
MUP	:	Motor Unit Potential
NCV	:	Nerve Conduction Velocity
NGC	:	Nerve Guidance Conduits
PASF	:	Polyaniline-Silk fibroin composite
PNI	:	Peripheral Nerve Injury
SCTM41	:	Rat Schwann cell line
SEM	:	Scanning Electron Microscope
SF	:	Silk Fibroin
SFI	:	Sciatic Function Index
TEM	:	Transmission Electron Microscopy
XRD	:	X-Ray Diffraction Spectroscopy

Chapter 1

Introduction

1.1 Peripheral Nerve Injury

Tissue damage to peripheral nerves can result from traumatic injuries caused by motor vehicle accidents as well as during surgical intervention. However, such neural trauma becomes more rampant during wartime which explains the extensive reports and research on nerve injuries during the World War I, World War II and subsequent wars. Extensive survey indicate that the radial and ulnar nerves are most prone to such trauma in the upper limbs while sciatic injuries are most common in the lower limb (Eser *et al*, 2009).

Peripheral nerve injuries (PNI) are often associated with fractures of nearby bones as well as central nervous system damage thereby compounding the disability and impeding proper diagnosis of peripheral nerve damages. PNI is primarily characterised by flaccid atrophy of surrounding muscles leading to partial or complete paralysis. Further sensory loss, including proprioception in the skin areas at the distal end is also observed. Depending on the extent of tissue damage Sunderland classified PNI into 5 degrees while Seddon described neuronal damage by three phases – neuropraxia, axonotmesis and neurotmesis (Seddon, 1947; Sunderland, 1951). **Table 1.1** summarizes the grading system of peripheral nerve injury.

According to the more commonly used Seddon's classification, neuropraxia is described as a mild injury with conduction block but no Wallerian degeneration. It is characterised by focal demyelination or ischemia leading to temporary sensory and motor loss which can be recovered within a few weeks without surgical intervention. Nerve crush injuries leading to axonal damage and loss of myelin are termed as axonotmesis. However, the Schwann cells, epineurium, and perineurium remain partially or completely intact thereby enabling axonal regeneration along the intact endoneurial tubes. The most severe form of nerve injury according to Seddon classification is neurotmesis where the nerve is completely severed with limited chance of axon regrowth making surgical intervention essential. Post surgical recovery is also quite limited. This classification has somewhat limited clinical utility as most nerve injuries are of mixed grade and there is no diagnostic test to discriminate between Sunderland grades II and IV. Currently these Sunderland grades can only be diagnosed histologically (Pfister *et al*, 2011). Mackinnon and Dellon modified

Sunderland's classification to include a mixed injury pattern better reflecting clinical practice (grade VI) (Mackinnon *et al*, 1988).

Sunderland	Seddon	Features
Type 1	Neuropraxia	Damage to local myelin only
Type 2	Axonotmesis	Division of intraneural axons only
Type 3	Axonotmesis	Division of axons and endoneurium
Type 4	Axonotmesis	Division of axons, endo- and perineurium
Type 5	Neurotmesis	Complete division of all elements including epineurium
Type 6 (Mackinnon and Dellon's modification to Sunderland's grading)	Mixed	Combination of types 2–4

Table 1.1: Grading of nerve injury (*Adapted with permission from* Grinsell *et al*, 2014**)**

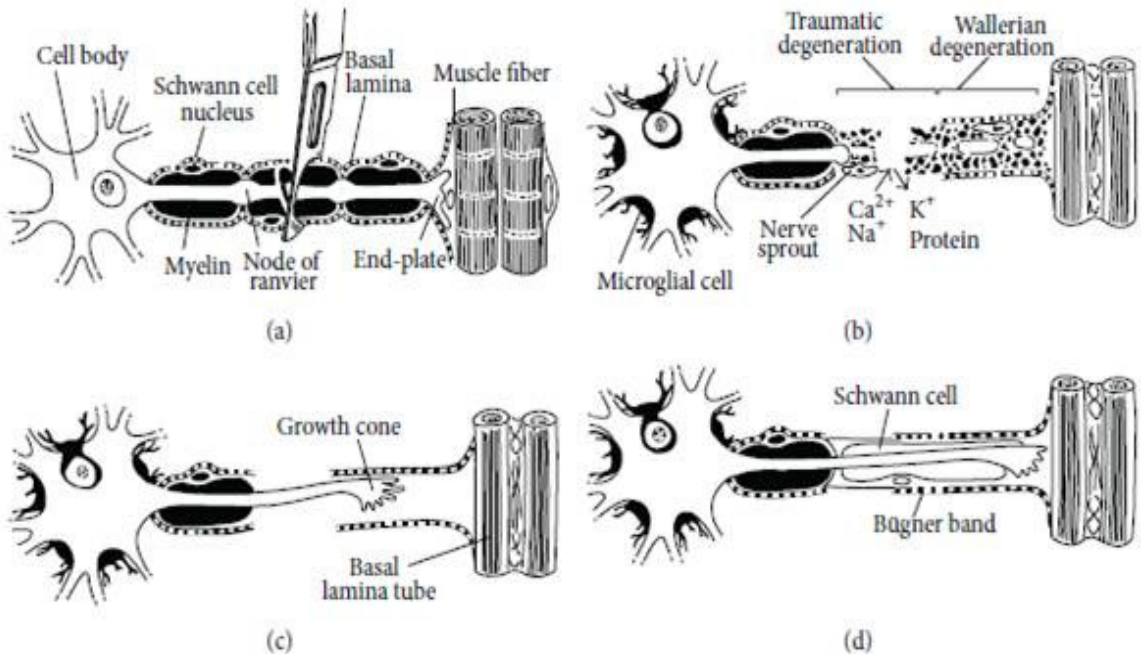

Fig 1.1: Progressive degeneration and regeneration of nerve post injury (*Adapted with permission from* Grinsell *et al*, 2014**)**

1.1.1 Physiological events post nerve injury

Immediately post nerve injury, a series of degenerative processes precedes actual axonal regeneration. Such degenerative processes occur after axonotmesis and neurotmesis grade injury and are referred to as Wallerian degeneration. Wallerian degeneration leads to physical fragmentation of axon and myelin within hours of injury. The axonal contour becomes irregular and by 96 hours post injury axonal continuity is lost with complete disintegration of myelin leading to loss of nerve conduction. The glial cells of the PNS i.e the Schwann cells play a pivotal role in Wallerian degeneration as well as regeneration of axons. Within 24 hours after injury, Schwann cells proliferate rapidly and initiate removal of myelin debris and degenerated axons along with macrophages that migrate through a hematopoietic route. The macrophage migration is facilitated by endoneurial mast cells which release serotonin and histamine within the first two weeks post injury.

During the late stages of Wallerian degeneration stacks of Schwann cells form columns called Bands of Bungner which act as guides for sprouting axons. In neurotmesis grade nerve injury, the nerve ends swell by accumulation of disorganised Schwann cells, fibroblasts and macrophages. This swollen mass at the nerve ends poses a major obstacle in the path of sprouting axons during regeneration. The magnitude of such inflammatory response depends upon the severity of injury caused to the nerve and surrounding tissues (Lee *et al*, 2000). The sequential degeneration and regeneration of nerves post neuro-trauma is depicted in **Fig 1.1.**

1.2 Peripheral Nerve Repair Strategies

1.2.1 Conventional methods of nerve repair

Peripheral nerve injuries having a nerve gap of more than 6mm rarely show complete axonal reconnection and functional regeneration. Hence for neurotmesis grade nerve injuries surgical intervention is the only option available. In case of smaller gaps, surgical apposition of the nerve stumps and accurate fascicular alignment followed by epineurial sutures is the preferred method of treatment. Surgical intervention in large nerve gaps generally involves autografting parts of other less important nerves like sural nerves, superficial cutaneous nerve, or lateral and medial antebrachii cutaneous nerves in the damaged area. Although autograft remains the clinical gold standard for repairing large nerve gaps, the technique is largely fraught with donor site morbidity a secondary surgical site and inefficient functional regeneration which may arise due to a mismatch in axonal size, distribution, and fascicular alignment (Arslantunali *et al*, 2014). Post autograft complications also include potential of infection and formation of painful neuroma. Alternative approaches to nerve autograft have included extensive attempts to bridge severed nerve endings with allografting nerve tissue from another individual or even xenografts. However their use presents limitations including especially immune rejection, risk of cross species disease transmission, secondary infection, and limited supply. Both allografts and xenografts requires long term administration of immunosuppressive drugs which decreases healing rate, increases chance of infection as well as tumor formation. The cellular components of an allograft or xenograft are generally responsible for immunogeneic reactions. Hence various nerve grafts of biological origin like veins, artery as well as decalcified bone channels have been decelluarized to remove the cellular elements but preserve the native extracellular matrix architecture which actually provides guidance to regenerating axons. Decellularization of a biological tissue can be achieved by several physical, chemical or enzymatic methods. Physical methods of decellularization include freezing of nerve tissues, application of direct pressure to tissue, sonication, and mechanical agitation to disrupt cell membrane (Arslantunali *et al*, 2014; Gilbert *et al*, 2006; Gulati *et al*, 1988; Freytes *et al*, 2004; Lin *et al*, 2004). Chemical methods are mostly used in combination with physical treatments and generally include treatment with alkaline and

acid solutions, (Yoo *et al*, 1998; De Filippo *et al*, 2002) nonionic, ionic, and zwitter ionic detergents, (Hudson *et al*, 2004; Dahl *et al*, 2003; Chen *et al*, 2004; Woods *et al*, 2005) and hypotonic and hypertonic solutions. These chemicals generally acheve removal of cellular components by disrupting and solubilising cell membranes and nucleic acids as well as cause cell lysis through osmotic shock. Decellularization of tissues can also be augmented upon treatment with enzymes such as exonucleases, endonucleases, and trypsin. Although a few decellularized nerve grafts like Avance (by Axogen Inc) have been approved by US-FDA, such biological grafts have been unable to match or surpass the results obtained by autograft repair.

1.2.2 Alternative surgical and therapeutic strategies

In addition to conventional methods of nerve grafting, alternative surgical strategies like nerve transfer and free functioning muscle transfer (FFMT) are also employed by neurosurgeons as and when required. Nerve transfer involves the surgical coaptation of a healthy donor nerve to an injured nerve. Here an expendable motor donor nerve supplying a less important limb/muscle is cut and is joined to the distal stump of the injured nerve. Such a technique is generally employed in case of important motor nerve reconstruction where there is no proximal nerve stump like in cervical nerve root avulsions (Grinsell *et al*, 2014; Lee *et al*, 2012). Successful nerve transfers have been reported to maximize functional recovery with fast reinnervation of denervated muscles (Grinsell *et al*, 2014; Lee *et al*, 2012). However, locating a suitable donor nerve having fascicular level synergy with the injured distal stump for the brain to accommodate the rewiring of the newly redirected fibers is a major challenge. Another alternative strategy for restoring functional activity post nerve injury is Free Functioning Muscle Transfer (FFMT). Here a healthy donor muscle along with complete neuro-vascular unit is transferred to the site of injury to assume a new function (Carlsen *et al*, 2009). Such a technique is reserved for severe injuries leading to traumatic loss of muscle, delayed reconstruction (>1 year) and where previous attempts of reconstruction have failed. Although a complex surgical procedure FFMT has been reported to achieve appreciable functional recovery in a large percentage of patients (Carlsen *et al*, 2009; Dodakundi *et al*, 2013). The surgical algorithm followed by a physician when presented with a case of nerve injury is depicted in **Fig 1.2.**

1.2.3 Enhancing axonal regeneration

Translational research for augmenting peripheral nerve repair is generally focussed at developing techniques which enhance axonal regeneration, guide regenerating axons across a gap, delay wallerian degeneration or shortens the denervation time of muscles. Axonal regeneration can be enhanced upon directly administering neurotrophins or growth factors (NGF,GDNF, FGF etc) to the proximal nerve stump after injury or in combination with nerve conduits (Grinsell *et al*, 2014;; Lee *et al*, 200; Konofaos *et al*, 2013). Direct electrical stimulation to the injured nerve also promotes a dramatic increase in the kinetics of target muscle reinnervation (Khuong *et al*, 2013).

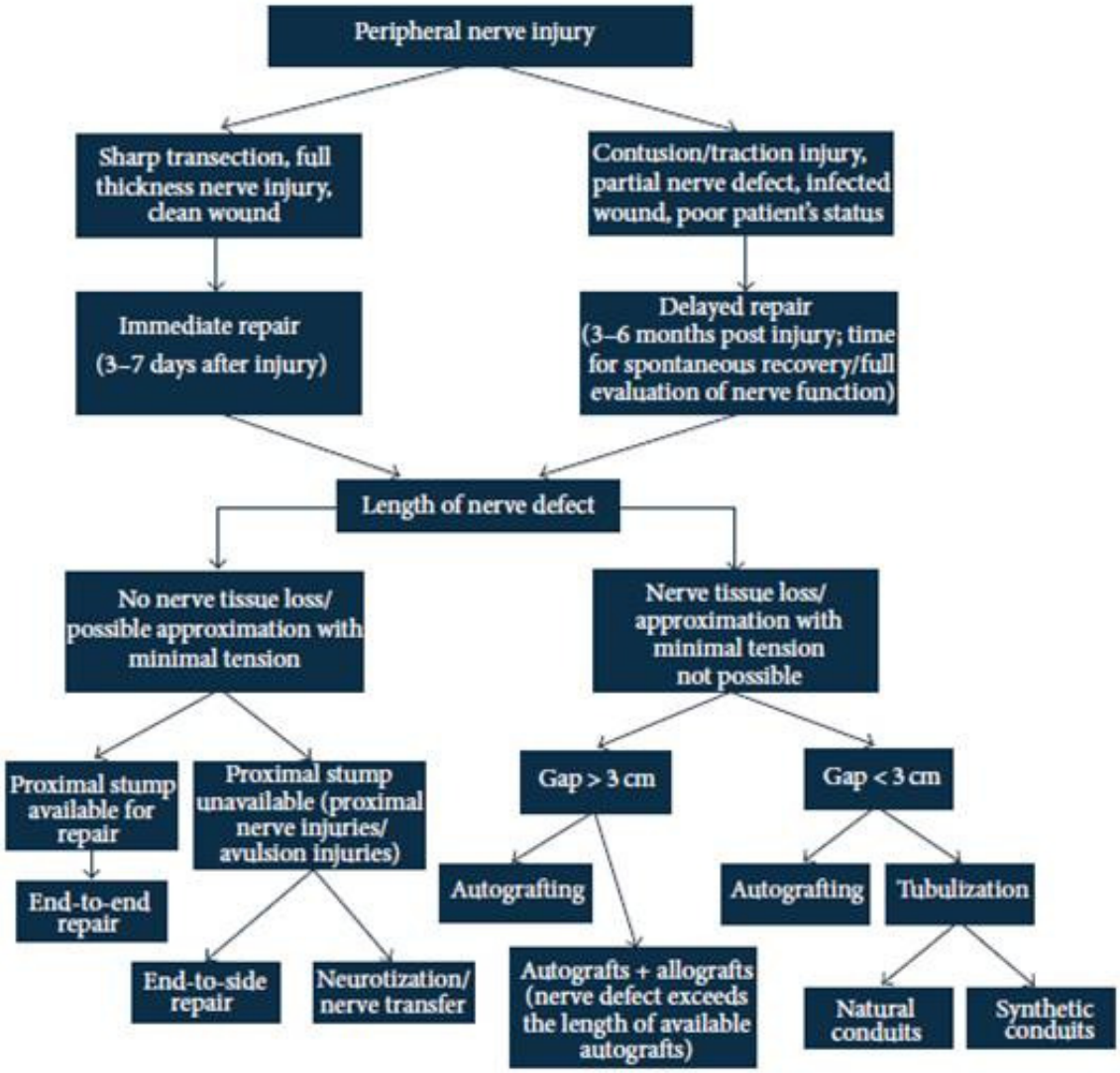

Fig 1.2 Surgical algorithm of peripheral nerve repair (Adapted with permission from Grinsell *et al*, 2014**)**

1.2.4 Entubulation strategies for nerve repair

Different artificial nerve guides have been developed over the years for providing topographical guidance to regenerating axons. Artificial nerve conduits which are tubular shaped scaffolds fabricated from natural/synthetic polymers have been mostly studied. The utility and characteristics of such nerve conduits are discussed in detail in subsequent sections. Neural wraps developed by photothermal tissue bonding (PTB) have also been employed to wrap around a nerve gap by covalent bonding. The PTB bonding is achieved by using an Nd/YAG laser, photoactive dye, and a non-immunogenic amnion wrap (O'Neill *et al*, 2009; O'Neill AC *et al*, 2009; Johnson *et al*, 2007; Henry *et al*, 2009) wherein the collagen present in the amnion wrap covalently bonds with the neural epineurium. The use of non-thermal solid state lasers minimise thermal injury to nerve. In vivo studies with such PTB bonded wraps reported improved axon counts and gait function when tested in rat sciatic nerve as well as rabbit peroneal nerve injury models (O'Neill *et al*, 2009; O'Neill AC *et al*, 2009; Johnson *et al*, 2007; Henry *et al*, 2009). The injured nerve tissue can also be welded by thermal laser whereby tissue bonding occurs due to initial thermal denaturation of structural proteins, followed by subsequent annealing when cooled. Limited in vivo reports are available regarding use of thermal lasers like CO2 laser in nerve injury models due to high rate of nerve dehiscence and thermal injury to axons and nerve tissue.

1.2.5 Glue based repair of nerve

The use of biocompatible adhesives is a non-invasive method for end-to-end coaptation of a nerve causing less tissue trauma, better fascicular alignment, and less scarring compared to microsutures (Tse *et al*, 2012). Ideally nerve glue should not induce fibrosis or act as a barrier to regenerating axons and should posses' sufficient mechanical strength so as to prevent occlusion of the lumen. Fibrin sealants are one of the most widely used glue in nerve repair especially in brachial plexus reconstruction (Tse *et al*, 2012). Extensive study employing fibrin glue in nerve repair on animal and human subjects revealed that it was possible to achieve results equal or superior to suture repair (Sameem *et al*, 2011). However, inferior tensile properties limit the use of fibrin sealants as a standalone technique and this is generally used as an adjunct to microsutures or to coapt nerves where suturing is not possible, for

example, intervertebral foramen (Temple *et al*, 2004). Polyethylene glycol (PEG) based hydrogels are another source of biocompatible glue and have been shown to successfully connect nerve tissue across a 5mm rat sciatic nerve defect (Lin *et al*, 2010). The superior tensile strength and longer degradation rate in vivo (4 weeks) as compared to fibrin establishes PEG as a promising material for nerve glue repair.

1.2.6 Delaying onset of Wallerian degeneration

The major hurdle to functional regeneration of peripheral nerves remains Wallerian degeneration which starts within hours of injury. Invertebrates like earthworms can inherently avoid/delay wallerian degeneration by reconnection of the proximal and distal ends immediately after injury. The complicated physiology of the mammalian nervous system is however unable to perform such phenomenon thereby limiting its regenerative potential. Applying fusogens like PEG promotes axonal membrane fusion between two cells thereby joining severed axonal ends within minutes to hours after injury (Bittner *et al*, 2000). Preliminary studies using PEG based axonal fusion have shown promising results after axonotmesis and neurotmesis grade injury maintain compound muscle action potential upto 7 days after surgery (Bittner *et al*, 2012; Britt *et al*, 2010; Sexton *et al*, 2012).

1.2.7 Minimising muscle denervation post nerve injury

Traumatic nerve injures are also accompanied by degeneration and atrophy of muscles supplied by the affected nerve which ultimately leads to loss of function. Continuous electrical stimulation at the distal end of the injured nerve can be a way of keeping the muscles in active state. The beneficial effect of distal electrical stimulation was experimentally demonstrated in vivo on limb and facial muscle using an implantable electrical stimulator. The method resulted in improved morphology and functional capacity with no evident signs of discomfort among the animals (Williams *et al*, 1996 a, b).

1.3 Neural Tissue Engineering and Artificial Nerve Conduits

Entubulation repair of nerve gaps with synthetic or natural polymers is central to the concept of neural tissue engineering (NTE). NTE involves the fabrication of natural and synthetic polymer based scaffolds having varying architecture which can be implanted as conduits to bridge a nerve gap. Such nerve conduits or nerve guides primarily enhance axonal regeneration by providing haptotactic, chemotactic and topographic guidance to sprouting axons. Additionally nerve conduits ensure localisation of neurotrophic factors protecting the regenerating axons from cellular invasion and prevent obstruction along the nerve gap that might be caused by lipid droplets and scar tissue.

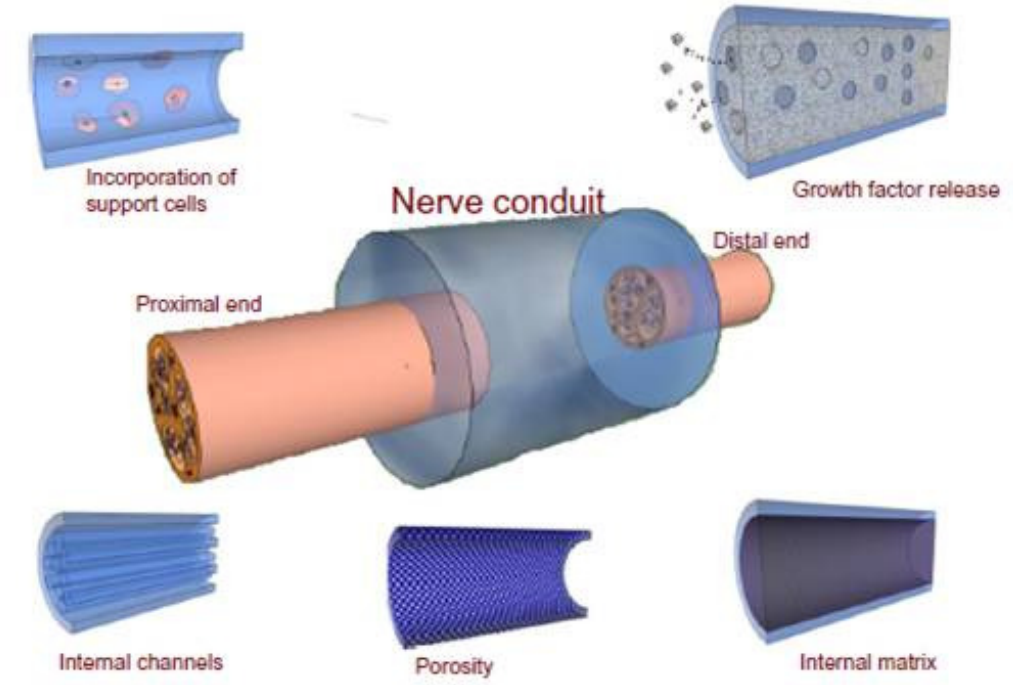

Fig 1.3: Properties of an ideal nerve conduit (*Reprinted with permission from Arslantunali et al, 2014***)**

The emergence of nerve conduits have also greatly helped in the study of cellular and molecular events that occur in the environment of regenerating peripheral nerves.

1.3.1 An ideal conduit

The physical properties of a conduit depend on the choice of biomaterial and the fabrication technique. By combining synthetic and natural polymers with the appropriate fabrication techniques it is possible to fine tune the flexibility, permeability, swelling and biodegradation properties of a nerve conduit. An ideal conduit should be permeable allowing diffusion of nutrients and adherence and proliferation of Schwann cells. Optimum flexibility and lower swelling tendency is desirable for a conduit to prevent occlusion of the lumen and compressing of regenerated nerve. Like all scaffolds used in tissue engineering, a nerve conduit should ideally remain intact till complete axonal regeneration inside the gap. However, it is also essential for the biomaterial to degrade post tissue regeneration in order to prevent any foreign body reaction. To enhance its neuro-regenerative potential, nerve guidance conduits have been incorporated with Schwann cells or stem cells and engineered to deliver therapeutic agents and growth factors into its lumen. The ideal properties of a nerve conduit are represented schematically in **Fig 1.3.**

1.3.2 Neural regeneration through a nerve conduit

The process of neural regeneration through a hollow conduit has been described in detail in a previous report (Daly *et al*, 2012; Heath *et al*, 1998) and is depicted here in **Fig 1.4**. The natural regenerative process occurring within hollow nerve conduits can be divided into five main phases: (i) the fluid phase; (ii) the matrix phase; (iii) the cellular migration phase; (iv) the axonal phase; and (v) the myelination phase (Daly *et al*, 2012; Heath *et al*, 1998). In the initial fluid phase, immediately after injury there is an influx of plasma exudate and tissue fluid from both the proximal and distal nerve stumps, which is rich in neurotrophic factors and extracellular matrix (ECM) precursor molecules (e.g. fibrinogen and factor XIII). The influxed ECM precursor molecules subsequently forms an acellular fibrin cable between the proximal and distal stumps, [Daly *et al*, 2012: Belkas *et al*, 2004; Williams *et al*, 1983; Hoffman-Kim *et al*, 2010] over one week. This fibrin cable later provides topographical guidance to Schwann cells (SCs), endothelial cells and fibroblasts to migrate from the proximal and distal nerve stumps [Mukhatyar *et al*, 2009; Belkas *et al*, 2004]. The migrating SCs subsequently align, forming a SC cable, i.e. the glial bands of Bungner. During the axonal phase of repair, this biological cable replaces the already degraded fibrin cable

and guides the regenerating axonal sprouts, from the proximal end towards the distal target over a period of 2-4 weeks. [Mukhatyar *et al*, 2009; Belkas *et al*, 2004; Williams *et al*, 1983; Kalbermatten *et al*, 2008; Pettersson *et al*, 2010].The aligned SCs mature over a period of 6−16 weeks and switch to 'myelinating' phenotype [Deumens *et al*, 2010]. wraping around the regenerated axons depositing myelin

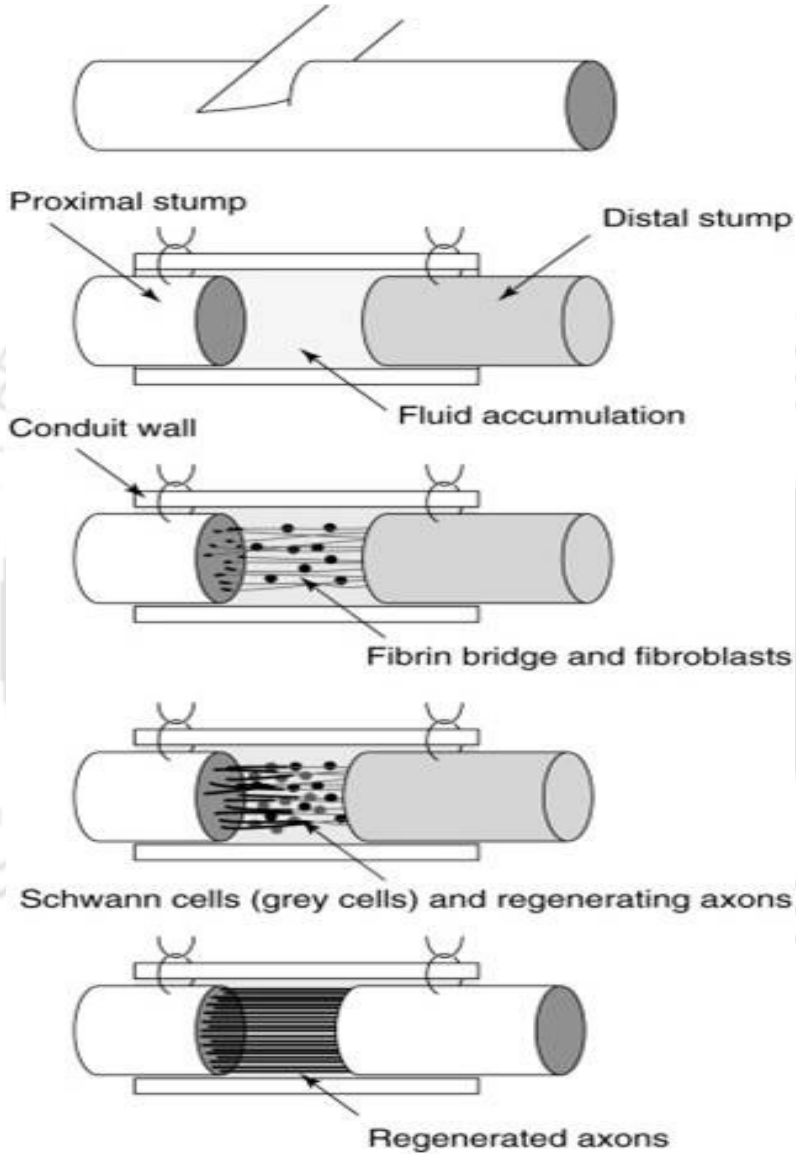

Fig 1.4: Progression of events upon implantation of nerve conduit *(Reprinted with permission from* Heath *et al,* 1998)

which results in functional repair of nerve fibres [Winter *et al*, 2002; Matsumoto *et al*, 2000]. This regenerative sequence takes place within hollow NGCs and can bridge a critical nerve gap of approximately 4 cm in humans and approximately 1.5 cm in a rat sciatic nerve model [Jiang *et al*, 2010; Deumens *et al*, 2010; Mosahebi *et al*, 2001;

Bellamkonda *et al*, 2006]. Although morphological regeneration is observed corresponding functional recovery however remains poor across all nerve gaps [Bellamkonda *et al*, 2006; Clements *et al*, 2009].

1.4 Rationale of the study and Objectives

Artificial nerve conduits with multiple biochemical as well as topographical cues have been fabricated over the years through a variety of fabrication methods. Although many advances have been made in the field of neural tissue engineering there are some unmet needs that limit the translation of laboratory materials to clinical products. This study is aimed at addressing some of the present limitations in the field as discussed below –

1.4.1 Long duration studies – Regeneration of nerves following severe neurotmesis grade injury with complete axonal loss and conduction failure is a highly complex, time consuming process marked with very low success rate even after surgical intervention. Most studies reported till date have been on an average for 3-4 months duration which is a short duration in terms of nerve regeneration and healing process. Only a handful of studies have been reported with post surgical observation time of 1year or more (Boeckstyns *et al*, 2013). Although the nerve is found to grow along the conduit filling the gap within 3-4 months of implantation, the innervations of muscles and regaining of strength as well as sensory function takes a much longer time. Hence it is essential to conduct long duration studies to ensire that the fabricated conduits remain safev(non-immunogeneic), stable and functional until complete neuro-muscular regeneration occurs. Such time tested materials would find it easier to make the transition from lab to clinic.

1.4.2 Using nanoparticles in Neural Tissue Engineering – There is at present much scope of using nanoparticles in fabricating scaffolds for neural tissue regeneration. Composite scaffolds containing nanofibers incorporated with nanoparticles would enable chemical modifications of biomaterial. Such nanocomposite can potentially act as platforms for delivery of nerve growth factors providing chemical cues for cellular proliferation and directing neurite outgrowth. Cohen-Karni *et al* first demonstrated the fabrication of silk-gold nano-composite scaffolds which holds the potential for use as smart biomaterials in tissue engineering applications (Cohen-Karni *et al*, 2012).

1.4.3 *In vivo* studies with conductive polymers - Conducting polymer based scaffolds are assumed to mimic the milieu and enhance regeneration of electrically

active nerve tissue. Although several in vitro reports with neuronal cells support such assumption there are limited in vivo studies till date which can corroborate the neuro-regenerative potential of conducting polymers.

1.4.4 Monitoring functional regeneration of muscle – Neurotmesis grade nerve injuries are not only associated with complete loss of a section of a nerve but also leads to severe degeneration and atrophy of muscles innervated by the damaged nerve. Nerve conduction studies recorded by surface electrodes measure the conduction velocity through the nerve as well as the amplitude (CMAP) of electrical response providing precise information about the diameter of axons and thickness of myelin sheath. Needle EMG uses a very fine bipolar needle electrode to penetrate a specific muscle area and measures the Motor Unit Potential (MUP). MUPs evaluate the integrity of the motor unit ie the motor neuron, motor axon and the muscle which the particular nerve innervates.

Although both nerve conduction study (NCS) and MUPs are monitored in clinical cases of nerve injuries, neurodegenerative diseases and neuropathies, mostly NCV and CMAP are the only parameters that are measured while evaluating nerve regeneration through a tissue engineered conduit. Hence to evaluate complete structural and functional regeneration of nerve and re-innervation of damaged muscle, it is essential to study the MUP patterns by needle EMG in neural tissue engineering applications.

1.4.5 Fabrication method – The human body contains a variety of peripheral nerves which differ from one another in morphology as well as functionality. Electrospining on a rotating mandrel, injection moulding, freeze drying and other fabrication methods used till date for developing nerve conduits only allow the formation of a single conduit of a particular dimension at a time. Further the shape and size of the conduits that can be designed by such methods is also restricted by the availability and dimensions of the mould. Hence, at present, there is an urgent need to develop fabrication methods for designing multiple nerve conduits of different dimensions at a single time.

1.4.6 Objectives of the study

To address the current gaps in knowledge the following objectives were formulated to fabricate artificial nerve conduits with the aim to simulate the native neural architecture and to provide a supportive environment for neural regeneration -

i) Fabrication of nerve conduits based on silk fibroin and *in vivo* evaluation of neuro-regeneration.

ii) Functionalization of nerve conduits with metallic nanoparticles and evaluation of neuro-regeneration in a rat sciatic nerve injury model

iii) Functionalization of nerve conduits with synthetic conducting polymers and evaluation of neuro-regeneration in a rat sciatic nerve injury model

iv) Formulation studies of cell-seeded nerve conduits and their *in vivo* evaluation and comparison with un-seeded nerve conduits.

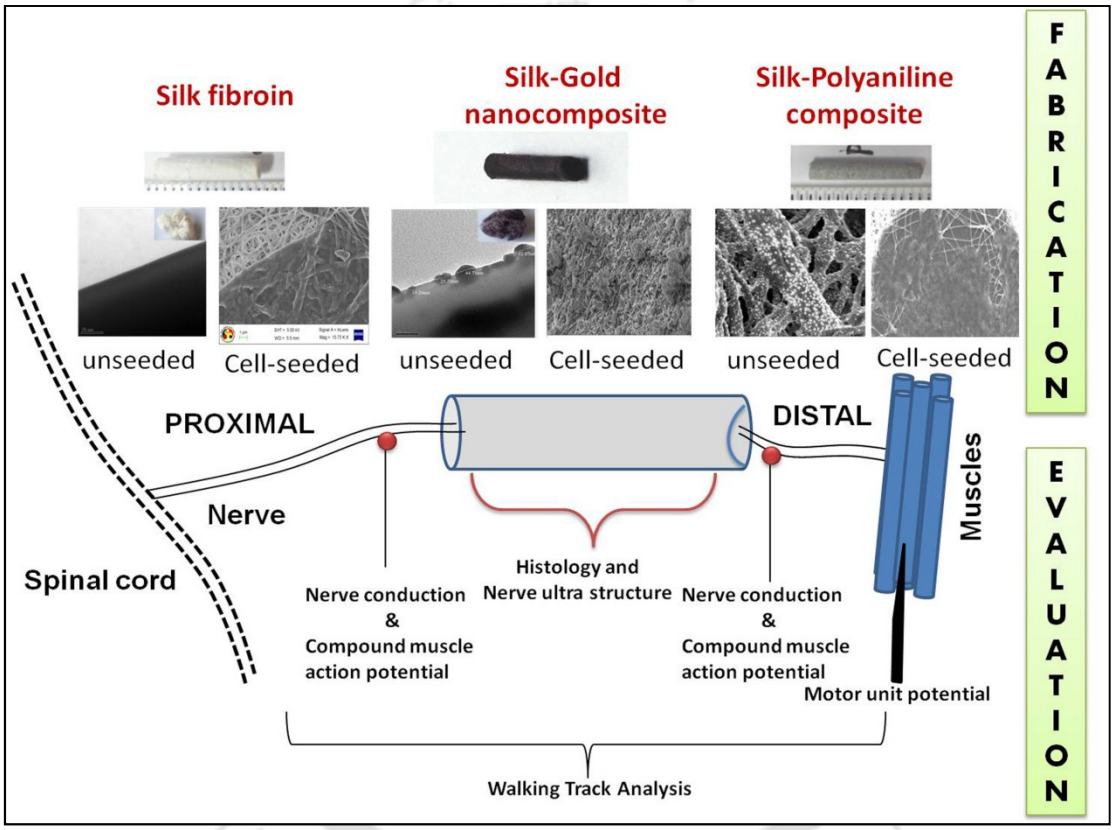

Fig 1.5: Schematic of thesis work – The figure is a schematic representation of the work carried out in the thesis. Three varieties of nerve conduits were fabricated using silk fibroin nanofibers, silk-gold nanocomposite nanofibers and silk-polyaniline composite nanofibers. In another objective the conduits were also pre-seeded with Schwann cells. Both cell-seeded and unseeded conduits were implanted in rat sciatic nerve injury model (nerve gap of 10mm). *In vivo* neural regeneration was evaluated through electrophysiological and histological studies along with monitoring nerve ultra-structure and walking track analysis.

Chapter 2

Review of Literature

2.1 Introduction

Tissue engineering evolved from the field of biomaterials and refers to the practice of combining scaffolds, cells, and biologically active molecules in order to fabricate functional constructs that restore, maintain, or improve damaged tissues or whole organs.

Regenerative medicine is a broad field that includes tissue engineering but also incorporates research on self-healing – where the body uses its own systems, sometimes with help of foreign biological material to recreate cells and rebuild tissues and organs.

2.1.1 Limitations of Neuroregeneration among mammals and potential of neural tissue engineering

In a pioneering experiment on spilt brain research, Dr. Robert Sperry, a neurobiologist pulled out an eye from a frog, rotated it 180^0 and put it back in. The animal was able to repair and rewire its neural circuits but had an inverted vision. As a result, when an insect was kept in front, instead of leaping forward, the frog jumped backward to catch it. Similar results were obtained even after the optic nerve was cut. The experiment proved the ability of neurons to regenerate and rewire neural circuits and for this revolutionary finding Dr Sperry was conferred with the Nobel Prize in 1981. Such remarkable neural regeneration and plasticity is found in many other animals like salamander, lampreys, gold fish etc which can regenerate entire limbs. Unfortunately, humans don't possess such ability. The number of neurons we are born with are all that we will ever have in our lifetime. However, adult stem cells called neural stem cells isolated from specific areas of the brain (olfactory bulb, dentate gyrus, and cerebellum) and spinal cord have been shown to differentiate into neural cells *in vitro*. Still the ability of the neural stem cells to regenerate new nerve cells *in vivo* is very much limited by the local inhibitory signals in the central nervous system (Shoichet *et al*, 2008). The major source of these inhibitory signals is the glial scar formed by the glial cells of the CNS (i.e. astrocytes) around the region of injury. The reactive astrocytes along with myelin and cellular debris forms the glial scar

which acts as an impenetrable barrier inhibiting the regenerating neurons from reaching the synaptic target.

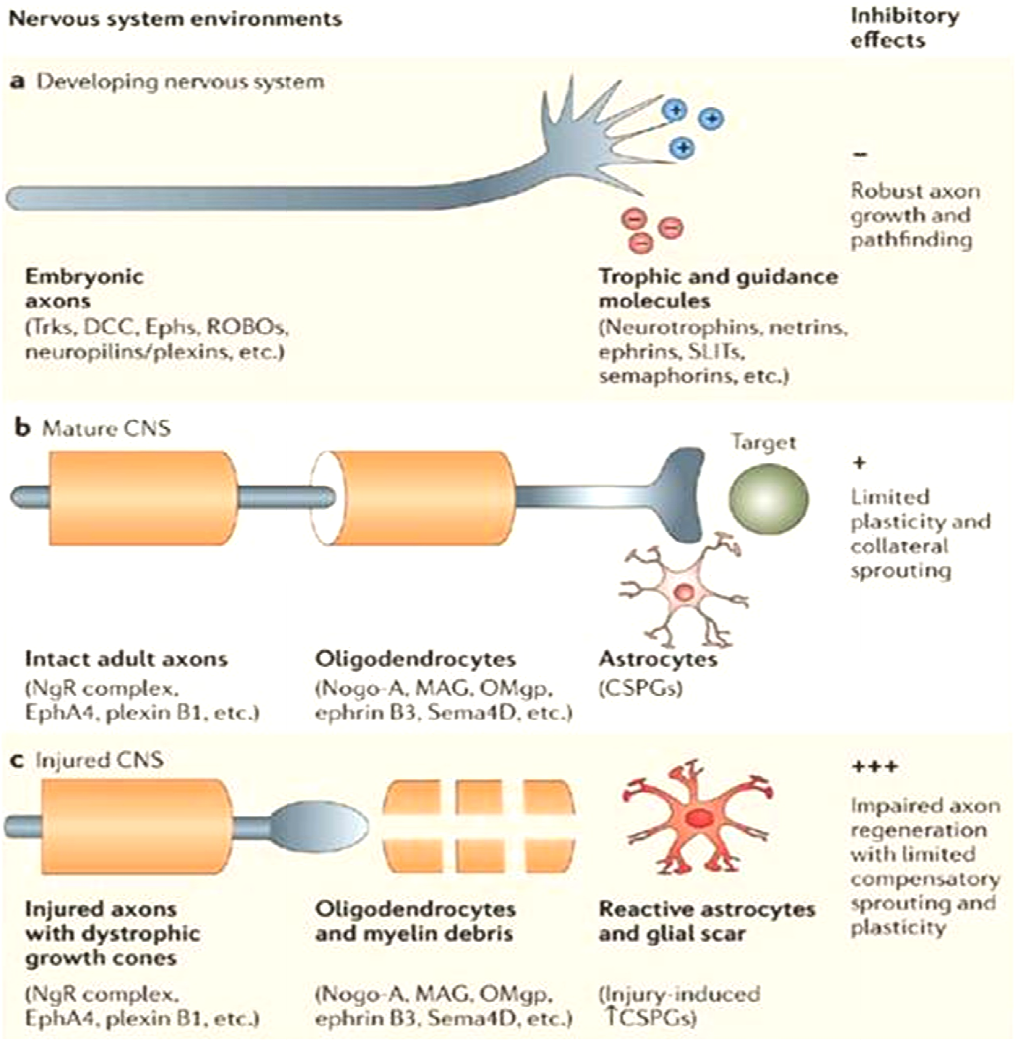

Fig 2.1: Changes in CNS environments after maturation and injury. During embryonic development, unmyelinated axons with motile growth cones can extend, retract and respond to various trophic and guidance molecules. This dynamic process allows the neural circuitry to be fine-tuned (**a**). As the nervous system matures after birth, myelination is finalized with oligodendrocytes ensheathing axons to prevent aberrant sprouting and astrocytes secreting chondroitin sulphate proteoglycans (CSPGs) to further limit structural plasticity in the adult (**b**). After CNS injury, axons become transected and reactive astrocytes further upregulate their secretion of CSPGs. The distal endings of severed axons form dystrophic growth cones and become exposed to CSPGs from the glial scar, as well as myelin-associated inhibitors from oligodendrocytes and myelin debris (**c**). As similar mechanisms prevent short-range plasticity in the adult and long-distance axon repair after injury, relieving these inhibitory influences might not only enhance the regeneration of severed axons, but might also promote compensatory sprouting. EphA4, the cognate neuronal receptor for ephrin B3; MAG, myelin-associated glycoprotein; NgR, Nogo-66 receptor; OMgp, oligodendrocyte myelin glycoprotein; Trk, tyrosine receptor kinase. (*Adapted with permission from Yiu et al, 2006*)

This unfavourable cellular milieu for neural regeneration makes even minor injuries/tissue damage in the CNS fatal. **Fig 2.1** describes the changes in CNS environment after nerve injury. However, the glial cells in the peripheral nervous system (PNS) i.e the Schwann cells play a much more constructive role in nerve regeneration than their CNS counterparts. Upon nerve damage, the Schwann cells shed their myelin sheath and release cytokines which triggers macrophages and monocytes to rush to the site of injury and clear the debris. Such phagocytic infiltration is aided by the easy physiological access to the peripheral nerves as compared to the heavily guarded CNS. The axonal sprouts arising from the Nodes of Ranvier in the proximal end are guided by the neurotrophins secreted by the Schwann cells towards the distal end at a rate of 2-5mm/day (Schmidt, 2003). Thus injuries resulting in small gaps in the peripheral nerves can be healed by regeneration. However, in case of gaps larger than 5mm, surgical intervention becomes essential (Cunha *et al*, 2011).

Neural tissue engineering (NTE) provides promising alternative therapeutic solutions to achieve functional regeneration in severe traumatic injuries which lead to large nerve gaps. NTE involves fabrication of tubular shaped scaffolds called nerve guides/nerve conduits which upon implantation in a nerve gap provide topographical guidance and biochemical cues by maintaining appropriate concentration of cells and growth factors in the lumen thereby facilitating axonal regeneration.

2.1.2 Components of an artificial nerve conduit

Artificial nerve conduits generally comprises of three components – Scaffolds, Support cells and Growth factors.

The scaffold is a template which provides a framework and initial support for the cells to attach, proliferate and differentiate and form an extra cellular matrix (ECM). The scaffolds are developed from a special class of materials called Biomaterials using carefully chosen fabrication method depending on the native architecture of the target tissue. A biomaterial can be described as a substance (other than a drug) or combination of substances synthetic or natural in origin, which can be used for any period of time, as a whole or part of a system to treat, augments, or replace tissue, organ, or its biological function (Williams DF, 2004). Biomaterials generally can be

subdivided to fall under different categories like metals, ceramics, polymers and composites (Williams DF, 2004).

Like any other tissue engineered graft, nerve conduits also should contain cells that are seeded over scaffold and grown in 3D to form the native extracellular matrix of the target tissue thereby making the regenerated tissue functional. Support cells may be autologous, allogeneic, xenogeneic or immortalised cell lines specific to the target tissue.

An ideal nerve conduit should be incorporated with biomolecules to provide biochemical cues to the regenerating axons. Such molecules are generally growth factors, hormones etc and can be delivered through scaffold functionalization or secreted by genetically engineered support cells.

Extensive in vivo studies are essential to establish the clinical significance of artificial nerve conduits. The importance of designing the animal experimentation with appropriate injury model is discussed in the following sections.

2.2 Scaffolds in Neural Tissue Engineering

Polymeric biomaterials are one of the cornerstones of tissue engineering. A wide range of materials has been used. Approaches have increasingly become sophisticated over recent years employing drug delivery functionality, micropatterning, microfluidics, and other technologies. Challenges such as producing three dimensional matrixes and rendering them deliverable through minimally invasive techniques have been addressed. The basic types of biomaterials used in tissue engineering can be broadly classified as synthetic polymers, which includes relatively hydrophobic materials such as the poly-hydroxy acid [a family that includes poly(lactic-co-glycolic) acid, PLGA], polyanhydrides, and others; naturally occurring polymers, such as complex sugars (hyaluronan, chitosan); and inorganics (hydroxyapatite). There are also functional or structural classifications, such as whether they are hydrogels, injectable, surface modified, capable of drug delivery, by specific application, and so on. The breadth of materials used in tissue engineering arises from the multiplicity of anatomical locations, cell types, and requirements of special applications. For example, relatively strong mechanical properties may be required in situations where the device may be subjected to weight-loading or strain, or where maintenance of a specific cyto-architecture is needed. In others, looser networks may be needed or even preferable. The type of materials used is also dependent on the anticipated mode of application (open implantation *vs.* injection or minimally invasive procedure), the nature of any bioactive molecules that might be released, the need for surface functionalization, the needs of the cell types of interest in terms of porosity, and other issues. Some of the materials and corresponding fabrication methods employed for developing nerve conduits are listed in **Table 2.1.**

2.2.1 Natural Polymers in Neural Tissue Engineering

Natural polymers utilized for fabricating nerve conduits include chitosan (Wang W *et al*, 2008;Wang X *et al*, 2005), collagen (Alluin *et al*, 2009; Li *et al*, 1992; Chamberlain *et al*, 2000; Harley *et al*, 2004; Yao *et al*, 2010), gelatin (Chang *et al*, 2009; Liu , 2008) and hyaluronic acid (HA) (Miyamoto *et al*, 2004;, Sakai *et al*, 2007), These natural polymers offer excellent biocompatibility, promotes cellular attachment and proliferation and are degrade naturally inside the body. (Chiono *et al*, 2009; Ciardelli

et al, 2006; Schmidt *et al*, 2003; Nisbet *et al*,2008). However, the widespread biomedical applications of such natural polymers are generally limited by batch-to-batch variation of bio-chemical and physical properties. (Chiono *et al*, 2009; Ciardelli *et al*, 2006; Schmidt *et al*, 2003). Further, most of them exhibit inferior mechanical properties as compared to synthetic polymers and degrade relatively fast *in vivo* (Chiono *et al*, 2009; Ciardelli *et al*, 2006; Schmidt *et al*, 2003). Hence there is often a need for chemical modification, crosslinking or blending with synthetic polymers to form a composite which can meet the requirements of a scaffold inside the body. Due to their low denaturing temperature and thermal stability, natural polymers are usually fabricated via injection molding, dip-coating, and electrospinning from their solutions at ambient or lower temperatures (Chiono *et al*, 2009; Ciardelli *et al*, 2006; Schmidt *et al*, 2003).

Chitosan in neural tissue engineering

Chitosan, a copolymer of d-glucosamine and *N*-acetyld-glucosamine, is a well-known biodegradable polysaccharide obtained from *N*-deacetylation of chitin, which can be extracted from the shells of crabs and shrimps (Chiono *et al*, 2009; Ciardelli *et al*, 2006; Schmidt *et al*, 2003). Chitosan has been used to fabricate nerve tubes and scaffolds because of its excellent biocompatibility and antibacterial activity (Chiono *et al*, 2009; Ciardelli *et al*, 2006; Nisbet *et al*,2008). Chitosan is usually processed in solutions due to its low thermal stability and high glass transition temperature (*Tg*) of $\sim 203\,^{\circ}C$. In one study, chitosan dissolved in trifluoroacetic acid (TFA) along with methylene chloride (MC) was electrospun onto a rotating Stainless Steel (SS) bar to form macro/nanofibrous scaffolds as the inner layer while chitosan-acetic acid solution is dip-coated on the SS bar to form an outer layer (Wang W *et al*, 2008). Immobilization of laminin peptides to these bilayered chitosan tubes was also achieved [Wang W *et al*, 2008]. Multi-channeled chitosan nerve conduits have been fabricated through soft lithography by molding chitosan/acetic acid solution in poly-dimethylsiloxane (PDMS) molds. (Wang DY *et al*, 2008). Chitosan scaffolds are often crosslinked or blended with reinforcing fibers or other polymers to improve its mechanical properties. (Wang X *et al*, 2005; Wang A *et al*, 2007; Freier *et al*, 2005; Xie *et al*, 2008; Pfister *et al*, 2007). Porous viscous gel formed by crosslinking chitosan dissolved with formaldehyde was injected in a tubular stainless-steel mold

to fabricate nerve conduits. Further longitudinally aligned poly (glycolic acid) (PGA) fibers were also inserted within the conduits as luminal fillers (Wang X *et al*, 2005). Chitosan tubes prepared using mold casting was strengthened by over 9 times with braided chitosan yarns (Wang A *et al*, 2007). In another study, chitosan solution was injected over poly (llactide- *co*-glycolide) (PLGA) coils which were mounted into a mold dried (Freier *et al*, 2005). Poly (lactic acid) (PLA) was also incorporated with chitosan in preparing nerve tubes using the dip-coating method to improve the resistance to tension and compression (Xie *et al*, 2008). Chitosan can be physically crosslinked with oppositely charged polysaccharides like alginate to form hydrogel based nerve tubes (Pfister *et al*, 2007).

Collagen in neural tissue engineering

Collagen is comprised of a group of 28 proteins with a same triple helical structure as an extended rod stabilized by hydrogen bonding (Chiono *et al*, 2009; Ciardelli *et al*, 2006, Yan *et al*, 2009, Chen *et al*, 2006). Collagen (types I and III) can be derived from animal tissues such as porcine skin (Alluin *et al*, 2009) and bovine deep flexor (Achilles) tendon (Li *et al*, 1992; Chamberlain *et al*, 2000; Harley *et al*, 2004; Ahmed *et al*, 2004,). Collagen, being the major form of extracellular matrix (ECM) protein, it provides excellent biocompatibility but is largely challenges by its inferior mechanical properties.. In order to provide structural stability to fabricated nerve conduits, collagen is often crosslinked between amine groups using formaldehyde, glutaraldehyde, or 1-ethyl-3-(3-dimethylaminopropyl)-1- carbodiimide (EDC)/*N*-hydroxysuccinimide (NHS). Among several commercially available nerve guides (Chiono *et al*, 2009, Alluin *et al*, 2009, Yao *et al*, 2010), there exists an FDA-approved nerve conduit made from crosslinked bovine collagen (type I). This collagen nerve conduit is known as NeuraGen (Integra) tube (Alluin *et al*, 2009, Yao *et al*, 2010). **Fig 2.2** describes the experimental protocol used to study the effect of another FDA approved nerve guide called RevolNerve composed of porcine type I and type III collagen. Besides conventional injection molding and dip-coating methods for preparing nerve conduits (Alluin *et al*, 2009; Li *et al*, 1992; Chamberlain *et al*, 2000; Harley *et al*, 2004; Yao *et al*, 2010), collagen can be extruded in its water solution and coagulated into filaments (Okamoto *et al*, 2010). These collagen filaments can be wound up around a mandrel to form a tubular structure and also used as longitudinally aligned luminal fillers (Okamoto *et al*, 2010). Collagen sponge

tubes with parallel oriented interconnected pores have been achieved through unidirectional freezing followed by lyophilisation [Bozkurt *et al*, 2009; Bozkurt *et al*, 2007; Kroehne *et al*, 2008]. Microwave irradiation was also used to crosslink collagen and this method is advantageous because potentially toxic crosslinking agents such as glutaraldehyde can be avoided [Ahmed *et al*, 2005; Ahmed *et al*, 2004]. The average tensile modulus of microwave crosslinked collagen tubes was enhanced from 16.7 $\pm$ 0.7 kPa for uncrosslinked tubes to 32.6 $\pm$ 0.6 kPa [Ahmed *et al*, 2004].

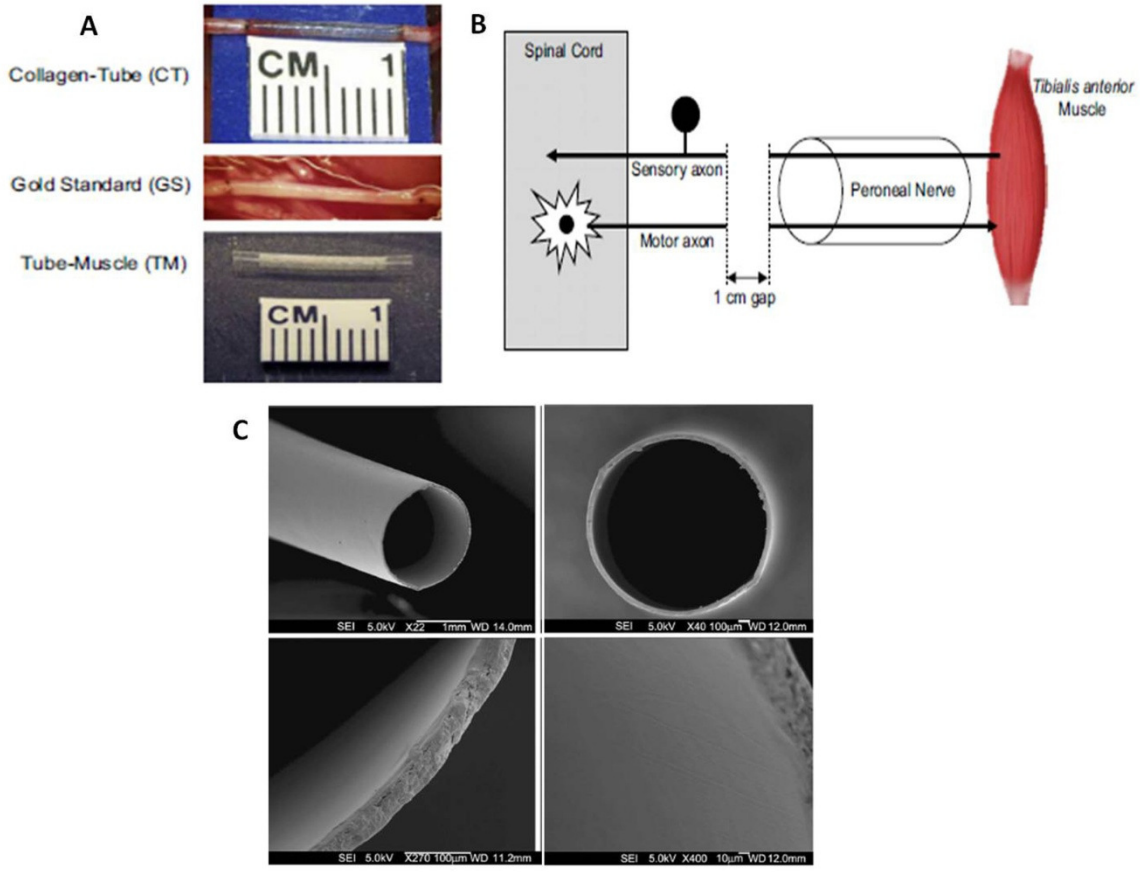

Fig 2.2: Overview of the experimental protocol. A) Mainly three types of conduits were used apart from untreated control group. Collagen tube (CT) was the RevolNerve tube, an EU-approved semipermeable and bioresorbable porcine collagen type I + III nerve conduit. Gold standard was the autograft. Tube-Muscle (TM) comprised of a RevolNerve tube filled with acellular skeletal muscle. **B)** 1 cm gap of peroneal nerve was cut and the respective conduits implanted. **C)** Scanning electron microscopy of a RevolNerve tube (ID: 2 mm). It can be noticed that the external and internal texture is smooth. (*Adapted with permission from Alluin et al, 2009*)

Collagen was blended with chitosan homogeneously in acidic solutions to fabricate nerve conduits [Hu *et al*, 2009; Wang *et al*, 2009], which exhibited much higher tensile modulus of 886 ± 3 kPa when the collagen:chitosan ratio was 4 : 3 after crosslinking and freezedrying [Wang *et al*, 2009].

Gelatin in neural tissue engineering

Gelatin is a biodegradable polymer derived from collagen by thermal denaturation of chemical and physical degradation. Gelatin has excellent biocompatibility, plasticity, and adhesiveness. The water solubility of gelatin renders convenient processing in aqueous solutions but the resulted products suffer from poor mechanical properties and handling characteristics [Chiono *et al*, 2009; Ciardelli *et al*, 2006]. Thus, subsequent crosslinking using proper crosslinking agents is crucial to improve the chemical and physical characteristics of gelatin for preventing toxicity and fabricating suitable tubular structures for nerve regeneration [Chiono *et al*, 2009; Ciardelli *et al*, 2006]. Gelatin tubes are prepared by injection molding or dip-coating followed by immersing the mold or mandrel into crosslinking agent solutions [Chang *et al*, 2009; Liu , 2008; Lu *et al*, 2007; Chen *et al*, 2005; Chang *et al*, 2007]. Styrenated gelatin was synthesized and photopolymerized into nerve conduits and fibers under visible light irradiation in the presence of camphorquinone [Gámez *et al*, 2004]. Other than chemical modification of gelatin, three commonly used agents, genipin, proanthocyanidin, and EDC/NHS, can be used to crosslink gelatin via primary amino groups along the chain backbone [Chang *et al*, 2009; Liu , 2008; Lu *et al*, 2007; Chen *et al*, 2005; Chang *et al*, 2007]. **Fig 2.3** depicts the morphology of genipin crosslinked gelatin based nerve conduits and its neuro-regenerative potential upon implantation. The residue free amino groups are a useful indicator for estimating the crosslinking density [Liu , 2008; Lu *et al*, 2007]. Crosslinking degree has been revealed to be crucial in tuning the degradation rate so as to influence nerve regenerative responses because a too low crosslinking density results in more degradation products to evoke more severe foreign body reaction while a too high crosslinking density impedes the degradation and causes nerve compression with thickened perineurium and epineurium [Lu *et al*, 2007].

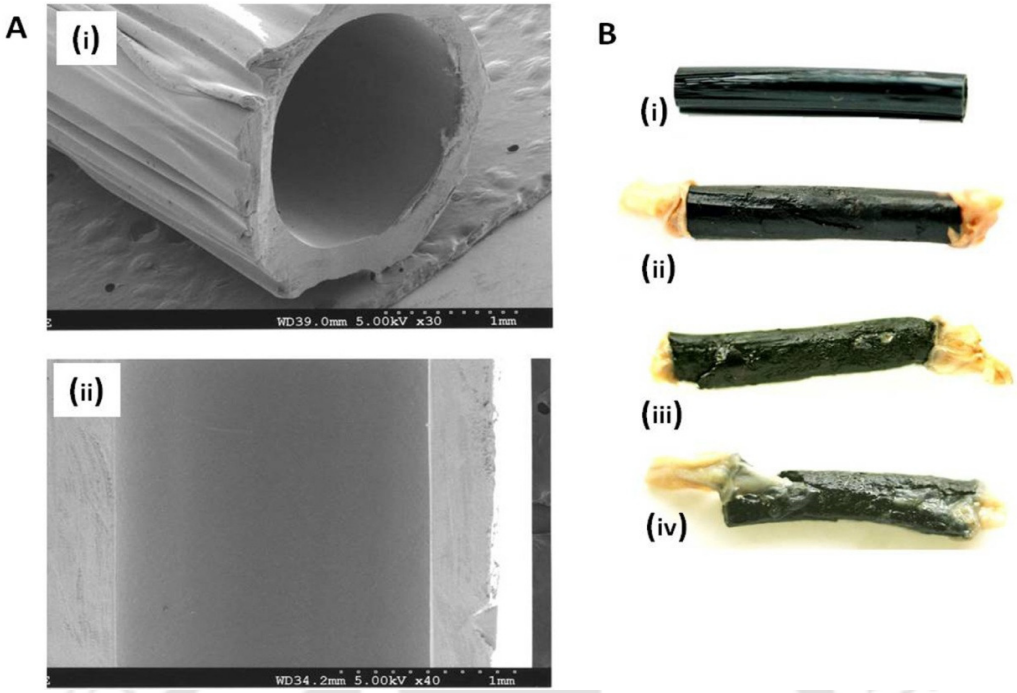

Fig 2.3: Genipin-cross-linked gelatin conduit (GGC). A) SEM micrographs of the GGC in longitudinal section (panel i) and cross section (panel ii). **B**) Macrographs of the GGCs at different implantation periods: intact (panel i), 1 week (panel ii), 4 weeks (panel iii), and 8 weeks (panel iv). Scale bars=5mm. (*Adapted with permission from Chen et al, 2005*)

Hyaluronic acid in neural tissue engineering

Hyaluronan (HA or hyaluronate) is a high molecular weight glycosaminoglycan (GAG) that can be found in ECM of humans. HA demonstrates a unique combination of advantages including nonimmunogenic, nonadhesive,bioactive GAG that has been associated with several cellular processes and axonal ingrowth [Nisbet *et al*, 2008;, Miyamoto *et al*, 2004;, Sakai *et al*, 2007; Leach *et al*, 2005; Jansen *et al*, 2004]. HA has to be modified to be crosslinkable for forming three-dimensional (3D) structures with mechanical strength. HA, conjugated by cinnamic acid to the carboxyl group using aminopropanol as a spacer, can be injected into a silicone mold and cured under ultraviolet (UV) light [Miyamoto *et al*, 2004;, Sakai *et al*, 2007]. Crosslinked HA is so weak for handling that augmentation of an outer layer made from another biodegradable material is required for the operation procedure and during the nerve regeneration period because the nerve conduits should keep their structure with sufficient elasticity and flexibility for the fixation to the nerve stumps [Sakai *et al*, 2007]. Another crosslinkable HA is glycidyl methacrylate HA or GMHA [Leach *et al*, 2005]. Nerve conduits based on an esterified hyaluronan derivative

(Hyaff) have been prepared from individually knitted strands and strengthened by coating a thin layer of the same polymer [Jansen *et al*, 2004]. Although Hyaff nerve tubes demonstrated excellent biocompatibility, a quick degradation, massive in growth of cells and fibrous tissue formation can possibly hamper the ultimate goal of the tubes in peripheral nerve repair [Jansen *et al*, 2004].

2.2.2 Synthetic Polymers in Neural Tissue Engineering

Producing a synthetic scaffold that would be biocompatible, biodegradable, conducting and resistant to infection in order to contribute to neurite outgrowth is a vital requirement (Subramanian *et al*, 2009). Synthetic polymers can be tailored to develop a wide range of mechanical features and degradation rates. They can also be processed to minimize immune response (Timnak *et al*, 2011). Biomaterial chemistry is influential on proteins that adsorb and this mediates interactions with immune cells and may lead to their activation (Boehler *et al*, 2011). Generally, hydrophobic materials tend to enhance monocyte adhesion relative to hydrophilic materials leading to a local immune response at the implant site. Studies have shown that the implantation of materials that are hydrophilic or neutral decrease monocyte/macrophage adhesion and reduce foreign body giant cell (FBGC) formation *in vitro*. However, adherent cells on hydrophilic or neutral biomaterials have been shown to produce a greater relative level of inflammatory cytokines (Boehler *et al*, 2011).

Non-biodegradable synthetic polymer based nerve conduits

Nerve guides made from non-biodegradable materials can lead to chronic nerve compression and may damage the regenerating nerves. Therefore, a secondary surgery is needed to remove these nondegradable conduits after nerve regeneration is fulfilled. Silicone rubber tubes are the earliest and widely used synthetic nerve tubes because of their inertness, availability, and flexibility [Jenq *et al*, 1985; Williams *et al* 1987; Cai *et al*,2005; Lundborg *et al*, 1997]. It can be processed directly without the need of a solvent, which may cause problems such as evaporation and toxicity. Because silicone nerve conduits are not biodegradable or permeable for large molecules, they only supply an isolated environment for nerve regeneration [Jenq *et al*, 1985; Williams *et al* 1987; Cai *et al*,2005; Lundborg *et al*, 1997]. PAN-PVC copolymer was used to fabricate nerve guides via a wet-phase inversion technique

[Wen *et al*, 2006; Broadhead *et al*, 2002]. Semipermeable membranes can be formed from the polymer solution using an annular spinneret with deionized water as a liquid precipitant [Wen *et al*, 2006; Broadhead *et al*, 2002]. Using different starting polymer solutions, various hollow fiber membranes were fabricated with different wall thicknesses and hydraulic permeabilities [Broadhead *et al*, 2002]. The wall architectures of these membranes were anisotropic and consisted of a fingerlike macrovoid structure [Broadhead *et al*, 2002]. Poly(2-hydroxyethyl methacrylate) (PHEMA) is an elastic and inert polymer. Hydrogel-based tubular structures made from PHEMA are too soft to be handled in implantation [Dalton *et al*, 2002]. A hydrophobic monomer methyl methacrylate (MMA) was copolymerized with HEMA in the presence of crosslinking agent ethylene dimethacrylate to obtain PHEMA-MMA hydrogel with a higher mechanical strength [Dalton *et al*, 2002]. A biphasic wall structure can be created with an inner porous sponge-like layer and an outer gel-like layer because of phase separation during the polymerization with centrifugal forces. Because PHEMA-MMA nerve conduits are still weak, PCL coils have been used to further enhance their mechanical strength and prevent tubes from partial collapse during implantation [Katayama *et al*, 2006]. The architecture of the coil-reinforced tubes formed through centrifugal casting (SpinFX) system and its effect on nerve regeneration is depicted in **Fig 2.4**. Mechanical stability can be also improved by wrapping small PHEMAMMA tubes in an expanded polytetrafluoroethylene (e-PTFE) membrane [Tsai *et al*, 2006].

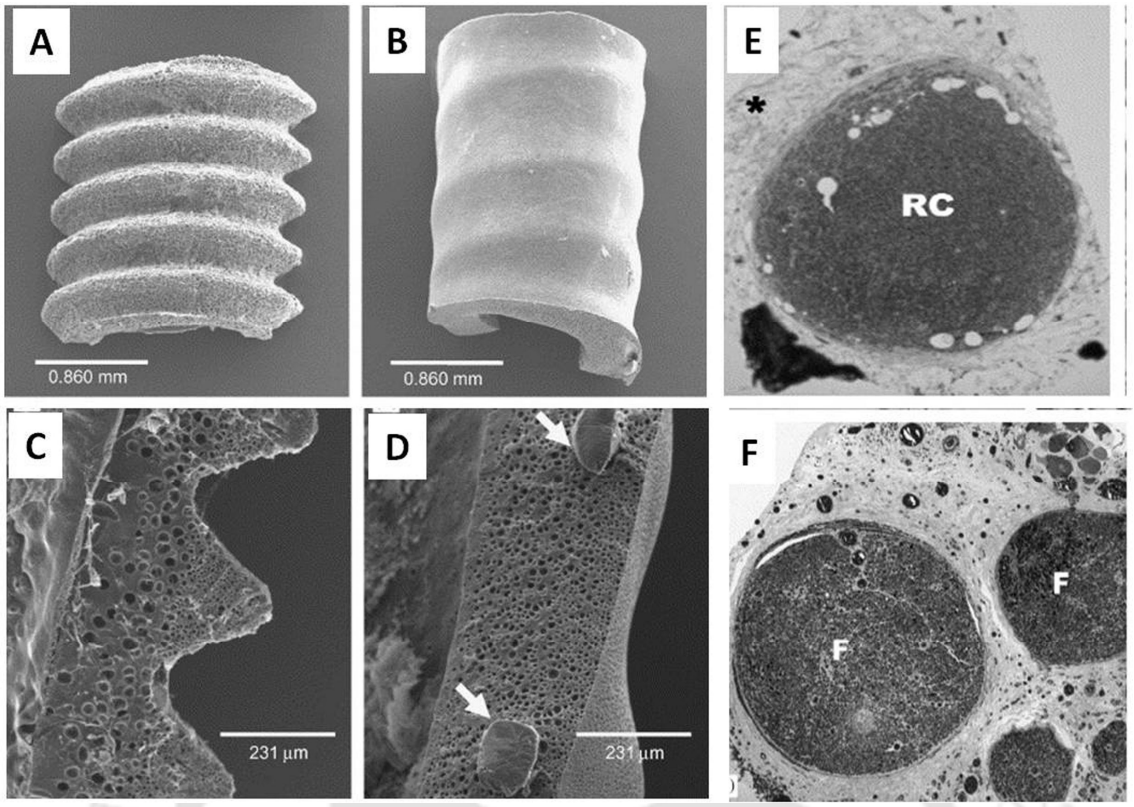

Fig 2.4: **Representative SEM micrographs of tubes synthesized by SpinFXs technology**: (**A**) corrugated tube, (**B**) coil-reinforced tube, (**C**) 130x magnification of the corrugated tube wall, and (**D**) 130x magnification of the coil-reinforced tube wall (arrow indicates coil). **Cross section of the mid section of grafts at 16 weeks** (**E**) 40x magnification of the regenerating cable (RC) within the tube (**F**) 40x magnification of the autograft. '*' indicates the tube wall. F is the fascicle of the autograft. (*Adapted with permission from Katayama et al, 2006*).

Biodegradable synthetic polymer based nerve conduits

Biodegradable nerve conduits are generally more promising in bridging nerve gaps as they can degrade away after accomplishing their task. Further, biodegradable nerve conduits offer possibilities of incorporating bioactive chemicals such as nerve growth factor (NGF), laminin, and fibronectin inside the wall and then releasing them in a controlled manner during polymer degradation [Chiono *et al*, 2009; Ciardelli *et al*, 2006]. In order to achieve this goal, polymer degradation rate should match the rate for axon growth along the gap. The thermal and mechanical properties of biodegradable polymers can be readily controlled at the molecular level using advanced synthetic routes. These properties are crucial for handling and implantation of conduits and axonal in-growth. Many biodegradable polymers are semi-crystalline and their thermal properties such as melting temperature (*Tm*),

crystallinity, crystallization rate, and morphology of crystalline domains are important for determining their bulk and surface physicochemical properties. The existence of crystalline regions can enhance mechanical strength and structural stability while it reduces the degradation rate and permeability of the nerve tubes made from these semicrystalline polymers, consequently affecting cellular and regenerative functions. Polyesters such as PGA, PLA, PCL, PDO, and their copolymers are most commonly used biodegradable polymers in constructing tubular structures for peripheral nerve regeneration. These polyesters are usually synthesized via ring-opening polymerization and can degrade via the hydrolysis of ester bonds along the polymer backbone [Chiono *et al*, 2009; Ciardelli *et al*, 2006]. Poly L-Lactic Acid (PLLA) is a biodegradable synthetic polymer applied as a biomaterial in different biomedical applications [Willerth *et al*, 2007]. Nano-structured PLLA scaffold has similarities with the natural extra-cellular matrix (ECM), such as ultrafine continuous fibers, high surface-to-volume ratio, high porosity and variable pore-size distribution. The presence of ester linkages in the polymer backbone also results in their bio-functionalization by covalent conjugation with different biomolecules. This polymer is considered as an ideal cell environment for tissue engineering of the nervous system (Vasita *et al*, 2006). Several studies have shown that neural stem cells (NSCs) can develop on PLLA scaffold and this supports neurite outgrowth Vasita *et al*, 2006; Tierney *et al*, 2009). Some disadvantages of this polymer are its poor biocompatibility, discharge of acidic degradation products, poor process ability and early failure of mechanical features during degradation (Vindigni *et al*, 2009). PLGA has been extensively used as a scaffold material for tissue engineering, as it is biodegradable and approved by the FDA for biomedical applications (Kramer *et al*, 2011). However, cell adhesion and growth can be impeded due to the deficiency of natural adhesion sites on the polymer. For this reason, many techniques have been explored to modify PLGA scaffolds and promote cell adhesiveness, such as hydrolysis, aminolysis, blending and covalent attachment of adhesive peptides (Kramer *et al*, 2011). Recent evidence showed that PLGA nano-fibers are appropriate scaffolds for nerve tissue engineering application and their biological properties can be promoted by applying poly-L-lysine (PLL) in the polymer matrix (Kramer et al, 2011).

Material used	Fabrication method	References
Alginate/Chitosan blend	Mandrel coating	Pfister et al, 2007
Chitosan	Dip-coating	Wang et al, 2008
	Injection molding	Wang et al,2005
	Soft lithography and molding	Wang DY et al, 2008
	Braiding and molding	Wang A et al, 2007
Chitosan/PLA blend	Mandrel coating	Xie F et al, 2008
Collagen	Dip-coating and crosslinking	Alluin O et al, 2009
	Injection molding and crosslinking	Chamberlain et al, 2000
	Fiber winding	Okamoto et al, 2010
	Unidirectional freezing and freeze-drying	Kroehne, et al, 2008
	Film rolling and crosslinking	Ahmed et al, 2004,2005
Collagen/Chitosan blend	Unidirectional freezing and freeze-drying	Hu X et al, 2009
	Freeze-drying and steam-extrusion	Wang X et al, 2009
Gelatin	Injection molding and crosslinking	Chang JY et al, 2009
	Dipcoating and crosslinking	Chen YS et al, 2005
PHEMA-MMA	Centrifuge casting and crosslinking	Piotrowicz et al, 2006
PPy	Electro-plating and molding	George et al, 2009
PCL	Dip coating	Kokai et al, 2010
	Braiding	Vleggeert-Lankamp et al, 2007
	Melt extrusion	Chiono et al, 2009
	Wire mesh and mandrel coating	Bender et al, 2004
PGA	Braiding and dip-coating with collagen	Nakamura et al, 2004
PHB	Film rolling	Kalbermatten et al, 2008
PLGA	Immersion precipitation	Oh et al, 2008
	Dipcoating and immersion precipitation	Chang CJ et al, 2006
	Wet phase inversion	Wen X et al, 2006
	Injection molding	Hadlock et al, 2000
	Electrospinning	Bini et al, 2004
PLLA	Extrusion	Widmer et al, 1998
	Braiding	Lu et al, 2009
	Dip coating	da Silva CF et al, 1985

Table 2.1: Overview of scaffold material and fabrication methods employed for fabricating nerve conduits (*Adapted with permission from Wang S et al, 2010***)**

In one report, the potential of biodegradable poly (l-lactide-co-glycolide)(PLGA) polymer with diverse microstructures, as scaffolds for nerve tissue engineering was analyzed. In this study porous nano-fibrous scaffolds were developed by the electro-spinning method. Polymer fibers with diameters in the nanometer range were created by applying a polymer fluid jet to a high electric field. microbraided and aligned microfiber scaffolds were also developed. The solvent casting method produced a polymer film scaffold. C17.2 nerve stem cells were seeded and cultured on all the four different types of scaffolds under static conditions for 3 days. Scanning electron micrographs detected that the nerve stem cells adhered to and differentiated on all the scaffolds and induced neurite outgrowth (Bini *et al*, 2006).

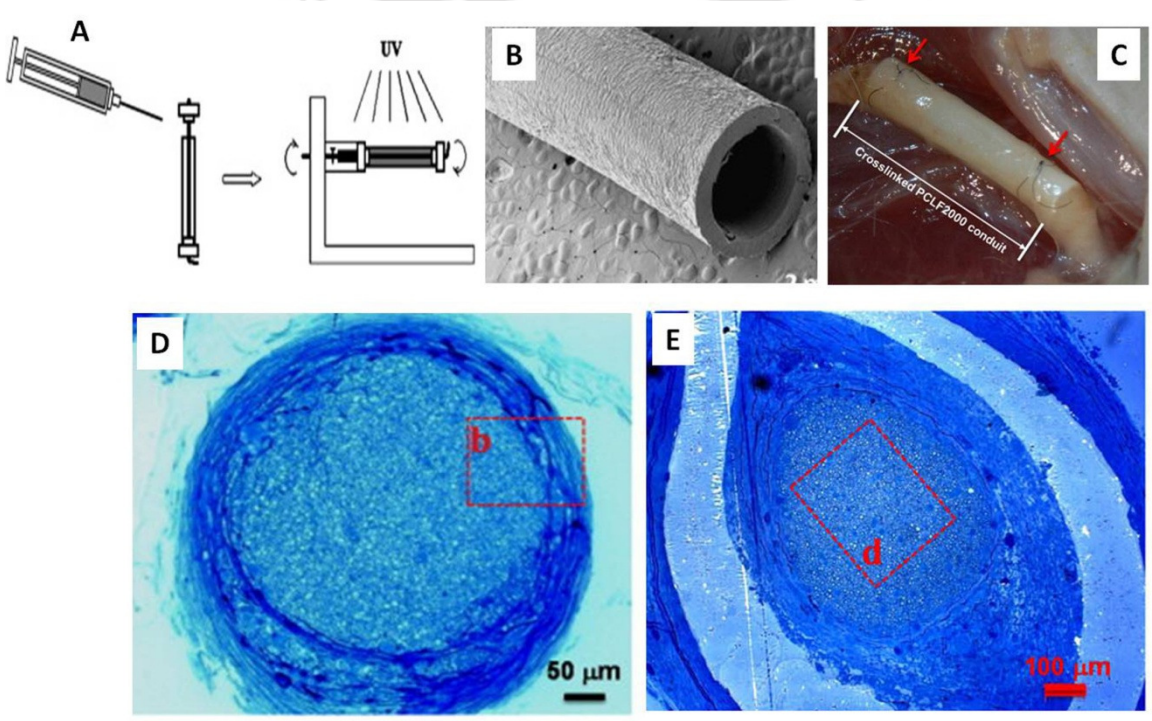

Fig 2.5: **Photo-crosslinked poly(e-caprolactone fumarate) based nerve conduits** (**A**) Fabrication of a photo-crosslinked PCLF conduit. (**B**) SEM pictures of crosslinked PCLF2000 conduits. **(C)** Gross view of a crosslinked PCLF2000 nerve conduit sutured with the proximal and distal sciatic nerve stumps (arrow headed) at 17 weeks post-implantation. Micrographs of toluidine blue-stained cross-sections of regenerated nerve cable at the mid-portion of a crosslinked PCLF2000 single-lumen conduit 6 weeks (**D**) and 17 weeks (**E**) after implantation. (*Adapted with permission from Wang et al, 2009*).

PCL-derived crosslinkable copolymers such as PCLF, PCLA, and PPF-PCL have been synthesized and nerve conduits have been fabricated via a technique that combines injection molding and photo-crosslinking [Cai *et al*, 2010; Wang *et al*, 2009; Wang *et al*, 2008; Runge *et al*, 2010, Wang *et al*, 2015].Well-tuned

architecture, crystallinity, mechanical and surface characteristic of crosslinked PCLAs and PCLFs have been shown to support and correlate with nerve cell attachment, proliferation, differentiation, and axon myelination [Cai *et al*, 2010; Wang *et al*, 2009; Wang *et al*, 2008; Runge *et al*, 2010]. Mechanical properties enhanced by PCL crystalline structures were found to play an important role in controlling Schwann cell precursor line (SpL201) cell behavior [Cai *et al*, 2010; Wang *et al*, 2009].

In vivo studies of crosslinked PCLF nerve conduits (**Figure 2.5**) showed no inflammatory reaction or existence of macrophages [Wang *et al*, 2009]. Nerve cable with myelinated axons has been found after 6 or 17 weeks of implantation [Wang *et al*, 2009]. Single lumen and multi-channel PPF-PCL nerve conduits have been fabricated using the molding and photo-crosslinking technique and implanted in the rat sciatic nerve transaction model for 4 and 16 weeks to demonstrate biocompatibility and guided axonal growth [Wang *et al*, 2015]. PHB is a granular constituent of bacterial cytoplasm, having the advantage of ease of synthesis via microorganisms and its adjustable mechanical properties, biocompatibility and biodegradability. PHB conduits have been fabricated by rolling PHB sheets around a mandrel followed by thermal sealing [Kalbermatten *et al*, 2008; Young *et al*, 2002].PHBHHx was developed with a better flexibility than PHB [Bian *et al*, 2009]. Conduits with uniform wall porosity and those with non-uniform wall porosity were fabricated using dip-coating and particulate leaching with NaCl-sized particles as porogen [Bian *et al*, 2009]. PHBV containing 95% PHB was blended with P(l-d,l)LA and PLGA to form a porous micropatterned film by solution casting from a silicon template and then the film can be rolled together with a electro-spun PHBV/PLGA aligned fibrous mat inside to prepare nerve conduits [Yucel *et al*, 2010]. A biodegradable polyurethane has been developed from PCL and PEG with 1,6-hexamethyl diisocyanate as the chain extender and dipcoated into tubes for repairing peripheral nerve injuries [Yin *et al*, 2007].The hydrophilic PEG segment can accelerate the degradation rate of hydrophobic PCL, making the degradation kinetics more compatible with the nerve regeneration rate [Yin *et al*, 2007].]. Porous nerve conduits can also be processed via rapid prototyping using a double nozzle, low temperature, deposition manufacturing system that combines phase separation and chemical crosslinking simultaneously [Yin *et al*, 2007].].

2.2.3 Electrical stimulation and electrically conductive scaffolds in Neural Tissue Engineering

Polymers with electrons in their backbones are often known as conducting polymers. Electrical stimulation has been shown to promote the nerve regeneration process and this has made the application of electrically conductive polymers very interesting for the manufacture of scaffolds for nerve tissue engineering. The main conductive polymers include Polypyrrole (PPy) carbon nanotubes, polyaniline and PEDOT.

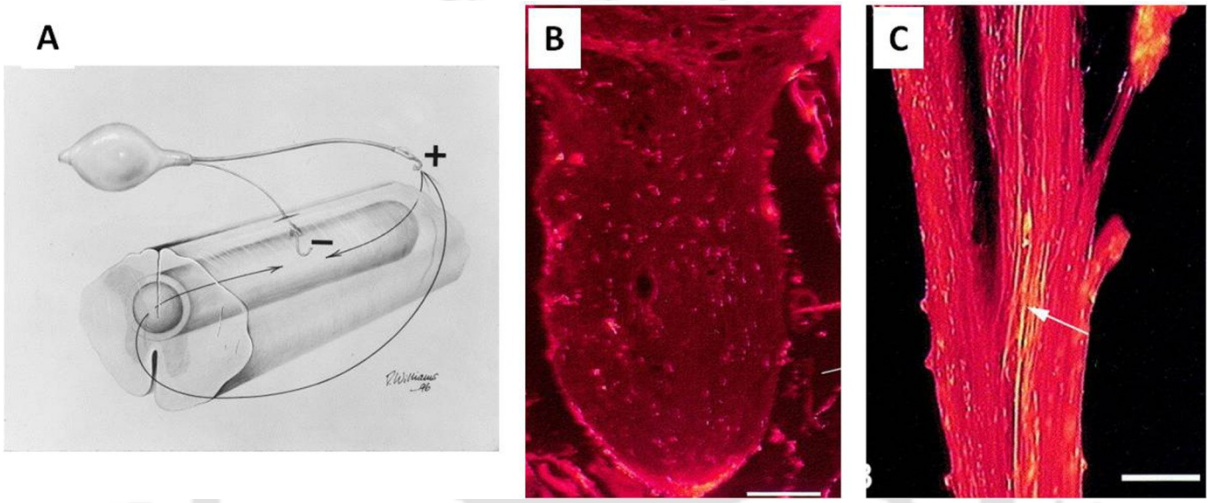

Fig 2.6: Electrically Mediated Regeneration of Mammalian Spinal Axons Into Polymeric Channels (**A**) Artist's drawing of the stimulator, silicone rubber tube or guidance channel, and the electrical circuit within the spinal cord. The tube was implanted into the dorsal spinal cord. The uninsulated tip of the cathodal electrode (negative) was sealed within the center of the tube, while the anodal electrode (positive) remained outside the vertebral column, sutured to paravertebral musculature. The body of the stimulator was surgically placed within the fat pad at the base of the guinea-pig's neck. To complete a circuit, current must flow initially into each end of the hollow tube as diagrammed. For diagrammatic purposes, the drawing is not made to scale. (**B**) Anatomical responses characteristic of sham-treated (control) tubes two months post-surgery. A high-magnification dark-field fluorescent image of the tissue plug protruding into a guidance channel is shown. (**C**) Anatomical responses typical of electrically facilitated guidance channels at two months post-implantation anterograde labeling of spinal axons. Higher magnification image of thin plug of tissue protruding into the channel is shown (compare with Fig. **B**) Note the numerous labeled axons (arrow) traced to project from the mouth of the guidance channel to the end of the scar plug forming tangles of axons at the tip. (*Adapted with permission from Borgens, 1999*)

Effect of electrical stimulation on nerve regeneration

An action potential can be elicited artificially by changing the electrical potential of a nerve cell by inducing an electrical charge to the cells, and the process is termed

electrical stimulation' (Kitchen *et al*, 2002). A variety of cellular responses to electric stimulation of different cell types, including fibroblasts, osteoblasts, myoblasts, chick embryo dorsal root ganglia and neural crest cells, have been reported (Schmidt *et al*., 1997; Kimura *et al*., 1998; Wong *et al*., 1994; Li *et al*., 2006; Bidez *et al*., 2006;Wood *et al*., 2006). Several theories have been suggested to explain the effect of electric stimulation on nerve regeneration. Patel *et al*. (1982) suggested three possible ways by which electrical stimulation could act directly on a neuron, including the redistribution of cytoplasmic materials, the activation of growth-controlling transport processes across the plasma membrane due to change in cell membrane potential, and the electrophoretic accumulation of surface molecules responsible for neurite growth or cell–substratum adhesion. Changes in ionic currents around the growing fibre tips induced by electric fields have been suggested by Freeman *et al*. (1985) as one possible mechanism through which electrical stimulation can affect nerve cells. Sisken *et al*. (1989) suggested that electrical stimulation affects protein synthesis in transected sciatic nerve segments and stimulates neurite outgrowth *in vitro*. Kimura *et al*. (1998) postulated that gene expression for nerve growth factor (NGF) is electrically activated for rat neuronal pheochromocytoma cells (PC12 cells) by alternative potential, while Kotwal *et al*. (2001) showed that fibronectin adsorption increased with immediate electrical stimulation and explained enhanced neurite extension on electrically stimulated PPy films. Initial studies investigating the effect of electrical stimulation on neurons were performed on *Xenopus* neurons after exposing them to a steady direct current field. Extracellular electric fields (0.1–10 V/cm) applied in solution reversibly influenced the direction of neurite growth and increased the neurite initiation and length in *Xenopus* (Li and Hoffman-Kim, 2008). Applied electrical fields have been shown to influence the rate and orientation of neurite outgrowth from cultured neurons *in vitro* (Valentini *et al*., 1992). For example, applied electric fields influenced the extension and direction of neurite outgrowth from neurons cultured *in vitro* and pulsed electromagnetic fields stimulated sciatic nerve regeneration *in vivo* (Wang *et al*., 2004). A separate study demonstrated that 7 days of electric field imposed within a damaged adult guinea-pig spinal cord can both induce the regeneration of axons and guide their growth into the ends of a hollow silicone rubber tube inserted into the dorsal half of the cord (Borgens *et al,*1999) (**Fig 2.6**).

Conductive polymer based scaffolds in neural tissue engineering

The importance of conductive polymeric composites is based on the hypothesis that such composites can be used to host the growth of cells, so that electrical stimulation can be applied directly to the cells through the composite, proved to be beneficial in many regenerative medicine strategies, including neural and cardiac tissue engineering (Bettinger *et al*., 2009). Conductive polymers show great promise in biomedicine and are stimulus-responsive polymers that can be synthesized to form composites that could serve as 'smart' biomaterials (Skotheim and Reynolds, 2007). The biggest limitation of conductive polymers for *in vivo* applications is their inherent inability to degrade, which may induce chronic inflammation and require surgical removal (Huang *et al*., 2007). To address the drawbacks of existing conductive polymers, attempts to blend them with suitable biodegradable polymers have been carried out. Zhang *et al*. (2010) synthesized a novel, electrically conductive and biodegradable polyphosphazene polymer containing aniline pentamer with glycine ethyl ester as side chains and evaluated its biocompatibility using Schwann cells. Their results showed that the polymer exhibited no cytotoxicity, indicating suitability of this polymer as a scaffold material for peripheral nerve regeneration or other biomedical devices that require electro-activity.

Polypyrrole

Polypyrrole (PPy) is a conductive synthetic polymer that has numerous applications in drug delivery and nerve regeneration and it has also been used in biosensors and coatings for neural probes (Sanghvi *et al*., 2005). **Figure 2.7 (i)** shows the chemical structure of PPy before and after doping. The high degree of conjugation in the molecular backbone of PPy makes it very rigid, insoluble and poorly processable. It is therefore very difficult to be used alone as a structural material and must be optimized and transformed into a mechanically manageable and processable form (Shi *et al*., 2004). Wang *et al*. (2004) showed that PPy has good biocompatibility with rat peripheral nerve tissue and showed it to be a suitable substrate for bridging the peripheral nerve gap. They reported that PPy extraction solution showed no evidence of acute and subacute toxicity, pyretogens, haemolysis, allergens and mutagenesis, and the migration of Schwann cells and the neurite extension from dorsal root ganglia on the surface of PPy membrane-coated glass were found to be

better than those on bare glass (Wang *et al*., 2004). George *et al*(2009) also fabricated conductive PPy tubes using the electrodeposition of PPy onto wire templates and subsequent separation from the template after electrochemical reduction. Conduits made of this material did not show any acute or active chronic inflammatory infiltrate or tissue damage in the surrounding tissues, for at least 8 weeks of *in vivo* implantation as sciatic nerve guides.

Polyaniline

Polyaniline (PANI) is the oxidative polymeric product of aniline under acidic conditions and is commonly known as aniline black (Nalwa, 1997). Depending on the oxidation level, PANI can be synthesized in various insulating forms, such as the fully reduced leucoemeraldine base, half-oxidized emeraldine base (PANI-emeraldine base) and the fully oxidized pernigraniline base. PANI emeraldine base is the most stable and widely investigated form of PANI (Le´on,2001). **Fig 2.7 (ii)** shows the reduced, oxidized and half oxidized forms of PANI (MacDiarmid and Epstein, 1994). Wang *et al*. (1999) investigated the *in vivo* tissue response to PANI and found no characteristic features resulting from tissue incompatibility after PANI implantation. In general, no significant inflammation at the implant site and no signs of abnormality of muscle and adipose tissues in the vicinity of the implants were observed (Guimarda *et al*., 2007).

Poly (3,4-ethylenedioxythiophene)

Poly (3,4-ethylenedioxythiophene) (PEDOT) is considered the most successful polythiophene derivative, with interesting properties.Its chemical structure is represented in **Fig 2.7** (**iii**) Luo *et al*. (2008) synthesized PEDOT films and investigated their biocompatibility by seeding NIH3T3 fibroblasts on PEDOT films, and carried out subcutaneous implantation of PEDOT films by *in vivo* study. Their results showed that PEDOT films exhibit very low intrinsic cytotoxicity and that their inflammatory response upon implantation was good, making them ideal for bio-sensing and bioengineering applications. Implantable electrodes can be used for the treatment of different disabilities and neurological disorders and can be used either to electrically elicit neural impulses or to record neuron signalling (Asplund *et al*., 2009). Asplund *et al*. (2009) coated platinum electrodes with PEDOT and investigated the biocompatibility of resultant electrode. Further *in vivo* study using

polymer-coated implants in rodent cortex indicated that platinum electrodes coated with PEDOT were non-cytotoxic and showed no marked differences in immunological response in cortical tissue compared to pure platinum controls. Green *et al*. (2009) used anionically modified laminin peptides, such as DEDEDYFQRYLI and DCDPGYIGSR, to dope PEDOT electrodeposited on platinum

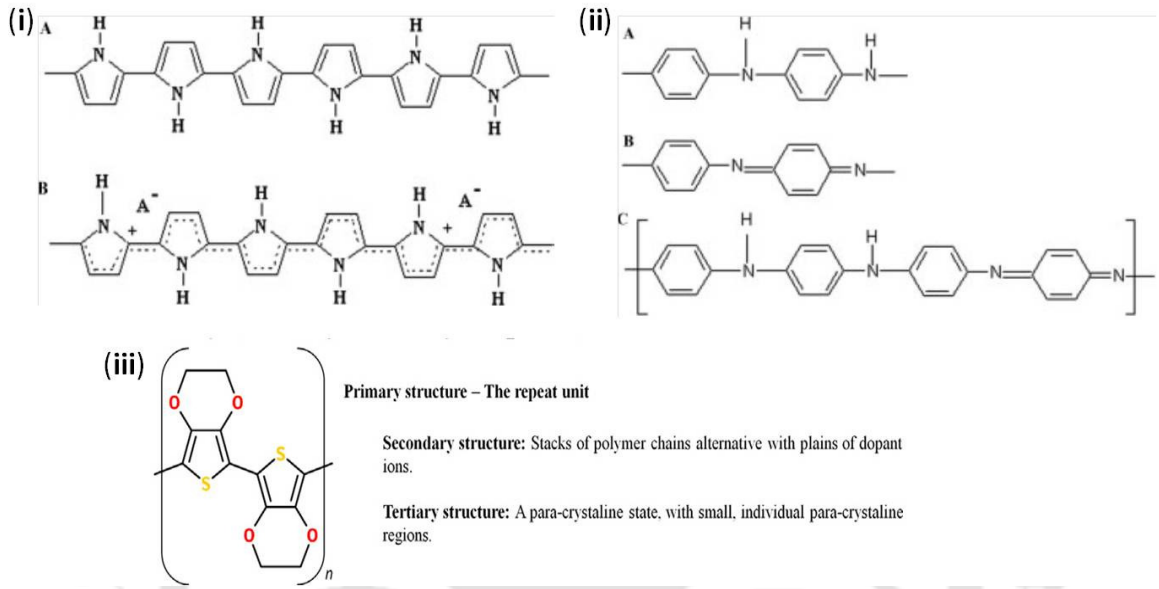

Fig 2.7: **Chemical structure of conducting polymers**. **(i)** Chemical structure of PPy: (A) before doping; (B) after doping, (**ii**) Polyaniline (PANI): (A) reduced; (B) oxidized; and (C) half-oxidized forms, (**iii**) The structure of PEDOT. (i) and (ii) *Adapted with permission from Ghasemi-Mobarakeh et al, 2011*, (iii) *Adapted with permission from Balint et al, 2014*).

electrodes and assessed the bioactivity of incorporated peptides and their effect upon nerve cell growth (PC12 cells). Longer neurite outgrowth was observed on PEDOT films doped with synthetic anionic laminin peptides than that on PEDOT films doped with conventional paratoluene sulphonate dopant. The interactions between neural cells and PEDOT for the development of electrically conductive biomaterials intended for direct and functional contact with electrically active tissues, such as the nervous system, heart and skeletal muscle, was also studied by Richardson-Burns *et al*. (2007).

Carbon nanotubes and Carbon nanofibers

Carbon nanotubes (CNTs) are another group of conducting polymers incorporated into non-conducting polymers to provide structural reinforcement and impart novel

properties, such as electrical conductivity, into the scaffolds and to direct cell growth (Harrison and Anthony,2007). CNTs are shown to be toxic to cells when used as a suspension in cell culture media in any given experiment, while they appear to be non-toxic if immobilized to a matrix or to a culture dish (Hussain *et al*., 2009). Potential cytotoxic effects associated with carbon nanotubes may be mitigated by chemically functionalizing their surfaces (Harrison and Anthony, 2007). Chemically functionalized CNTs have been used successfully as potential devices to improve neural signal transfer while supporting dendrite elongation and cell adhesion. These results strongly suggest that the growth of neuronal circuits on a CNT grid is accompanied by a significant increase in network activity. In a study dissociated embryonic rat hippocampal neurons on a mat of multi-walled CNTs (MWNTs) were deposited onto a polyethyleneimine (PEI) covered glass. In this condition, neurons could grow and elongate their neurites in all directions. In fact, CNTs represent a scaffold composed of small fibres or tubes that have diameters similar to those of neural processes such as dendrites (Lovat *et al*., 2005). Interest in carbon nanofibres has also been growing exponentially due to their unique electrical, mechanical and surface properties. Webster *et al*. (2004) developed a carbon nanofibre-reinforced polycarbonate urethane composite in an attempt to determine the possibility of using carbon nanofibres as either neural or orthopaedic prosthetic devices. Their results showed that this composite supports neural cell function and has the ability to tailor electrical properties for polyurethane composites containing carbon nanofibers. However, there are several limitations to the application of carbon nanotubes being non-degradable (Harrison and Anthony, 2007).

2.3 Support cells in Neural Tissue Engineering

2.3.1 Schwann cells/Glial cells and macrophages

Schwann cells play a critical role in guiding regenerating axons to the distal nerve stump by providing a supportive environment for nerve regeneration and producing ECM, cell adhesion molecules, integrins, neurotrophins and in as well as facilitating synapse formation (Son *et al*, 1996; Thanos *et al*, 1998). Recent studies of Schwann cells in central and peripheral nerve injuries have primarily centered on techniques to deliver these cells to the injury site. Nerve grafts with a monolayer of Schwann cells implanted in a 7 mm gap in rat sciatic nerve increased functional regeneration after 10 weeks (Hadlock *et al*, 2001). In the CNS, the glial cells consist of astroctyes, oligodendrocytes and microglia. Streit *et al* showed grafts of cultured microglial cells promoted neurite extension in rat spinal cord after injury (Rabchevsky *et al*, 1997). Furthermore, in the CNS, glial cells contribute to the formation of scar tissue, which inhibits neuro-regeneration. Therefore, a greater understanding of CNS glia is imperative to develop dependable therapies for spinal cord repair.

Like Schwann cells, macrophages also play a vital role in promoting peripheral nerve repair by clearing myelin debris. Neural transplants along with macrophages used in peripheral nerve injuries resulted in a significant decrease in myelin-associated glycoprotein, as well as increased angiogenesis, Schwann cell infiltration, and axonal regeneration (Franzen *et al*, 1998).

2.3.2 Olfactory Ensheathing Cells (OEC)

Olfactory Ensheathing cellls or OECs are found in the nasal epithelium along the PNS-CNS transition zone from where they aid axon outgrowth through the olfactory bulb to the central nerves in the olfactory glomeruli. OECs support axonal outgrowth and survival by producing neurotrophins and cell adhesion molecules (Lu *et al*, 2002). OECs also share phenotypic similarities to Schwann cells and astrocytes (Bartolomei *et al*, 2000). For all of these reasons, this unique glial cell has been found to benefit regeneration in both the PNS (Verdu *et al*, 1999) and CNS (Ramon-Cueto *et al*, 1998,2000) (**Fig 2.8**)

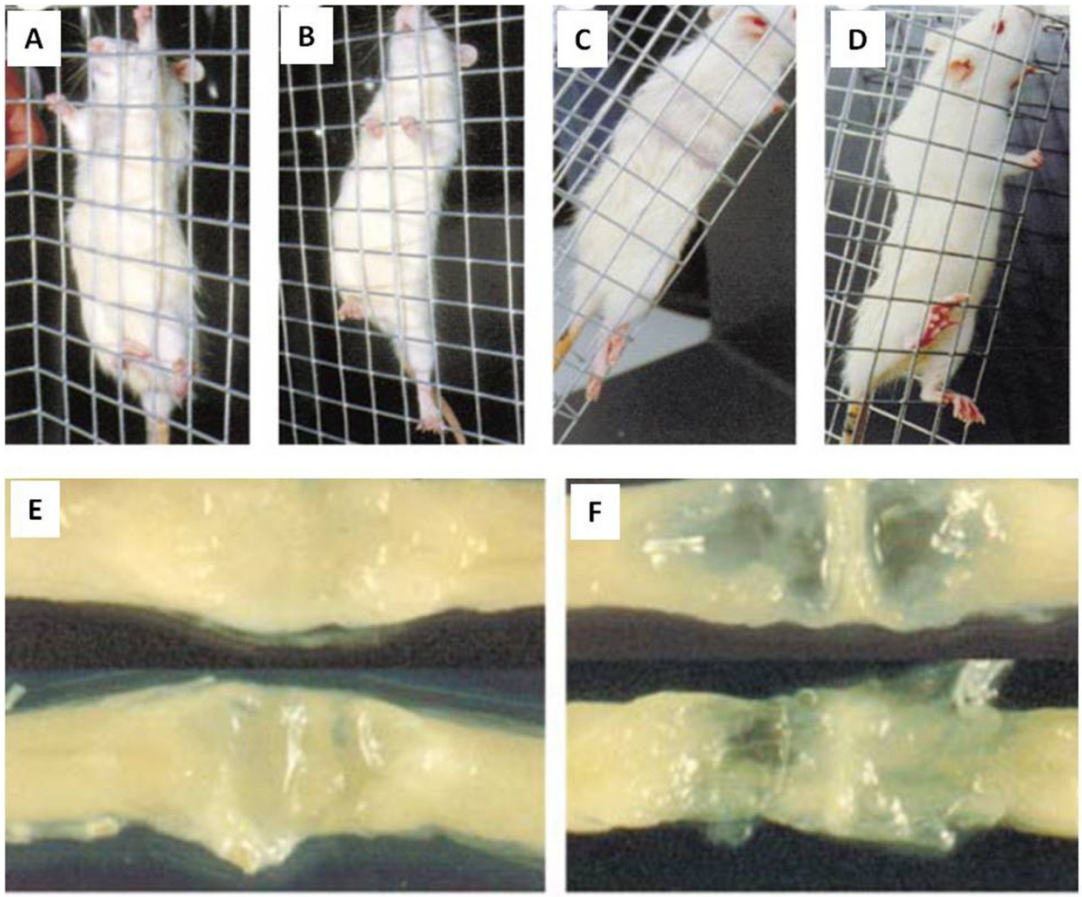

Fig 2.8: Effect of Olfactory Ensheathing Glial (OEG) cells in Functional and morphological regeneration of axons. Functional Recovery of Rats with Completely Transected Spinal Cords after OEG Transplantation Nontransplanted rats (**A and C**) and OEG-transplanted rats (**B and D**) 3 months (**A and B**) and 7 months (**C and D**) post surgery. (**A**) An example of a nontransplanted rat on a vertical grid. The animal hangs with its forelimbs; it does not place the hindlimbs on the rungs and supports its body weight with the forelimbs.(**B**) OEG-transplanted rat 2 (see below) climbing onto a vertical grid (level 4). This animal is pushing with its left hindlimb upward to reach an upper rung with the right one. This animal properly steps and places its hindlimbs on the rungs and is capable of supporting its weight with the hindlimbs. (**C**) An example of a nontransplanted rat climbing and supporting its weight with the forelimbs but not using the hindlimbs.(**D**) OEG-transplanted rat 5 (see below) climbing onto a level 3 grid (75^0). This animal is stepping and placing both hindlimbs on rungs of different heights, supporting its weight with the hindlimbs.
Macroscopic Repair and Motor Axon Regeneration through the Lesioned Region of OEG-Transplanted Spinal Cords, 8 months Post Surgery (**E**) Dorsal aspect of two injured OEG-transplanted spinal cords from the best (top) and the worst (bottom) performing rats in the behavioral tests (rats 1 and 9, respectively). Rostral and caudal stumps are bridged by a white and opaque tissue that covers the black background. (**F**) Dorsal surface of two representative injured spinal cords. Both cord stumps are joined by a translucent membrane, and the black background can be visualized through it. (*Adapted with permission from Ramon-Cueto et al, 2000*)

2.3.3 Stem Cells

The use of stem cells has shown great potential to facilitate nerve regeneration applications (Keirstead, 2001). Neural stem cells have been isolated from rodent brain (Kocsis *et al*, 2002) or spinal cord (Kalyani *et al*, 1998) and have shown promising results when cultured over electrospun scaffolds (Christopherson *et al*, 2009).

Glial progenitor cells isolated from the spinal cord (Horner *et al*, 2000) have been shown to act as a precursor of astrocytes and oligodendrocytes in rat spinal cord following injury.

Mesenchymal stem cells derived from bone marrow samples have been shown to differentiate into neuronal cells under appropriate induction factors. These cells grown over electrospun poly (l-lactic acid)-co-poly-(3-caprolactone)/Collagen (PLCL/Coll) nanofibrous scaffolds showed neuronal morphology, with multipolar elongations and expressed neurofilament and nestin protein (Prabhakaran *et al*, 2009).

Recently adipose tissue derived stem cell were expanded in vitro and later differentiated into neuronal cells using two procedures – chemical induction and culturing them in neurobasal medium (Ahmadi *et al*, 2012).The stem cells were cultured in differentiation medium and were found to express Schwan cell marker protein S100, nerve growth factor receptor etc. The results revealed the therapeutic potential of adipose-derived stem cells in nerve reconstruction (Orbay *et al*, 2011). Further, another study demonstrated the fabrication of a 3D scaffold less neural conduit using adipose tissue derived stem cell and differentiating them into neural lineage (Adams *et al*, 2012).

2.3.4 Genetically Modified Cells

The application of neurotrophins can result in significant increases in nerve regeneration. However, it is difficult to deliver active growth factors controllably over the entire duration of regeneration. Transplanted genetically modified cells, on the other hand, pose advantages as a means to deliver a continual supply of active neurotrophins (Blesch *et al*, 2002). Genetically modified fibroblasts have been a highly studied model for the delivery of neurotrophins. For example, fibroblasts have been engineered to produce NGF, BDNF, bFGF (Nakahara *et al*, 1996) and GDNF (Blesch *et al*, 2001). Implants of transfected fibroblasts have provided information regarding the application of active neurotrophins locally to the nerve injury site.

Schwann cells also have been modified to release BDNF alone (Menei *et al*, 1998) as well as modified to secrete NGF (Tuszynski *et al*, 1998). Researchers have also begun to transfect other cell types like neural stem cells and olfactory ensheathing cells.

2.4 Growth factors in Neural Tissue Engineering

The role of neurotrophic factors in neural regeneration has been the focus of extensive research. The influence of these factors in neural development, survival, outgrowth, and branching has been explored on various levels, from molecular interactions to macroscopic tissue responses. One family of neurotrophic factors, the neurotrophins, has been heavily investigated in nerve regeneration studies. The neurotrophins include nerve growth factor (NGF), brain derived neurotrophic factor (BDNF), neurotrophin-3 (NT-3), and neurotrophin-4/5 (NT-4/5). Outside of the neurotrophin family, other factors of importance are ciliary neurotrophic factor (CNTF), glial cell line-derived growth factor (GDNF), and acidic and basic fibroblast growth factor (aFGF, bFGF).

Nerve growth factor (NGF)

NGF is vital to the development and regeneration of the nervous system; consequently, NGF is the most thoroughly characterized neurotrophic factor (162, Yin *et al*, 1998). NGF is expressed at low levels in healthy peripheral nerve and is upregulated in the distal stump upon injury (Heumann *et al*, 1987). Similarly, following spinal cord transection, NGF accumulates in both the distal and proximal stumps (Murakami *et al*, 2002). On the cellular level, NGF promotes survival, outgrowth, and branching in sensory neurons, but does not aid motor neuron regeneration (Tuszynski *et al*, 1996; Oudega *et al*, 1996;Matheson *et al*, 1997). Nonetheless, much work has focused on delivering NGF to neuronal injuries. Studies using nerve guidance channels filled with NGF solutions have provided conflicting results (Derby *et al*, 1993; Hollowell *et al*, 1990; Rich *et al*, 1989), perhaps due to leakage from the channel or NGF inactivation. Continuous delivery devices (discussed in more detail below) offer a more reliable means of administering NGF, and such work has been associated with increased regeneration in both the PNS (Fine *et al*, 2002) and the spinal cord (Oudega *et al*, 1996, Nakahara *et al*, 1996; Ramer *et al*, 2000). Application of exogenous NGF has also been linked to increased sensory neuron regeneration from the dorsal root ganglia, through the PNS-CNS transition zone, and into the spinal cord (Ramer *et al*, 2000;Romero *et al* ,2001;

Priestley *et al*, 2002). However, the use of NGF is not without disadvantages: the application of exogenous NGF to spinal cord injuries has been associated with significant sprouting of uninjured sensory axons (Romero *et al* ,2001). This sprouting has been linked to serious side effects, including chronic pain (Romero *et al* ,2001; Priestley *et al*, 2002) and inappropriate neuronal reflexes (Romero *et al* ,2001).

Brain derived neurotrophic factor (BDNF)

BDNF supports motor neuron survival (Henderson *et al*, 1993; Yan *et al*, 1992) and promotes the axonal growth of motor (Braun *et al*, 1996) and sensory (Oudega *et al*, 1999) neurons. However, research investigating the effects of BDNF on nerve regeneration has provided inconclusive results in both the PNS (Utley *et al*, 1996) and the spinal cord (Nakahara *et al*, 1996, Oudega *et al*, 1996).

Neurotrophin-3 (NT-3)

NT-3, like BDNF, promotes motor neuron survival (Henderson *et al*, 1993) and outgrowth (Braun *et al*, 1996) as well as sensory axon growth. In vivo, NT-3 plays a vital role in aiding the regeneration of peripheral nerves (Sterne *et al*, 1997) and spinal cord (Oudega *et al*, 1999, Bradbury *et al*, 1999) NT-3 has also been associated with the increased ability of sensory axons to grow from the dorsal root ganglia, across the PNS-CNS transition zone, and into the spinal cord (Ramer *et al*, 2000, Priestley *et al*, 2002; Bradbury *et al*, 1999).

Ciliary neurotrophic factor (CNTF)

CNTF promotes motor neuron survival (Sendtner *et al*,1990; Gravel *et al*, 1997), outgrowth (Oyesiku *et al*,1996), and sprouting (Siegel *et al*, 2000). The application of exogenous CNTF has been associated with increased levels of regeneration following injury in both the spinal cord and peripheral nerve (Newman *et al*, 1996). A drawback, however, is that CNTF has been demonstrated to play a role in glial scarring (Winter *et al*, 1995).

Glial cell line-derived growth factor (GDNF)

GDNF promotes the survival of motor (Henderson *et al*, 1994), sensory (Levison *et al*, 1996), and autonomic (Buj-Bello *et al*,1995) neurons. GDNF also promotes the

growth of motor neurons in the CNS (Blesch *et al*, 2001) and has been correlated with improved peripheral nerve regeneration.

Acidic and basic fibroblast growth factor (aFGF, bFGF)

aFGF and bFGF have been associated with enhanced regeneration following injuries in the peripheral nerve (Cordeiro *et al*, 1989, Danielsen *et al*, 1988) and spinal cord. The fibroblast growth factors are strong promoters of angiogenesis (Friesel *et al*,1995) and could, therefore, directly and indirectly aid in the healing of injured nerves.

Although neurotrophic factors promote regeneration in PNS and CNS the in vivo responses can vary due to the method of delivering the growth factor. Therefore, the continued use and development of highly controllable delivery devices are required for the study of these extremely complex systems.

2.5 Silk based scaffolds in Tissue Engineering

Silk has directly or indirectly influenced the medical field for centuries dating back to the times of Louis Pasteur (who saved the French silk industry from bacterial infection) and Dr. Ishiwata Shigetane; who while studying silkworm diseases first identified the bacterium *Bacillus thuringiensis*. However, the journey of silk as a biomedical material began only in the 19th century when surgeons began using it as a suture material replacing traditional metal wires.

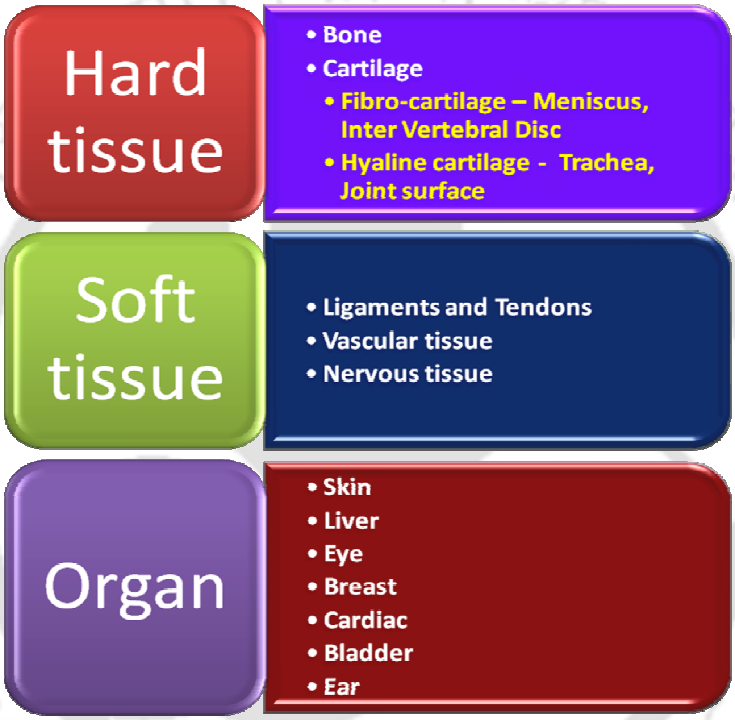

Fig 2.9: Silk in engineering various forms of tissues (Reprinted with permission from *Das et al, Elsevier, 2014*)

Silk proteins (outer glue like sericin and inner core fibroin) are produced by the epithelial cells in specialized glands by most members of the Arachnida class like silkworms, spiders, scorpions, flies etc to provide structural support, protection of eggs or for catching prey. The fibers are characterized by excellent mechanical strength, biocompatibility and controlled degradation *in vivo.* These unique features along with its hydrophobic nature and ease of genetic manipulation have urged researchers to use it as a biomaterial for three decades in engineering various types of tissues and organ (**Fig 2.9**). The sericin protein, earlier reported to trigger

immunological reactions, is also being used recently as a scaffold for controlled release of drugs and a variety of cosmetic products.

Among the natural polymers, silk has now emerged as one of the foremost biomaterial to be used in tissue engineering due to its easy availability, low cost of processing and a long history of use as a suture.

Silk based scaffolds in bone tissue engineering

In developing osteoid composites the initial focus was on fabricating highly porous silk scaffolds which would allow easy transport of fluids and provide higher surface area for cell adhesion and proliferation. Macroporous scaffolds developed from silk using water based and organic solvent (HFIP) based techniques were found to support the growth of human mesenchymal stem cells (hMSCs) invitro. Comparatively higher transcript levels for osteogenic markers like collagen type I (Col I), osteopontin (OP) and alkaline phosphatase (ALP) were observed on the water based scaffolds as compared to the HFIP based ones [Kim *et al*, 2005]. These results encouraged researchers to implant the scaffolds on mouse calvarial bone defect [Meinel *et al*, 2005] (**Fig 2.10**). Engineered bones made of pre-differentiated hMSCs grown over silk scaffolds led to successful in vivo osteogenesis with enhanced expression of a variety of osteogenic marker proteins. But bones of axial skeleton require additional tensile and stress related properties for load bearing. Constructs of pre differentiated hMSCs grown over scaffolds when tested on critical size defects in rat femur were found to have improved bone regeneration along with increased load and torque bearing capacities [Meinel *et al*, 2006 a].

With time, studies exploring ways to improve the simple silk scaffolds were initiated leading to the development of composites. These mainly focused on ways to deliver osteoinductive proteins like bone morphogenetic protein (BMP-2) either by adenovirus mediated transfection of growing mesenchymal stem cells [Meinel *et al*, 2006 b], by fabricating BMP-2 loaded silk scaffolds through electrospinning **[**Li *et al*, 2006] or by simple solvent casting method [Kirker-Head *et al*, 2007]. Cells grown over scaffolds in dynamic conditions have been widely reported to increase density of viable cells spread evenly over the scaffolds, higher calcium deposition and alkaline phosphatase activity in vitro compared to static cultures [Kim *et al*, 2007; Hofmann *et al*, 2007]. Using a rotating bioreactor based dynamic cell culture system

it was possible to develop bone and cartilaginous tissues from the same population of human mesenchymal stem cells (hMSCs) under osteogenic and chondrogenic differentiation media. High deposition of glycosoaminoglycans (GAG) and alkaline phosphatase in the chondrogenic and osteogenic medium respectively were also reported **[**Marolt *et al*, 2006**]**. Although mulberry silk fibroin became a popular material for fabricating scaffolds for load bearing tissues due to its high mechanical strength and tunable compressibility, it inherently lacked moieties necessary for cell adherence. To improve upon this aspect, scientists developed scaffolds blending mulberry silk fibroin with synthetic spidroin protein containing cell recognition RGD moieties [Morgan *et al*, 2008]. Alternatively, non-mulberry varieties of silk believed to have RGD sequences were also explored for use as potential biomaterial. Three dimensional scaffolds were developed from silk protein directly isolated from the silk glands of non-mulberry variety (Tasar - *Antherea myllitta*) of silkworms. The mechanically robust scaffolds were found to support cell adhesion and osteogenic differentiation of hMSCs leading to extensive mineralization and higher alkaline phosphatase activity [Mandal *et al*, 2009].

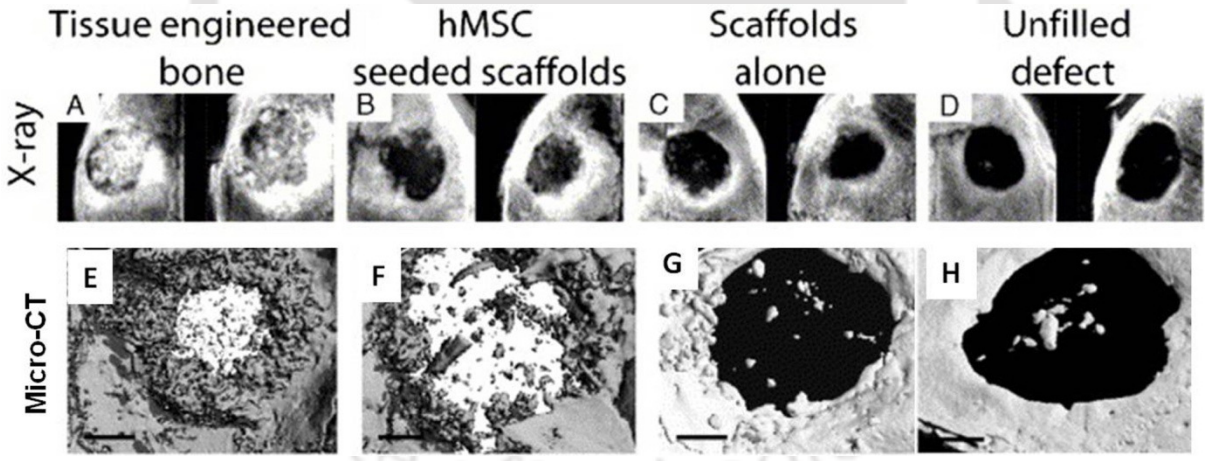

Fig 2.10: Effect of silk implants for the healing of critical size bone defects. X-ray analysis of mouse calvarial bone defects 5 weeks after surgery. Defects were treated with tissue-engineered bone on silk scaffolds (silk-TE bone cultured for 5 weeks; column 1), silk scaffolds seeded with mesenchymal stem cells (silk-MSC; column 2), plain silk (silk; column 3), or left unfilled (empty; column 4). (**A–D**) Two defects per group as seen by X-rays. Microcomputer tomography (μCT) images of cranial defects taken 5 weeks after implantation (**E-H**). (*Adapted with permission from Meinel et al, 2005*).

Further improvements to scaffold architecture were forthcoming towards improved mechanical strength and enhanced bio-mimetic properties. Since tissue is composed

of several types of cells in a specific ratio adhering to the extracellular matrix, it is imperative to grow more than one cell type over a scaffold to improve the functionality of the implant. In an innovative study osteoblasts and osteoclasts were co-cultured in a ratio of 1:100 over silk scaffolds [Jones *et al*, 2008]. The results clearly indicated that methanol stabilized silk scaffolds seeded with both the cell types were superior to synthetic polymers in terms of cell adhesion and faster degradation in vivo. Additionally fabricating pre-mineralized silk scaffolds [Kim e al, 2008; Jiang *et al*, 2009**]** and silk nanofibrous scaffolds [Wei *et al*, 2011] along with prevascularised silk fibroin scaffolds using endothelial cells [Fuchs *et al*, 2009] have shown to have favorable impact on cell adhesion and successful bone regeneration at the site of transplantation. Till date, hMSCs have remained the preferred cells to grow over scaffolds and induce osteogenesis. But attempts are being made to differentiate more easily available human adipose tissue derived stem cells (hASCs) to osteogenic lineage by culturing them over 3D silk fibroin scaffolds **[**Correia *et al*, 2012**]**. Silk fibroin has been found to promote mineralization in presence of calcium or phosphate containing solutions. It was later reported that only the amorphous hydrophilic region of silk protein is responsible for formation of carbonated hydroxyl apatite in presence of stimulated body fluid (SBF) [Marelli *et al*, 2012]. This electronegative amorphous region leads to rapid mineralization within 6 hours and formation of carbonated hydroxyl apatite crystals by a week. In future, such fibroin derived peptides (FDP) may be hybridized with other scaffold materials to enhance the degree of mineralization at the site of transplantation.

Silk based scaffolds in inter-vertebral disc (IVD) tissue engineering

The intervertebral disc (IVD) is composed of fibro-cartilage made up of fibrous connective tissue which has a tough outer layer i.e. annulus fibrosus (AF) and an inner soft but non-compressible nucleus pulposus (NP). The complex architecture of the tissue has captivated the imagination of many tissue engineers and poses a tough challenge for tissue engineers to mimic it in vitro and develop a successful graft. In the beginning attempts were made to develop porous silk scaffolds loaded with AF cells and decorated with cell binding RGD peptides to patch a ruptured annulus and treat inter vertebral disc disorder. The scaffolds were found to enhance collagen type II and aggrecan gene expression in vitro [Chang *et al*, 2007]. Further studies revealed that culturing the cells in a dynamic environment and over scaffolds

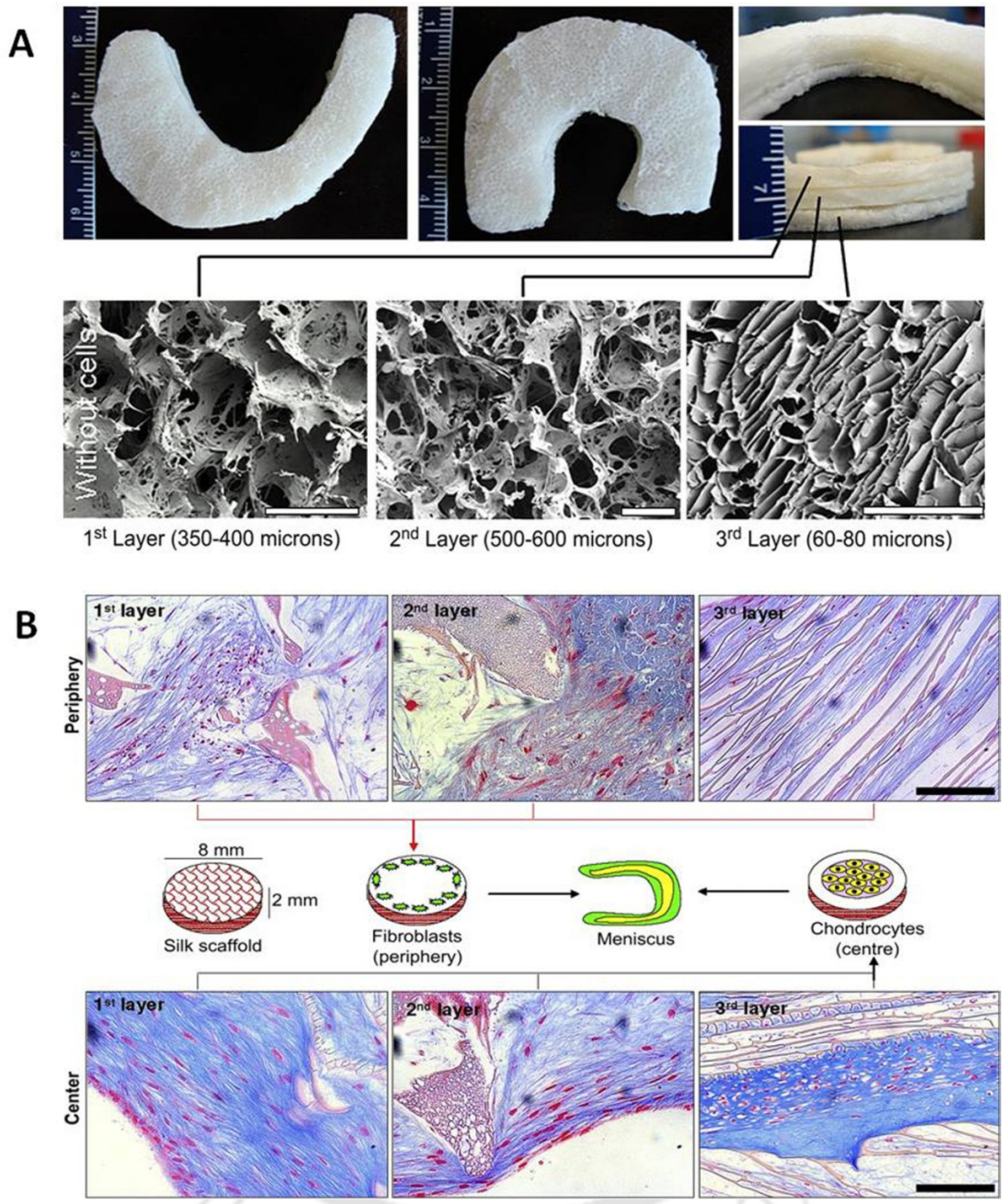

Fig 2.11: **Regenerated silk scaffolds for functional meniscus engineering**.
(**A**) Representative images of fabricated meniscus shaped scaffolds with three stacked layers (Top). SEM images showing porosity and interconnections within pores of individual silk layers without cells (bottom) (**B**) Schematic representation showing central and peripheral cell seeding on silk scaffold layers mimicking native meniscus tissue cell organization along with histology sections showing matured tissue outcomes. (*Adapted with permission from Mandal et al, 2011* b).

having larger pores (200-1000µm) yielded better results in terms of cell growth and matrix deposition [Chang *et al*, 2010]. The main challenge however was to develop a scaffold that would simulate the native intercrossed lamellar architecture of collagen

in the annulus fibrosus. Lamellar scaffolds with toroidal shape were developed from both mulberry and non mulberry (*Antheraea mylitta*) varieties of silk fibroin and were shown to support growth and proliferation of AF cells and chondrocytes leading to the genesis of lamellar shaped neo-tissue [Park *et al*, 2012]. But effective treatment of IVD disorders would require simultaneous regeneration of both the outer AF and inner nucleus pulposus (NP). Soon afterwards, the IVD assembly was simulated by wrapping silk scaffolds around a silicone NP and then culturing bone marrow stem cells on the construct which showed increased collagen II formation and GAG deposition [See *et al*, 2012**]**. Silk fibroin composite hydrogels replacing the NP appeared to perfectly fit the cavity [Hu *et al*, 2012] Very recently; success has been met for the first time in fabricating both the outer and inner parts of IVD i.e. AF and NP simultaneously using silk fibroin based composite scaffolds. AF formed with silk fibroin and NP formed with fibrin-hyaluronic acid hydrogel was seeded with AF cells and chondrocytes respectively. Such biphasic scaffold was found to effectively regenerate an entire IVD in vitro [Park *et al*, 2012].

Another tissue structure that draws considerable attention because of its susceptibility to permanent traumatic damage is the meniscus present in the knee. It is made of fibro-cartilaginous tissue having unique biomechanical and shock absorption properties. Meniscus damage predisposes the patient to osteoarthritis. Originally highly porous silk scaffolds were prepared and evaluated for their efficacy in vitro [Yan *et al*, 2012] followed by culture and differentiation of bone marrow stem cells over such scaffolds [Mandal *et al*, 2011 a]. In a further improvement, a three layered wedge shaped silk scaffold was developed resembling the meniscal tissue. The outer layer was seeded with human fibroblasts while the inner layer had chondrocytes. In presence of chondrogenic medium the cells showed higher levels of sulfated GAG and collagen II formation indicating that the construct could be applied as a potential scaffold in meniscus tissue engineering [Mandal *et al*, 2011 b] (**Fig 2.11**).

Silk based vascular grafts for vascular tissue engineering

Coronary artery bypass grafting (CABG) is the most common type of vascular surgery performed all over the world. Though many synthetic grafts have been introduced into the market for large and medium vessels, their main drawback is

thrombogenicity which renders them ineffective for small diameter (<6mm) blood vessel repair [Stegemann *et al*, 2007] restricting their use in CABG. Tissue engineered small blood vessels can overcome this problem but the complex architecture of the vascular wall and its unique mechanical properties required for perfect dynamics of blood flow remains a major challenge [Nerem *et al*, 2001].

The practice of using silk as scaffold for vascular grafts started on a different note. The unique ability of silk based scaffolds to promote angiogenesis and endothelialization was noticed while experimenting on bone and cartilage tissue engineering,. At the outset, growth of various endothelial cells over silk scaffolds was monitored. Human umbilical vein endothelial cells (HUVEC), dermal microvascular endothelial cells (HDMEC), endothelial cell lines like HPMEC-ST1.6R and ISO-HAS-1 were seeded over silk scaffolds separately. Coating of nets with collagen, gelatin or fibronectin showed favourable effects by promoting cell adhesion, proliferation and neo-vascularisation [Unger *et al*, 2004]. The compatibility of silk fibroin with endothelial cells prompted the development of silk fibroin based prosthetic devices to be used as vascular graft. Enhanced blood compatibility was attained by the sulfonation of the silk scaffolds and inclusion of heparin as an anticoagulant, the detailed gains of which are summarized as below;

(i) Sulfonated silk fibroin-heparin scaffold exhibited excellent biological and mechanical properties required for small caliber grafts [Ma *et al*, 2005]. Recent, investigations on the effect of sulfated silk fibroin scaffolds on hemocompatibility showed growth and expression of markers by endothelial [Liu *et al*, 2011 a**]** and smooth muscle cells cultured on the scaffolds [Liu *et al*, 2011 b].

(ii) The addition of heparin on silk scaffolds increased the expression of elastin – a protein essential to maintain pliability and prevent stenosis [Saitow *et al*, 2011]. Microvascular grafts (1.5mm diameter) prepared with silk fibroin scaffolds having heparin as an additive has a relatively long term patency (1year) [Enomoto *et al*, 2010].

Synthetic grafts for large vessels which are porous and allow tissue in-growth are not desirable as high permeability allow exudation of fluids and serum for a considerable time along the pressure gradient that exists across its walls. In vivo studies in abdominal aorta of dogs employing porous polyester grafts impregnated with silk

fibroin showed the efficacy of fibroin as a sealant, reducing water permeability to > 99% while maintaining high porosity tissue in-growth, enhancing host cell migration and reducing thrombosis [Huang *et al*, 2008].

Tubular scaffolds of silk fibroin ideal for use as vascular grafts and nerve conduits are fabricated by several methods like, molding, dip coating and electrospinning [Lovett *et al*, 2008]. Silk scaffolds of various diameters (1-6mm) were synthesized by dip-coating stainless steel wires of different sizes with 20-30% silk fibroin solution. By controlling the microtube porosity through addition of polyethylene oxide (PEO) [Lovett *et al*, 2007] or poly ethylene glycol diglycidyl ether (PEGDE) [Min *et al*, 2009] both medium and low porosity tubes could be fabricated for use as microvascular grafts. Such tubular scaffolds evaluated in vivo for implantation in the abdominal aorta of rats were found to be non-thrombogeneic and induce growth of endothelial cell lining [Lovett *et al*, 2010]. Tubular scaffolds made by winding braided silk films over a polymer tube of appropriate diameter have also proven to be successful both in vitro and in vivo [Zhao *et al*, 2010; Nakazawa *et al*, 2010]. Electrospun silk fibroin nanofibrous scaffolds provided higher surface area for adhesion and proliferation of human aortic endothelial (HAEC) and human coronary artery smooth muscle cell (HCASMC) [Zhang *et al*, 2008]. These could withstand arterial pressure comparable to native blood vessels (upto 15% elongation and pressures upto 575±17mm Hg) [Soffer *et al*, 2008; Marelli *et al*, 2010].

Scaffolds made from a single polymer do not mimic all attributes of a given tissue; but composites improve both mechanical properties and biodegradability. Electrospun composite scaffolds have been reported with silk fibroin-gelatin **[**Wang *et al*, 2010], silk fibroin-collagen [Zhou *et al*, 2010], silk fibroin-poly (L-lactic acid-co-epsilon-caprolactone (PLLA-CL) [Zhang *et al*, 2010], polydioxanone-polycaprolactone-silk fibroin [McClure *et al*, 2009**]**, polylactide/silk fibroin-gelatin [Wang *et al*, 2009]. Composites fabricated with silk fibroin and collagen by freeze drying enhanced the growth and proliferation of fibroblasts and vascular smooth muscle cells (VSMC) [Lu *et al*, 2009].

Cocultures of human microcapillary endothelial cells (HDMEC) and primary human osteoblast cells (HOS) on 3D silk scaffolds promote angiogenesis through formation of micro-capillary like structures which is essential for incorporation of grafted bone

at the implant site [Unger *et al*, 2010]. This cocultured prevascularised implant enhanced infiltration of host capillaries into the implanted scaffold. A dual loop bioreactor simulating the pulsatile flow of blood was designed to provide a dynamic environment for growing vessels. HAEC and HCASMC when seeded over silk scaffolds and grown in the dual loop reactor indicated increased metabolic activity of cells as seen from transcript and protein level studies **[**Zhang *et al*, 2009**]**.

Silk based scaffolds for skin tissue engineering

Silk has long been used to suture skin wounds. However, the use of silk fibroin as film or patch for wound healing was reported as late as the year 2000. Transparent silk fibroin films applied over full thickness dermatotomies in mice led to rapid and improved wound healing compared to the conventional materials used at that time [Sugihara *et al*, 2000]. The cyto-compatibility of silk based composite scaffolds like silk-alginate [Roh *et al*, 2006], silk-chitin [Yoo *et al*, 2008] silk-chitosan [Altman *et al*, 2009; Luangbudnark *et al*, 2012] and silk-aloevera gel films **[**Inpanya *et al*, 2012] were evaluated by growing dermal fibroblasts, keratinocytes or human adipose derived stem cells. The scaffold architecture was further improved by treating silk fibroin fibers with oxygen plasma to increase its hydrophilicity leading to enhanced adhesion and proliferation of keratinocytes and fibroblasts [Jeong *et al*, 2009]. Formic acid cross-linked 3D silk fibroin scaffolds were also reported to have better biocompatibility in dermal fibroblasts and keratinocytes [Dal Pra *et al*, 2006]. Bioactive scaffolds were formulated by electrospinning silk fibroin along with epidermal growth factor (EGF). The composite scaffold was able to release EGF into the surrounding environment in a time dependant manner. Its effect on wound healing process was studied using an organotypic coculture model for human-skin equivalent developed by deposition of collagen invitro. The biofunctionalised scaffold promoted rapid wound healing by reepithelialization at the wound site [Schneider *et al*, 2009]. Silk fibroin hydrogels functionalized with polarized hydroxyapatite exhibited favourable effect on full thickness wound healing [Okabayashi *et al*, 2009]. Studies with silk fibroin peptides also showed that silk peptides possess antioxidant activity capable of reducing inflammation in mice edema model [Kim *et al*, 2011] and ameliorate atopic dermatitis [**I**kegawa *et al*, 2012].

The silk protein sericin has been largely ignored in biomedical applications due to its unfavourable property of eliciting host immune response, which however remains one of the unresolved queries so far. Sericin possesses an inherent antimicrobial property which could be beneficial for wound healing. Electrospun PCL-sericin 3D scaffolds were found to promote adhesion and proliferation of human primary skin fibroblast cells (FEK4) [Li *et al*, 2011]. Recently, sericin derived from Tasar silk worms *(A.mylitta)* when used to synthesize (a) 2D cross linked sericin membranes and (b) sericin-polyacrylamide gels for dermal reconstruction exhibited excellent water uptake capacity, compressive strength, cell adhesion and proliferation [Nayak *et al*, 2012; Kundu *et al*, 2012].

Silk based scaffolds for cardiac tissue engineering

Atheromatous blocks of coronary arteries cause ischaemic dysfunction of cardiac muscles or frank infarctions for which revascularization surgery with autologous bypass graft is the standard of care. Similarly, damaged heart valves are replaced with prosthetic valves. Engineered tissue for both conditions may provide more efficient and economic alternatives. Current tissue engineering methods have involved growing cardiac cells over collagen scaffolds or over decellularised porcine heart tissue which are expensive and often lead to immune rejection.

Silk fibroin coated over synthetic polymers like poly(3-hydroxybutyrate-co-3-hydroxyhexanoate) (PHBHHx) was found to increase its biocompatibility and enhance growth of human smooth muscle cells[Zhang *et al*, 2007]. Composite scaffolds of silk crosslinked (by genipin) with other polysaccharides like chitosan and hyaluronic acid were recently used to construct hybrid cardiac patches which supported growth and expansion of rat MSCs as well as cardiomyogenic differentiation upon induction with 5-azacitidine [Yang *et al*, 2009]. Extensive molecular analysis indicated that such cardiomyogenic differentiation was influenced by CD 44 surface markers over rat MSCs [Yang *et al*, 2010]. In another study, cardiomyocytes isolated from rats were cultured over *A.mylitta* silk fibroin scaffolds. The presence of RGD sequences on non-mulberry scaffolds lead to enhanced cell adhesion, expansion and activity as compared to those growing over mulberry scaffolds. The cardiomyocytes were also observed to mimic the cardiac syncitium leading to formation of sarcomeres and contract synchronously in culture [Patra *et al*,

2012]. Although these exhibit the potential of silk fibroin in cardiac regenerative therapy more research is required to unravel the hidden potential.

Silk based scaffolds for bladder tissue engineering

The urinary bladder is an elastic musculo-membranous sac which acts as a temporary storage for urine till it can be conveniently voided. It is primarily composed of three layers of tissue –the inner mucosa (composed of transepithelial cells called urothelial cells), the middle submucosal layer and the detrusor muscle which helps to expel urine from the bladder by contraction. Reconstruction of damaged or deficient urinary bladder is done by replacement with an intestinal patch which is frought with early and delayed complications such as infections, improper voiding and malignancy [Atala, 2011]. Tissue engineered scaffolds made of cell-polymer constructs are now being developed to overcome these limitations.

In early 1980s it was first observed that silk sutures used for bladder surgery also promote the growth of urothelial cells on the bladder wall [Shimamura *et al*, 1987]. Later in 2007, the cytocompatibility of silk films to urinary epithelial cells was evaluated and reported to promote tissue regeneration in rabbit urethral defect model [Liu *et al*, 2008; Liu *et al*, 2007]. In a recent study, gel spun silk scaffolds was developed and tested in vivo for bladder regeneration. 70 days post implantation; both urinary epithelial and smooth muscle cells had infiltrated leading to prominent expression of uroplakin and other contractile proteins [Mauney *et al*, 2011] **(Fig 2.12).** The degradation rate of these silk scaffolds could also be regulated by modifying the winding and post-winding fabrication parameters [Gomez *et al*, 2011].

Intractable adult urinary incontinence which is a major problem worldwide is usually managed by implantation of a sling to voluntarily maintain control of the bladder sphincter. Slings made of knitted silk on which human bone marrow derived mesenchymal stem cells were cultured gave encouraging results when tested on rat urethral stress incontinence model [Zou *et al*, 2010].

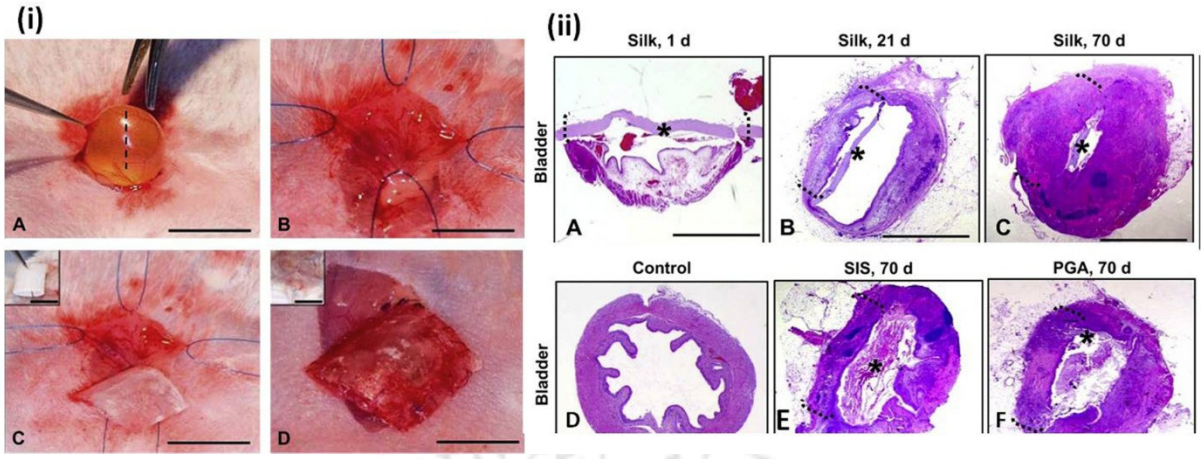

Fig 2.12: **Evaluation of gel spun silk-based biomaterials in a murine model of bladder augmentation** (**i**) Murine bladder augmentation model. Photomicrographs of various surgical stages of gel spun silk matrix implantation. (**A**) Abdominal incision and extrusion of bladder. Hashed line denotes defect site. (**B)** Cystotomy and exposure of the bladder lumen. (**C)** Scaffold tailored to area of the defect site. Inset: Initial tubular configuration of matrix following fabrication. (**D)** Integration of the implant into the bladder wall. Inset: Placement of bladder into the abdominal cavity and surgical closure of the defect site. (**ii**) Hematoxylin and eosin analysis of bladder defect regeneration. Photomicrographs of total (A-F) non surgical controls and bladders augmented with different scaffold groups over the course of the 70 d implantation period. (*) denotes scaffold fragments. Brackets denote area of tissue regeneration. *(Adapted with permission from Mauney et al, 2011*).

Silk based scaffolds for ocular tissue engineering

Human eye is an amazingly complex organ surpassed only by the complexity of the function it serves – vision. It may be divided into three major regions – the cornea, lens, and retina. While artificial intraocular lens are used to replace opacified lenses in cataract to restore vision, no such therapy exists for the damaged cornea or retina. The four regions within the cornea and retina which offer possibilities of tissue engineering are - the corneoscleral limbus, the corneal stroma, the corneal endothelium, and the outer blood retinal barrier also known as Ruysch's complex consisting of retinal pigment epithelium and Bruch's membrane [Harkin *et al*, 2011]. Re-engineering each of the four regions requires is a high order to achieve as their mechanical, optical and biological properties have to be replicated with fidelity.

As in any other branch of tissue engineering, silk was primarily used as a suture during lens fixation in the eye. Silk was well tolerated within the eye over a prolonged time without any leading noticeable inflammation or endopthalmitis [Peyman *et al*, 1979]. However, no attempts to use silk fibroin for tissue regeneration were made for

the next three decades. It was in 2008, when silk fibroin membranes were first evaluated as a substratum for corneal limbus regeneration. Human limbal epithelial cells were cultured over the scaffolds and expanded profusely in vitro in serum-free conditions [Chirila *et al*, 2008]. Soon afterwards, highly patterned and porous (0.5-5µm diameter) 3D silk films mimicking the corneal stroma architecture were fabricated leading to improved growth and proliferation of human and rabbit corneal fibroblast cells [Lawrence *et al*, 2009]. The response of these cells to surface features of the scaffold was studied in detail by culturing stromal fibroblast cells over scaffolds with different groove patterns. The depth and width of the grooves were found to influence cell attachment and proliferation leading to expression of corneal stromal tissue markers like collagen type V and proteoglycans [Gil *et al*, 2010 a]. Such patterned scaffolds further conjugated with cell recognition moieties (RGD), enhanced adhesion and proliferation of human cornea fibroblast with formation of corneal stromal tissue like helicoidal multilamellar structured ECM composed of collagen and proteoglycans [Gil *et al*, 2010 b]. Simultaneous attempts to regenerate corneal epithelial and endothelial layer were also in progress. Primary corneal endothelium cells and B4G12 cell line were grown over collagen coated 5µm thick transparent silk fibroin membranes providing a potential substratum to regenerate corneal endothelium [Madden *et al*, 2011]. Similar porous silk films seeded with rabbit limbal epithelial cells produced stratified ECM in vitro, replicating the structure of corneal epithelium. These cells also expressed cornea specific cytokeratins K3 and K12, corneal epithelial marker pax6 along with collagen type IV and integrin β1 [Higa *et al*, 2010]. Engineered fibroin membranes exhibited similar ability to maintain the morphology of human limbal epithelium (HLE) cells as compared to amniotic membrane (AM), which are used for corneal epithelium replacements. Although, cellular attachment on fibroin was almost 6 times less than on AM, the cells still retained their corneal phenotype by expressing K3 and K12 markers **[**Bray *et al*, 2011]. For a successful reconstruction of the entire corneal limbus both the outer epithelium sheet and underlying stroma must be regenerated. In such an endeavor, a dual layer construct of silk fibroin was engineered with one layer (porous/nonporous membrane) seeded with HLE cells and another layer (fibrous mat of fibroin) with mesenchymal stromal cell population. Both the cells maintained corneal phenotype indicating the possible use of such a scaffold in corneolimbal repair [Bray *et al*, 2012].

The retina is more complex part of the eye bearing photoreceptor epithelial cells. The Bruch's membrane along with the retinal epithelium provides support and controls the movement of biomolecules in and out of retina [Shadforth *et al*, 2012]. Attempts to replicate the complex architecture in vitro using retinal pigment epithelium cell line ARPE-19 cultured over porous silk fibroin membranes resulted in the expression of F-actin and ZO1 markers **[**Shadforth *et al*, 2012]. Although, till date only preliminary studies have been reported, silk shows promise as a potential material for corneal and retinal tissue engineering necessitating advanced fabrication techniques along with extensive in vivo studies.

Silk based scaffolds for neural tissue engineering

The complex physiology of the nervous system combined with the intricate process of nerve regeneration poses a unique challenge to tissue engineers. Nerve damage may result from trauma, aging or other neurological disorders. The process of regeneration also differs greatly between the central nervous system (CNS) and peripheral nervous system (PNS). Peripheral nerves, supported by Schwann cells have a capacity to regenerate on their own and hence end to end anastomosis by surgery can bridge most small gaps. However, in the CNS, a physical gap in the nerve is bridged by a glial scar made of clumps of regenerating glial cells (i.e astrocytes) which blocks infiltration by macrophages preventing removal of myelin debris [Schmidt *et al*, 2003]. Thus, neural tissue engineering till date, have focused primarily on bridging of large gaps in the PNS which can't be treated by surgical intervention alone with the aid of nerve guidance conduits (NGC). An overview about the surgical implantation of these conduits in a rat sciatic nerve defect model is presented in **Figure 2.13**.

A Chinese group first experimented with conduit shaped scaffolds made of silk fibroin in facial nerve regeneration [Lu *et al*, 2006] publishing in a national journal, which had little visibility. However, during the same time, another group reported biocompatibility of silk fibroin against peripheral nerve tissues and cells in vitro in an internationally renowned journal which received attention. [Yang *et al*, 2007]. Silk fibroin scaffolds fabricated into nerve guidance conduits by casting on stainless steel tubes were eventually evaluated for in vivo biocompatibility [Chen *et al*, 2007] followed by implantation on a 10mm sciatic nerve gap in rats [Yang *et al*, 2007].

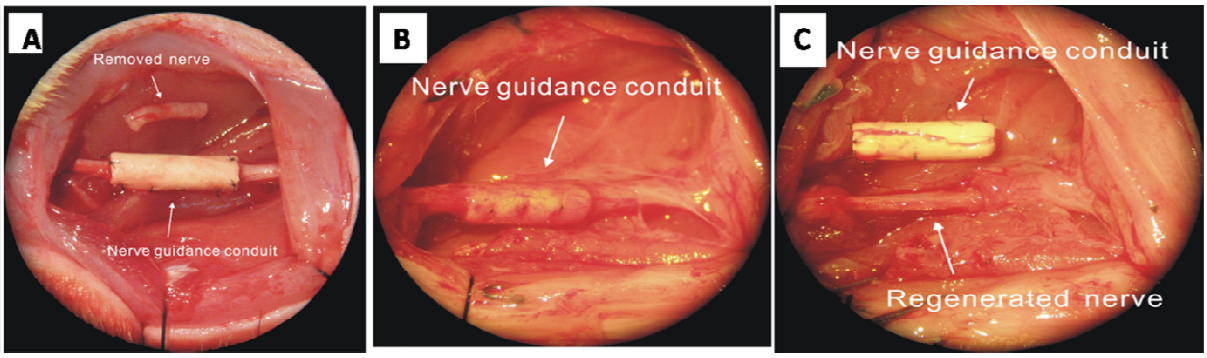

Fig 2.13: **Silk fibroin based composite scaffold in neural tissue engineering. A**) Surgically implanted aligned NGC to bridge a 10mm rat sciatic nerve defect (10x magnification), (**B, C**) Contour of the NGC 8 weeks after implantation. *(Adapted with permission from Wang et al, 2011).*

An ideal nerve conduit should degrade in vivo by the time regeneration is complete. The degradation rate of SF-NGCs both in vitro (in protease XIV solution) and in vivo was investigated by subcutaneous implantation of graft in rabbits. The time dependant changes in the expression of lysozyme related genes (Hip1R, cathepsin D, and tPA) further helped in understanding the mechanism of degradation and absorption of SF-NGC in vivo [Yang *et al*, 2009]. Several modifications were introduced to improve upon the functionality of the existing scaffolds. As nerve regeneration occurs unidirectionally from the proximal end to the distal end, aligned fibers are necessary to provide direction to the regenerating axons. One of the simplest methods to obtain aligned nanofibers is by electrospinning. Nanofibers have been shown to promote outgrowth and formation of complex interconnections by Schwann cells [Hu *et al*, 2012] while aligned fibroin nanofibers functionalized with nerve growth factors led to unidirectional outgrowth of axo-glial cells from the conduit [Madduri *et al*, 2010].

Generally, Schwann cells and dorsal root ganglion (DRG) cells are the preferred cells to culture over nerve conduits. However, other support cells, especially stem cells like adipose-derived stem cells [Wei *et al*, 2011], bMSCs [Yang *et al*, 2011], human embryonic stem cells [Wang *et al*, 2012] and rat pheochromocytoma cell line PC12 [Rao *et al*, 2011], have also been used. Moreover, olfactory ensheathing cells grown over silk fibroin nanofibers were also found to secrete neurotrophic factors emerging as a potential construct for treatment of spinal cord injury [Qian *et al*, 2009; Shen *et al*, 2010].

Silk based composites have also been used in neural tissue engineering. Silk fibroin-poly (L-lactide-coglycolide (PLGA) films were first shown to promote adhesion and proliferation of schwann cells in vitro [Kim *et al*, 2011]. Electrospun nanofibers of the same formulation were reported to promote peripheral nerve regeneration in 10mm sciatic nerve defects of rats [Li *et al*, 2012]. Similarly, chitosan-silk fibroin [Wei *et al*, 2011], poly (L-lactic acid-co-e-caprolactone) (P(LLA-CL)) – silk fibroin [Wang CY *et al*, 2011] and PLGA-silk fibroin-collagen composite scaffolds [Wang G *et al*, 2011] were fabricated by solvent evaporation and electrospinning methods and were found to promote cell growth in vitro [Wang G *et al*, 2011] and nerve regeneration in vivo [Yang *et al*, 2011, Wang CY *et al*, 2011].

In an attempt to precisely mimic the fascicular organization of nerve several structural modifications like introduction of multiple channels or luminal fillers within the conduit were implemented to provide multiple stimuli through a single therapy [Schmidt *et al*, 2003]. Recently silk fibroin conduits having linearly oriented multiple channel structure were fabricated by vertical sequential cooling-thermal induced phase separation (TIPS) processing technique mimicking the nerve fascicular structure thereby promoting cellular adhesion and secretion of nerve growth factors [Rao *et al*, 2011]. Another group developed silk conduits having silk fibers as intraluminal filler material. The conduit seeded with bone marrow mesenchymal stem cells resulted in excellent nerve regeneration and functional recovery in a 10mm rat sciatic nerve defect model [Yang *et al*, 2011]. Further, uniaxial multichannel conduits were fabricated by a directional freezing technique. Concentrated silk solutions were poured into silicon tubes (3mm diameter) fixed to the bottom of a metal box immersed in liquid nitrogen. The tube was surrounded by adiabatic materials to ensure a directional temperature gradient. The resulting multichanneled conduit with channels of 120µm diameter was found to promote the growth of primary hippocampal neurons along with enhanced expression of βIII-tubulin and microtubule associated protein **[**Zhang *et al*, 2012**].** Similarly, luminal fillers made of Spidrex® (a silk-based biomaterial with properties similar to those of spider silk.) were used to fabricate multichannel conduits which promoted axonal regeneration and functional recovery in vivo [Huang *et al*, 2012].

Functional silk fibroin scaffolds for spatially controlled delivery of neurotrophic factors like glial derived neurotrophic factor (GDNF) and brain derived neurotrophic factor

(BDNF) were found to promote regeneration in the PNS as well as in CNS [Lin *et al*, 2011; Wittmer *et al*, 2011]. Attempts to culture more than one type of cells over the scaffold are also being made currently. Silk based tissue-engineered nerve graft (TENG) using coculture of dorsal root ganglion cells and Schwann cells were reported to cause improved functional as well as structural recovery from nerve damage [Tang *et al*, 2012]. Indigenous Tassar silk fibroin (nonmulberry wild variety) was also recently used by another group for production of electrospun nanofibrous scaffolds. Such scaffolds were also found to promote neuronal differentiation of hESCs [Wang *et al*, 2012].

The unique property of nervous tissue is its ability to transmit electrical signals. Thus it is imperative to incorporate electrical conductive properties in fabricating nerve conduits for proper functioning of the regenerated nerve. As silk fibers and fabric are well known insulators; blending conductive polymers for conductivity is essential. Silk based composites fabricated with conductive polymers like polypyrrole, polyaniline and poly3,4-ethylene-dioxythiophene (PEDOT) were [Xia *et al*, 2008] reported to be cytocompatible to mesenchymal stem cells and human fibroblast cells [Aznar-Cervantes *et al*, 2012]. Recently silk-carbon nanotube (a highly conductive synthetic material) composite scaffold was also found to promote neuronal differentiation of hESCs in vitro [Chen *et al*, 2012]. Stimulating nerve cells from the outside through conductive scaffolds may also help in enhancing cell proliferation and neurite outgrowth [Ghasemi-Mobarakeh *et al*, 2009]. Such modifications including advanced fabrication techniques and multiple functionalities aimed to accurately mimic the native architecture of nerve tissue are required to develop an ideal nerve guidance conduit.

A detailed timeline describing the development of silk based scaffolds is presented in **Figure 2.14**. At first, simple knitted or braided forms of silk were used to develop scaffolds catering to the needs of patients with bone, cartilage or ligament defect. The promising results encouraged fabrication of silk scaffolds for more complex tissues like vascular and nervous tissue. Its excellent biomechanical properties combined with its ability to form a versatile range of products have urged many to develop innovative fabrication methods with the help of modern state-of-the-art technology which can be used to develop silk based scaffolds for engineering more complex tissues at the organ level.

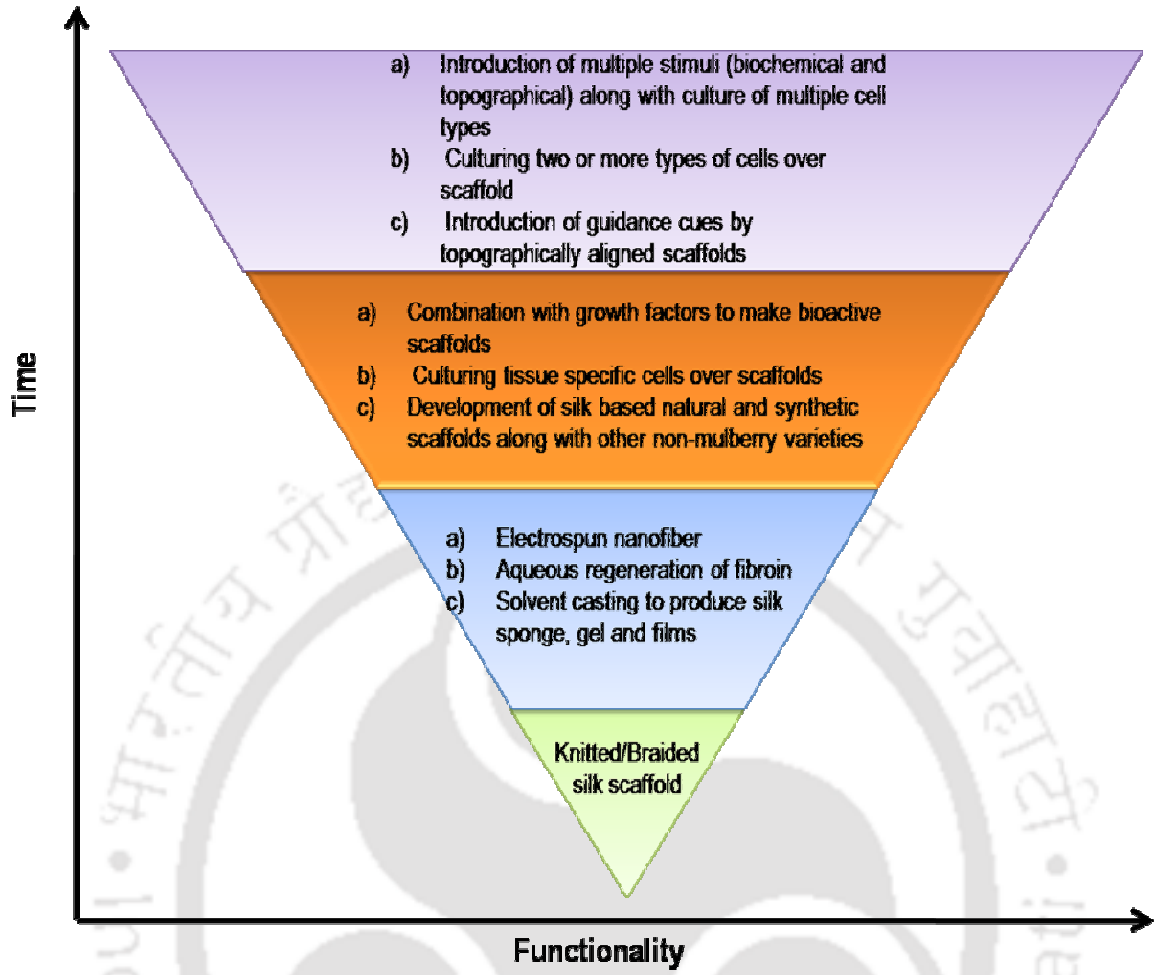

Fig 2.14: Schematic description of the evolution of silk based scaffolds. (Reprinted with permission from Das *et al*, Elsevier, 2014)

2.6 Application of Nanotechnology in Neuroscience

2.6.1 Evolution of nano-scale materials and concept of nanotechnology

Richard Feynman's epic lecture in 1965 on "There is plenty of room at the bottom" at Caltech urged scientists to look beyond the micro- dimension and explore material properties in the atomic scale. The plethora of research activity that followed over the years lead to the coining of the term "nanotechnology" by Professor Norio Taniguchi, development of scanning tunnelling microscope, discovery of fullerenes, synthesising colloidal semiconducting nanocrystals like quantum dots and developing the atomic force microscope. Such has been the impact of this technology that within a span of three decades around 6 Noble prizes has been conferred upon scientists working with nanotechnology. Although it appears to be a very new and advanced technology belonging to the modern era when compared to neurology, nanotechnology also has been around for thousands of years. Nanoparticle loaded drug delivery dates back to the Charak Samhita (100 BC) that describes unique metallic-mineral formulations called "*Bhasmas*" which have now been reported to be biologically prepared nanoparticles. One of the best examples of carbon nanotubes, Damascus steel was made by Indian craftsmen from Wootz steel more than 2000 years ago. The swords made from this steel had cementite nanowires encapsulated by carbon nanotubes which lead to its exquisite sharpness and ultralight weight.

Nanomaterials can be conceived as structures having at least one dimension in the nano-meter scale. Materials engineered to such a small scale exhibit high surface-to-volume ratio along with unique optical, magnetic, and electrical properties. The difference in the physiochemical characteristics of nanomaterials in contrast to macromolecules can be attributed to their high surface-to-volume ratio. Further to fine tune different physico-chemical and biological properties of the nanomaterials, several routes of synthesis have evolved employing physical as well as biological means.

Nanotechnology is being extensively employed in various disciplines of science ranging from computer and electronics to chemistry and biomedical applications. The section, is focused on the impact nanotechnology on the progress of neurological sciences through its role in neuro-imaging techniques, drug delivery platforms and providing topographical guidance in the nano scale to regenerating nerve tissues. Simultaneously we also attempt to elucidate how the barriers posed by the complex physiology of the nervous system has been overcome by the advancement of nanotechnology through development of bio-inspired nanomaterials which are biomimetic and biocompatible.

2.6.2 Nanotools for Neuro-imaging

Visualizing the mind at work and acquiring knowledge about its functioning has always been the ultimate aim of neurologists. However, the anatomical and physiological barriers always remained a major challenge. Nanotechnology has had a profound impact on improving the diagnosis of neurological disorders by enhancing the specificity and clarity of neuro-imaging techniques.

2.6.2.1 Magnetic nanoparticles in Neuro-imaging

Liposomes and iron-oxide nanoparticles are the most used nanomaterials in MRI because of their ability to cross the BBB and tunable magnetic properties respectively. Like most other biomedical innovations, the use of super-paramagnetic nanoparticles as contrast agents for neuro-MRI was also inspired from natural physiology itself. It was back in the late 80s and early 90s that the role of iron imbalance in neurodegenerative diseases was observed. In the body, iron remains in nano-form as ferritin comprising of a 1nm thick protein coating called apoferritin and a 25nm iron oxide core (Theil *et al*, 1987). A separate investigation revealed that Parkinson's patients exhibited an increased ferritin level corresponding to enhanced MR signal in the substantia nigra region (Gorell *et al*, 1995). Although ultra small iron oxide particles (USPIO) were already used in MR studies of liver, kidney and respiratory diseases, the correlation of ferritin levels with Parkinson's lead to exponential increase in research activity involving application of USPIO in neuro-MRI. These USPIOs possessed long circulating life and were found to accumulate at the margins of brain tumor leading to improved delineation of tumors in MR images (Enochs *et al*, 1999). However, their limited ability to cross the BBB as well as

toxicity concerns was a major impediment towards the use of USPIOs in therapeutic applications and intracellular imaging in the brain. Once again, the solution lay with nature herself. Taking cue from viruses like HIV which can easily cross the BBB, a Harvard group conjugated USPIOs with HIV derived Tat peptide (responsible for cellular uptake of HIV). They further coated the nanoparticles with dextran thereby making them more biocompatible (Josephson *et al*, 1999). The high degree of cellular uptake by lymphocytes encouraged them to develop USPIO based multifunctional systems. They further conjugated the dextran coated USPIO-Tat complex with near-infrared fluorescent probes (NIRF) like Cy5.5 rendering a multimodal aspect to the system. Such a system could be used in preoperative MRI to delineate tumor margins as well as in intra-operative imaging of brain tumors (Kircher *et al*, 2003). The enhanced cellular uptake of surface functionalized iron-oxide nanoparticles encouraged studies using USPIOs as vehicles for drug delivery to brain tumors (Chertok *et al*, 2008). Further, glioma specific USPIOs were also designed by conjugation with Chlorotoxin, a peptide having high affinity and specificity for matrix-metalloproteinase (MMP-2) expressing tumors of neuro-ectodermal origin (Sun *et al*, 2008). Conjugating such target specific iron-oxide nanoparticles with NIRF probe Cy5.5 enabled MRI as well as intra-operative pathology detection at cellular level (Veiseh *et al*, 2005). A Chinese team designed and reported similar glioma specific super-paramagnetic iron oxide nanoparticles (SPIONs) by conjugating with Transferrin which can bind with the Transferrin receptors over-expressed in glioma cells. MR imaging even 2 days post administration of SPIONs revealed significant contrast enhancement on T2-weighed images of glioma as well as Prussian blue staining of tumor indicated enhanced retention of nanoparticles inside the tumor cell cytoplasm (Jiang *et al*, 2012). Enhanced permeability and retention (EPR) of such magnetic nanoparticles were obtained by temporary disruption of BBB by focused ultrasound prior to injecting the nanoparticles. The technique was found to be useful in delivering macromolecular chemotherapeutic agents inside the CNS (Liu *et al*, 2010). The advent of several commercial varieties of SPIOs like Feridex (Ferimoxides by AMAG Pharma), Resovist (Ferucarbotran by Bayer Healthcare), Combidex (Ferumoxtran-10 by AMAG Pharma) and Clariscan (PEGylated SPIO suspended in glucose) led to their comparison with conventional gadolinium based MRI contrast enhancers. Gadolinium based agents suffer low circulation time and fast diffusion from cells with

low target tissue specificity and certain side effects (Jiang *et al*, 2012). Studies comparing commercial SPION - based contrast enhancers and gadolinium reported identical efficiency of both as MRI contrast enhancers. Notably, the SPIONs were found to accumulate along the periphery of tumor and hence were primarily effective in determining the tumor margins (Varallyay *et al*, 2002; Manninger *et al*, 2005). A separate study by the same group with Ferumoxtran-10 (Combidex), a dextran coated SPION, showed TI and T2 MR signals even in very low magnetic field of up to 0.15 Tesla, which did not enhance with gadolinium. Further, Ferumoxtran derived T1 signal enhancement was persistent for longer duration (2-5 days) which could be advantageous for postoperative imaging (Neuwelt *et al*, 2004). Although many SPION based commercial contrast enhancers were approved in the past, most were banned or got discontinued at a later stage. Hence, presently, gadolinium chelate based complexes remain the preferred MRI contrast enhancers. Recent reports of application of SPIOs in monitoring cerebral blood volume (CBV) have been encouraging. Due to their long half-life and enhanced sensitivity, USPIO nanoparticles can play an important role in estimating CBV through CBV weighted functional MRI (fMRI). The CBV being a critical indicator of tissue viability and vascular activity, fMRI involving USPIOs have been reported to provide enhanced spatial specificity and better monitoring of neurological changes induced upon functional activity and pharmacological interventions (Kim *et al*, 2013).

2.6.2.2 Liposomes in Neuro-imaging

Liposomes are microscopic artificial phospholipids which have been recognized as promising vehicles for delivery of therapeutic and diagnostic agents to various tissues in the body. Moreover, the ability of such colloidal particles to cross the BBB and accumulate in the CNS along with their easily tunable surface properties makes liposomes an attractive vehicle for neuro-diagnostic applications. It was back in the early 1990s, that a group of radiologists from Connecticut Health Centre, USA experimented with lipid coated microbubbles (air filled bubbles which were efficient reflectors of sound) as contrast agents for neurosonography. They observed that the lipid coated microbubbles were stable for over 6 months in vitro with an in vivo half-life of 20 hours (Simon *et al*, 1990). Upon direct injection of these microbubbles as contrast agents into brain parenchyma it was possible to detect growing lesions in

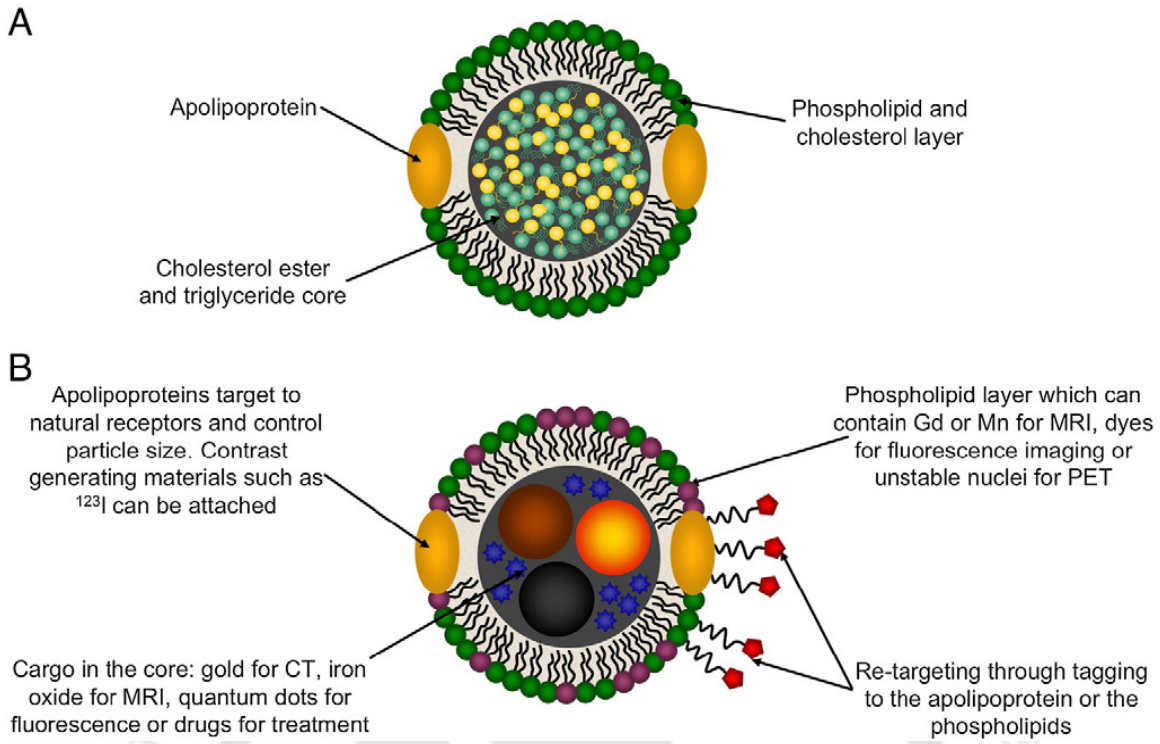

Fig 2.15: Lipoproteins as contrast agents. **A**) Schematic depiction of lipoprotein structure. **B**) The ways in which lipoproteins may be modified to act as contrast agents. *(Adapted with permission from Cormode et al, 2010*).

40% less time as without the micro bubbles (D'Arrigo *et al*, 1991). Further, using these lipid coated micobubbles, they were also to directly correlate signal intensity from the accumulated microbubbles in the glioma with the rate of tumor enhancement thereby providing a quantitative assessment of tumor progression (Simon *et al*, 1992). The unique ability of liposomes to trap any drug or contrast agent within its aqueous core or within its membranes has drawn special attention of radiologists. Although these artificial phospholipids have been widely useful in imaging various vital organs across different imaging modalities (Rozenberg *et al*, 1985; Passaridlo *et al*, 1990; Kabalka *et al*, 1991; Schwendener *et al*, 1994), there use in CNS imaging till the late 1980s were comparatively limited (Turski *et al*, 1988). The application of liposomes as contrast agents in gamma and magnetic resonance imaging till early 1990s as well as the various methods available to design target specific liposomes by surface modifications were reviewed in detail by another radiologist and biochemist from Harvard Medical School (Torchilin VP, 1996; Torchilin VP, 1997). Delivery of therapeutic or diagnostic agents in the CNS especially in brain tumors is largely limited by poor diffusion of molecules through tumor and brain interstitium. Although smaller molecules like nanoparticles have

higher diffusivity, their therapeutic efficacy is largely diminished due to loss via capillaries. In order to overcome this challenge, a team of neurosurgeons from NIH came up with the concept of using fluid convection or bulk flow to deliver molecules in the brain instead of diffusion. They were able to enhance the distribution of large and small molecules by maintaining pressure gradient during infusion through brain interstitium (Bobo *et al*, 1994). This technique of convection-enhanced delivery (CED) of molecules into the brain was later used to target chemotherapeutic agents like Taxol into brain tumor and its response monitored by diffusion weighted MRI (Mardor *et al*, 2001). Liposomes were also eventually administered into rodent brains and brain tumor models using convection enhanced delivery. In comparison to direct injection method, CED was able to achieve extensive distribution of liposomes loaded with gadodiamide and fluorochromes or gold nanoparticles in brain tissue as monitored by MRI and fluorescence microscopy respectively (Mamot *et al*, 2004; Saito *et al*, 2004). Similar results were obtained in primate (monkey) models by real time monitoring of liposomal distribution by MRI (Saito *et al*, 2005). Extensive in vivo studies in rodent and non-human primate models subsequently led to the clinical application of CED based administration of liposomes. At present, convection based delivery of liposomes loaded with chemotherapeutic drug Irinotecan and its monitoring by MRI in recurrent high grade glioma is under Phase 1 clinical trials (ClinicalTrials.gov Identifier: NCT02022644).

2.6.2.3 Quamtum dots in Neuro-imaging

Real time imaging of brain tumor under intra-operative conditions is a much needed utility in a neuro-surgeon's arsenal. Although intraoperative MRI and ultrasound using USPIO nanoparticles have been reported in some cases, their clinical relevance is largely limited by huge costs and difficult data interpretation techniques. Thus optical microscopy based imaging provides a cheaper and simpler alternative. However, tagging nanoparticles with fluorescent dyes does not appear to be particularly helpful under the highly lit conditions of operating room which results in rapid photobleaching of fluorophores. Seminconductor nanocrystals like Quantum dots (QDs) have been proved to have excellent fluorescence quantum yield, higher brightness and are resistant to photobleaching as compared to fluorophores. Quantum dots administered in sufficient doses in rat glioma model were found to be sequestered by macrophages and microglia which infiltrated the tumor tissue. The

deep red fluorescence of QDs could be easily detected thereby optically outlining the brain tumor and augmenting surgical resection and biopsy of the tumor (Jackson *et al*, 2007). These findings were extensively analysed along with the QDs toxicity concerns and methods to improve its biocompatibility in order to accurately assess their potential as in vivo optical imaging agents for management of brain tumors (Popescu *et al*, 2006). QDs engineered to emit fluorescence in the NIR region (750nm) were able to achieve higher tissue penetration of upto 5mm from the skull corresponding to the hypothalamic region of mouse brain. The fluorescence signal peaked within 3 hours of QD administration and gradually decreased over 3 days (Youn *et al*, 2008). Further, to increase their stability and BBB permeability, QDs were incorporated within the core of PEG-polylactic acid (PLA) nanoparticles conjugated with Lectin protein. These nanoprobes were reported to be stable, hydrophilic and could efficiently deliver higher amount of payload specifically into the brain (Gao *et al*, 2008). Novel surface modification strategies for increasing the biocompatibility and bio-inertness of QDs have resulted in its successful application for in vitro and in vivo tumor imaging. The biofunctionalization of CdSe/CdS/ZnS quantum dots and iron oxide nanocrystals enabled MRI imaging of tumors. Surface coating of the nanoprobes with PEG-polyisoprene complex was reported to enhance its stability, bio-inertness and tumor specificity (Pöselt *et al*, 2012). Although not applied till date in neurological cases, such platforms can enable quantum dot based MRI imaging of brain tumors. Conventional imaging techniques like X-ray, ultrasound, MRI, CT and PET were all developed for imaging the tissues and organs. The advent of nanomaterials like QDs have strengthened the field of fluorescence based in vivo optical imaging which can now detect tumor progression at the cellular level. In vitro studies with human glioblastoma cells (U87) proved that QDs can indeed be used to specifically label cancer cells by conjugating it with transferrin (Tf). As tumor cells highly over expressed Tf receptor, the QD-Tf complex could selectively bind to malignant cells with very high efficiency and prolonged red fluorescence signal for two days (Yukawa *et al*, 2013). Similar studies have also been reported to use QDs for tracking single particle like neurotransmitters in astrocyte augmenting a better understanding of neuron-astrocyte communication (Arizono *et al*, 2014).

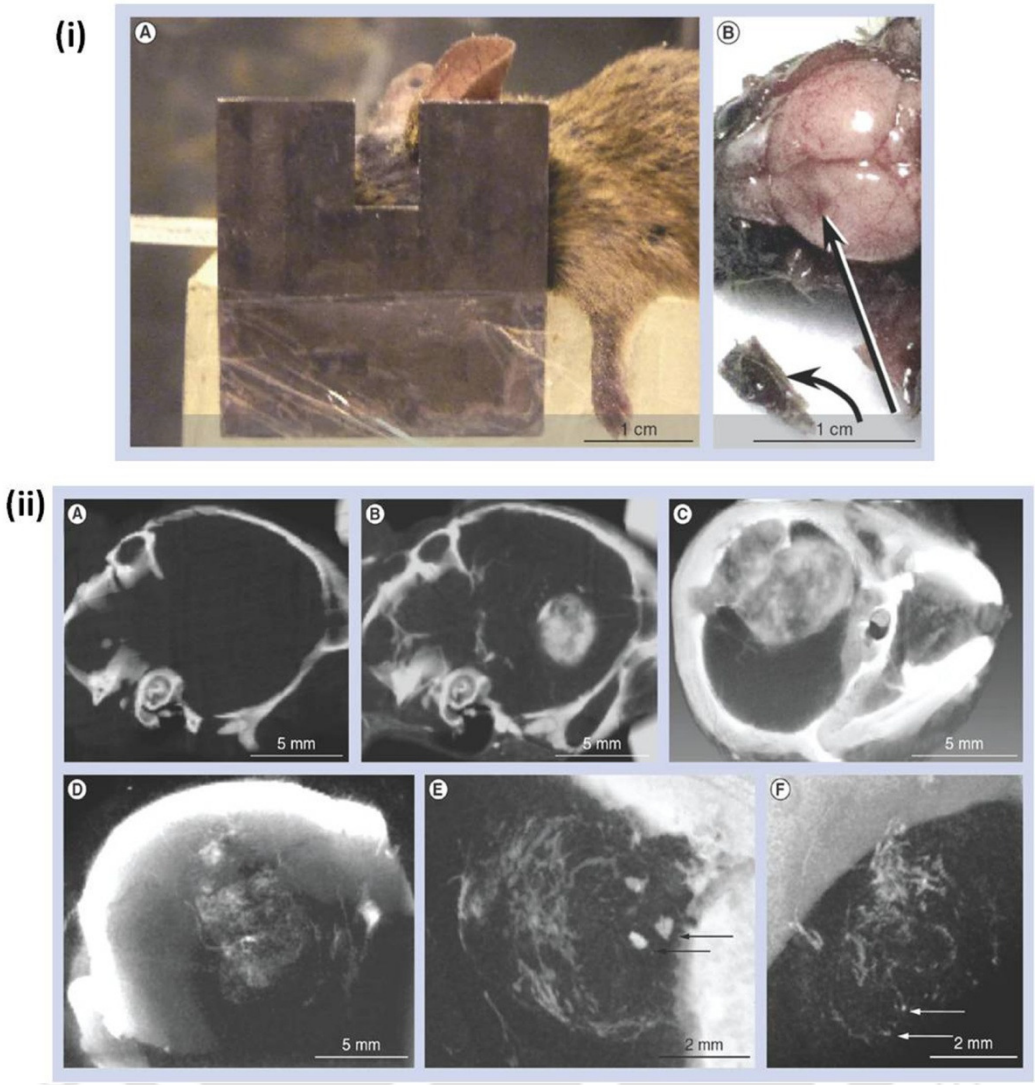

Fig 2.16: **Gold nanoparticle imaging and radiotherapy of brain tumors in mice** (**i**) Irradiation and tumor dissection **(A)** Irradiation setup showing mouse with a lead collimator. **(B)** Mouse brain and glioma at necropsy 10 days after tumor initiation and 4 h after gold nanoparticle intravenous injection (4 g Au/kg). The tumor (curved arrow) was removed (place of removal: straight arrow). The removed tumor was black compared with normal brain tissue due to gold nanoparticle uptake.
(**ii**) Microcomputed tomography imaging of brain tumors after intravenous gold nanoparticle injection **(A–C)** Live mouse microcomputed tomography images of brain tumors 9 days postimplantation and 15 h after intravenous (iv.) gold nanoparticle (AuNP) injection. **(A & B)** Same mouse **(A)** before and **(B)** 15 h after iv. injection (4 g Au/kg). **(C)** Larger tumor imaged after iv. injection of 1.7 g Au/kg. **(D–F)** Live mouse microcomputed tomography images of a typical brain tumor 9 days postimplantation and 1 h after iv. AuNP injection (1.7 g Au/kg). **(D)** Individual blood vessels in the tumor could be discerned. **(E)** Focal spots of gold were also observed (arrows). **(F)** AuNP leakage was very irregular in some vessels (arrows). *(Adapted with permission from Hainfield et al, 2013*)

2.6.2.4 Gold nanoparticles in Neuro-imaging

Elements with high atomic number (Z) like Iodine have been used for long as radiosensitizing agents in X-ray based radiotherapy and imaging due to their ability to locally absorb X-ray. Progress in nanotechnology, has led to the use of metallic nanoparticles like gold nanoparticles (GNP) as X-ray contrast agents exhibiting better contrast as well as higher tumor localisation than Iodine based agents. Although several groups have contributed in the progress of GNP in X-ray based therapy and imaging, the work done by Nanoprobes Inc for over a decade stands out. The research and innovation driven company formed by scientists of renowned US laboratories, first reported the use of GNP as a novel X-ray contrast agent. As a prelude to the important innovation, the group previously proved that enhancement of radiation dose in tumor bearing mice could be achieved with high spatial specificity by using GNPs which had a propensity to localize in high number within tumors (Hainfeld *et al*, 2004). The team later went on report that administration of GNP in high concentration had no toxic effect in tumor bearing mice. High resolution imaging of tumor, kidneys and even tumor vasculature was possible by X-ray using GNP as contrast agent (Hainfeld *et al*, 2006). Recently, they further used GNPs in micro-CT imaging and radiotherapy for management of brain tumors. The results indicated that GNPs were able to selectively localize in tumors over normal tissue leading to high resolution micro-CT imaging of tumor as well as a prolonged tumor free survival (Hainfeld *et al*, 2013) (**Fig 2.16**). Plasmonic nanoparticles like GNPs have the capacity to track molecular events and the cellular level. A detailed kinetic analysis of gold nanocages in brain tumor model in vitro and in vivo provided a quantitative understanding of the distribution and clearance of the nanoparticles. Two photon microscopy and photo-acoustic microscopy revealed that 10-20% of initial gold was cleared by the 6^{th} day of administration in vitro and in vivo respectively (Cho *et al*, 2013). Similarly, using GNPs in synchrotron based computed tomography provided high resolution images of brain tumor detecting even small groups of cells (Schültke *et al*, 2014). Conjugating GNPs with FePt nanoparticles and chelating with Gadolinium agents enables the tracking of the nanoprobes by MRI. Such heterogenous nanocomplexes have been shown to be water stable, biocompatible and provide high resolution MRI of brain tumor with accurate location

of particles enabling determination of optimal dose of irradiation (Choi *et al*, 2006; Miladi *et al*, 2014).

2.6.3 Nanomaterial based assay platforms for Neuro-diagnostics

Although nano-scale imaging techniques like electron microscopy and atomic force microscopy can detect protein misfolding associated with neuro-degenerative diseases, it is usually possible at very severe stages of the disease (Lyubchenko *et al*, 2010). Most of the biomarkers for such diseases appear at young age, devoid of any clinical symptoms and hence early detection of these biomarkers is essential. Nanomaterials with their high sensitivity and specificity have been integrated into biosensors which can detect ultra-low concentrations of these biomarkers in a non-invasive, inexpensive and rapid manner.

2.6.3.1 Gold nanoparticle based assays for early detection of Alzheimer's disease

Alzheimer's disease (AD) is the most common form of dementia affecting millions of people worldwide every year. Several hypotheses have been put forward in an attempt to explain the disease mechanism. According to the most accepted hypothesis, amphipathic peptides called amyloid beta (Aβ) polymerize, aggregate, accumulate and deposit in Alzheimer's affected brain and forms protofibrils and fibrils. These amyloid fibrils are highly neurotoxic inducing neuronal cell death possibly by triggering oxidative stress. Another hypothesis suggests that such oxidative stress can lead to hyper-phosphorylation of a microtubule associated protein called 'τ'. Hyperphosphorylated *τ*-protein results in destabilization of microtubules which in turn compromise synaptic connections. Another possible factor in AD pathogenesis is thought to be amyloid derived diffusible ligands (ADDL) which is a synthetic A*β* derivative produced from A*β* monomers. ADDL has been shown to be more toxic than Aβ even at nanomolar concentrations. The initial steps towards developing an assay for AD detection were taken by scientists from Northwestern University, USA. They were able to study the binding kinetics of ADDL and anti-ADDL antibody using silver nanotriangles and localised surface plasmon resonance (LSPR) (Haes *et al*, 2004). The study was extended further to diagnose ADDL in CSF of patients using a gold nanoparticle based bio-barcode assay. The assay could detect below femtomolar concentrations of ADDL rapidly, thereby

providing the first significant example of nano based diagnostic assay for early detection of AD (Georganopoulou *et al*, 2005). Nanoparticle based plasmonic sensors for detection of Aβ peptide aggregates can be a potent device for early detection of AD. Gold nanoparticle coated with anti-Aβ antibody have been reported to detect ultra-low concentrations of amyloid-beta peptide across various platforms like surface plasmon resonance, dot blot assay and even by naked eye (Lee *et al*, 2009; Wang *et al*, 2012; Sakono *et al*, 2012). Further the application of anti Aβ labelled quantum dots enabled real time imaging of protein aggregation, oligomerization and fibrillation (Tokuraku *et al*, 2009). Similar biosensors were developed using gold nanoparticle to detect ultra-low concentrations of other AD biomarkers like τ-protein and acetylcholine esterase (AChE) in CSF using two-photon Rayleigh scattering property and colorimetric assay techniques respectively (Neely *et al*, 2009; Liu *et al*, 2012). Multifunctional nanoparticles capable of detecting as well as inhibiting Aβ fibril formation have been designed using gold and iron oxide for potential theranostic applications in AD (Choi *et al*, 2013; Skaat *et al*, 2013).

2.6.3.2 Nanomaterial based assays for early detection of Parkinson's disease

Like AD, another neurodegenerative disease primarily affecting the aged called Parkinson's disease (PD) is also characterised by abnormal protein accumulation. The deposition of high amounts of alpha-synuclein protein leads to formation of Lewy bodies inside neurons. However, the major cause of PD is thought to be the drastic depletion of neurons in the substantia nigra region of the brain primarily involved in secretion of a catecholamine neurotransmitter called dopamine (DA). Tyrosine hydroxylase, a critical enzyme in catecholamine biosynthesis pathway was monitored by gold-nanoparticle based DNA barcode assay. Its quantification could provide a direct indication to the levels of dopamine and hence detect the onset of PD (An *et al*, 2013, 2012). Similar attempts at measuring dopamine were made by other groups using different transducer platforms. For example, a single walled carbon nanotube based voltammetric biosensor was designed to simultaneously detect DA and Adenosine (metabolic indicator of neuronal activity) with very low detection limit (34.7μM for adenosine, 7μM for dopamine) (Goyal *et al*, 2008). Another team reported a voltammetric biosensor designed to detect three potential PD biomarkers – Uric Acid (UA), DA and Ascorbic Acid (AA). The biosensor was fabricated with ZnO nanowire arrays on 3D grapheme foam and was capable of

detecting all three analytes with high sensitivity and accuracy from clinical samples of PD patients (Yue *et al*, 2014) (**Fig 2.17**). Recent attempts to detect PD biomarkers in exhaled breath by using nanotechnology platforms are undergoing clinical trials (ClinicalTrials.gov Identifier**:** NCT01246336).

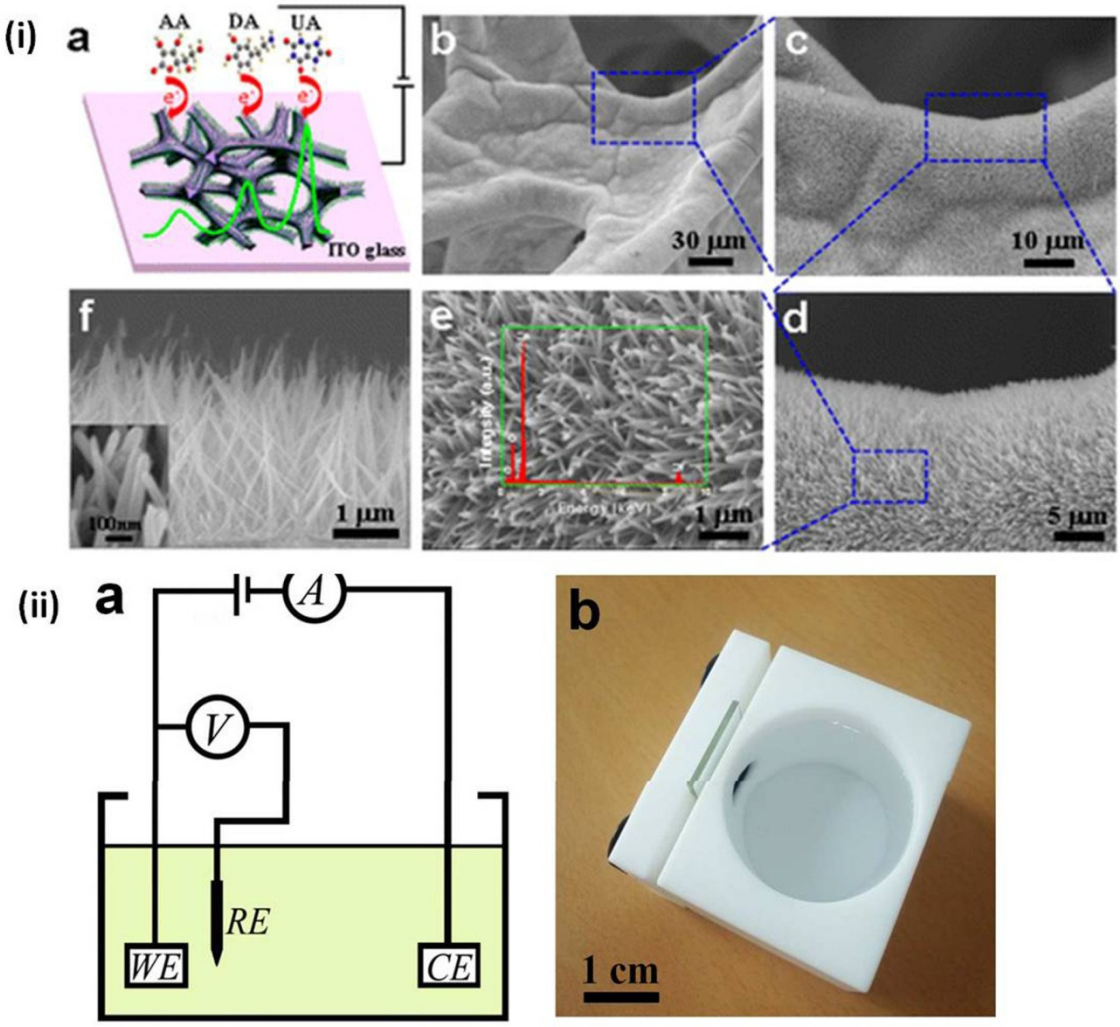

Fig 2.17: ZnO nanowires on 3D grapheme foam for detection of Parkinson's disease (**i**) Structural analysis of the integrated ZnO NWA/GF. (**a**) Schematic of the ZnO NWA/GF electrode and detection of UA, DA, and AA. (**b-e**) SEM images of the ZnO NWAs on the 3D GF at different magnifications. Inset: EDX of the ZnO NWAs. (**f**) SEM images of the height of the ZnO NWAs, ~2 µm. Inset: diameter of the ZnO NWAs, ~40 nm.
(**ii**) Electrochemical cell**. (a)** Schematic of three-electrode electrochemical cell setup. The ZnO NWA/GF on the ITO glass served as the working electrode (WE), coupled with a platinum as the counter electrode (CE) and an Ag/AgCl (sat. KCl) as the reference electrode (RE). (**b)** Photograph of the electrochemical cell used in our experiment. *(Adapted with permission from Yue et al, 2014*).

The need for a cost effective, rapid and highly sensitive diagnostic platform for early detection of biomarkers related to neurodegenerative diseases prompted the European union to initiate a multi-institute collaborative initiative for development of nanosystems for early diagnosis of neurodegenerative diseases (NADINE) in 2010.

2.6.4 Nanotools for Neurotherapy

The complex physiology of the BBB and the restricted neuroanatomical access poses major challenge to surgical intervention and drug delivery in the nervous system. However, the rapid progress in fabrication of nanomaterials has provided solutions to many of the neurological challenges as discussed in earlier sections.

2.6.4.1 Nanotherapeutics in Glioblastoma multiforme

Glioblastoma multiforme, is the most aggressive form of intracranial malignancies, arising from the astrocytes with a very high mortality rate. Its an unique form of malignancy which displays polymorphism by gross examination, at the microscopic level as well as at the genetic level with a variety of genetic mutations contributing to disruption of multiple biochemical and cell-cycle pathways (Holland *et al*, 2000). The BBB and the Blood-Brian Tumor Barrier (BBTB) poses the major hurdles for drug delivery inside the tumor depending on the stage of malignancy. At the initial stages of the disease, the tumor cells rely on the normal BBB for supply of nutrients and benefits from the high TEER of the endothelial cells which restricts drug transport. However, at advanced stages of malignancy, when tumor cells invade normal tissue, neo-vasculatures are formed with continuous fenestrated microvessels allowing only molecules less than 12nm to pass through (Liu *et al*, 2012). Thus strategies targeting therapeutic agents inside brain tumors have mainly evolved using dual targeting nanoparticles functionalised with molecules specific for tumor cells as well as tumor neo-vasculature. Over the years, Chinese groups have reported extensively on a variety of functional coatings on polymeric nanoparticles to obtain dual targeting of brain tumor. Nanoparticles were functionalized with Interleukin-3 peptide (Gao *et al*, 2014) and Lactoferrin (Miao *et al*, 2014) to enhance uptake by tumor cells. These were further decorated with tumor neovasculature targeting RGD moieties (Gao *et al*, 2014) and tLyp-1 peptides (Miao *et al*, 2014) to cross the BBTB. In some cases, lipoprotein receptor protein binding molecules like Peptide-22 (Zhang *et al*, 2013) and Angio-pep-2 (Xin *et al*, 2012) could individually achieve efficient delivery of

paclitaxel by dual targeting of neo-vascualture and malignant cells. In another study, the same team managed to decorate the polymeric nanoparticles with aptamers specific for nucleolin which is over-expressed in both cancer cells and tumor vasculature (Guo *et al*, 2011). Nano-formulations of naturally occurring anti cancer compounds like reservatol was delivered by lipid based nanocapsules and were reported to inhibit glioma growth in vitro and in vivo (Figueiró *et al*, 2013). Another group demonstrated the efficiency of polymeric nanoparticles as vehichles for targeted gene delivery inside glioma. The Chlorotoxin conjugated PEG-PLA nanoparticles could efficiently cross the BBB and reach the perinuclear region, thereby facilitating the delivery of GFP encoding DNA inside tumor cells (Kievit *et al*, 2010). In order to obtain sustained release of drugs in situ, scaffolds in the form of nanofibers were found to hold potential as implants for glioma therapy. PLGA nanofibers loaded with paclitaxel exhibited sustained release of drug over 60 days in vitro on culture of C6 glioma cell line (Xie *et al*, 2006).

2.6.4.2 Nanotherapeutics in Alzheimer's disease

Alzheimer's disease (AD) is mainly caused by aggregation and accumulation of Aβ fibrils in the brain tissue. Hence most of the therapeutic strategies developed for AD has focussed on inhibition of amyloidogenesis and destruction of Aβ fibrils by targeted irradiation methods and localised delivery of anti-amyloid molecules. Metal ions like (Cu, Fe and Zn) tend to accumulate in ageing brain and have been shown to interact with and stabilize Aβ fibrils thereby facilitating progression of AD. By using Cu-chelator D-penicillamine conjugated with nanoparticles, scientists observed that it was possible to resolubilize $A\beta_{1\text{-}42}$ aggregates (Cui *et al*, 2005). This showed that nanoparticle based platforms could be used to reduce metal ion accumulation thereby reversing many neurodegenerative diseases. Enhanced delivery of natural anti-oxidant and anti-amyloid compounds like curcumin can be achieved by employing biocompatible nanomaterials tagged with moieties that direct the nanoprobes into neuronal cells. Studies with curcumin loaded polymeric nanoparticles conjugated with Tet-1 peptide as well as enhanced delivery of curcumin into mice brain by PBCN-NP are some examples (Matthew *et al*, 2012; Sun *et al*, 2010). Metallic nanoparticles like gold nanoparticles have been reported to inhibit Aβ fibril formation as well as aid in targeted photothermal (Triulzi *et al*, 2008) and microwave irradiation (Araya *et al*, 2008) for Aβ aggregates. Surface

modification of GNPs with COOH groups provided a net negative charge which was found to inhibit and redirect Aβ fibrillation (Liao *et al*, 2012). Apart from GNPs, Quantum dots (QDs) have also been conjugated with anti-amyloid molecules like N-acetyl-L-cysteine (NAC) which can inhibit fibrillation by quenching the nucleation and elongation processes (Xiao *et al*, 2010). Nano-formulations of polymeric materials like PEGylated poly-lactic acid (PLA) and polysaccharide nanogels (cholesterol bearing pullulan) also exhibited potential as platforms for targeting amyloid plaques (Zhang *et al*, 2014) and as chaperones inducing conformational change in Aβ fibrils respectively (Ikeda *et al*, 2006). Similarly, estradiol loaded polymeric nanoparticles were given orally in rat AD model, keeping in mind the enhanced risk of the disease in post menopausal women due to reduced estrogen levels. Nanoparticle mediated delivery aided in brain localisation of estradiol increasing bioavailability and therapeutic efficiency at lower drug concentration (Mittal *et al*, 2011). In a separate approach towards AD treatment an Italian group delivered Acetylcholine esterase inhibitor drug Tacrine via albumin nanoparticle. The intranasal delivery of the drug through nanocarrier was expected to increase bioavailability, enhance permeation and circulation time of the active ingredient (Luppi *et al*, 2011).

2.6.4.3 Nanotherapeutics in Parkinson's disease

The second most prevalent neurodegenerative disorder after AD is Parkinson's disease (PD). Although the pathophysiology of PD has been extensively studied, the disease etiology largely remains unknown (idiopathic) till date. PD is primarily associated with loss of dopaminergic neurons in the substantia nigra leading to deficiency of the neurotransmitter – Dopamine. In order to combat this deficiency, Levo-dopa (L-DOPA) which is a biological precursor of dopamine is generally administered to PD patients. The low bioavailability of L-DOPA upon systemic or oral administration has necessitated nanotechnology based delivery platforms to ensure efficient transport of dopamine across the BBB and maximum localization of the molecule in the brain. Initial attempts for site-specific delivery of dopamine to minimise its peripheral side effects were focussed on designing and biometric simulation of a prototype nano-enabled scaffold device (NESD) comprising of alginate scaffold embedded with dopamine loaded cellulose acetate phthalate (CAP) nanoparticles (Pillay *et al*, 2009). The device was implanted in the parenchyma of the frontal lobe of rats and was found to deliver dopamine over 30 days with 10 fold

more dopamine in CNS as compared to systemic concentration. Similar attempts for dopamine delivery were also made with chitosan nanoparticles (De Giglio *et al*, 2011). Intraperitoneal administration of dopamine loaded chitosan nanovectors were found to induce dose dependent increase of dopamine presence in the striatum as observed through in vivo brain microdialysis experiments. Other neuro-protecting molecules like corticotrophin hormone urocortin and genes encoding growth factors like GDNF also arrests development of Parkinsonism when administered through polymeric nanoparticles conjugated with lactoferrin (Hu *et al*, 2011;Huang *et al*, 2010). Similarly, angiopep conjugated dendrimers have been used to transport human GDNF genes into the affected areas of the brain for recovery of dopaminergic neurons and restore locomotory activity in Parkinson's induced animal models (Huang *et al*, 2013). Oxidative stress is one of the main causes which result in loss of dopaminergic neurons in PD. Hence, attempts to specifically deliver antioxidants into the substantia nigra of diseased brain have also been reported. Cationic block copolymer polyethyleneimine-PEG (PEI-PEG) of 60-100nm size were loaded with catalase enzyme to form a nanozyme complex which exhibited longer stability in vitro and in vivo with 0.6% of the injected dose reaching the brain (Batrakova *et al*, 2007). Besides dopamine deficiency, another pathophysiology associated with PD is the accumulation of α-synuclein protein forming inclusions called Lewy bodies which are found distributed throughout a diseased brain. Gold nanoparticles were observed to act as chaperones, preventing the misfolding of α-synuclein and hence can be used as a therapeutic to sequester and regulate α-synuclein homeostasis (Yang *et al*, 2014; Yang *et al*, 2013). These pathophysiologies are ultimately responsible for deterioration of electrical activity in the thalamic, subthalamic nucleus, globus pallidus and medial globus pallidus region of the parkinsonian brain. Temporal administration of magneto electric nanoparticles facilitates non-invasive stimulation of these regions thorugh an external magnetic field thereby improving the brain's electrical activivty (Yue *et al*, 2012).

2.7 Nanotechnology in Neuroregeneration

Through the use of structures which actively encourage and guide axons to reconnect with their targets, nanotechnology is gradually revolutionising the field of regenerative neuroscience. Some of the nanomaterials used in promoting neuro-regeneration are listed in **Table 2.2.**

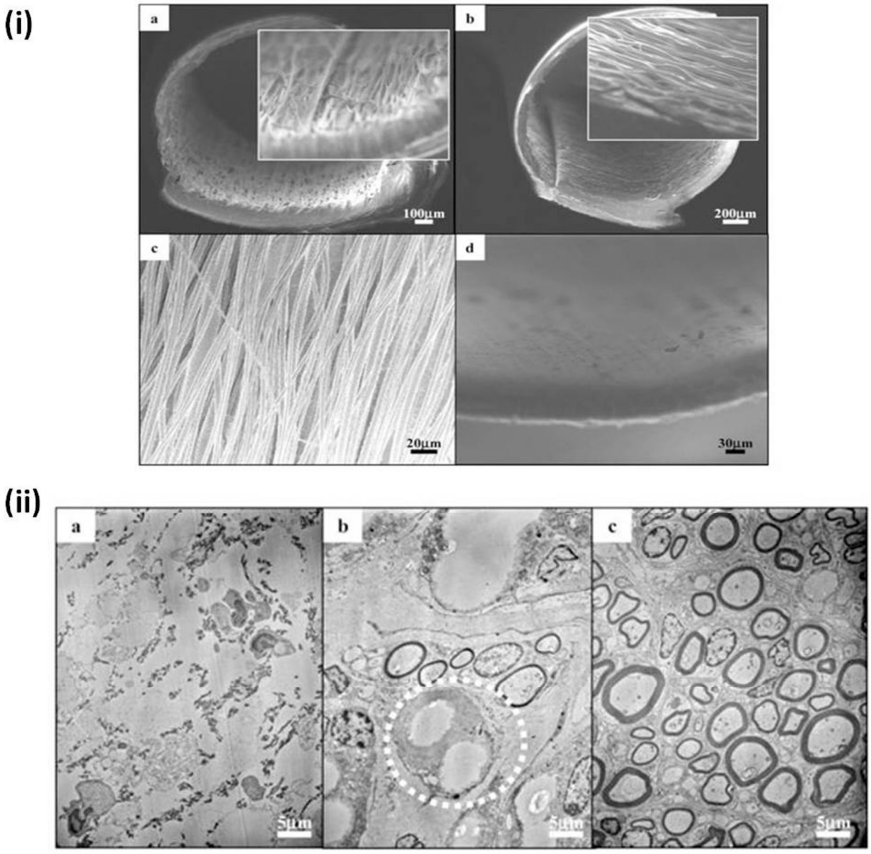

Fig 2.18: **Poly(*ε*-caprolactone-*co*-ethyl ethylene phosphate) (PCLEEP) and aligned GDNF-PCLEEP electrospun fiber based conduits**. (**i**) Cross-sectional views of nerve conduits with aligned electrospun fibers (EF), **a**) Longitudinally aligned (EF-L) and **b**) circumferentially aligned (EF-C). Insets: higher-magnification views of the cross sections. c) Aligned PCLEEP fibers in nerve guide conduits, GDNF-encapsulated fiber diameter, *φ*=(3.96 ±0.14) μm and plain PCLEEP fiber *φ*= (5.08 ± 0.05) μm. d) Inner surface of an empty nerve guide conduit.
(**ii**) TEM images of cross sections of regenerated sciatic nerve, 8–10 mm from the proximal end of nerve conduits. **a**) In the control group, showing the absence of myelinated axons and the presence of fibrous tissues. b) In the EF-L group, showing the tendency of myelinated axons regenerating in close proximity to PCLEEP fibers (circled). c) In the EF-L-GDNF group, demonstrating the presence of a large number of myelinated axons. *(Adapted with permission from Chew et al, 2007*).

Although axonal regeneration in the PNS occurs much more efficiently than in the CNS, reinnervation and functional recovery are often poor. This is particularly the case for lesions in which large spaces between nerve stumps are created. This gap, lacking the Schwann cells necessary for axonal regrowth, poses a major obstacle for regenerating axons. In these cases, the golden standard for treatment of PNS damage has been the use of autologous nerve grafts for bridging the two ends. However, as discussed above, these grafts pose several disadvantages. Instead, nanotechnology may hold the answer for the development of alternatives to these autologous grafts, in the form of tissue engineered nerve grafts (TENGs). Although in the most classical sense a TENG consists essentially of a hollow tube connecting the two nerve stumps, more recently developed TENGs rely on a combination of physical and biochemical cues to actively facilitate the growth of axons through it. These cues are often introduced in the form of nanofibers.Nanofibers possess a number of advantages for their use as scaffolds for neural regeneration, since (1) their physical properties can be tailored to specifically meet the requirements of a particular type of lesion; (2) their large surface area – to – volume ratio enhances the presentation of biochemical cues; and (3) they can be made from a number of biocompatible and degradable materials.

Electrospinning is one of the most used methods for the fabrication of nanofibers. This technique allows for the production of fibers with a wide range of dimensions, which can be easily regulated through variations in the polymer solution, electric field strength, and field pattern used in the fabrication process. Synthetic materials, including poly(ε-caprolactone) (PCL) (Panseri *et al*., 2008), poly(ε-caprolactone-co-ethyl ethylene phosphate) (PCLEEP) (Chew *et al*., 2007), and poly(L-lactic acid) (PLLA) (Yang *et al*., 2005); are the most common component used for the fabrication of electrospun nanofibers for nerve regeneration. **Fig 2.18** describes a study with GDNF incorporated aligned PCLEEP electrospun nanofibrous conduits. Kim *et al*. (2008), for example, used poly(acrylonitrile-co-methylacrylate) (PAN-MA) fibers (with a diameter of 400–600 nm) to bridge a 17 mm rat tibial nerve lesion gap. They observed that, following a 16 week recovery period, these rats exhibited a sensory and motor recovery on par with that of rats with autologous grafts. Notably, this effect was only seen in animals with PAN-MA fibers aligned with the axis of axonal regeneration, suggesting that the topographical cues provided by the nanofibers are

a crucial component of their regenerative potential. Similarly, in a recent study Jiang *et al*. (2012) implanted either PCL microfibers (981±83 nm diameter) or nanofibers (251 ±32 nm diameter) into a 15 mm rat sciatic nerve lesion. Regeneration through the graft, as seen by retrograde labelling, was much greater in nanofiber than in microfiber grafts; a finding which serves to highlight the importance of nanofiber scale in their properties as regenerative scaffolds. Naturally occurring materials, such as chitosan (Wang *et al.,* 2008), have also been employed as nanofibers scaffolds.

Material used	Fabrication method	Target tissue	Reference
Poly(lactic-co-glycolic acid) (PLGA)/Poly(ε-caprolactone) (PCL)	Electrospinning	Rat sciatic nerve	Panseri et al, 2008
Copolymer of caprolactone and ethyl ethylene phosphate (PCLEEP) with GDNF	Electrospinning	Rat peripheral nerve	Chew et al,,2007
Poly(acrylonitrile-co-methylacrylate) (PAN-MA)	Electrospinning	Rat tibial nerve lesion	Yang et al, 2005
Poly(ε-caprolactone) (PCL)	Electrospinning	Rat sciatic nerve	Jiang et al, 2012
Chitosan	Electrospinning	Rat sciatic nerve	Wang et al, 2008
Polyamide nanofibers bound with tenascin-C	Electrospinning	Rat spinal cord	Meiners et al, 2007
Single-walled carbon nanotubes functionalized with polyethylene glycol (SWNT-PEG)	Purchased	Rat spinal cord	Roman et al,, 2011
PLGA nanospheres	oil-in-water with co-solvent single emulsion solvent evaporation technique	Rat optic nerve	Robinson et al, 2011
IKVAV (isolucine-lysine-valine-alanine-valine) peptide	Self assembly	Mice spinal cord injury	Tysseling-Mattiace et al, 2008
Peptides of Arginine–Alanine–Aspartate (RAD)16-I and RAD16-II	Self assembly	primary neurons and neuronal cell lines (PC12)	Holmes et al, 2000

Table 2.2: Nanomaterials used in Neuroregeneration

Although these materials more closely resemble the tissue they are intended to replace, potentially exhibiting greater biocompatibility, their weak mechanical properties limit their usefulness as nerve graft scaffolds.

The other major alternative to electrospinning for the fabrication of nanofibers is self-assembly. This technique consists in the design of molecules, particularly peptides, capable of assembling by noncovalent bonding into polymeric structures directly in their target areas (Zhang *et al*., 2003). Self-assembled peptide nanofibers(SAPNs)

are characterised by a very small diameter (5-10 nm) in contrast to electrospun fibres, which often are orders of magnitude larger. These dimensions closely resemble those of extracellular matrix (ECM) proteins, making SAPNs a close imitation of the natural cellular environment. Additionally, these fibersbreak down intoL-amino acids which, being common in all organisms, are non-toxic. Several self-assembling peptide (sapeptide) sequences have been used for the formation of SAPN scaffolds. Arginine-alanine-aspartate sequences (RAD16), for example, have been shown to support adhesion and facilitate neurite outgrowth of primary neurons and neuronal cell lines (PC12) in vitro(Holmes *et al*, 2000).Sapeptides can also be modified so as to include certain motifs, introducing functional properties in the final SAPNs which may be desirable in the final scaffold. For example, Gelain *et al*. (2006) studied the effect of functionalisation of RADA16(arginine-alanine-aspartate-arginine) sapeptides with bone marrow homing motifs. Functionalised SAPN scaffolds were found to support neural stem cell proliferation to a greater degree than pure RADA16 SAPN scaffolds.

Axonal regeneration in the CNS often fails, due to a combination of inhibitory environment and lack of growth supporting factors. Although these limiting factors have often been addressed individually, no therapy currently exists to treat CNS lesions in humans. It is likely that, given the multimodal nature of the problem, the issues limiting regeneration in the CNS will have to be addressed simultaneously to achieve successful regeneration. Given the wide range of unique properties that they can exhibit, nanotechnologies are thus an attractive platform for the development of these therapies.

As in the PNS, nanofiber scaffolds have been used to promote the regeneration of axons through lesions in the CNS. Although electrospunfibers have sometimes been used for this purpose (Meiners *et al*., 2007), SAPNs are more commonly employed due to their ability to polymerise in situ, minimising the need for surgical intervention. Tysseling-Mattiace *et al*. (2008) injected laminin motif-derived IKVAV (isolucine-lysine-valine-alanine-valine) sapeptidesinto mouse thoracic (T10) spinal cord compression injuries. These mice not only had reduced glial scar formation, but also exhibited enhanced functional recovery 9 weeks after injury. RADA16 sapeptide scaffolds have also been used in in vivo CNS regeneration studies, in both spinal

cord (Guo *et al*., 2007) and optic tract (Ellis-Behnke *et al*., 2006) lesion models (**Fig 2.19**).

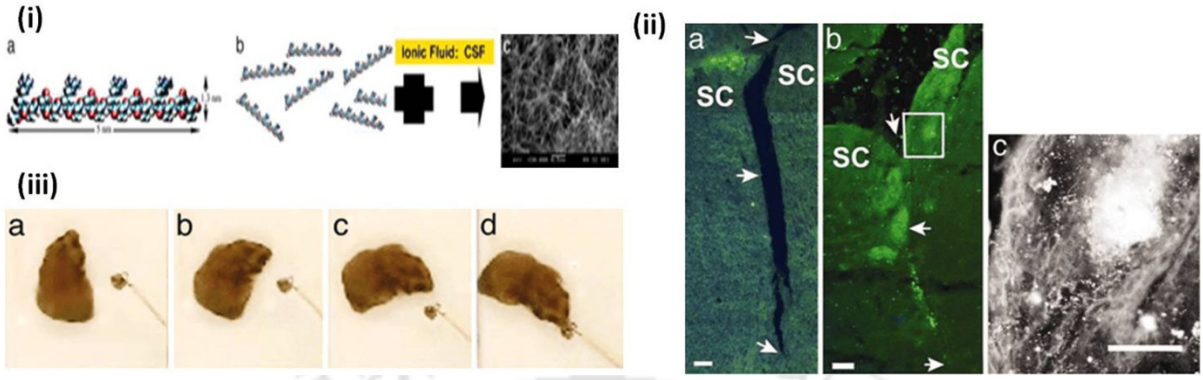

Fig 2.19: **Self-Assembling Peptide Nanofiber Scaffold (SAPNS) mediated repair for the animal brain**. (**i**) (*a*) Molecular model of the RADA16-I molecular building block. (*b*) Molecular model of numerous RADA16-I molecules undergo self assembly to form well ordered nanofibers with the hydrophobic alanine sandwich inside and hydrophilic residues on the outside. (*c*) The SAPNS is examined by using scanning electron microscopy. (Scale bar,500 nm.) (**ii**) SAPNS allows axons to regenerate through the lesion site in brain. The dark-field composite photos are parasagittal sections from animals 30 days after lesion and treatment. (*a*) Section from brain of 30-day-old hamster with 10 µl of saline injected in the lesion at P2. The cavity shows the failure of the tissue healing. The retinal projections, in light green at the top left edge of the cavity, have stopped and did not cross the lesion. Arrows indicate path and extent of knife cut. (*b*) A similar section from a 30-day-old hamster with a P2 lesion injected with 10µl of 1%SAPNS. The site of the lesion has healed, and axons have grown through the treated area and reached the caudal part of the superior colliculus (SC). Axons from the retina are indicated by light-green fluorescence. The boxed area is an area of dense termination of axons that have crossed the lesion. Arrows indicate path and extent of knife cut. (*c*) Enlarged view of boxed area in *b*. The regrown axons, shown in white, were traced with cholera-toxin fragment B labeling by using immunohistochemistry for amplification of the tracer. (**iii**) Optic tract regeneration and functional return of vision. This SAPNStreated adult animal turns toward the stimulus in the affected right visual field in small steps, prolonged here by movements of the stimulus away from the animal. Each frame is taken from a single turning movement, at times 0.00 (*a*), 0.27 (*b*), 0.53 (*c*), and 0.80 (*d*) sec from movement initiation. The animal reached the stimulus in the last frame. This is 29% slower than most turns by a normal animal. The recording was made 6 weeks after surgery and treatment when the animal started to show a response.(*Adapted with permission from Ellis-Behnke et al, 2006*)

More complex approaches to CNS regeneration have also been taken. One such example is the combination of nanofiber scaffolds with stem cell therapy. Neural stem cells (NSCs) can aid regenerating axons through the formation of a growth-supportive microenvironment, and are considered to hold great therapeutic potential

for the treatment of CNS injury and disease(Martino and Pluchino, 2006). Poly(lactic-co-glycolic acid) (PLGA) scaffolds containing pores for axonal guidance, and an underlying layer seeded with NSCs, were implanted in rats with spinal cord hemisection lesions (Teng *et al*., 2002). Implantation of this scaffold led to axonal regeneration and a functional recovery which was superior to that seen in rats implanted with the scaffold or NSCs alone.

The conductive properties of certain nanomaterials also make them well suited to combine neural scaffolding with electrical stimulation. Although studies have mainly limited to *in vitro* testing, neuronal cultures have been reported to exhibit increased neurite outgrowth in response to electrical stimulation (Kimura *et al*., 1998). Electrospun nanofibers coated with electrically conductive polymers have been studied by several groups as potential platforms for the fabrication of regenerative scaffolds. Lee *et al*. (2009) cultured cells of the PC12 neuronal cell line ona mesh of poly(lactic-co-glycolic acid) (PLGA) nanofibers coated with a nano-thick layer of electro-conducting polypyrrole (PPy).Not only did the nanofibers support the extension of neurites from the cells, but neurite length and number was greatly increased when cells were electrically stimulated. Carbon nanotubes also hold great potential for the development of multifunctional scaffolds. Although they are non-degradable; their size (~1 nm diameter),electrical conductivity, and excellent mechanical properties make them good candidates for their use as scaffolds for neural regeneration. Moreover, *in vivo* studies in rat SCI lesion models have shown that carbon nanotube scaffolds, functionalised with polyethylene glycol, are capable of supporting axonal regeneration through the lesion and promote functional recovery (Roman *et al*., 2011).

Finally, more traditional treatments like the direct delivery of growth-supportive compounds to lesions have also benefitted from nanotechnology. Although agents such as Epidermal growth factor receptor (EGFR) inhibitors have been shown to reduce the inhibitory effect of CSPGs and myelin on axon regeneration (Koprivica *et al*., 2005), sustained delivery is necessary for its therapeutic effects to be seen. Since systemic administration is not a desirable delivery route due to associated side-effects, consequence of the role played by EGFR in other tissues (Fakih and Vincent, 2010), a nanotechnology platform was developed for the sustained, local delivery of EGFR inhibitors (Robinson *et al*., 2011). PLGA microspheres and

nanospheres loaded with the EGFR inhibitor Tyrosine Kinase Inhibitor (TKI) AG1478 were administered to the eye of rats following injury of the optic nerve. Although both microspheres and nanospheres caused axons to regenerate through the site of injury 2 weeks later, survival of these axons at 4 weeks post-lesion was only observed in nanosphere-injected animals. This observation was attributed to the ease of administration and more stable drug release profile of nanospheres compared to their larger counterparts, and serves as an example of the advantages that nanotechnology can have over seemingly similar approaches to axonal regeneration (**Fig 2.20**).

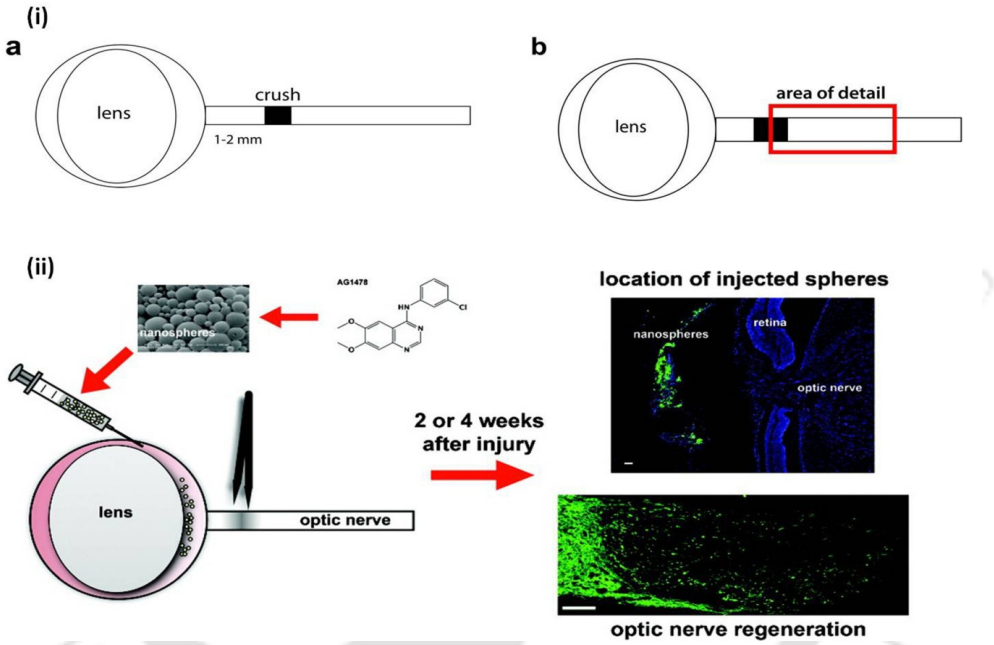

Fig 2.20 Promoting Optic Nerve Regeneration through sustained delivery of EGFR TKI AG1478 by nanospheres (**i**) Optic nerve crush injury model. (**a**) Diagram of the rat eye and optic nerve illustrating the surgical approach for the animal studies testing the effectiveness of the microspheres and nanospheres. (**b**) Diagram illustrating the area of detail for the immunohistological images examining nerve regeneration. (**ii**) Poly(lactic-co-glycolic acid) (PLGA) microspheres and nanospheres containing the EGFR TKI 4-(3-chloroanilino)-6,7-dimethoxyquinazoline (AG1478) were fabricated for intravitreal administration in a rat optic nerve crush injury model. Two weeks after intravitreal delivery, microspheres and nanospheres could be detected in the vitreous using coumarin-6 fluorescence, but fewer microspheres were observed compared to the nanospheres. At four weeks only nanospheres could be detected. AG1478 microspheres and nanospheres promoted optic nerve regeneration at two weeks, and at four weeks evidence of regeneration was found only in the nanosphere-injected animals. This observation could be attributed to the ease of administration of the nanospheres *versus* the microspheres, which in turn led to an increased amount of spheres delivered to the vitreous in the nanosphere group compared to the microsphere group.(*Adapted with permission from Robinson et al, 2011).*

2.8 Sciatic Nerve Injury Model in Neuro-regenerative research

Pre-clinical experiments in neuro-regeneration research is mainly carried out in animal models since, so far, in vitro investigation of nerve regeneration is very limited due to the structural complexity of this organ which can hardly be reproduced in vitro (Geuna *et al*., 2009). The most used experimental paradigm for the pre-clinical investigation of peripheral nerve regeneration is represented by the sciatic nerve injury (SNI) model. Among the various reasons that might explain the preponderance of SNI employment, two are the most important: (i) the large size of the sciatic nerve which facilitates surgery; (ii) the easy surgical access;(iii) the sought for data that can be comparable with previous studies, the very large majority of which have been carried out using the SNI model.

2.8.1 Sciatic Nerve Injury Model in compression lesions

Experimental models based on the mechanical compression of the sciatic nerve have been widely used in experimental research in order to investigate the changes occurring to the nerve, proximal and distal to the lesion, as well as to the other central (e.g. neuronal cell bodies) and distal (e.g. muscles) anatomical structures. Sciatic nerve compression can be obtained by either ligation or crush of the epineurium. The compression is applied with the goal of interrupting the continuity of all axons axons (axonotmesis) without interruption of the connective scaffold of the nerve (especially the epineurium) and thus without losing continuity of the nerve trunk. Therefore, the nerve segments proximal and distal to the lesion site remain connected allowing severed axons to regrowth along an optimal regenerating pathway. Independently of the procedure, the main advantage of the crush lesion is that it does not require microsurgical skills and inter-individual variability in tissue regeneration as well as in functional recovery is also limited. These features make the sciatic nerve crush injury model particularly suitable for the study of the biology of peripheral nerve regeneration as well as the treatment strategies to improve it. In fact, its high reproducibility makes easier the identification of the changes occurring not only to the entire tissue but also at the cellular and molecular level (Chen *et al*., 2008; Toth *et al*.,2008; Lou *et al*., 2012; Long *et al*., 2013; Wright *et al*., 2014).

Further this experimental model is also particularly suitable for investigating regeneration-related time course changes (De Leon *et al*., 1991; Gupta and Channual, 2006; Sta *et al*., 2014).

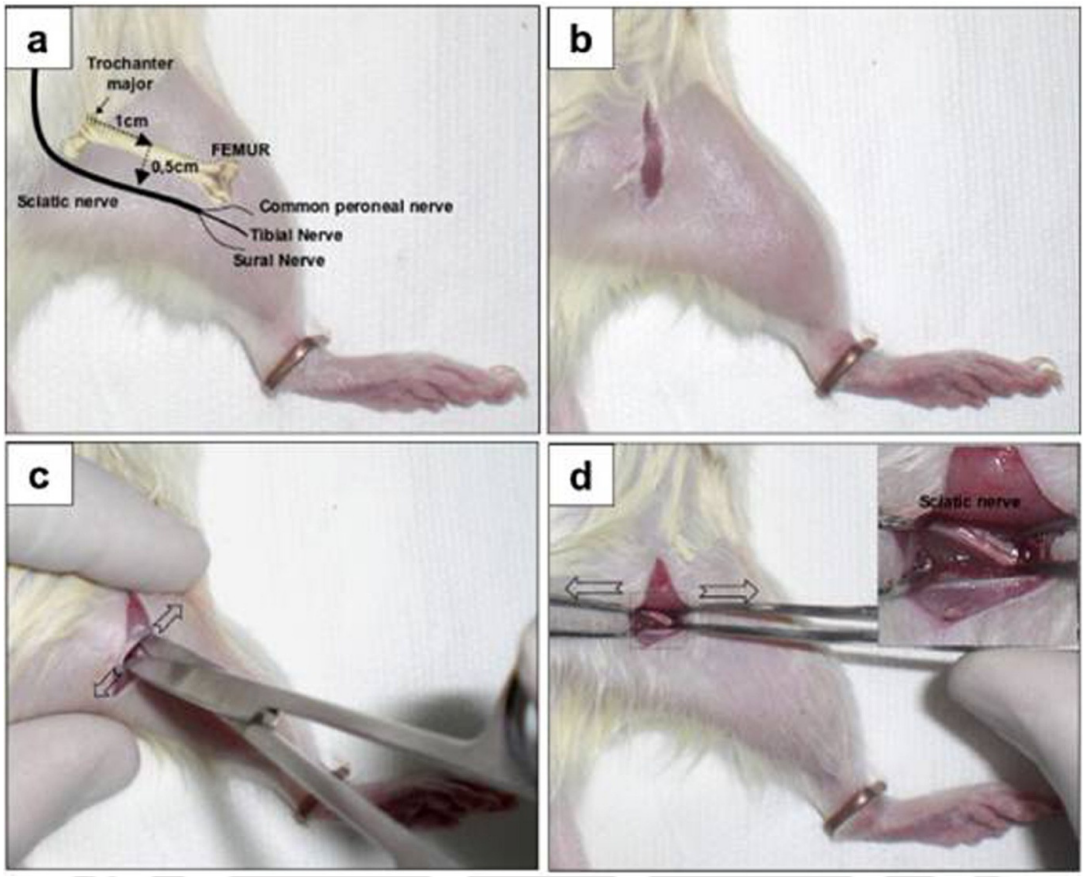

Fig 2.21. **Procedure for performing an axonotomesis of the sciatic nerve at mid-leg level**. (a) Right hind leg of the anesthetized and shaved animal immobilized with a staple. To orient the operator, images of the femur in its anatomical location and the general path of the sciatic nerve up to its trifurcation have been superimposed onto the animal's leg. (b) The bone can be palpated in order to estimate the site of the incision, near to the position of the sciatic nerve, and above the level of its trifurcation. (c) Using the landmarks in (a), the scissors are placed 1 cm distal to the femur (trochanter major) and 0.5–1 cm orthogonal in the caudal direction and carefully inserted while tensingthe muscle with the fingertips of the other hand. The muscle fibers are separated by simultaneously opening and retracting the scissors, which are then removed without completely closing them. (d) The incision is held open using a pair of forceps in either hand, and the superficial muscular layer is moved backwards and forwards until the sciatic nerve is identified. The magnified inset shows the presence of blood vessels along the sciatic nerve, distinct from the gluteal and pudendal arteries, and the three nerve bundles that, more distally, trifurcate to innervate different targets. The inset contrasts a bright strand of connective tissue on the lower lip of the incision with the duller nerve, which could be confused by inexperienced operators. (*Adapted with permission from Savastano et al, 2014)*

Finally, changes in the outcome of nerve regeneration after a crush injury of the sciatic nerve might be used as a pre-clinical end-point predictor of the effectiveness of a therapeutic agent and/or tissue engineering strategy on nerve regeneration (Fleming *et al*., 2007; Amado *et al*., 2008; Baptista*et al*., 2008; Gigo-Benato *et al*., 2010; Dadon-Nachum *et al*., 2011;Kilic *et al*., 2013; Wang *et al*., 2014).

Although the experimental model based on the sciatic nerve crush injury has several advantages in terms of feasibility and reproducibility, its translational potential is limited for two main reasons. First, most surgically relevant nerve lesions in human patients are characterized by at least partial transection/laceration of the nerve. Second, crush lesions in patients have a different clinical history in comparison to experimental crush lesions in lab-oratory animals, namely spontaneous axon regeneration observed in laboratory animals does not often occur in humans due to frequent extensive fibrosis at the lesion site; thus, in many cases, crush lesions in patients require surgery for removing the damaged tissue and replace it with a conduit (Tos *et al*., 2012).

2.8.2 Sciatic Nerve Injury Model in chronic denervation

The most severe clinical condition that can be met in a patient is the chronic denervation, i.e. a complete transection of a nerve not followed by reconstruction of the nerve continuity. This induces the permanent disconnection between neurons and the respective distal nerve targets with definitive loss of sensory and/or motor function.

Chronic denervation can be reproduced by complete transection of the sciatic nerve not followed by its surgical reconstruction. Since in laboratory animals axonal regeneration is more pronounced than in humans and can occur spontaneously after complete transection even in absence of nerve repair, particular attention should be paid in avoiding this occurrence by turning the proximal nerve stump and suturing it to a neighboring tissue (e.g. a muscle). Since changes in both distal nerve segment and target muscle occur very early, the model can be used to study both early and late events post-denervation.

2.8.3 Sciatic Nerve Injury Model in autograft studies

Autograft repair of the sciatic nerve isstill today widely used in pre-clinical research since it represents the benchmark condition toward which alternative types ofnerve guides are tested (Siemionow and Brzezicki, 2009; Griffin *et al*., 2013). However, it should be clearly pointed out that thetechnique used for autograft sciatic repair in laboratory animals (i.e. the removal of a nerve segment followed by its immediate re-implant with or without 180◦rotation) significantly differs from the autograft technique used in patients (i.e. interfascicular nerve grafting of the damaged nerve using multiple segments of a sensory nerve, usually the sural one), a discrepancy that should be always taken into consideration in the interpretation of the experimental results in a pre-clinical perspective.

2.8.4 Sciatic Nerve Injury Model in nerve conduit studies

A number of alternatives, both biological and synthetic, have been assessed in a pre-clinical setting in order to substitute nerve autografts. Un-doubtfully, the search for alternatives to nerve autografts is the field where SNI model has seen most extensively employment. The SNI model has been used for testing conduits for nerve repair of both biological and synthetic origin. In spite of the effectiveness of some types of biological nerve guides, some of which have been successfully translated to the clinics (Chiu and Strauch, 1990; Pereira *et al*., 1991; Marcoccio and Vigasio, 2010; Tos *et al*., 2012; Manoli *et al*., 2015), most research along the last 30 years has been dedicated to artificial scaf-folds based on the recent advancements in bio-nanotechnologies. A number of innovative artificial nerve guides have been developed and this body of experimental research has been mainly based on experiments made using the SNI model.

2.8.4 Surgical considerations of using Sciatic Nerve Injury Model

Experimental surgery on the sciatic nerve is relatively easy due to its large size (the largest nerve in mammals). The sciatic nerve is a mixed nerve (Schmalbruch, 1986) which originates from the lumbo-sacral plexus and ends at the knee level with its terminal division that is usually represented by a trifurcation: the tibial nerve (the biggest one) the common peroneal nerve and the sural nerve (Rupp *et al*., 2007b). However, there is a high anatomical variability in the number and site of origin of

sciatic nerve terminal branches which should be always taken into consideration, especially in the identification of the lesion site. The anatomy of sciatic nerve and the surgical procedure for performing an axonotmesis is described by Savastano *et al,* 2014 *(***Fig 2.21***)* A second methodological consideration about surgery is the maximum length of the sciatic nerve defect that, in the rat, should be limited to 1.5 cm. Although the bridging of gaps longer than1.5 cm have been described in the rat (Dodla and Bellamkonda, 2008), it is preferable to move to larger animal models (e.g. rabbit or sheep) when long nerve prostheses have to be tested in vivo.

2.8.5 Functional assessment in Sciatic Nerve Injury Model

Although the assessment of the functional outcome is the more important evaluation parameter in the pre-clinical perspective, most currently available methods for measuring functional recovery after SNI are characterized by a high degree of variability which, unfortunately, limits data interpretation. As regards motor function recovery, the most commonly used test is the calculation of the sciatic functional index (De Medinaceli *et al*., 1982; Varejão *et al*., 2001). Although this method is very popular in peripheral nerve regeneration research, its validity has been questioned (Varejão *et al*., 2004a,b).Therefore, more recently, the availability of high-performing video cameras has allowed the development of more reliable computerized gait analysis system based on the video recording of the animals (Bozkurt *et al*., 2008a,b; Costa *et al*.,2009).

2.8.6 Electrophysiological assessment in Sciatic Nerve Injury Model

The electrophysiological assessment of the nerve recovery is the predictor of nerve regeneration which is closer to the direct assessment of the motor or sensory function. Being a mixed nerve, the electrophysiological assessment of the sciatic nerve can be carried out both for the efferent and afferent component. Since recovery of motor function is the most relevant postoperative achievement that is sought in the pre-clinical perspective the most used electrophysiological method is the recording of evoked compound muscle action potentials (CMAPs) after electrical stimulation proximal and distal to the lesion site (Navarro and Udina, 2009; Nijhuis *et al*., 2013).

2.8.7 In vivo imaging in Sciatic Nerve Injury Model

Recent advances in vivo imaging techniques of tissues and organs have more and more expanded their use to small animal species. As regards SNI investigation, two methods are receiving growing interest for monitoring in vivo the nerve regeneration process: ultrasonography and magnetic resonance. Ultrasound imaging has the advantage that can be obtained using relatively cheap instruments. This technique can thus be used also in rat sciatic nerve to monitor the progression of nerve tissue regeneration, e.g. along a nerve prosthesis (Chen *et al*., 2014). Magnetic resonance requires much more expensive devices that should adapted to the size animal species under investigation (Behr *et al*., 2009). However, if a dedicated facility is available, magnetic resonance imaging holds great expectations for in vivo SNI investigation in experimental models (Liao *et al*., 2012; Yamasaki *et al*., 2015).

2.8.8 Ethical issues in Sciatic Nerve Injury Model

SNI induces significant limitations in the movements of the affected limb accompanied by loss diffuse of sensation, especially in the foot. Motor function loss, besides walking impairment, often induces muscle contractions (Dellon and Mackinnon, 1989). On the other hand, the main drawback of sensory function loss is the progressive autotomy of variable degree, from simple nail lost to extensive mutilation of the entire foot (Krˇsljak and Stajˇci´c, 2004). If the experimental paradigm leads to fast nerve regeneration e.g. the crush injury model, functional impairment is transitory with reduced discomfort to the animal. On the other hand, in an ethical view point, the impact of the functional impairment induced by SNI on animal wellbeing should be taken into serious consideration in case of experimental conditions that induce long term functional impairment, e.g. chronic denervation and/or complex reconstruction treatments which require a long-term regeneration process.

2.9 Commercially available artificial nerve conduits

The majority of recent research efforts in the field of peripheral nerve grafting has emphasized enclosing (entubulating) opposing nerve stumps (of the severed nerve) in a non-neural tube (Nerve Guidance Conduit or NGC) fabricated from natural or synthetic materials (Johnson *et al*, 2008; Evans *et al*,2001; Udina *et al*,2004). The desired effect of nerve entubulation: is to increase the (i) number; (ii) speed, and (iii) length of the regenerating axons (Jordan *et al*, 2001) In addition, such biomaterials and their contiguous devices must have the appropriate dimensions to facilitate bridging the nerve gap defect without tension and the conduit width must also be able to house securely the two nerve end stumps without any compression (Archibald *et al*, 1995; Wang *et al*, 2001; Taras *et al*, 2005) The internal diameter and wall thickness of NGCs appears to influence the rate of nerve regeneration and, as such, the tube must be large enough to accommodate any swelling of the nerve without resulting in any compression of the nerve by swelling during degradation of the tubular construct (Kokai *et al*, 2009) The use of artificial NGCs enables the fabrication of a wide specification of conduit sizes to suit site-specific nerve lesions in mass production and as such offer significant advantages over autograft and allograft material. In brief, the design specification required: is a biocompatible and bioresorbable scaffold that supports outgrowing axons (neurite extension) within a microenvironment known to favour peripheral nerve regeneration, whilst minimizing the interactions between the myofibroblasts and axon growth. With these specifications for preparing optimum NGCs in mind, the FDA have approved the following products (devices) with regards their safety and efficacy in addressing the requirements to promote complete peripheral nerve regeneration across inter sump gaps (nerve lesions) and nerve crush injuries post traumatic injury (**Table 2.3**).Further the clinical trial data of some commercially available conduits are described in brief in **Table 2.4.**

2.9.1 Polyvinyl alcohol hydrogel (Salubridge^{TM}; SaluTunnel^{TM})

The Salubridge^{TM} nerve cuff device is composed of a hydrophilic and non-degradable biomaterial (called Salubria^{TM}) which is thermally crystallized from a

repeatedly freeze−thawed organic polymer solution containing the PVA molecular backbone in 20% (w/w) (CAS Registry Number 9002-89-5, −CH2CH(OH)−) and 0.9% sodium chloride (Seal *et al*, 2001; Stammen *et al*, 2001). Salubria™ can be easily moulded into customized anatomic shapes because it is gelatinous prior to the freeze/thaw processing (US Patent no. 5, 981, 82651). Salubridge™ nerve cuff (Salumedica LLC (Atlanta, GA) is a nerve protectant wrap based on the Salubria™ biomaterial. Salubridge™ is a flexible tubular sheath developed to provide a protective environment for peripheral nerve repair after injury. Salumedica LCC have also received 510k approval for the SaluTunnel™ nerve protector (August 2010); a device of identical composition and structure to the Salubridge™ device, with the only difference being a longitudinal slit to facilitate ease of surgical placement. SaluTunnel™ is indicated for the management of peripheral nerve injuries in which there has been no substantial loss of nerve tissue. Salubridge™ and SaluTunnel™ are currently available in different sizes (2, 5 and 10 mm internal diameter), with each device provided in a standard length of 6.35 cm. Both devices are provided sterile, hydrated in saline for presentation onto the operative field, and are single use only. However, the non-resorbable nature of this material lends itself to issues relating to nerve compression and tension at the suture lines after nerve regeneration has occurred.

2.9.2 Type I Collagen based devices (NeuraGen; Neuroflex; NeuroMatrix; NeuraWrap and NeuroMend)

NeuraGen (Integra Life Sciences Corporation (Plainsboro, NJ) was the first semi-permeable Type I collagen NGC to receive approval from the FDA in 2001. The NeuraGen1 device is available in two different lengths (2 and 3 cm) and a varying range of inner diameters (1.5−7 mm). The fibrillar structure of the collagen is maintained throughout the manufacturing process, permitting the construction of a biocompatible tubular matrix that has sufficient mechanical strength, defined permeability and a controlled rate of resorption (Archibald *et al*, 1991; Li *et al*, 1991; Li *et al*, 1992) However, this material is not expected to fully resorb for a period of up to 4 years post implantation (Jiang *et al*, 2010) Initial clinical experience using NeuraGen was reported by Taras *et al* (Taras *et al*, 2005) in a clinical study on 73

Product Name	Material	Degradation (months)	Diameter (mm)	Length (cm)	FDA approval no	FDA approval date	Company
NERVE CONDUIT DEVICES							
Neurotube	Polyglycolic acid (PGA)	3	2.3–8	2–4	K983007	22nd March, 1999/1995	Synovis Micro Companies Alliance Inc
NeuraGen	Type I collagen	36-48	1.5-7	2-3	K011168	22nd June, 2001	Integra Life Sciences Corp
Neuroflex	Type I collagen	4-8	2-6	2.5	K012814	21st Sept, 2001	Collagen Matrix Inc.
NeuroMatrix	Type I collagen	4-8	2-6	2.5	K012814	21st Sept, 2001	Collagen Matrix Inc.
AxoGuard Nerve Connector	Porcine small intestinal submucosa (SIS)	3	1.5-7	10	K031069	15th May, 2003	Cook Biotech Products
Neurolac	Poly(DL-lactidee-caprolactone); PCL	16	1.5-10	3	K032115/ K050573	10th October, 2003/4th May, 2005	Polyganics B.V.
SaluTunnel Nerve Protector	Polyvinyl Alcohol (PVA)	Nonabsorbable	2-10	6.35	K100382	5th August, 2010	Salumedica,
NERVE CUFF/NERVE WRAP DEVICES							
Salubridge	Polyvinyl Alcohol (PVA)	Nonabsorbable	2-10	6.35	K002098	24th November, 2000/2001	Salumedica.
AxoGuard Nerve Protector	Porcine small intestinal submucosa (SIS)	3	2-10	2-4	K031069	15th May, 2003	Cook Biotech Products
NeuraWrap	Type I collagen	36-48	3-10	2-4	K041620	16th July, 2004	Integra Life Sciences Corp
NeuroMend	Type I collagen	4-8	4-12	2.5-5	K060952	14th July, 2006	Collagen Matrix Inc.

Table 2.3. FDA approved nerve guidance devices (*Adapted with permission from* Kehoe et al, 2012**)**

NEURAGEN							
Study design	**Number**	**Nerve Location**	**Gap size (mm)**	**Follow-up (mths)**	**Complications**	**Results/Outcome**	**Ref**
Retrospective chart review	126 repairs 96 patients	Sensory	Range: 2.5–20; mean: 11.7 and 12.8	256 days to last follow-up	2 minor and 1 case of pulmonary embolism. All postoperative.	40/126 lost to follow-up. 26/126 quantitative testing: 35% reporting improvement and 31% requiring revision. 60/126 qualitative testing: with 45% reporting improvement and 5% requiring revision	Wangensteen *et al* 2009
Prospective cohort study	15 repairs 14 patients	Digital	Mean: 12.5_3.7	12	None	4/12 excellent; 5/12 good; 1/12 poor; 2/12 none.	Lohmeyer *et al*, 2009
Retrospective human	12 repairs	Digital	<20	12–22	None	4/9 excellent; 4/9 good; 1/9 fair	Bushnell *et al*, 2008
Retrospective human	9 repairs	Lingual and inferior alveolar	15	12-30	None	4/9 good; 4/9 some; 1/9 none	Farole *et al*, 2008
Retrospective human	5 repairs	Brachial plexus	<20	18–26	None	4/5 good (1 year follow-up); 3/5 excellent (2 years follow-up).	Ashley *et al*, 2006
Retrospective human	73 repairs	Median, ulna, radial, posterior interosseous common digital, superficial radial	<20	24	None	1/5 poor; Ongoing clinical study	Taras *et al*, 2005
NEUROTUBE							
Retrospective chart review	6 repairs	Median and ulnar	Range: 15–40; mean 28	Range: 4–66; mean 39	None	100% return to useful motor function. All patients had some return of motor function rated as M3a or greater by physical exam.	Rosson *et al*, 2009
Retrospective human	2 patients; 4 repairs	Median	30	Not available	None	Each patient recovered two-point discrimination with good localization in the thumb, index,	Donoghoe *et al*, 2007

NEUROTUBE Contd..							
Study design	**Number**	**Nerve Location**	**Gap size (mm)**	**Follow-up (mths)**	**Complications**	**Results/Outcome**	**Ref**
						and middle finger by 2 years after the nerve reconstruction. Almost 4 years post surgery, one had recovered 2PD to _4mm in the thumb and middle finger and 8mm in the index finger	
Retrospective human	1 patient 2 repairs	Digital	25	30	None	S2PD of the hallux was 4mm at 14.7g/mm2. The cutaneous pressure threshold for 1-point static touch was 0.7g/mm2.	Dellon *et al*, 2006
Series	13 patients received muscle-vein combined NGCs. 17 patients (19 repairs) PGA	Digital	Range: 10–40; mean 20	Range: 6–74; mean 30	None	77% showed VGa results (S3+ or S4)a, and 18% showed Ga results (S2+ or S3)a in the PGA group. 76.9% showed VGa results, whilst only 23.1% showed G results in the muscle-vein-combined group. There was no difference between the two groups in terms of functional recovery.	Battiston *et al*, 2005
Retrospective human	7 repairs	Facial	Range: 10–30	Range: 7–12	None	1 VGa, 4 Ga, 2 Pa	Navissano *et al*, 2005
Retrospective human	2 repairs; 1autograft 1 PGA	Cranial			None	PGA reconstructed nerve reached M5a trapezius function by 3 months, whilst the patient with the autograft reached M4a function by 6 months after reconstruction, and had persistent numbness of the ear lobe	Ducic *et al*, 2005
Prospective human	24 patients; 28 repairs	Palmar digital			None	93% Ga	Larao s *et al*, 2003
Retrospective human	1 repair	Medial plantar	20	Range 1–10	None	Pain resolved. At 8 months, Measurements for moving two-point discrimination were 3.8mm and 2.6 g/mrrr2 for the right and 3.8rnm and 5.0 g/mrn2 for the left hallux.	Kim *et al*, 2001

NEUROTUBE Contd..							
Study design	**Number**	**Nerve Location**	**Gap size (mm)**	**Follow-up (mths)**	**Complications**	**Results/Outcome**	**Ref**
RCMT-	98 patients; 136 repairs 46 PGA 56 controls	Digital	7.0 (a gap of 5mm was left intentionally, even in defects of 0–4mm); control 4.3	mean 9.4; control 8.1	In 9 patients, a delayed primary amputation was performed, whilst 3 patients had a partial NGC extrusion as a result of loss of the initially crushed skin flap.	There were no statistical differences between the 2 groups (control and NGC) overall. Excellent results obtained in 91% in the PGA group (3.7mm m2PD), whereas in the end-to-end group only 49% achieved excellent results (6.1mm m2PD), with P levels of 0.02 and 0.03, respectively. The PGA NGC provided superior results and eliminated donor-site morbidity over the standard end-to-end repair group.	Weber *et al*, 2000
Prospective human study	17 patients	Digital	20–35	4		All modalities tested demonstrated successful recovery.	Casanas *et al*, 2000
Retrospective human	1 repair	Right inferior alveolar	25	24		No recurrence of pain. At 24 months follow-up, pain relief remained excellent, and perception of pressure and vibration was similar to the thresholds for these perceptions on the contralateral lip.	Crawley *et al*, 1992
Series	15 patients; 16 repairs	Digital	5.0–30; mean 17	5.0–30; mean 17	11–32; mean 22.4	Excellent functional sensation (moving two-point discrimination less than or equal to 3mm and/or static two-point discrimination less than or equal to 6mm) was present in 33% and good functional sensation (moving two-point discrimination of 4–7mm and/or static two-point discrimination of 7–15mm) in 53% of the digital nerve reconstructions.1patient with poor sensory recovery and one with no recovery were judged as functional failures (14%). Absence of pain at the site of reconstruction was judged by the patient to be excellent in 40%, good in 33%, and poor in 27%.	Mackinnon *et al*, 1990

Neurolac							
Study design	**Number**	**Nerve Location**	**Gap size (mm)**	**Follow-up (mths)**	**Complications**	**Results/Outcome**	**Ref**
RCMT 5 hospitals (August 2002–March 2003)	30 patients 34 repairs 21 NGCs 13 controls (end-to-end suture)	Digital	<4–<20	3, 6, 9 and 12 months	Gap remained in the NGC group. Wound healing problems in the NGC group	Both groups comparable onsidering the demographics. More complications in the NGC group but none directly device related. Recovery of sensibility in the NGC group as least as good as in the control group. Nerve gaps of 2 cm can be treated with the NGC	Bertleff *et al*, 2005

Table 2.4. Brief Clinical Trial Data of commercially available nerve conduits (*Adapted with permission from Kehoe et al, 2012*)**.**

peripheral nerves (including median, ulnar, radial, posterior inter-osseous common digital, proper digital, and the superficial radial sensory nerve). Therapeutic observations of the peripheral nerve repairs utilizing NeuraGen yielded no rejection and only two cases of scar sensitivity. Patients tolerated splinting and range of motion (ROM) exercise, and resisted exercise without negative clinical consequences. Bushnell *et al*.,(Bushnell *et al*, 2008) published results of 14 digital nerve repair procedures with NeuraGen. Follow-up periods of 12 and 22 months were used for patients. The outcome showed four of the repairs exhibited good results; four patients achieved good sensibility and one patient demonstrated poor sensibility. In October 2010, Integra Life Sciences announced the results of the multi-centre human clinical trial comparing NeuraGen with direct suture repair for presentation at the joint meeting of the American Association for Hand Surgery (AAHS), American Society for Reconstructive Microsurgery (ASRM), and American Society for Peripheral Nerve (ASPN), 2011. 32 patients completed the 2-year postoperative follow-up period, during which they were routinely examined for sensory and motor electrophysiological function, post-operative pain assessments and overall hand-function. Results showed that patients who received NeuraGen had lower post-operative pain than those treated with direct suture repair. The overall study conclusion was that entubulation nerve repair using the NeuraGen is as

effective a method of joining severed nerves as direct microsurgical suture for short gap graft repair.

In the same year that NeuraGen received FDA approval, Collagen Matrix, Inc. (Franklin Lakes, NJ) received approval for the use of two (Collagen Type I) NGC devices; NeuroMatrix™ and Neuroflex™. Neuroflex™ is a white resorbable, flexible, non-friable, semi-permeable tubular matrix designed to create a favourable environment for axonal growth across a nerve gap defect and is kink resistance up to 1408 (US Patent No. 6,716,22572). The device slowly resorbs in vivo over a period of 4–8 months whilst its highly purified Type I collagen fibre structure provides the required mechanical strength at the site of repair. Neuroflex™ is currently the only flexible and kink resistant Type 1 collagen NGC on the market which has been designed to bridge nerve gap defects not exceeding 2.5 cm (Meek *et al*, 2008) Both devices are presented as crimped semi-permeable matrices having a pore size in the range of 0.001–0.005 mm to allow for nutrient transfer (Yuen *et al*, 2003)

In addition to the above devices, NeuraWrap™ (Integra Life Sciences Corporation, Plainsboro, NJ), a Type I collagen nerve protectant wrap, received approval for human use by the FDA in 2004. NeuraWrap™ is indicated to provide a non-constricting encasement for injured peripheral nerves. The wall of the NeuraWrap device has a longitudinal slit that allows the wrap to be positioned easily over the injured nerve. NeuraWrap has a porous outer membrane that mechanically resists compression from surrounding tissues whilst excluding scar tissue formation and a semi-permeable inner membrane that allows for nutrient permeation. NeuraWrap™ is available in inner diameter ranging from 3 to 10 mm of varying lengths: 2–4 cm.

NeuroMend™ (Collagen Matrix, Inc., Franklin Lakes, NJ) is also a Type I collagen nerve protectant wrap approved in 2006, and is compositionally identical to the above devices. NeuroMend™ has been designed to wrap a protective environment around an injured (crushed) peripheral nerve in which there has been no substantial loss of nerve tissue as opposed to addressing a complete peripheral nerve discontinuity. It is designed to unroll and self curl to best match the dimensions of the injured nerve (Li *et al*, 2004) It has also been shown to be well received by soft tissue and provokes limited inflammatory response, whilst exhibiting full levels of resorbability Li *et al*, 2004; Bostman *et al*, 2000)

2.9.3 Polyglycolic acid (Neurotube)

Polyglycolide (PGA) is a rigid thermoplastic, highly crystalline polymer (45–55% crystallinity) (Gunatillake *et al*, 2006; Stang *et al*, 2009) which exhibits a high tensile modulus with very low solubility in organic solvents (Tabesh *et al*, 2009). The device may be fabricated to from a knitted or woven tubular device, which is set (dry heat) to improve the tubes in vivo strength; followed by crimping of its exterior to have a corrugated exterior surface. Neurotube (Synovis Micro Companies Alliance, Birmingham, AL) is the first synthetic highly porous bioresorbable NGC to receive 510k approval by the FDA in 1999. Characteristics of this tube include, (i) porosity, which provides an oxygen-rich environment for the regenerating nerve; (ii) flexibility, to accommodate movement of joints and associated tendon gliding; (iii) corrugation, to resist the occlusive force of surrounding soft tissue; and (iv) bioabsorbability, eliminating the need for removal at a subsequent operation (Wolford *et al*.2003). An animal study comparing three commercially available, synthetic, bioabsorbable nerve conduits (NeuraGen, Neurotube and Neurolac) against the currently accepted gold standard autograft procedure however, has shown the Neurotube to exhibit the poorest results for functional motor recovery in the rat model; with a recovery rate of 15% for compound muscle action potentials (CMAPs) and 29% for muscle force (Shin *et al*, 2009). Moreover, Neurolac and NeuraGen remained structurally stable after 12 weeks, whilst the Neurotube had completely collapsed. The first clinical study for Neurotube was reported by Mackinnon and Dellon105 on a series of 15 patients; in which they used PGA NGCs to repair digital nerve defects up to 3 cm. In that study, excellent results were reported for 5 patients (33%), good results for 8 patients (53%), and poor results for 2 patients (14%) (Mackinnon and Dellon *et al*, 1990). Weber *et al*. reported results for the first large multicenter clinical trial for Neurotube which generated very encouraging results (Weber *et al*, 2000). This prospective randomized trial used Neurotube to reconstruct sensory nerve defects in 136 nerve repairs in the hand, was divided between two groups. Group 1 comprised patients receiving repairs with either end-to-end anastomosis (for gaps less than 8 mm) or nerve graft repairs (for gaps exceeding 8 mm) Group 2 comprised patients treated with Neurotube. The observations after 1 year showed superior sensory results were obtained in the Neurotube1 groups with excellent and good outcomes in 44% and 30% of the repairs respectively; compared with 43% of both excellent and

good outcomes after standard repairs. Further clinical reports have investigated the Neurotube conduit for motor reconstruction and specifically their efficacy in the reconstruction of the spinal accessory nerve due to cautery injury (Ducic *et al*, 2005); the reconstruction of several facial nerves injuries (Navissano *et al*, 2005) and median nerves in the forearm (Donoghoe *et al*, 2007). Rosson has published a retrospective chart review of six patients having received bioabsorbable Neurotube NGCs across short gap motor nerve injuries over a 7-year period. The outcome demonstrated favourable results with all patients having some return of motor and sensory function (Rosson *et al*, 2009).

2.9.4 Poly D,L lactide-co-e-carprolactone (Neurolac)

Poly D,L lactide-co-e-carprolactone (PCL) in the form of a hydrophobic semi-crystalline polyester (crystallinity decreases with increasing molecular weight (Woodruff *et al*, 2010; Nair *et al*, 2007) has also received approval as a resorbable device for peripheral nerve repair. PCL has gained considerable interest in the research field due to its ease of fabrication and low processing costs. Its high processibility is attributed to the fact that PCL is highly soluble in a wide range of organic solvents (Stang *et al*, 2009) and moreover, its crystalline nature enables easy formability at relatively low temperature (Casanas *et al*, 2000). PCL has a relatively low tensile strength of 23 MPa coupled with an extremely high elongation at breakage (>700%). Degradation of PCL occurs in the form of hydrolysis due to the presence of hydrolytically labile aliphatic ester linkages and may also occur actively (enzymatically) with a slow rate of degradation between 2 and 3 years.(Nair *et al*, 2007; Meek *et al*, 2008). Its degradation products consist of succinct acid, butyric acid, valeric acid and caproic acid, which are non-toxic and do not cause an inflammatory response (Sanchez *et al*, 2000) These degradation products are less acidic than PLA and may cause less damage to the surrounding tissue environment (Luis *et al*, 2007; Meek *et al*, 2008) Meek and den Dunnen138 evaluated the short term (in vivo) effects of Neurolac across a 10 mm nerve gap defect for evaluation after 12 weeks implantation in 10 male Black Hooded rats (Meek *et al*, 2009). After 5 weeks, no improvement of nerve regeneration was evident and the NGC walls were so swollen that lumen blockage and crack formation was evident. At 8 weeks, some myelinated nerve fibres appeared distal to the NGC due to lumen blockage. After 12 weeks, only some myelinated nerve fibres were evident, as at this time period.

Neuromas had occurred proximal to the NGC with further evidence of fragmentation. In the same year, Meek *et al* published results on 4 Neurolac NGCs implanted into adult male wistar rats across a 15 mm nerve gap defect; whose results indicated that the sciatic nerve function was not measurable due to automutilation and flexion contractures, whilst the gait stance duration showed no improvement with time coupled with the presence of a disturbed walking pattern. Whilst some clinical reports have been negative (Meek *et al*.2006) Neurolac NGCs have been the basis of a randomized clinical trial (30 patients with up to 20 mm long lesions of hand nerves were repaired (Meek *et al*, 2007) Patients were randomized for treatment either with autologous nerve grafts or with Neurolac. Whilst more complications were reported for the Neurolac group; none were directly device related.

2.9.5 Conclusions

Since 1995, 11 devices (NGCs and nerve protectant wraps) based on natural and synthetic materials have been approved by the FDA for the repair of peripheral nerve injuries. Whilst autograft remains the gold standard, a large amount of published prospective and retrospective clinical studies have been performed with NeuraGen (collagen type I NGC) and have demonstrated its comparable efficacy to autograft in discontinuities up to 20 mm. In respect, of synthetic materials, and based on the weight of published clinical evidence (including prospective, series, retrospective and RMCTs), Neurotube (PGA NGC) has the most comprehensive history when compared with other synthetic devices.

Chapter 3

Silk-Gold nanocomposite based scaffolds for neural tissue engineering

3.1 Introduction

Damage of peripheral nerve results from traumatic injuries caused by accidents, physical conflict as well as during surgical intervention. Peripheral nerve injuries are primarily characterised by flaccid atrophy of surrounding muscles leading to partial or complete paralysis. Seddon had classified neurotmesis as the most severe form of peripheral nerve injury where the nerve is completely severed with limited chance of axon re-growth making surgical intervention essential. Neurotmesis grade injuries with a gap larger than 5 mm rarely show complete axonal reconnection and functional regeneration (Cunha et al, 2011). Surgical intervention in large nerve gaps generally involves grafting a part of nerve harvested from a healthy area into the damaged area. Although autografts remain the clinical gold standard for repairing large nerve gaps, the technique is largely fraught with donor site morbidity in the secondary surgical site and inefficient functional regeneration. While many studies have shown autografts to be superior to the available conduits there have been reports indicating an increased growth of nociceptive fibers along autografts which result in high autotomy among animals (Daly et al, 2013; Berrocal et al, 2013). An alternative approach to nerve autograft is entubulation of nerve gaps using nerve conduits or nerve guides made of synthetic or natural polymers.

In the present study, silk fibroin nanofibers have been used to fabricate functional nerve conduits, exploiting the biocompatibility and biomimetic properties of silk protein. Silk fibroin films functionalized with nerve growth factor (NGF) promotes neurite outgrowth and modulates functional properties of dorsal root ganglion (DRG) neurons (Benfenati et al, 2012**).** Silk based nanofibers have been proven to facilitate neural regeneration along artificially fabricated nerve guides, both in the CNS and PNS by providing topographical guidance along the length of a nerve conduit. Further the incorporation of nerve growth factor (NGF) and glial-derived nerve factor (GDNF) within silk fibroin nanofibers leads to trophical functionalization of nerve guidance conduit thereby potentially enhancing functional recovery of injured peripheral nerves (Madduri et al, 2010; Dinis et al, 2013). The ability of aligned nano-scale fibers to direct the neurite outgrowth and Schwann cell migration enables scientists to influence cell-biomaterial interaction and design appropriate conduit

architecture to enhance functional nerve regeneration (Wang et al, 2010; Qu et al, 2013).

The use of nanoparticles in neurology has been largely limited to applications in drug delivery and diagnostics. There are very few reports on the use of nanoparticles for enhancing nerve regeneration. An US group described the neuroprotective abilities of autocatalytic ceria nanoparticles in adult spinal cord neurons (Das et al, 2007). Uptake of magnetic nanoparticles in regions of spinal cord injury was also studied by another team to evaluate the potential of magnetic nanoparticles as vector systems for in situ gene delivery in nerve injury sites.

Electrically active silk scaffolds based on carbon nanotube (CNT) have been explored to facilitate signal transmission across a nerve gap through the conduit. Such conduits can easily interface with neuronal circuits, synapses and facilitate conduction of nerve impulse thereby promoting neural regeneration (Fabbro et al, 2013). Silk-single walled carbon nanotubes (SWCNT) based composite conduit was also found to promote neural regeneration when implanted across a 10mm sciatic nerve injury model (Mottaghitalab et al, 2013). The present study demonstrates the fabrication of nanocomposite comprising of gold nanoparticle-silk fibroin nanofiber (GNP-SF) which appreciably decreases the resistance of an electrically insulating material like silk thereby making the scaffold more suitable for neural tissue engineering applications.

3.2 Materials and Methods

3.2.1 Cytotoxicity of synthesized GNPs

Cytotoxic effect of *Centella asiatica* mediated synthesized gold nanoparticles (GNP) was assessed by MTT assay on rat schwann cell line (SCTM41) following standard assay procedures (Mosmann et al, 1983). Briefly, the nano-particle solution was lyophilized to get GNP as powder form. A stock solution (10mg/ml) was prepared in Dulbecco's modified eagle's medium (DMEM) without serum. This solution was used to make further working concentrations (5µg/100µl to 500µg/100µl) of GNP against which MTT assay was done. The cells were cultured in 96 well cell culture plates and incubated with various concentrations of GNP (5µg/100µl to 500µg/100µl) in serum free DMEM for 24 hour in a CO_2 incubator (Make - Healforce) under 37^0C and relative humidity 90%. This was followed by addition of DMSO and recording absorbance at 570nm using a UV-VIS multiwell plate reader (Make-TECAN) (Ribble et al, 2005)

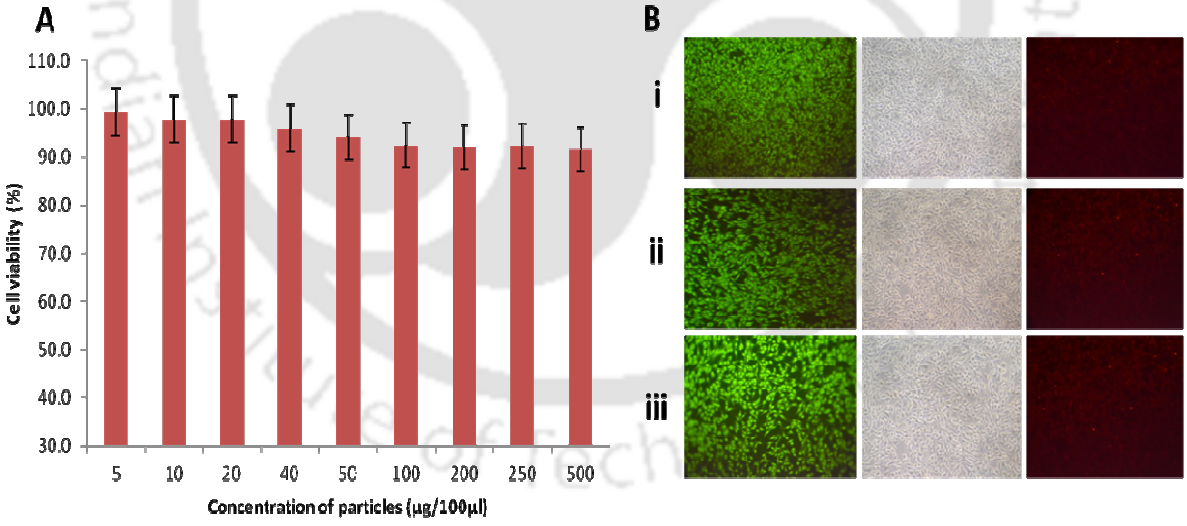

Fig 3.1: Cytotoxicity of GNPs. A, MTT assay of GNPs on rat Schwann cell line SCTM41. Each concentration was done in triplicate to generate standard deviation. **B**, Live-dead staining assay with acridine orange (AO) and ethidium bromide (EtBr).The assay was done by treating the cells with GNP concentration of 5µg/100µl (i), 50µg/100µl (ii) and 500µg/100µl (iii). The live cells are stained green from AO while the dead cells stain red with EtBr.(*Reprinted with permission from Das et al, Data in Brief, 2015*)

3.2.2 Fabrication and characterization of nanocomposite mat

Bombyx mori silk cocoons were purchased from local market in Guwahati, Assam. Degumming of cocoons was done by standard protocol reported earlier (Rockwood et al, 2011). The degummed silk fibroin fibers were rinsed thoroughly with distilled water and dried at 50^{o}C overnight. Gold nanoparticles (GNP) were synthesized following a method reported earlier by our laboratory and were stored at 4^{0}C (Das et al, 2010). Degummed silk fibroin fibers (1g) were kept submerged in the GNP solution (100ml) and stirred at room temperature for 10 minutes until most of the particles were adsorbed onto the silk fibroin fibers. Both the pristine silk fibroin and the GNP incorporated silk fibers were dissolved in a chaotropic solvent (e.g Lithium bromide) and subsequently dialysed against distilled water and finally freeze dried as per standard procedures (Kim et al, 2005). The freeze dried powder of pristine and GNP incorporated silk fibroin protein were separately dissolved in formic acid (98% pure) at a concentration of 100mg of protein/ml along with 1mg/ml of polyethylene oxide (PEO). The mixture was electrospun using an electrospinning machine (Make – Physics Equipment Company; Model – ESPIN-NANO) to form silk fibroin nanofibrous scaffold (SF) and gold nanoparticle-silk fibroin nanocomposite (GNP-SF) following standard procedures (Rockwood et al, 2011).

The uptake of GNPs by the degummed silk fibers was monitored by UV-Visible Spectrometer. The GNP incorporated silk fibers as well as the pristine degummed silk fibers were visualised under transmission electron microscope (TEM). The electrospun nanocomposite mat was dried overnight and scraped before X-Ray Diffraction studies. The mats were further viewed under Field Emission Electron Microscope (FESEM) to study the architecture of the nanofibers. Energy dispersive X-ray analysis (EDAX) was also performed on multiple locations over the nanocomposite mat to check for the presence of gold (Au).

For electrical conductivity measurements the electrospun mats were placed on aluminium coated corning glass and adhered with silver paste**.** (Das et al, 2015) A piece of corning glass was first coated with aluminium using a suitable masking agent to generate a 2mm thick uncoated strip in the middle. In order to study the electrical resistance, a 1cm x 1cm portion of the electrospun silk fibroin (SF) and

gold nanoparticle-silk fibroin nanocomposite (GNP-SF) sheet was placed over the uncoated strip with its edges fixed on the aluminum coated section by silver paste.

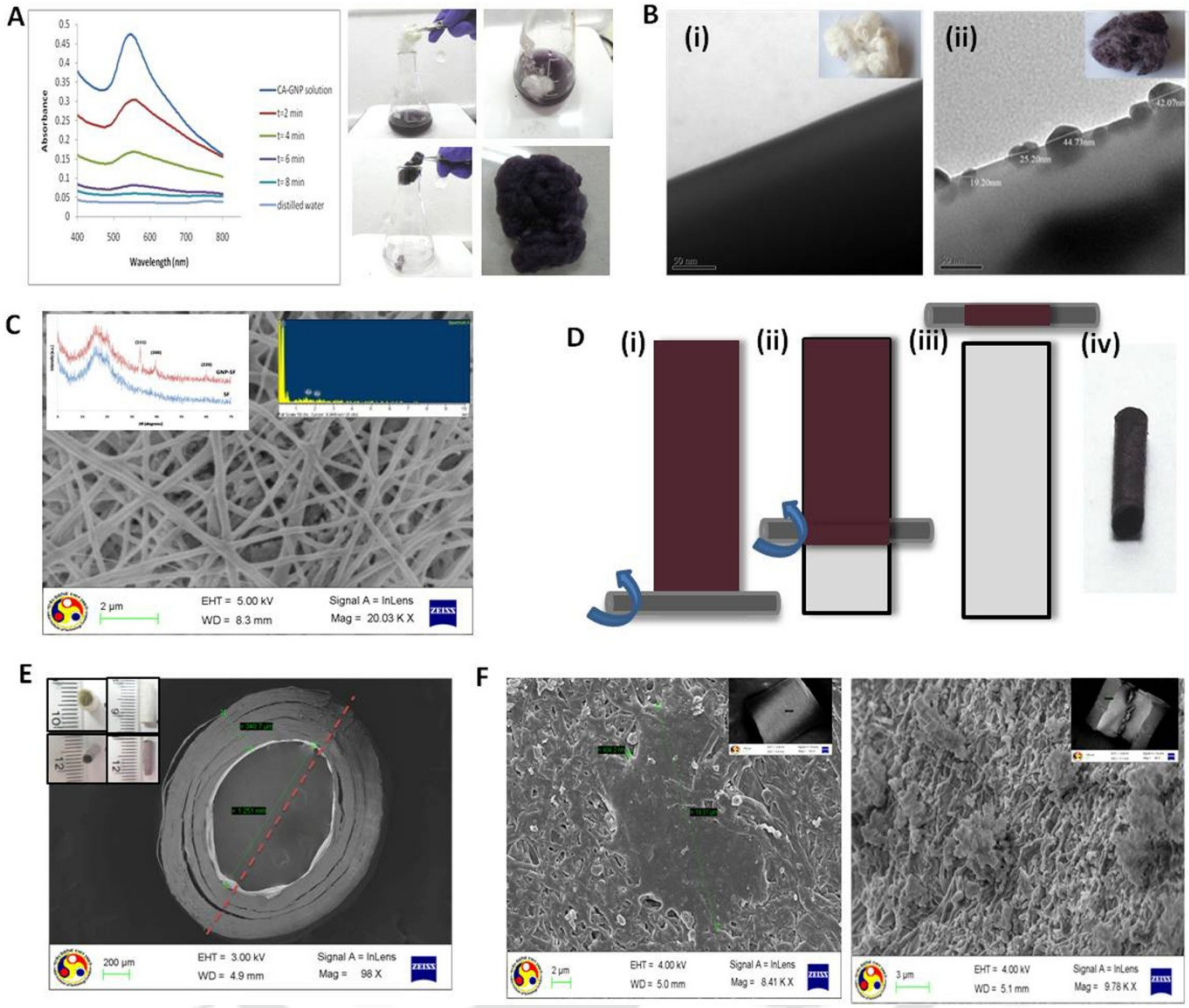

Fig 3.2: Fabrication and characterization of pre-seeded nanocomposite conduits. A, Adsorption of gold nanoparticles by degummed silk fibroin fibers and subsequent colouration of silk fibers with concomitant decrease in intensity of 540 nm peak as recorded by UV-VIS spectrometer. **B**, TEM micrographs of (i) pristine degummed silk fibers and (ii) gold nanoparticle-silk fibroin composite. **C**, FESEM image of gold nanoparticle-silk fibroin nanocomposite nanofibers without gold sputter coating of the sample. Scale bar 2µm. The nanocomposite formation was confirmed by XRD and EDAX analysis (inset). **D**, Fabrication of nerve conduits by novel sheet rolling method. The electrospun sheet was peeled off and rolled on a stainless steel mandrel of specific dimensions (**i-iii**) to form a nerve conduit (iv). **E**, Cross-sectional view of a typical nerve conduit as observed under FESEM. Scale bar 200 µm. Digital photographs of silk fibroin (white) and gold nanoparticle-silk fibroin nanocomposite nerve conduit (purple) prepared for implantation in rat (inset). **F**, Culturing Schwann cells (SCTM41) on nerve conduits with the gross pictures of conduit portions in the inset. Cells were found to adhere and proliferate on the outer (left) as well as on the inner surface (right) of the nerve conduits. (*Reprinted with permission from Das et al, Biomaterials, 2015*)

An I-V graph was generated for GNP-SF sample (**Fig 3.6**) and the resistance of the materials was calculated.

3.2.3 Culture of Schwann cells over nanofibrous scaffolds

Pristine silk fibroin and GNP incorporated silk fibroin nano fibers were collected in cover slip separately for 2D culture of cells. Cover slips were treated with methanol and UV ray for conversion to ß sheet and sterilization. They were then washed 3-4 times with sterile phosphate buffer saline (PBS) and incubated with DMEM containing 10% FBS for 24hrs in CO_2 incubator for conditioning. SCTM 41 cells (Rat Schwann cell) were seeded over cover slips and incubated for 10 days. On fifth day cover slips were processed for FESEM analysis to monitor cell adhesion. Cellular proliferation was also quantitatively studied over the cover slips by MTT analysis at 0, 5^{th} and 10^{th} day.

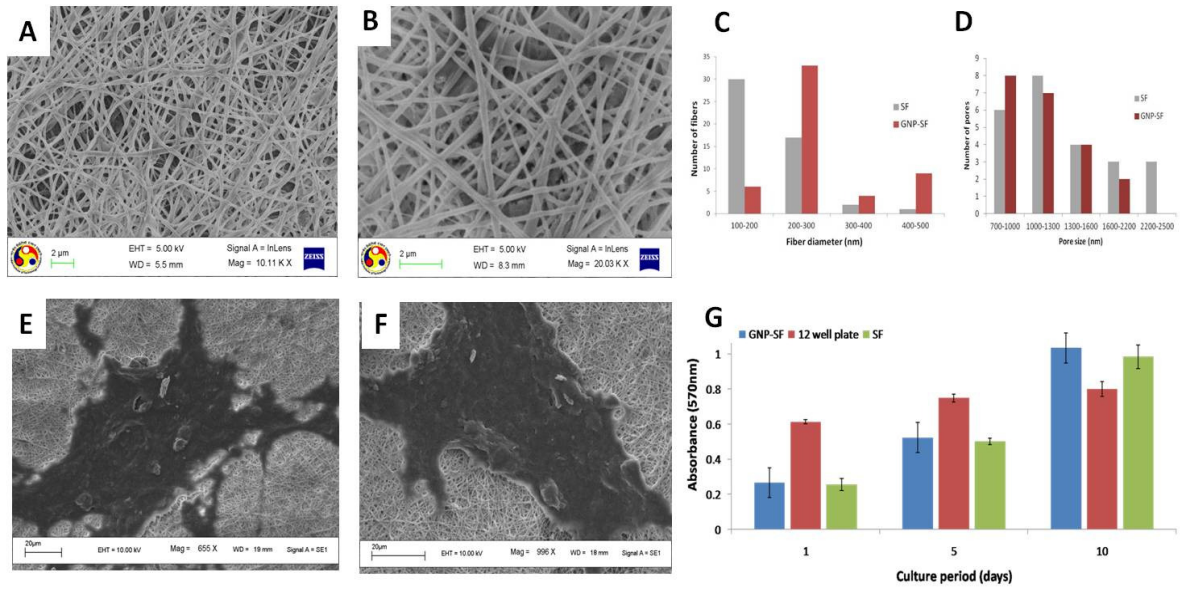

Fig 3.3: Architecture of nanofibers and culture of Schwann cells over nanofibrous scaffolds. A, FESEM image of SF nanofibrous scaffold and **B**, nanocomposite (GNP-SF) nanofibrous scaffold. **C**, Size distribution of nanofibers calculated using Image J (NIH, USA), **D**, Pore size distribution of the nanofibrous scaffolds calculated using Image J (NIH, USA), **E**, FESEM image of SF nanofibrous scaffold after 5 days of culturing Schwann cells (SCTM41) and **F**, FESEM image of GNP-SF nanocomposite nanofibrous scaffold after 5 days of culturing Schwann cells (SCTM41), **G**, Cell proliferation study by MTT assay by culturing Schwann cells for 10 days over GNP-SF and SF scaffolds keeping one well of 12-well culture plate as control.(*Reprinted with permission from Das et al, Data in Brief, 2015*).

3.2.4 Fabrication of nerve conduit and pre-seeding with Schwann cells

Immediately after electrospinning, the nanofibrous mat (made either of GNP-SF or SF) was slowly peeled off the aluminum sheet and rolled onto a stainless steel needle and pressed together so that each layer adhere to one another **(Fig 3.2 D**). The rolled conduits were sterilized by treatment with methanol followed by UV exposure. All fabricated conduits were washed with sterile phosphate buffered saline (PBS), pH=7.4 to remove residues of methanol. Conduits were then conditioned by keeping in Dulbecco's Modified Eagle's Medium (DMEM) with 10% Fetal Bovine Serum (FBS) in CO_2 incubator for 24 hours. Conduits were washed again with sterile PBS following UV sterilisation before implantation in rat.

For preparation of cell loaded conduit the same was seeded with SCTM 41 (rat Schwann cell) and incubated for five days with regular replacement of media. These conduits were also washed 3-4 times with sterile PBS before implantation.

3.2.5 Porosity and Swelling ratio of Nerve conduits

The porosity of the conduits was determined by a previously described ethanol displacement method (Tang et al, 2013). Briefly, the dimensions of the conduits (n=4) were precisely measured using a vernier caliper and the volume (V) calculated according to the following formula –

$V = \pi(R^2 - r^2)h$, where R was the outer radius of the conduit, r was the inner radius of the conduit and h was the length of the conduit. The conduits were then weighed in dry condition (M_o) and immersed in ethanol for 24 hours before being weighed again to get M_t. The porosity of the conduit was calculated according to the following formula –

$$Porosity\ (\%) = \frac{(M_t) - (M_o)}{V \times \rho} \times 100$$

Where, ρ is the density of ethanol (0.79g/cc). Both SF and GNP-SF conduits were found to have low porosity.

The dynamic swelling ratio of the nerve conduits was measured according to a previously described method (Wang et al, 2014)The conduits were immersed in

phosphate buffered saline (pH 7.4) and the swelling ratio was calculated periodically every hour according to the following formula –

$$Swelling\ ratio\ (\%) = \frac{(W_s - W_d)}{W_d} \times 100$$

Where W_s is weight of the conduit in swollen state and W_d is the dry weight.

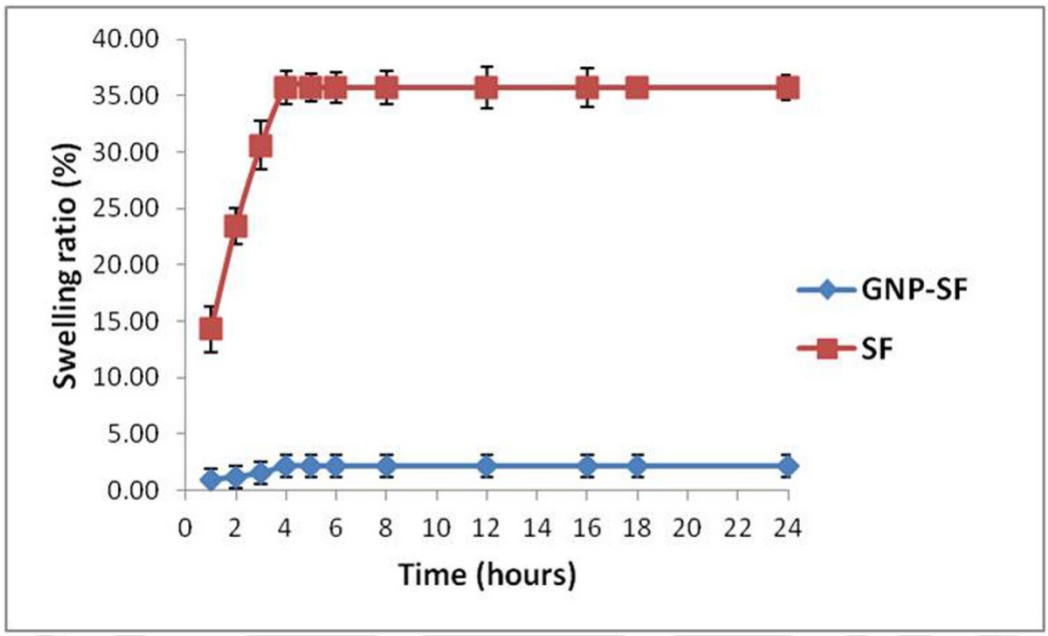

Fig 3.4: Swelling ratio of conduits. The dynamic swelling ratio of the conduits were calculated periodically every hour upto 24 hours. (*Reprinted with permission from Das et al, Data in Brief, 2015*)

3.2.6 *In vivo* intra dermal test

Intra-cutaneous irritation and toxicity studies were performed on Sprague Dawley rats (n = 9) following standard procedures as described in ASTM standard protocol for "Standards Used in Meeting Requirements for a Model Pre-Market Approval (PMA) of a Neural Guidance Conduit" (ASTM STP 1452). Briefly, 24 hour saline extract of the silk fibroin (n=3) and GNP-incorporated silk fibroin conduit (n=3) were taken and injected intradermally. Normal saline was injected in the control group (n=3) (**Fig 3.5C**). The animals were observed for 72 hours.

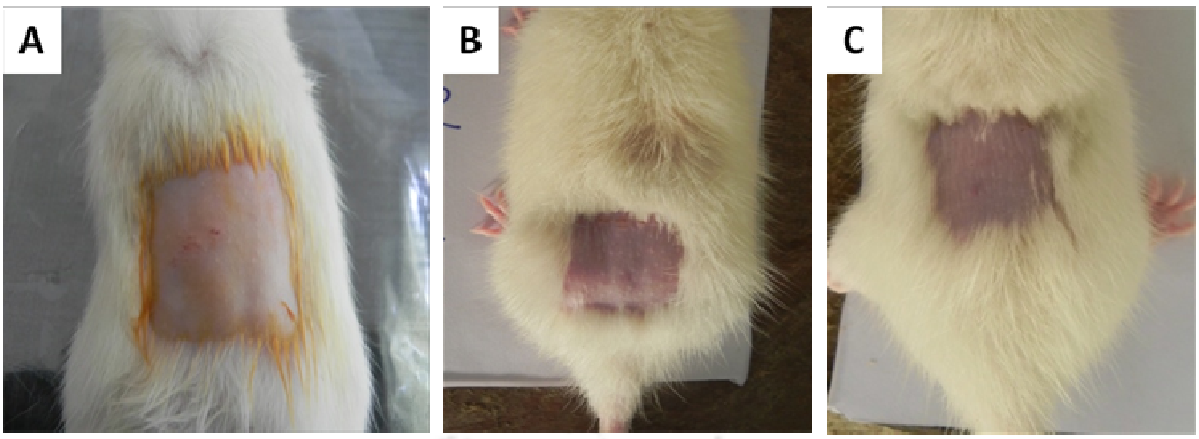

Fig 3.5: In vivo intra cutaneous irritation test. The animals observed after 72 hours of injecting saline extract of **A**, GNP-SF conduit and **B**, SF conduit. **C**, In the control group only saline was injected. (*Reprinted with permission from Das et al, Data in Brief, 2015*)

3.2.7 Surgical implantation of nerve conduits and Magnetic Resonance Imaging (MRI)

Clinically healthy sub-adult (12weeks) Sprague Dawley rats with average body weight of 250g considered for the study were procured from authorized supplier and were housed under good managerial condition under veterinary supervision following CPCSEA, India and Institutional Animal Ethical Committee (IAEC) guidelines at College of Veterinary Sciences, AAU, Khanapara, Assam. An outline of the surgical procedure performed is depicted in the data article (Das et al, 2015).

All animals were anaesthetized using Ketamine (50-100mg/kg bwt, i/p) and Xylazine (5mg/ kg bwt, i/p) after Atropine (0.05mg/ kg bwt, i/p) as pre-anaesthetics. The region below the hip joint was prepared for surgery and an incision was made on the right leg covering the upper thigh and lower gluteal region to expose the sciatic nerve. 10mm length of sciatic nerve was transected out before it branches to fibular, tibial and sural nerve. The nerve gap was left untreated in the control group. In other groups conduit was sutured to both proximal and distal end of the nerve stumps by 7-0 polypropylene suture (Ethicon). Surgical wound was closed with 6-0 black braided silk suture (Ethicon). Post operatively antibiotic and NSAID were followed for seven days with regular dressing and antiseptic spray. Suture was removed on tenth day. The implantation of all the conduits was evaluated by magnetic resonance imaging (MRI) of the operated leg one week after implantation. [23] The details of all the groups maintained are delineated in **Table 3.1.**

Groups	Name	Number of animals	Description
1	Control	8	10 mm nerve gap was created and left without treatment.
2	SF	8	10 mm nerve gap was created and gap was filled up with SF Plain conduit.
3	SF Cell	8	10 mm nerve gap was created and gap was filled up with SF conduit seeded with Rat Schwann Cell.
4	GNP-SF	8	10 mm nerve gap was created and gap was filled up with GNP Plain conduit.
5	GNP-SF Cell	8	10 mm nerve gap was created and gap was filled up with GNP conduit seeded with Rat Schwann Cell.

Table 3.1: Outline of animal groups maintained

For confirming the accuracy of implantation, the animals were subjected to MRI imaging using a 1.5 Tesla MRI machine (Make-Philips Model- Achieva) and a 40mm diameter coil one week post implantation.

3.2.8 Functional analysis of regenerated sciatic nerve

The functional regeneration of sciatic nerve was monitored by electrophysiological studies and walking track analysis. The electrophysiological studies were conducted using an electromyogram (EMG) machine (Make – Nicolet Model- Viking Quest). Animals were chemically restrained using sedative dose of Xylazine **(**1mg/kg body wt**)** and Ketamine (100mg/kg body wt) and placed on ventral recumbency over a wooden table. Area concerned was shaved and disinfected before recording. Grounding electrode was attached to the base of tail as shown in the data article [23]**.**

For recording nerve conduction velocity (NCV) and compound muscle action potential (CMAP), percutaneous stimulation of sciatic nerve with bipolar electrode was done first at the proximal end of the implanted conduit at the level of hip joint

and second distal stimulation point was at level of poplieal fossa. Distance between the two points was measured for calculating NCV.

Motor unit potentials (MUPs) were recorded by inserting a bipolar needle electrode into the gastrocnemius muscle. Sensory stimulus was provided by interdigital pinch.

For walking track analysis a blank white paper was placed on a walking track of 16 inch length and 3 inch breadth for obtaining the foot prints. The hind limbs of the animals were painted with methylene blue and they were allowed to walk through the track. Subsequently Sciatic Functional Index (SFI) was calculated using the following formula.

$$\text{SFI} = -38.3\left(\frac{EPL - NPL}{NPL}\right) + 109.5\left(\frac{ETS - NTS}{NTS}\right) + 13.3\left(\frac{EITS - NITS}{NITS}\right) - 8.8$$

where , EPL – Experimental print length

NPL - Normal print length

ETS –Experimental toe spread

NTS – Normal toe spread

EITS – Experimental inter toe spread

NITS - Normal inter toe spread

3.2.9 Morphological analysis of regenerated sciatic nerve

Samples for histological analysis were collected in 10% neutral buffer formalin (Make-Sigma Aldrich) at an interval of nine and eighteen months after surgery by euthanizing the animal with intravenous over dose of Thiopentone sodium. Conduit was isolated and processed for Hematoxylin & Eosin (H&E) staining and cross sectional images were taken at 400X magnification. For TEM studies, cross-sections of the regenerated nerve after 18 months were stained with osmium tetra-oxide and processed by standard protocol.

3.3 Results

3.3.1 Cytotoxicity of synthesized GNPs

The gold nanoparticles synthesised using ethanolic extract of *C. asiatica* were found to be non-toxic to Schwann cells upto a concentration of 500µg/ml (**Fig 3.1A**). Live dead assay with Acridine orange and Ethidium bromide conducted with GNP concentration of 5 µg/ml (**Fig 3.1B i**), 50 µg/ml (**Fig 3.1B ii**) and 500 µg/ml (**Fig 3.1B iii**) revealed normal cellular morphology upto the highest concentration of 500µg/ml. The live cells preferentially take up Acridine orange (green) whereas Ethidium bromide (red) stains the nuclei of dead cells (Ribble et al, 2005).

3.3.2 Fabrication and Characterization of nanocomposite mat

The rapid discolouration of the gold nanoparticle (GNP) solution was found to be accompanied by purple colouration of the degummed silk fibroin fibers with a concomitant decrease in peak intensity at 540nm of visible spectra. (**Fig 3.2 A**). We observed that the GNPs were impregnated along the surface as well as inside the silk fibroin fibers (**Fig 3.2B**). The electrospun silk fibroin nanofibers had diameters in the range of 100nm – 200nm and pores of size 1000-1300nm whereas diameters of the nanocomposite nanofibers were mostly in the range of 200nm – 300nm with pores predominantly in the range of 700-1000nm as evident from FESEM analysis [23]. Elemental analysis by EDAX revealed the presence of gold (Au) upto a concentration of 1.71% by weight of the nanocomposite mat (**Fig 3.2C**). XRD analysis of the electrospun nanocomposite scaffolds showed sharp peaks around 2θ = 38.5, 44.5 and 64.95 degrees and a broader peak around 2θ = 21 degrees (**Fig 3.2C**). The I-V characteristic obtained for GNP-SF nanofibers was found to be mostly ohmic. Electrical resistance of the nanocomposite scaffolds, calculated from the slope of the I-V curve was found to be $0.48 \times 10^{9}\Omega$ for GNP-SF nanofibers as compared to $12 \times 10^{9}\Omega$ (graph not shown) for silk fibroin nanofibers.

3.3.3 Culture of Schwann cells over nanofibrous scaffolds

The cells were found to adhere and grow over the surface of electrospun nanofibers (**Fig 3.3 A-B, E-F**). MTT assay of cells growing over the scaffolds exhibited

subsequent increment of absorbance with time over a period of 10 days as compared to a more saturated growth in control group of 12 well tissue culture plate (**Fig 3.3 G**).

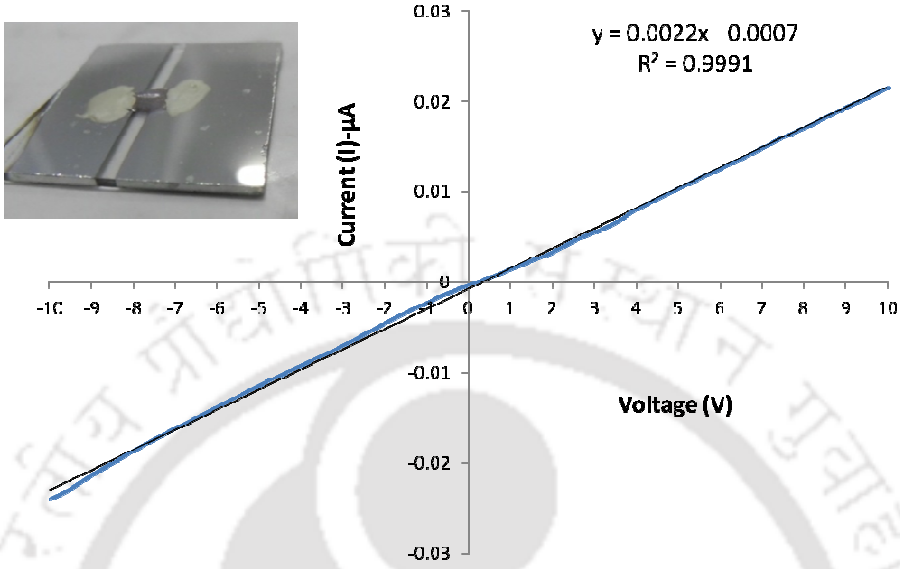

Fig 3.6: Electrical property of GNP-SF nanocomposite scaffold. The figure shows the ohmic nature of the I-V characteristic of the GNP-SF nanocomposite scaffold with the experimental setup in inset. (*Reprinted with permission from Das et al, Data in Brief, 2015*)

These results indicate enhanced cellular proliferation over porous nano-scaffolds with higher surface area to volume ratio than conventional tissue culture plates with similar dimensions. However, no appreciable difference was observed in rate of proliferation between GNP-SF and SF scaffolds.

3.3.4 Morphology of nerve conduits and Schwann cell adhesion and proliferation

FESEM images showed that the fabricated conduits had an internal diameter of 1.25mm and a wall thickness of 0.34mm with a lamellar architecture comprising multiple layers of nanofibers (**Fig 3.2 E**). Electron microscopic observations of conduits cultured with rat Schwann cell line (SCTM41) showed adherence of cells, formation of cell clusters and growth of cells in three dimensions on both inner and outer surface of GNP-SF as well as SF conduits (**Fig 3.2 F**).

3.3.5 Porosity and Swelling ratio of Nerve conduits

The porosity of SF nerve conduit was found to be 15.6% ($\pm$ 0.3) while GNP-SF conduits exhibited minute porosity of 5.37% ($\pm$0.08).

The SF conduits saturated at a swelling ratio of 35.7% while GNP-SF conduits showed a maximum swelling of only 2.1% (**Fig 3.4**).

3.3.6 *In vivo* intra dermal test

The 24 hour saline extract of the GNP-SF (**Fig 3.5A**) and SF conduits (**Fig 3.5B**) did not produce any abnormal clinical symptoms, oedema or erythema in the animals. The site of administration of the extract did not exhibit any abnormality as compared to the control saline group upto 72 hours from the time of intra-dermal injection.

3.3.7 Surgical implantation of nerve conduits

The dimensions of the conduits were found to be suitable for implantation in a rat sciatic nerve. The texture and strength of the conduits were also appropriate and could withstand the implantation and suturing process without any deformation. The MRI image of the thigh region post implantation reveals accurate implantation of the conduits and no deformation or delocalisation of the conduits from their implanted position was observed.

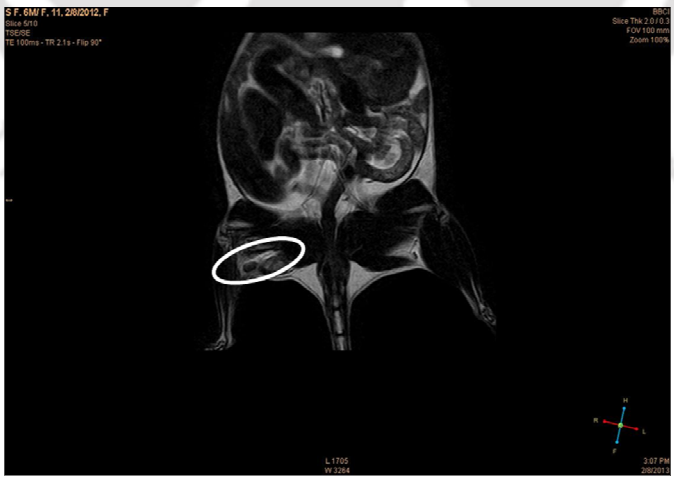

Fig 3.7: Magnetic resonance imaging of animals. The implanted conduit could be visualized (encircled area) by MRI after a week of implantation. *(Reprinted with permission from Das et al, Data in Brief, 2015*)

3.3.8 Functional analysis of regenerated sciatic nerve

A normal nerve was found to exhibit NCV of 59m/sec, CMAP of 17.5mV, MUP of 152μV and an ideal SFI of 0. The results of electrophysiological studies and walking track analysis are presented in **Fig 3.9 and Fig 3.10**. Immediately post implantation of the conduits a minute MUP of 32μV was observed in all the groups. At 9 months after implantation the animals with nanocomposite conduits without Schwann cells (GNP-SF) exhibited NCV of 54m/sec, CMAP of 3.4mV, MUP of 105μV and SFI of -55. Animals having pre-seeded nanocomposite conduits with Schwann cells (GNP-SF cell) after 9 months showed NCV of 58m/sec, CMAP of 7.8mV, MUP of 112μV and SFI of -47. The silk fibroin conduits without Schwann cells (SF) exhibited NCV of 22m/sec, CMAP of 4.3mV, MUP of 85μV and SFI of -75 after 9 months. Pre-seeded silk fibroin conduits with Schwann cells (SF cell) after 9 months showed NCV of 29m/sec, CMAP of 4.4mV, MUP of 105μV and SFI of -73.

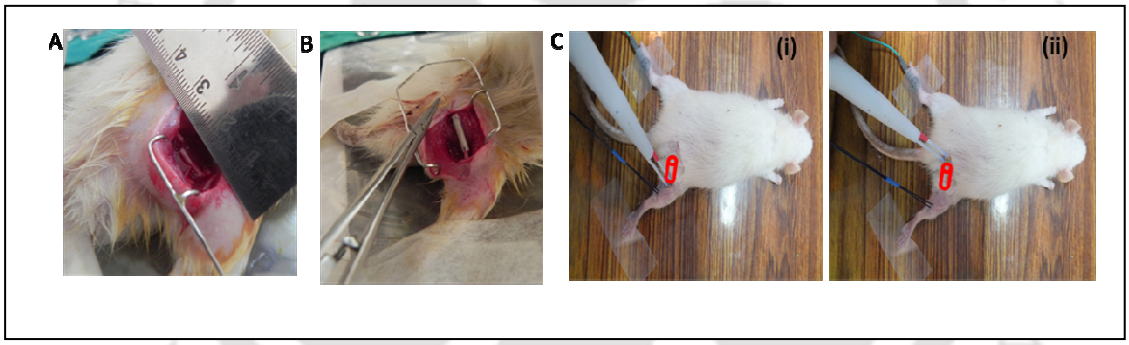

Fig 3.8: Surgical implantation and electrophysiological study. **A,** Rat sciatic injury model having a 10mm gap was created. **B,** The fabricated nerve conduits were implanted within the gap and sutured to the proximal and distal ends of the nerve stump. **C**, Experimental setup for conducting NCV and CMAP studies with the nerve stimulator (white) and recording electrode (black). The nerve stimulator is placed once at the distal end (**i**) and again at the proximal end (**ii**) of the implanted conduit (apparent position shown in red) to record NCV through the conduit. The recording electrode is kept fixed near the ankle of the animal. (*Reprinted with permission from Das et al, Data in Brief, 2015*)

After 18 months, the animals implanted with GNP-SF conduits exhibited NCV of 42m/sec, CMAP of 16.5mV, MUP of 116μV and SFI of -43.4. Animals with GNP-SF cell conduits showed NCV of 50m/sec, CMAP of 29.7mV, MUP of 133μV and SFI of -38.4 after 18 months. Implantation of SF conduits led to a NCV of 50m/sec, CMAP of 6mV, MUP of 87μV and SFI of -70 after 18 months. Animals implanted with SF cell nerve conduits exhibited NCV of 50m/sec, CMAP of 10mV, MUP of 123μV and

SFI of -64 after 18 months. The control group showed a more or less constant SFI of around -100 throughout their life span.

The locomotory activities of the animals implanted with nanocomposite conduits after 10 months are presented in **Fig 3.11 A-D.**

3.3.9 Morphological analysis of regenerated sciatic nerve

All the conduits were found to be structurally intact up to 18 months maintaining adherence to micro-sutured proximal and distal nerve ends. In the animals implanted with GNP-SF and GNP-SF cell conduits, growth of nerve along the nerve gap was complete 18 months post implantation and the regenerated nerve appeared morphologically normal (**Fig 3.11 E-F**). However, even after 18 months in the animals with silk fibroin conduits (both SF and SF cell) the gap along the conduit was found to be filled with tissue which appeared to be fibrous in nature (**Fig 3.11 G-H**). Histological analysis of the regenerated tissue in the nanocomposite group by H&E staining revealed large recruitment of Schwann cells inside the lumen and as well as within the interlayer gaps of the conduits (**Fig 3.12 A-B**). Upon closer observation Schwann cells were found to be aligned in characteristic wave like fashion in the GNP-SF cell group. Fewer Schwann cells and more inflammatory cells were found inside the silk fibroin conduits (**Fig 3.12 C-D**). TEM analysis of the regenerated sections after 18 months showed presence of many myelinated fibers with thick myelin deposition in the nanocomposite group. However, few myelinated axons with fragmented myelin sheath was observed within the silk fibroin conduits (**Fig 3.13**).

3.4 Discussions

Fabrication of Gold-Silk nanocomposite fibers have been previously performed using a co-electrospinning technique wherein a mixture of silk fibroin solution and colloidal gold nanoparticles were electrospun to incorporate nanoparticles on and within the nanofibers(Cohen-Karni et al, 2012). However, the need for multiple reduction steps employing strong alkaline reagents like tetrakis (hydroxymethyl) phosphonium chloride **(**THPC) and potassium carbonate (K_2CO_3) with proven neural toxicity limits the prospect for clinical deployment of grafts fabricated by such methods (National Toxicology Program, 1987).

In the present study, gold nanoparticles (GNPs) were formed by reduction with ethanolic extract of *Centella asiatica* (CA), an herb reported to facilitate neuro-regeneration and wound healing (European Medicines Agency, 2009). The CA extract mediated synthesis of GNP and particle characterization have been standardised earlier in our laboratory (Das et al, 2010). In this current work we found these GNPs to be non-toxic to rat Schwann cell line SCTM41. GNPs produced using synthetic reducing agents like malate, citrate and tartarate exhibit a net negative surface charge and have been studied as potential dyes for colouration of silk due to LSPR properties of plasmonic nanoparticles. One possible mechanism that was postulated for the rapid incorporation of GNPs on and within silk fibers was the electrostatic attraction between negatively charged GNPs and amine groups present on the fibroin protein which gets protonated in the acidic environment of the reaction (Tang et al, 2011). In the present study, a similar phenomenon could have led to the purple colouration of silk fibers upon treatment with GNP solution due to the presence of free –COOH groups in CA extract (Das et al, 2010).. Further, the highly acidic (pH 2.0) nature of the GNP solution could have facilitated the protonation of amine groups present on silk fibroin protein.

The gold nanoparticle incorporated silk fibroin fibers and the pristine degummed silk fibers were processed and electrospun following standard procedures to convert them into nano-dimension (Rockwood et al, 2011). The hence formed silk fibroin nanofibers (SF) could not be visualised under scanning electron microscope (SEM) without gold coating. However, we found that no sputter coating with gold was

necessary to observe the gold nanoparticle-silk fibroin nanocomposite (GNP-SF) nanofibers under electron microscope (**Fig 3.2 C**). This is due to the improved electrical conductivity of GNP-SF nanofibers arising from the presence of GNPs on silk

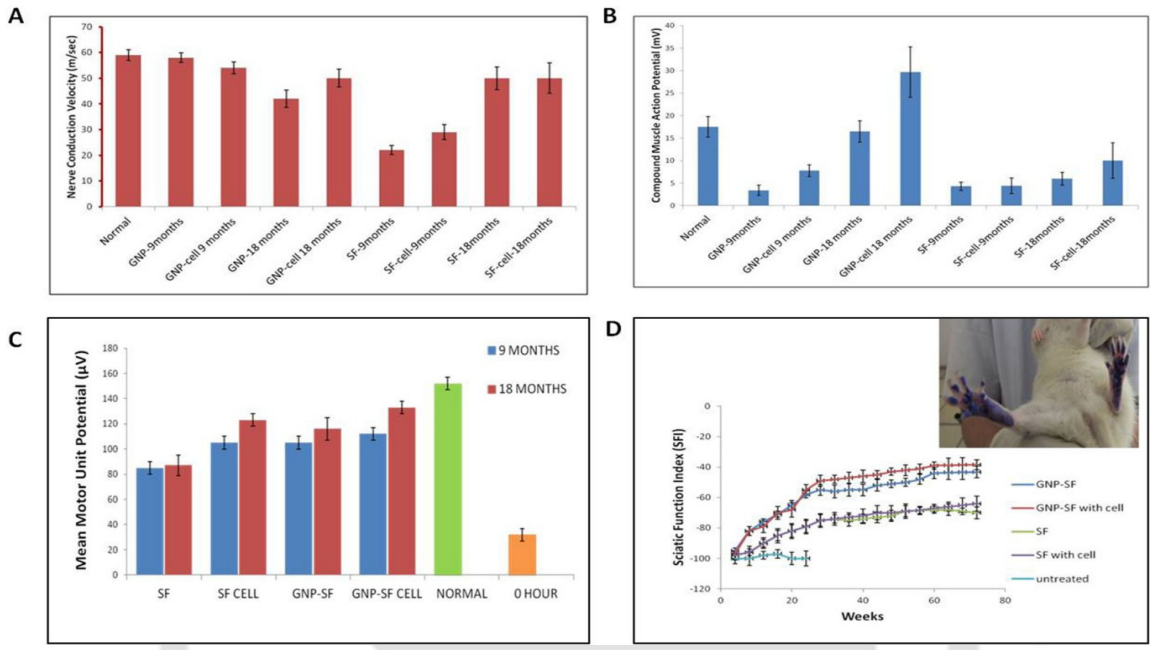

Fig 3.9: Functional analysis of regenerated nerve. A, Nerve conduction velocity (NCV) recorded after 9 months and 18 months (n=8). **B**, Compound muscle action potential (CMAP) values recorded after 9 months and 18 months (n=8). **C**, Mean Motor unit potential (MUP) recorded from the gastrocnemius muscle after 9 months and 18 months. **D**, Sciatic function index (SFI) calculated by walking track analysis at 2 week interval for 18 months (n=8). The hind limbs of the animals were stained with methylene blue for obtaining footprints (inset). (*Reprinted with permission from Das et al, Biomaterials, 2015*)

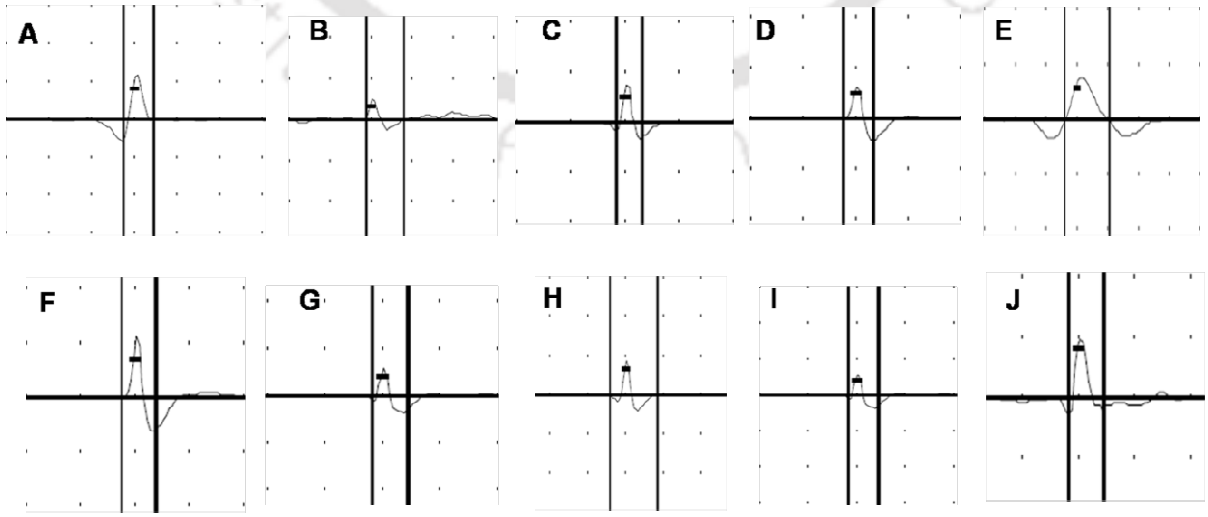

Fig 3.10: Motor unit potential wave patterns. A, A representative image of MUP pattern of normal rat, **B**, MUP recorded immediately after nerve transection (0 hour group), **C**, GNP-SF

conduit group after 9 months, **D**, GNP-SF conduit group after 18 months, **E**, GNP-SF cell conduit group after 9 months, **F**, GNP-SF cell conduit group after 18 months, **G**, SF conduit group after 9 months, **H**, SF conduit group after 18 months, **I**, SF cell conduit group after 9 months, **J**, SF-cell conduit group after 18 months. (*Reprinted with permission from Das et al, Biomaterials, 2015*)

nanofibers. The formation of the nanocomposite (GNP-SF) was confirmed through XRD analysis by the presence of characteristic sharp peaks for crystalline GNP corresponding to (111), (200), (220) fcc structure of gold. The broad peak around 2θ = 21^{o} corresponds to amorphous silk fibroin protein (**Fig 3.2 C inset**). The ohmic nature of the I-V characteristics obtained for GNP-SF nanofibers was indicative of the electronic tunnelling/hopping effect as reported previously for similar ultrathin films (Hill, 1969). The 25 fold decrease in resistance of silk nanofibers upon incorporation of GNPs indicates the enhanced electronic conduction through the silk-gold nano-composite scaffold. Further the GNP-SF and SF scaffolds were also found to promote Schwann cell adhesion and proliferation[23]. The nano-architecture of the electrospun scaffolds provided higher surface area to volume ratio for cellular attachment as compared to a single well of 12 well-culture plates having similar diameter.

Most of the fabrication methods used for developing nerve conduits like electrospinning, injection moulding, solvent casting etc predominantly rely on a mould like a teflon mandrel of specific dimension to provide the scaffold a conduit shaped architecture. Hence conduits with one particular dimension can only be made at a time. In the present study we have used a novel sheet rolling method to fabricate multiple conduits with varied length and diameters from a single electrospun sheet. Another advantage of the fabrication method is that the wall thickness of the conduits can be manipulated simply by the number of rotations of the electrospun sheet around the axis**.** Such layer by layer stacking of densely packed nanofibers lead to low porosity and limited swelling of the nerve conduits**.**[23]

For our experiments we fabricated conduits by rotating the electrospun sheets on 16 gauge sterile needles with multiple rotations. The dimensions of the conduits were chosen after thorough standardization to match the dimensions of a rat sciatic nerve. The conduits were treated with methanol upon fabrication to induce β-sheet formation. This also served as a measure for sterilizing the implants. The conduits were further UV-sterilized prior to seeding with rat Schwann cell line (SCTM41) to

ensure minimum possibility of contamination to cells or infection *in vivo*. The three dimensional environment of the lamellar conduits was found to mimic the native architecture of the nerve and promote Schwann cell growth in the form of clusters (**Fig 3.2 F**).

Regeneration of nerves following neurotmesis grade injury (complete axonal loss and conduction failure) is a highly complex, time consuming process often shackled with very low success rate inspite of surgical intervention. Most studies reported till date has been on an average for 3-4 months duration which is a short duration in terms of nerve regeneration and healing process. Only a handful of studies have been reported with post surgical observation time of 1 year or more (Boeckstyns et al, 2013). Although the nerve is found to grow along the conduit filling the gap within 3-4 months of implantation, the innervations of muscles to restore strength and sensory function takes a much longer time.

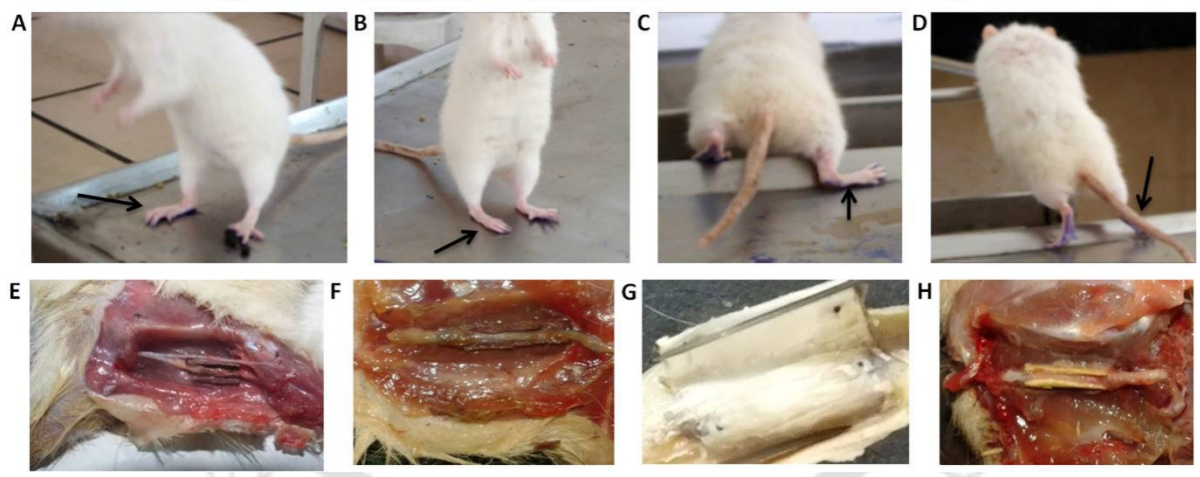

Fig 3.11: Gait analysis and neural regeneration. A-D, The animals implanted with GNP-SF cell conduits exhibited improved gait and could stand, stretch and jump by the end of 10 months. Black arrows indicate the operated leg. **E-H**, The implanted conduits were slit open after 18 months to monitor tissue regeneration. Growth of tissue was observed in GNP-SF (**E**), GNP-SF cell (**F**), SF (**G**) and SF cell (**H**) groups. (*Reprinted with permission from Das et al, Biomaterials, 2015*)

One of the major goals of this study was to observe the long term effect of a metal-polymer nanocomposite based neural implant fabricated with GNPs and a non-absorbable natural polymer like silk on the structural and functional regeneration of nerve tissue as well as its impact on surrounding muscles. No signs of erythema or edema were observed upon intra-cutaneous irritation and toxicity tests of the

conduits, thereby establishing the non-immunogenicity of the nanocomposite material inside the body. Further the fact that all the animals survived their normal life span before being sacrificed indicates the biocompatibility and safety of the silk-gold nanocomposite conduits.

A nerve injury is immediately followed by a series of degenerative processes called Wallerian degeneration leading to physical fragmentation of axon and disintegration of myelin sheath and ultimately loss of nerve conduction. Nerve conduction velocity (NCV) measurements along the nerve gap and the compound muscle action potential (CMAP) in the region of conduit implantation provide information about the extent of remyelination and conduction of nerve impulse through the grafted nerve conduit.

Electrophysiological measurements among all the groups immediately (within 1 hour) after surgery revealed minute generation of action potential in the distal region while no signal could be recorded by stimulating from the proximal side of the nerve gap (data not shown). This was particularly necessary to ascertain whether using an electrically conductive conduit with metallic nanoparticles can lead to conduction artefacts in nerve conduction studies. We found the NCVs of the group implanted with GNP-SF conduits (with and without cells) to be close to the normal values after a period of 18 months (**Fig 3.9 A**). They also exhibited near normal CMAP values which are possible only if the regenerating axons have been remyelinated. Rats implanted with GNP-SF conduits containing pre-seeded Schwann cells were found to have higher CMAP values than normal rats which may be due to high amount of myelin deposition by the Schwann cells (**Fig 3.9 B**). The data also indicated that there was no conduction block along the conduit. Rats implanted with SF conduits (with and without Schwann cells) exhibited increase in conduction velocities over a period of 18 months (**Fig 3.9 A**). However the low CMAP values exhibited by these groups can be attributed to the loss of myelin sheath and incomplete neural regeneration due to persistent axonal damage (**Fig 3.9 B**).

Neurotmesis grade nerve injuries are associated with complete loss of a nerve which leads to severe degeneration and atrophy of muscles innervated by the damaged nerve. Motor Unit Potential (MUP) evaluates the integrity of the motor unit comprising of the motor neuron, motor axon and the muscle which the particular

nerve innervates. Both nerve conduction (NCV and CMAP) and electromyogram (MUP) are performed in clinical cases of nerve injuries, neurodegenerative diseases and neuropathies. However for evaluating nerve regeneration through a tissue engineered conduit only nerve conduction parameters have been measured so far. Hence to evaluate complete structural and functional regeneration of nerve and re-innervation of damaged muscle, it is essential to study the MUP patterns in neural tissue engineering applications. The MUP wave patterns observed for all the groups are presented in **Fig 3.10**. MUPs recorded immediately after surgical transection of nerve (0hour group) and implantation of conduit exhibit very low amplitude of 32μV trailed by fibrillation (**Fig 3.9 C and Fig 3.10 A**) suggesting complete loss of sciatic nerve activity. The minute MUP recorded in the region are due to the action potential of other minor nerves that innervate the gastrocnemius muscle. The GNP-SF group were observed to have similar MUP wave pattern with slight increase in amplitude after 18 months as compared to 9months (**Fig 3.9 C and Fig 3.10 C-D)**. The GNP-SF conduits seeded with Schwann cells however exhibited marked improvement in MUP wave pattern with decrease of duration, area and increased amplitude after 18 months. The mean MUP amplitude of the GNP-SF cell group was found to be 133μV which is almost comparable to normal control group value of 152μV (**Fig 3.9C and Fig 3.10 E-F)**. The animals implanted with SF conduits were found to have identical MUP pattern and amplitude with no appreciable improvement over the duration of the study (**Fig 3.9 C and Fig 3.10 G-H**). SF conduits seeded with Schwann cells did reveal enhanced MUP amplitude after 18 months as compared to the 9 month old MUP but fibrillation patterns similar to 0 hour group was also evident (**Fig 3.9 C and Fig 3.10 I-J**). Hence electrophysiological studies over 18 months suggested that near normal functional regeneration of nerve as well as re-innervations of surrounding muscles was achieved in the GNP-SF conduit group containing pre-seeded Schwann cells.

The sciatic nerve is one of the major nerves supplying to the muscles of hind limbs and is particularly responsible for proprioception in the feet as well as locomotion. The ability of the animals to regain locomotor activities following surgical implantation of conduits was studied by walking track analysis on the operated leg by sciatic function index (SFI) measurement (**Fig 3.9 D**). The rats implanted with GNP-SF conduits seeded with Schwann cells (GNP-SF cell) performed better than the GNP-

SF, SF and SF-cell groups with SFI values approaching normal level after 18 months. We noted that none of the animals in the negative control group survived more than 6 months and exhibited SFI values close to -100 indicating complete neuromuscular degeneration. In all the other groups the SFI values were observed to rise sharply in the initial 12-16 weeks thereby gradually saturating over a period of 36-40 weeks.

Collagen remains the most preferred biopolymer for fabricating nerve conduits which is reflected in numerous collagen based conduits that have been approved by the US FDA in the recent past (Kehoe et al, 2012). The described nanocomposite conduits upon implantation exhibited high degree of functional neuro-muscular regeneration that is superior to even collagen based implants (Yu et al, 2011). In a comparative study of 4 synthetic conduits the maximum CMAP amplitude reported was around 1mV with poly-caprolactone fumarate (PCLF) and PLGA conduits in comparison to autografts showing amplitude of 2.5mV (Daly et al, 2013). However, normal nerves show CMAP amplitude of 15-20mV. Although most studies keep autograft as the control we have compared our results with a normal nerve thereby setting a higher standard. In the present study, the animals with nanocomposite conduits seeded with Schwann cells exhibit near normal values of CMAP, NCV and motor unit potentials after 18 months which conclusively proves that these conduits significantly enhance neural regeneration to a far more extent than previously reported.

In addition to electrophysiological tests, the rats were regularly monitored for signs of pain, discomfort and incidental abnormalities. The initial implantation of nerve conduit was done on three month old animals and thereafter monitored over a period of 18 months. The rats were found to lead a normal life span (except the control group which did not survive more than 6 months). No behavioural or clinical anomalies (like autotomy) were noted in any of the groups. The animals with GNP-SF conduits pre-seeded with Schwann cells displayed near-normal locomotor activities. Although the digits of the operated leg (right leg) remained flexed, the rats were able to stand, stretch and jump at will by the end of 10 months (**Fig 3.11 A-D**). Such activities put strain on the toe and thigh of the animals and could not be possible without functional regeneration of the sciatic nerve and regaining of strength in the gastrocnemius region.

To physically examine nerve growth by histo-morphometric analysis, the conduits were harvested along with the proximal and distal sections of the sciatic nerve 9 and 18 months post implantation. All the conduits were found to be structurally intact up to 18 months maintaining adherence to micro-sutured proximal and distal nerve

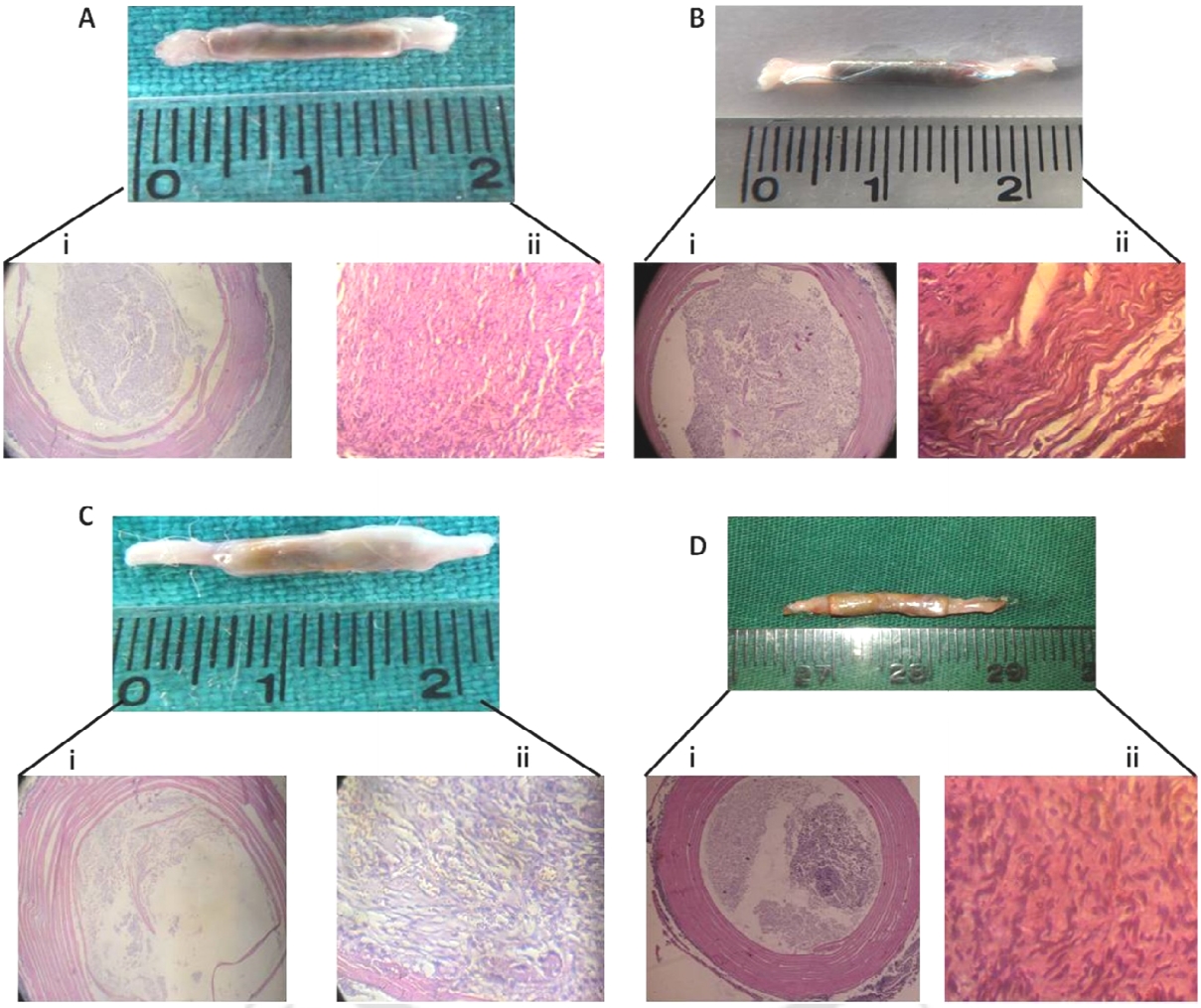

Fig 3.12: Gross examination and histology of harvested conduits. A, GNP-SF conduit harvested and stained with haematoxylin-eosin (H&E) after 9 months (i) and 18 months (ii). **B**, GNP-SF conduits with cell (GNP-SF cell) harvested after 9 months (i) and 18 months (ii) and stained with H&E exhibiting characteristic wave like organisation of Schwann cells and nervous tissue. **C**, SF conduit and **D**, SF conduit with cell (SF-cell) harvested and histological analysis by H&E staining after 9 months (i) and 18 months (ii).(*Reprinted with permission from Das et al, Biomaterials, 2015*)

ends. This could be attributed to the minimal swelling tendency of the conduits which helped it to retain its structural integrity over 18 months *in vivo*. In the groups implanted with GNP-SF and GNP-SF cell conduits, growth of nerve along the nerve gap was complete 18 months post implantation and the regenerated nerve appeared

morphologically normal (**Fig 3.11 E-F**). However, in the silk fibroin group (SF and SF cell) after 18 months, the gap along the conduit was found to be filled with tissue which appeared to be fibrous in nature (**Fig 3.11 G-H**). The nanocomposite conduits

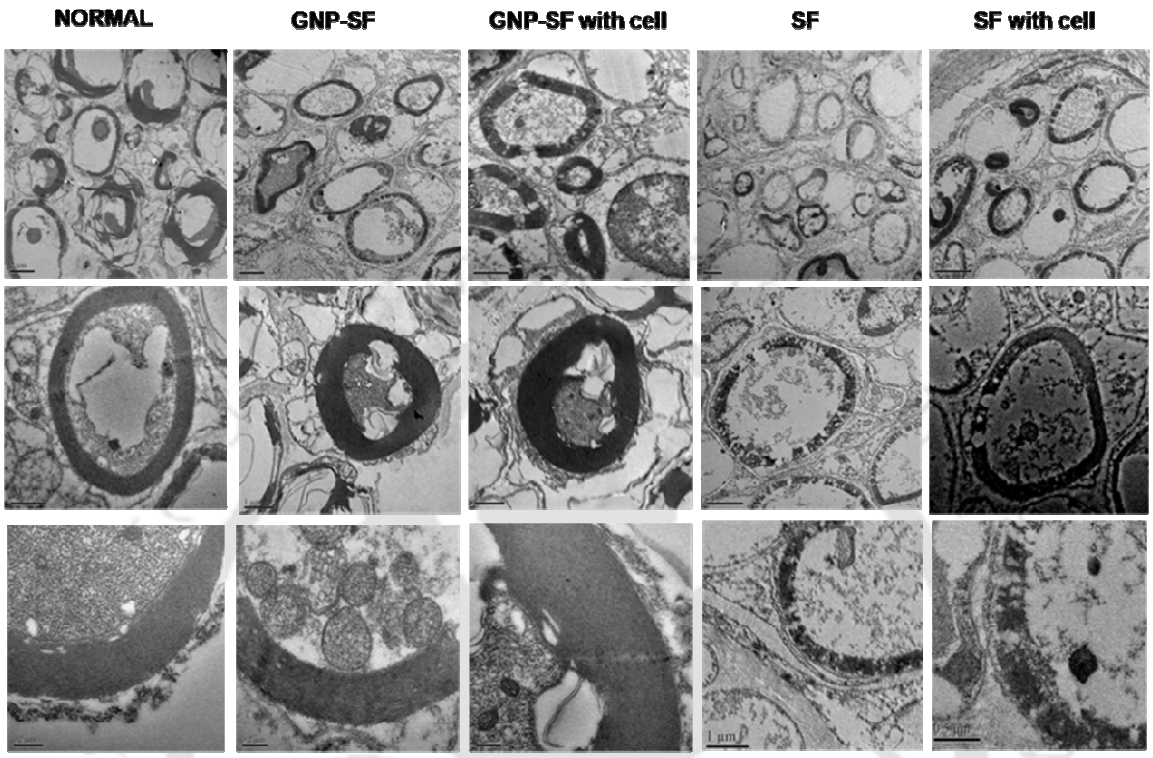

Fig 3.13: Ultra structure of regenerated tissue. Normal, Ultra structure of a normal sciatic nerve as observed under TEM. Closer look at each axon reveals the myelin sheath encapsulation stained black due to osmium tetra-oxide treatment. The myelin sheath is seen being deposited in a lamellar fashion over the axon. **GNP-SF and GNP-SF cell**, Many axons with thick deposition of myelin were observed in both groups after 18 months. A closer look revealed lamellar architecture of the myelin sheath similar to the normal nerve. **SF and SF cell**, Few myelinated axons were observed after 18 months. Higher magnification images reveal discontinuous deposition of myelin over the axons and absence of lamellar architecture of myelin sheath. (*Reprinted with permission from Das et al, Biomaterials, 2015*)

(GNP-SF and GNP-SF cell) were found to be encapsulated by fascia and fibrous tissue. No signs of inflammation were visible and both the proximal and distal ends appeared normal (**Fig 3.12A and Fig 3.12B**). In histological studies the conduits lamellar architecture appeared to be intact with cellular proliferation along the lumen as well as the interlayer gaps of the conduits (**Fig 3.12A i and Fig 3.12 B i**). A closer look at the regenerated nerve tissue of GNP-SF group after 18 months indicated recruitment of large amount of Schwann cells (**Fig 3.12A ii**) whereas the Schwann cells were observed to be aligned in characteristic wave like fashion in the GNP-SF cell group **(Fig 3.12B ii**). Upon gross examination, the silk fibroin conduits (SF and

SF-cell) appeared to be associated with inflammation at the distal end **(Fig 3.12C-D**). Histology of the SF conduits after 9 months showed little recruitment of neuronal cells with most of the lumen empty (**Fig 3.12C i**). Further, 18 months post surgery also cellular proliferation inside conduit remained minimal (**Fig 3.12C ii**). The SF conduits seeded with Schwann cells (SF-cell) did have more cells inside the lumen after 9 months as compared to SF group (**Fig 3.12D i**). However over 18 months it was found that the cells were mostly inflammatory in nature indicating possible neuroma formation (**Fig 3.12D ii**).

In order to evaluate the degree of myelination, the regenerated nerve tissue was observed under transmission electron microscope following lipid specific osmium tetraoxide staining **(Fig 3.13**). The animals implanted with gold nanoparticle containing conduits (GNP-SF and GNP-SF cell) exhibited neural ultra-structure similar to that of a normal nerve. Thick coating of myelin sheath along with characteristic lamellar structure was evident in the GNP-SF and GNP-SF cell groups indicating sufficient deposition of myelin in aligned fashion by Schwann cells. On the contrary, the animals with silk fibroin conduits (SF and SF cell) displayed fewer myelinated axons along with incomplete deposition of myelin in a more granular fashion rather than the desired lamellar organization. Although SF cell group exhibited more number of myelinated axons as compared to SF, there was no significant improvement in the myelin architecture.

The pre-seeding of Schwann cells forms an inner and outer sheet of cells on the conduit. When the conduit is sutured to the two ends of the nerve stump the Schwann cell sheath inside the conduit serves as natural guidance for the migration of endothelial cells and fibroblasts from the proximal and distal nerve stumps. This helps in formation of a biological tissue cable augmenting axonal regeneration and myelination (Daly et al, 2012). The porous nature of the conduit facilitates the transport of nutrients as well as growth factors and signalling molecules released by the outer layer of Schwann cells into the interior. Overall this enhances neuro-regeneration across the nerve gap as compared to animals implanted with un-seeded conduits.

3.5 Conclusions

A major accomplishment of the present study is the fabrication of a metal-biopolymer based nano-composite for deployment as a nerve conduit. Here, we have demonstrated in principle how the nanocomposite nerve conduits exhibited improved structural and functional neuro-muscular regeneration as compared to silk fibroin and control group. Pre-seeding the nerve conduits with Schwann cells was found to enhance its neuro-regenerative potential. The GNP-SF cell group exhibited increased CMAP, better MUP patterns and improved SFI values over 18 months. Histological and TEM analysis of regenerated nerve harvested from GNP-SF cell group revealed increased recruitment of Schwann cells leading to better myelination of axons in a lamellar fashion.

We also report here for the first time the utility of motor unit potentials (MUP) recorded from surrounding gastrocnemius muscle in studying nerve regeneration through an implanted conduit. The MUP patterns obtained through electromyogram along with nerve conduction studies helped us to accurately analyse nerve continuity across the gap as well as re-innervation of surrounding muscles which is of direct clinical relevance.

The novel sheet rolling approach adopted in the present study for fabrication of multidimensional conduits from a single electrospun sheet can be scaled up through automation in future. Such a process would aid in fabricating conduits which can fit nerves of varied dimension in the human body.

The present study convincingly demonstrates that neural implants comprising of gold nanoparticles are safe, stable and remain functional *in vivo* for a long duration. The presence of GNPs in the conduits neither elicited any inflammatory response in the host nor in situ at the site of implantation. This may be attributed to the fact that such particles were synthesised using biological agents like herbal extracts. Further the strong interaction between the nanoparticles and nanofibers kept the GNPs embedded in the nanofibers limiting their migration into the surrounding tissue as evident from by the retention of colour of the GNP-SF nerve conduits after 18 months of implantation. Such well characterised materials would be able to withstand

the complex and lengthy process of neuromuscular regeneration and prove to be ideal for clinical translation.

Further the formation of nanoparticle-nanofiber nanocomposite also opens up new opportunities for fabricating advanced scaffolds. Such nanocomposites would enable chemical modifications of biomaterial and can potentially act as platforms for delivery of nerve growth factors providing chemical cues for cellular proliferation and directing neurite outgrowth. The method demonstrated herein can potentially be used as a platform to fabricate smart materials having applications not only in tissue engineering but also in optoelectronics, sensing technologies and development of e-textiles. Research on extending the applicability of the method to different polymers using a variety of nanoparticles as well as attempts to better understand the possible mechanism behind such nanocomposite formation are presently underway in our laboratory.

Chapter 4

Silk-Polyaniline nanocomposite based scaffolds for neural tissue engineering

4.1 Introduction

Intrinsically conducting polymers like Poly-3,4-ethylenedioxythiophene (PEDOT), polypyrrole, polyaniline etc have conjugated π-electron system, low ionization potential and high electron affinity which are responsible for its electrical conductivity through electron delocalisation. These conducting polymers have been extensively studied for a wide range of biomedical applications like biosensors (Gao *et al*, 2014), drug delivery platforms (Thompson *et al*, 2010), fabricating electro-responsive artificial muscles and as a biomaterial in developing electrically conductive scaffolds for enhancing nerve regeneration (Peramo *et al*, 2008; Huang *et al*, 2010).

Polyaniline is one of the most common intrinsically conducting polymers explored for multidisciplinary applications. The superior thermal stability, easy processing into various forms (solutions or micro/nanostructure) using an inexpensive monomer (aniline) are some of the properties which makes polyaniline an attractive choice as a scaffold material. (Beesabathuni *et al*, 2013; Reddy *et al*, 2009; Bhadra *et al*, 2009). Polynaniline based films or powders have been found to support cellular adhesion and proliferation and did not elicit any toxic or immune response upon subcutaneous implantation in rats over a period of 50 weeks thereby proving its biocompatibility (Wang *et al*, 1999). Further the ability of polyaniline based scaffolds to support the growth of neuronal cells, differentiation of neural stem cells as well as promote neurite extension upon external electrical stimulation indicates its potential in fabricating artificial nerve conduits for neural tissue engineering applications (Bhang *et al*, 2012; Prabhakaran *et al*, 2011). The present study is the first report of fabricating polyaniline based artificial nerve conduits and evaluating its efficacy in promoting functional and morphological regeneration of nerves.

Peripheral nerve damage following trauma or other neuropathic manifestations often lead to permanent disability through loss of sensory and motor function. Artificial nerve conduits fabricated using biocompatible synthetic and natural polymers are essential to bridge nerve gaps larger than 5mm and augments nerve regeneration by guiding the sprouting axons from the proximal and distal stumps (Cunha *et al*, 2011). However, to address the loss of nerve impulse transmission following nerve injury it is imperative that the artificial nerve grafts favor electrical conduction. Conductive

polymers like polypyrrole, carbon nanofiber etc have been used as dopants to fabricate scaffolds and develop artificial nerve guides **(**George *et al*, 2005; Ahn *et al*, 2015**).** Although electrically conductive polymers have been reported to favor growth and functional regeneration of nerve cells and tissue, the exact mechanism behind such neuro-regenerative effect is yet to be fully understood. **(**George *et al*, 2009; Williams *et al*, 1994**).** In addition, the biodegradability and chronic *in situ* toxicity effects of degradation by-products of synthetic conducting polymers remains doubtful due to limited *in vivo* studies as neural implant.

Among the natural polymers, silk fibroin and silk based composites have been extensively used in neural tissue engineering due to its excellent biological and mechanical properties, tunable architecture, high permeability to body fluids and controlled degradation in vivo. However, the poor electrical conductivity of the silk polymer has to be improved in order to achieve better results in regeneration of electrically active tissues like cardiac muscles and nerve fibers. Our group has recently reported that incorporating metallic nanoparticles into silk nanofibers can considerably decrease the resistance of silk and augment near-normal functional and morphological regeneration of a transected sciatic nerve (Das *et al*, 2015). Silk nanofiber based meshes coated with polypyrrole were found to be compatible with human mesenchymal stem cells and human fibroblast cells (Aznar-Cervantes *et al*, 2012**).** Electrospun core-sheath nanofibrous meshes comprising of polyaniline-silk fibroin-poly(L-lactic acid-co-3-caprolactone) have been reported to promote the growth and differentiation of rat PC12 cell line (Zhang *et al*, 2014). Silk threads have also been combined with the conductive polymer poly(3,4-ethylenedioxythiophene) - poly(styrenesulfonate) (PEDOT-PSS) in order to develop biocompatible electrodes to record signals during electrophysiological tests such as electrocardiography (ECG), electroencephalography (EEG) and evoked potential data (Tsukada *et al*, 2012). In vivo studies with silk fibroin-single walled carbon nanotubes based porous nerve conduits along with intraluminal fillers of fibronectin nanofibers exhibited more number of myelinated axons and higher nerve conduction velocities upon implantation on a rat sciatic nerve injury model (Mottaghitalab *et al*, 2013).These studies indicate that the efficacy of silk fibroin as a biomaterial for facilitating nerve regeneration can be increased by incorporation of electrical cues in the nerve conduits upon combination with synthetic conducting polymers.

In the present study we have fabricated nerve conduits based on polyaniline-silk fibroin nanocomposite (PASF). The nerve conduits were tested for their biocompatibility in vitro and in vivo, pre-seeded with rat Schwann cell line SCTM41 cells and implanted in a 10mm sciatic nerve gap. The electrophysiological and histomorphometric outcomes of the nanocomposite group was compared with those of animals with pure silk fibroin nanofibers based conduits over a period of 12 months in order to understand the long term safety of such synthetic polymers as well as their effect on nerve regeneration *in vivo*.

4.2 Materials and Methods

4.2.1 Synthesis and cytotoxicity of polyaniline

Polyaniline (PA) was synthesised from aniline monomer upon polymerization following previously described procedure (Ai *et al*, 2010; Jiang *et al*, 2009). Briefly, 1 mL of aniline monomer was added to 20 mL 0.1 M HCl solution at room temperature and stirred for 15 min. There after 2.49 g of ammonium persulfate (APS) in 10 mL of 0.1 M HCl solution was added to above solution in one portion. The mixture solution was allowed to polymerize without stirring at room temperature for 24 h. After filtering the resulted product was washed with deionised water and methanol. There after it was dried under vacuum at 60° C for 24 h to obtain a green amorphous powder.

Cytotoxic effect of the polyaniline (PA) was assessed by MTT assay on rat schwann cell line (SCTM41) following standard assay procedures (Mosmann, 1983). Briefly, PA were dispersed in Dulbecco's modified eagle's medium (DMEM) without serum to make a stock solution of 10mg/ml. This solution was used to make further working concentrations (100µg/ml to 1000µg/ml) of PA against which MTT assay was done. The cells were cultured in 96 well cell culture plates and incubated with various amounts of PA (10µg to 100µg) dissolved in 100µl of serum free DMEM for 24 hour in a CO_2 incubator (Make - Healforce) under 37^0C and relative humidity 90%. This was followed by addition of DMSO and recording absorbance at 570nm using a UV-VIS multiwell plate reader (Make-TECAN). Live-dead staining assay was performed using Acriding orange (AO)-Ethidium bromide (EB) mixture. For the AO-EB staining assay, the Schwann cells after 24 h incubation with PA (1000µg/ml) were treated with 20µl of AO-EB mixture dye solution. After 2-3 mins incubation period, both the samples were observed under an inverted fluorescent microscope. The same procedure was followed with untreated Schwann cells as control.

4.2.2 Molecular mass characterization of synthesised polyaniline

Matrix-assisted laser desorption/ionization (MALDI) was used to characterise the molecular mass of synthesised polyaniline. MALDI was performed separately on polyaniline samples dissolved in tetrahydrofuran (THF) and acetonitrile. Solventless MALDI was also performed by mixing the sample directly with the MALDI matrix. The

samples were prepared following standard procedure reported earlier [Dolan *et al*, 2014].

4.2.2.1 *Sample preparation for solvent based MALDI*

Two different solvents were used i.e. acetonitrile and Tetrahydrofuran (THF). 5 mg of polyaniline was dissolved in both acetonitrile and THF separately. After 10 min, the samples were centrifuged and the solid polyaniline that had not dissolved was decanted off. For the preparation of matrix, 0.1% of trifluoroacetic acid (TFA) solution in distilled water was mixed with acetonitrile in the ratio of 60:40 respectively. 15 mg of 2,5-dihydroxybenzoic acid (DHB) matrix was added to 1 ml of the prepared solution. This was further sonicated in a water bath sonicator for 5 min. This matrix solution and polyaniline containing sample solution were mixed in a 1:1 ratio. The samples were then spotted onto the sample plate and allowed to air dry.

4.2.2.2 *Sample preparation for solvent-less MALDI*

For solvent-less MALDI, the DHB matrix was prepared as mentioned above. Polyaniline powder was then mixed and grounded with the DHB matrix using mortar-pestle in a sample: matrix ratio of 1:50. The sample was then spotted onto the sample plate and allowed to air dry.

All analysis were performed in the MALDI-TOF mass spectrometer (Make - Bruker) equipped with nitrogen laser (wavelength = 333nm). The analyzer was operated in the reflectron mode with the mass range of 500-1500 m/z. All spectra were generated with an acceleration voltage of 19 kV and with average of 500 laser shots. Data acquisition and analysis was done using Bruker Flex Control program. Representative structures of polyaniline shown in **Fig 4.9** were drawn using ChemDram Ultra 12 software.

4.2.3 Fabrication and characterization of electrospun SF and PASF nanofibrous mat

Bombyx mori silk cocoons were purchased from local market in Guwahati, Assam. Degumming of cocoons was done by standard protocol reported earlier (Rockwood *et al*, 2011)**.** Briefly**,** B. mori silk cocoons were boiled for 30 mins in distilled water. There after cocoons were rinsed and immersed in an aqueous solution of 0.2%

Sodium carbonate and 0.025% detergent (like triton x-100) and kept at 90^{o}C for 3hours to completely remove sericin protein. The degummed silk fibroin fibers were left to dry at 60^{o}C overnight after rinsing thoroughly with distilled water. The degummed silk fibers were then dissolved in a highly concentrated chaotropic solvent (9M Lithium bromide) in a material: liquor ratio of 1:10. The procedure was carried out under magnetic stirring condition and a temperature of 60^{0}C till all the fibers dissolved. Subsequently, the solution was dialysed against distilled water (MW cut off – 8000) for 3-4 days with frequent changes of water. The aqueous solution of pristine silk fibroin thus obtained was concentrated by further dialysis against polyethylene glycol (MW = 20,000) till the concentration of the protein solution reached about 15%. The protein solution was stored at -20^{0}C overnight followed by freeze drying for 2-3 days.

The lyophilized powder of pristine silk fibroin protein (SF) was dissolved in formic acid (98% pure) at a concentration of 10% w/v (i.e. 100mg/ml) for electrospinning. Polyaniline powder was also added into the formic acid in a Polyaniline:Silk ratio of 1:100 and left under constant stirring overnight. The spinning solution was taken in a 2ml syringe and electrospun under optimized conditions where the operating voltage ranged from 20KV to 25KV, working distance (i.e distance between needle tip and collector) of 15cm and flow rate of 0.5ml/hr to 1ml/hr. and the nanofibers were collected on a rotating drum covered with an aluminum sheet.

The polyaniline-silk fibroin (PASF), pristine silk fibroin (SF) electrospun mats as well as PA powder were dried overnight and scraped before X-Ray Diffraction (XRD) and Fourier Transform Infrared (FTIR) spectroscopic studies. In order to study the electrical resistance, a 1cm x 1cm portion of the electrospun mats (SF and PASF) were placed over the uncoated portion of a aluminum coated corning glass with the edges of the mat fixed on the aluminum coated section by silver paste. The electrical resistance of the materials was measured by a sub-femto-ampmeter (Make-Keithley). Thermal properties of the scaffolds (PASF and SF) as well as polyaniline (PA) powder were analyzed by TGA (Make: Netzsch). The temperature range for the analysis was set from 30-800℃.

Pristine SF and PASF nano fibers were collected in cover slip separately for culture of cells. Nanofiber coated cover slips were treated with methanol and UV radiation

for conversion to ß sheet and sterilization. They were then washed 3-4 times with sterile phosphate buffer saline (PBS) and incubated with DMEM containing 10% FBS for 24hrs in CO_2 incubator for conditioning. SCTM41 cells (Rat Schwann cell) were seeded over cover slips and incubated for 10 days. On fifth day the cover slips were processed for FESEM analysis to monitor cell adhesion. Cellular proliferation was also quantitatively studied over the cover slips by MTT analysis at 0, 5^{th} and 10^{th} day.

4.2.4 Fabrication and characterization of pre-seeded and un-seeded nerve conduits

Immediately after electrospinning, the nanofibrous mat (made either of PASF or SF) was slowly peeled off the aluminum sheet and rolled onto to a stainless steel needle and pressed together so that each layer adhere to one another. The rolled conduits were sterilized by treatment with methanol followed by UV exposure. All fabricated conduits were washed with sterile phosphate buffered saline (PBS), pH=7.4 to remove residues of methanol. Conduits were then conditioned by keeping in DMEM medium with 10% Fetal Bovine Serum (FBS) in CO_2 incubator for 24 hours. Conduits were washed again with sterile PBS following UV sterilisation before implantation in rat.

For preseeding conduits, SCTM 41 (rat Schwann cell) cells were seeded into the conduits and incubated for five days with regular replacement of media. These conduits were also washed 3-4 times with sterile PBS before implantation.

The porosity of the conduits (n=4) was determined by a previously described ethanol displacement method according to the following formula (Tang et al, 2013) –

$$Porosity\ (\%) = \frac{(M_t) - (M_o)}{V \times \rho} \times 100$$

where ρ is the density of ethanol (0.79g/cc), V is the volume of the conduits, M_t is the mass of the conduit upon immersion in ethanol and M_o is the mass of the dry conduit. The dynamic swelling ratio of the nerve conduits (n=4) was periodically measured by immersing the conduits in phosphate buffered saline (pH7.4) according to a previously described method as per the following formula **(**Wang *et al*, 2014) –

$$Swelling\ ratio\ (\%) = \frac{(W_s - W_d)}{W_d} \times 100$$

where W_s and W_d are the wet and dry weight of the conduit.

4.2.5 *In vivo* intra dermal test

Intra-cutaneous irritation and toxicity studies were performed on Sprague Dawley rats (n = 9) following standard procedures as described in ASTM standard protocol for "Standards Used in Meeting Requirements for a Model Pre-Market Approval (PMA) of a Neural Guidance Conduit" (ASTM STP 1452). Briefly, 24 hour saline extract of the silk fibroin (n=3) and polyaniline-silk fibroin conduit (n=3) were taken and injected intradermally. Normal saline was injected in the control group (n=3) (**Fig 4.6 A**). The animals were observed for 72 hours.

4.2.6 Surgical implantation of nerve conduits

All the animal experimentations were performed under veterinary supervision following CPCSEA, India and Institutional Animal Ethical Committee (IAEC) guidelines at College of Veterinary Sciences, AAU, Khanapara, Assam. The study was approved by IAEC and CPCSEA vide approval no 770/ac/CPCSEA/FVSc/AAU/IAEC/11-12/117 dated 27.03.2012. The animals were housed in a temperature and humidity controlled room with access to food and water *ad libitum*.

The fabricated nerve conduits were subsequently implanted in clinically healthy female Sprague Dawley rats (age 3 months and weighing 250gm). A total of 40 rats were taken for the study. The animals were divided into five groups, each comprising of 8 animals and a gap of 10mm was created in the sciatic nerve. Group I was treated with silk fibroin (SF) nanofiber nerve conduit (n=8), Group II consisted of Schwann cell preseeded SF conduits (n=8), Group III were implanted with Polyaniline-silk fibroin nanocomposite (PASF) nerve conduit (n=8) and Group IV were treated with Schwann cell preseeded PASF conduits. Group V was the negative control group where the sciatic nerve gap was left untreated (n=8). The surgical procedure followed is described in **Fig 4.8(B-D)**. The operation was done under balanced anesthesia using a combination of Xylazine (5mg/kg body weight) and Ketamine (50 to 100mg/kg body weight) intra-peritoneally. The right sciatic nerve was surgically exposed and subsequently separated from the underlying muscles and fascia. A 10mm long nerve segment of the sciatic nerve was transacted

and removed. The proximal and distal stumps of the nerve were slowly inserted inside the conduit and sutured along with the conduit using 7-0 polypropylene sutures. Subsequently, the muscles and skin were sutured using 7-0 polypropylene and 6-0 black braided silk sutures respectively and sealed with Tincture Benzoin cotton seal. Animals were then maintained on antibiotic (Ceftriaxone) and non-steroidal anti-inflammatory drug (Meloxicam) for 5 days postoperatively. Regular dressing was done with 5% Povidine iodine solution (Betadine) and antiseptic solution spray for 7 days. Skin suture was removed after 8-10days.

4.2.7 Functional analysis of regenerated sciatic nerve

The functional regeneration of sciatic nerve was monitored by electrophysiological studies and walking track analysis. The electrophysiological studies were conducted using an electromyogram (EMG) machine (Make – Nicolet Model- Viking Quest). Animals were chemically restrained using sedative dose of Xylazine **(**1mg/kg body wt**)** and Ketamine (100mg/kg body wt) and placed on ventral recumbency over a wooden table. Area concerned was shaved and disinfected before recording. Grounding electrode was attached to the base of tail**.**

Nerve conduction velocity (NCV) and compound muscle action potential (CMAP), were recorded by percutaneous stimulation of sciatic nerve with bipolar electrode first at the proximal end of the implanted conduit at the level of hip joint followed by a distal stimulation near the popliteal fossa. Distance between the two points was measured for calculating NCV.

Motor unit potentials (MUPs) were recorded by inserting a bipolar needle electrode into the gastrocnemius muscle. Sensory stimulus was provided by interdigital pinch.

For walking track analysis a blank white paper was placed on a walking track of 16 inch length and 3 inch breadth for obtaining the foot prints. The hind limbs of the animals were painted with methylene blue and they were allowed to walk through the track. Subsequently Sciatic Functional Index (SFI) was calculated using the following formula.

$$\text{SFI} = -38.3\left(\frac{EPL - NPL}{NPL}\right) + 109.5\left(\frac{ETS - NTS}{NTS}\right) + 13.3\left(\frac{EITS - NITS}{NITS}\right) - 8.8$$

where , EPL – Experimental print length

NPL - Normal print length

ETS –Experimental toe spread

NTS – Normal toe spread

EITS – Experimental inter toe spread

NITS - Normal inter toe spread

4.2.8 *Morphological analysis of regenerated sciatic nerve*

Samples for histological analysis were collected in 10% neutral buffer formalin (Make-Sigma Aldrich) at an interval of 6 and 12 months after surgery by euthanizing the animal with intravenous over dose of Thiopentone sodium. Conduit was isolated and processed for Hematoxylin & Eosin (H&E) staining and cross sectional images were taken at 400X magnification. For nerve ultrastructure studies, cross-sections of the regenerated nerve after 12 months were stained with osmium tetra-oxide and processed by standard protocol to be visualised by transmission electron microscopy (TEM).

4.3 Results

4.3.1 Synthesis and cytotoxicity of polyaniline

The polyaniline amorphous powder formed after subsequent polymerization was dark green in colour with a fluffy texture. Scanning electron microscope observation of the powder showed presence of aggregates (**Fig 4.1A**). Rat Schwann cell (SCTM41) exhibited high cellular viability by MTT assay when treated with maximum concentration of polyaniline i.e. 1000µg/ml (**Fig 4.1B**). Live-dead assay of SCTM41 cells treated with 1000µg/ml PA revealed normal cellular morphology compared to control untreated cells **(Fig 4.1C-H)**.

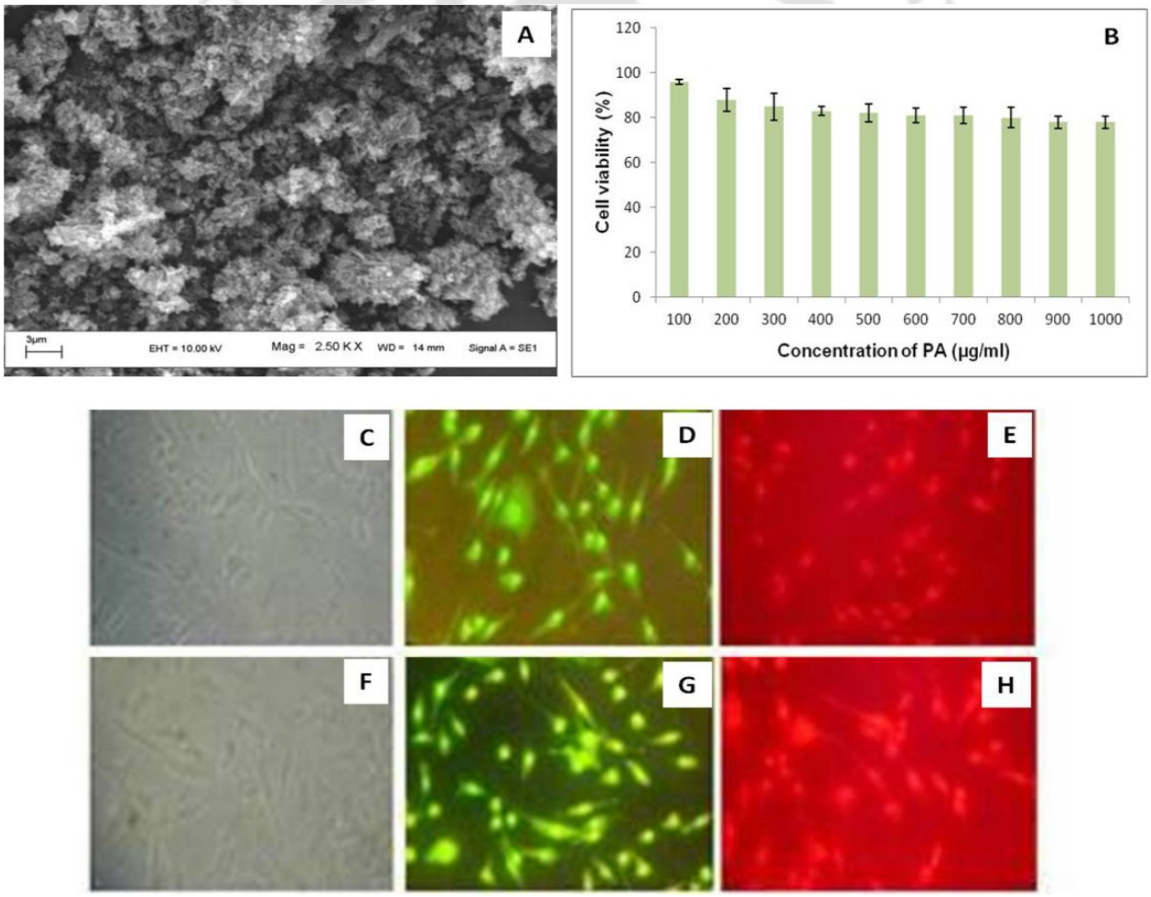

Fig 4.1 ***Fabrication and cytotoxicity of polyaniline powder***. **A**) Scanning electron microscope (SEM) image of polyaniline (PA) powder, **B**) Viability of rat Schwann cells (SCTM41) against PA measured by MTT assay. (**C-E**) Live-dead staining assay of untreated SCTM41 under normal light (C), green fluorescence (AO stained) (D) and red fluorescence (EB stained) (E). (**F-H**) Live-dead staining assay of SCTM41 cells treated with 1000µg/ml under normal light (F), green fluorescence (AO stained) (G) and red fluorescence (EB stained) (H).

4.3.2 Molecular mass characterization of synthesised polyaniline

4.3.2.1 Solvent based MALDI with polyaniline dissolved in acetonitrile showed prominent peaks at m/z = 542, 558, 574, 634, 650, 666 and low intensity peaks corresponding to m/z = 725 and 741 (Fig 4.2A). Similar peaks were found using THF as a solvent with one extra peak at m/z = 757 (Fig 4.2B).

4.3.2.2 Solvent less MALDI was performed over m/z range 530 – 730 and 800 – 1200. Prominent peaks were found at m/z = 544, 560, 576, 635,651,667 and 726 (Fig 4.2C). In the higher m/z range sharp peaks were observed at m/z = 816,832, 907,923, 998, 1014, 1089 and 1105 (Fig 4.2D).

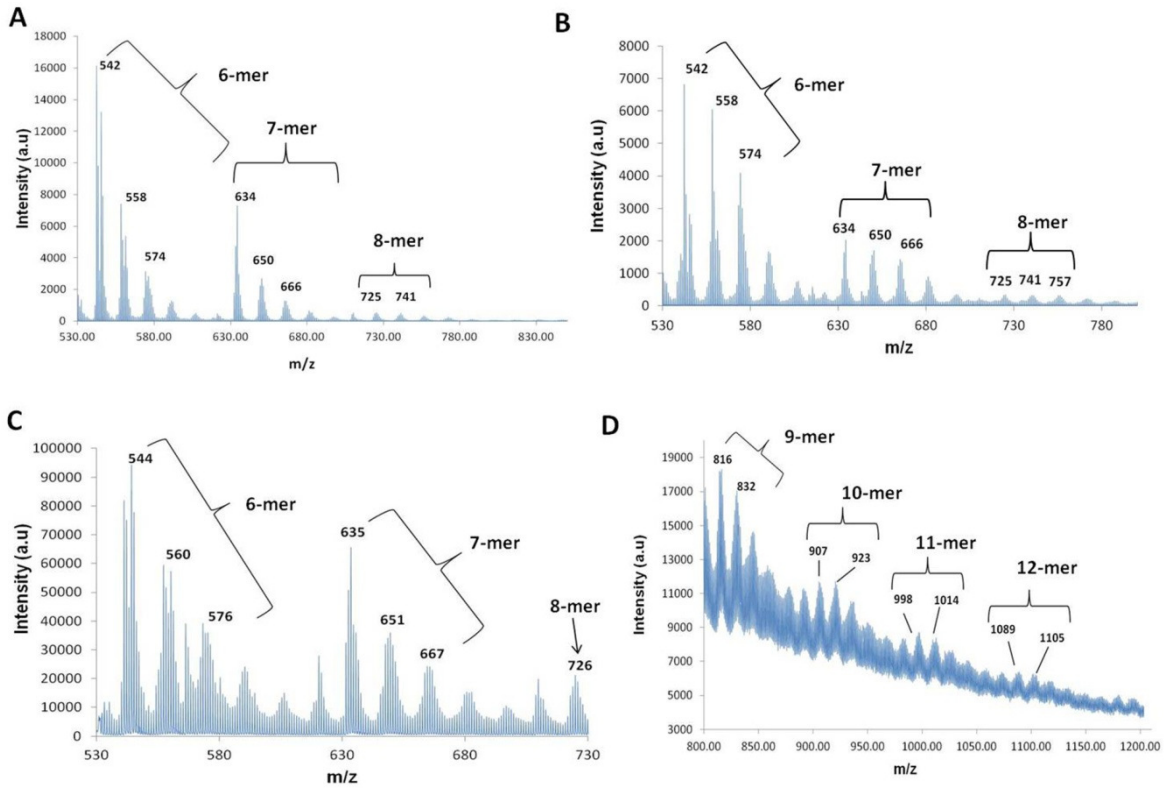

Fig 4.2: Molecular mass distribution of synthesised polyaniline (PA). **A**) PA in THF; **B**) PA in Acetonitrile; **C-D**) Solvent-less MALDI showing low molecular weight oligomers (**C**) and higher molecular weight oligomers of PA (**D**).

4.3.3 Fabrication and characterization of electrospun SF and PASF nanofibrous mat

The morphology of the electrospun mats (SF and PASF) were observed under electron microscope. FESEM analysis revealed formation of nanofibrous mesh in

both SF and PASF scaffolds with average fibre diameter of 150-250nm in case of SF and 350-450nm for electrospun PASF mat (**Fig 4.3A-B, Fig 4.3D**). PASF nanofibers were found to be coated with numerous nano sized particles with an average particle diameter of 40-60nm (**Fig 4.3C**). Rat Schwann cells (SCTM41) were observed to adhere over both the electrospun mats (SF and PASF) (**Fig 4.3E-F**). MTT assay of cells cultured over the scaffolds for 10 days indicated enhanced cellular proliferation in case of nanofibrous mat as compared to control 12 well plate (**Fig 4.3G**).

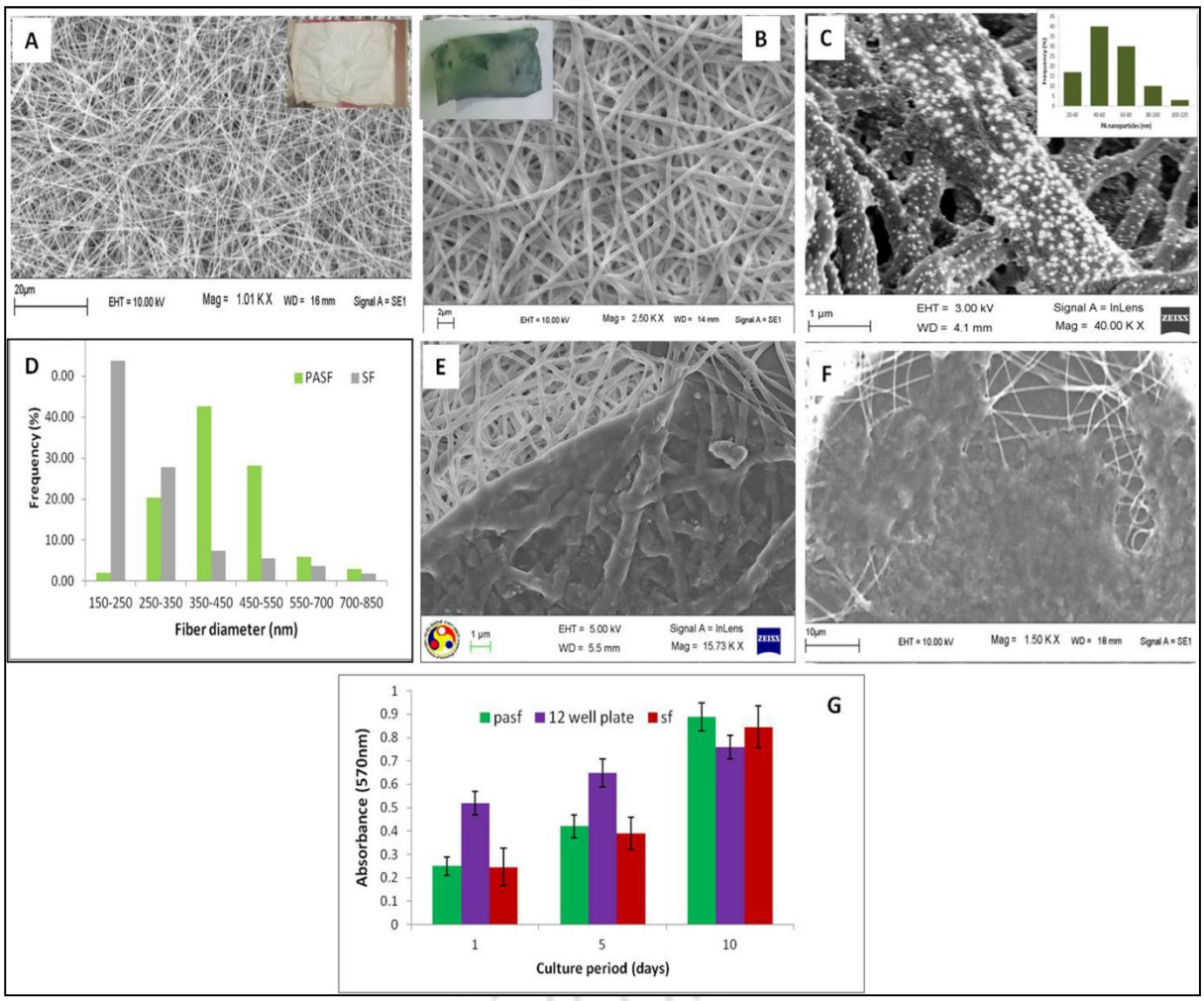

Fig 4.3: Fabrication of electrospun scaffolds and cellular proliferation. **A**) FESEM image of silk fibroin (SF) nanofibers with SF sheet in the inset, **B**) FESEM image of polyaniline-silk fibroin (SF) composite nanofibers with PASF sheet in the inset, **C**) Higher magnification of FESEM image of PASF nanofibers showing uniform coating with polyaniline nanoparticles. The particle size distribution is depicted in the inset, **D**) Variation of fiber diameter in SF and PASF nanofibrous scaffolds, **E**) FESEM image of Schwann cell growth on SF scaffold and **F**) FESEM image of Schwann cell growth on PASF scaffold, **G**) Cellular proliferation over electrospun scaffolds measured by MTT assay.

The electrical resistance of SF nanofibers mat was found to be $12.39x10^{12}\Omega$ whereas PASF nanofibers had a resistance of $1\ x10^{12}\Omega$.

FTIR analysis of the SF electrospun mat exhibited peaks around 1668 cm^{-1}, 1514 cm^{-1}, 1240cm^{-1} and 1146 cm^{-1}. PA powder was also found to have peaks identical to SF with few additional peaks corresponding to 931 cm^{-1},777 cm^{-1}, 725 cm^{-1},644 cm^{-1}, 517 cm^{-1}. PASF nanocomposite scaffolds were found to exhibit peaks around 1614 cm^{-1}, 1541 cm^{-1}, 1257 cm^{-1}, 1119 cm^{-1} and 663 cm^{-1}(**Fig 4.4A**).

Polyaniline powder exhibited a single broad peak at $2\theta = 24^0$ in XRD analysis while SF electrospun mat had a broad peak around $2\theta = 21^0$ (**Fig 4.4C-D**). The electrospun PASF nanocomposite mat showed a broad peak around $2\theta = 20.65^0$ and a minor peak around $2\theta = 24.8^0$ (**Fig 4.4B**).

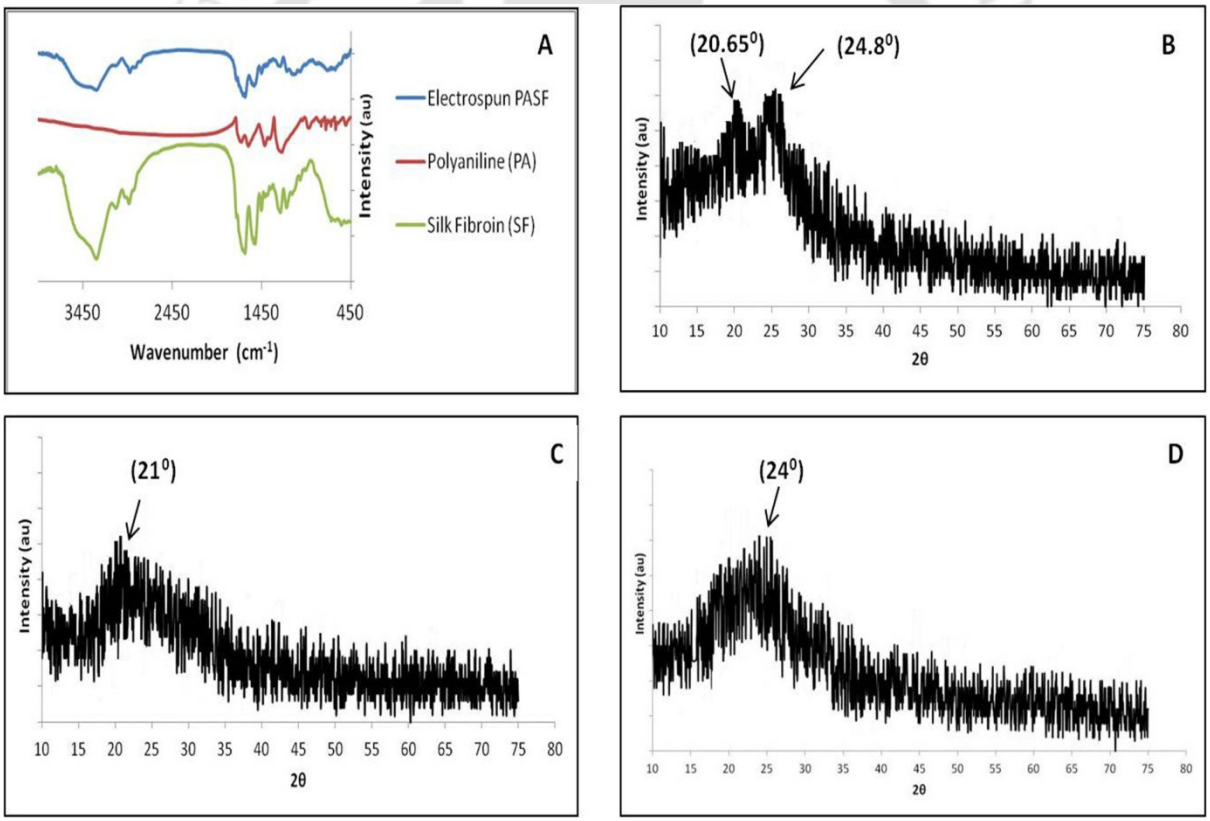

Fig 4.4: Characterization of electrospun scaffolds. **A**) FTIR spectrum of PA, PASF and SF scaffolds, XRD data of **B**) PASF nanocomposite, **C**) SF nanofibers and **D**) PA powder samples.

Thermogravimetric analysis of PA showed a major weight loss around 205^0C while SF and PASF exhibited similar weight loss around 244.7^0C and 245.9^0C respectively (**Fig 4.5**).

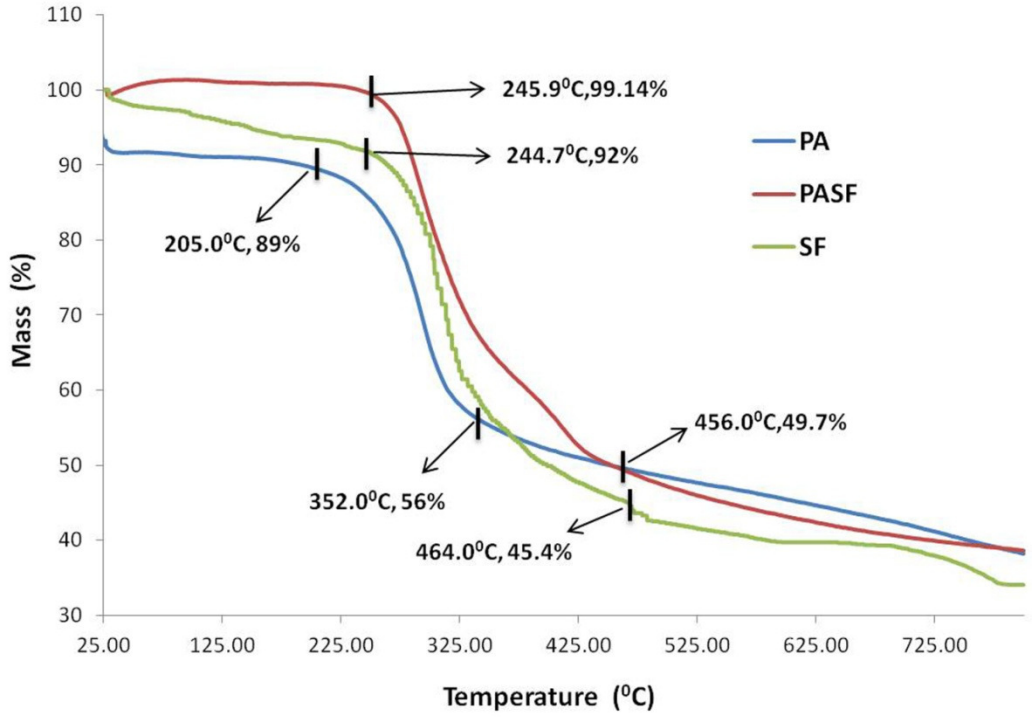

Fig 4.5: Thermo-gravimetric analysis of scaffolds. Thermal curves of polyaniline (PA), composite (PASF) nanofibers and silk fibroin (SF) nanofibers.

4.3.4 Fabrication of pre-seeded and un-seeded nerve conduit and implantation in rats

The fabricated nerve conduits had an internal diameter of around 1.3mm and wall thickness of 0.5mm comprising of multiple layers organized in a layer by layer fashion (**Fig 4.6A-D**). Rat Schwann cells (SCTM41) were also found to adhere and proliferate on both PASF and SF conduits (**Fig 4.6E-F**). The porosity of SF and PASF nerve conduits was observed to be 15.8% ($\pm$ 0.2) and 11.2% ($\pm$ 0.3) respectively. The SF conduits exhibited maximum swelling ratio of 33.5% whereas PASF conduits were found to have a swelling ratio of 15.3% after 24 hours (**Fig 4.7**).

4.3.5 *In vivo* intra dermal test

The 24 hour saline extract of the PA-SF (**Fig 4.8A ii**) and SF conduits (**Fig 4.8A iii**) did not produce any abnormal clinical symptoms, oedema or erythema in the animals. The site of administration of the extract did not exhibit any abnormality as compared to the control saline group (**Fig 4.8A i**) upto 72 hours from the time of intra-dermal injection.

4.3.6 Surgical implantation of nerve conduits

The dimensions of the nerve conduit were found to be suitable for implantation in a rat sciatic nerve injury model. The strength and texture of the conduits were also suitable for suturing and the conduits did not show any dislocation or deformation upon implantation in the sciatic nerve gap.

4.3.7 Functional analysis of regenerated sciatic nerve

The functional recovery of sciatic nerve was monitored by walking track analysis as well as electrophysiological tests like NCV,CMAP and MUP.

The wave patterns of compound muscle action potential (CMAP) obtained from both SF and PASF nanocomposite groups following stimulation near the proximal as well as distal end of the implanted conduits are represented in **Fig 4.10**.

The electrophysiological parameters for evaluating extent of functional regeneration as well as the percentage of recovery compared to a normal rat are tabulated in **Table 4.1**. A normal nerve was found to exhibit an average CMAP of 16mV upon quantitative analysis of the peak amplitude obtained from action potential signals. In comparison, the PASF nanocomposite group exhibited CMAP of 4.8mV and 12mV after 6 months and 12 months of implantation respectively. The animals treated with pre-seeded nanocomposite conduits (PASF- cell) were found to have CMAP of 5.7mV and 12.8mV after 6 months and 12 months of implantation respectively. Animals with SF conduits had an average CMAP of 3.4mV and 5.5mV after 6 and 12 months of conduit implantation respectively. Schwann cell seeded SF conduits were found to exhibit CMAP of 4.2mV and 11mV after 6 and 12 months post surgery respectively.

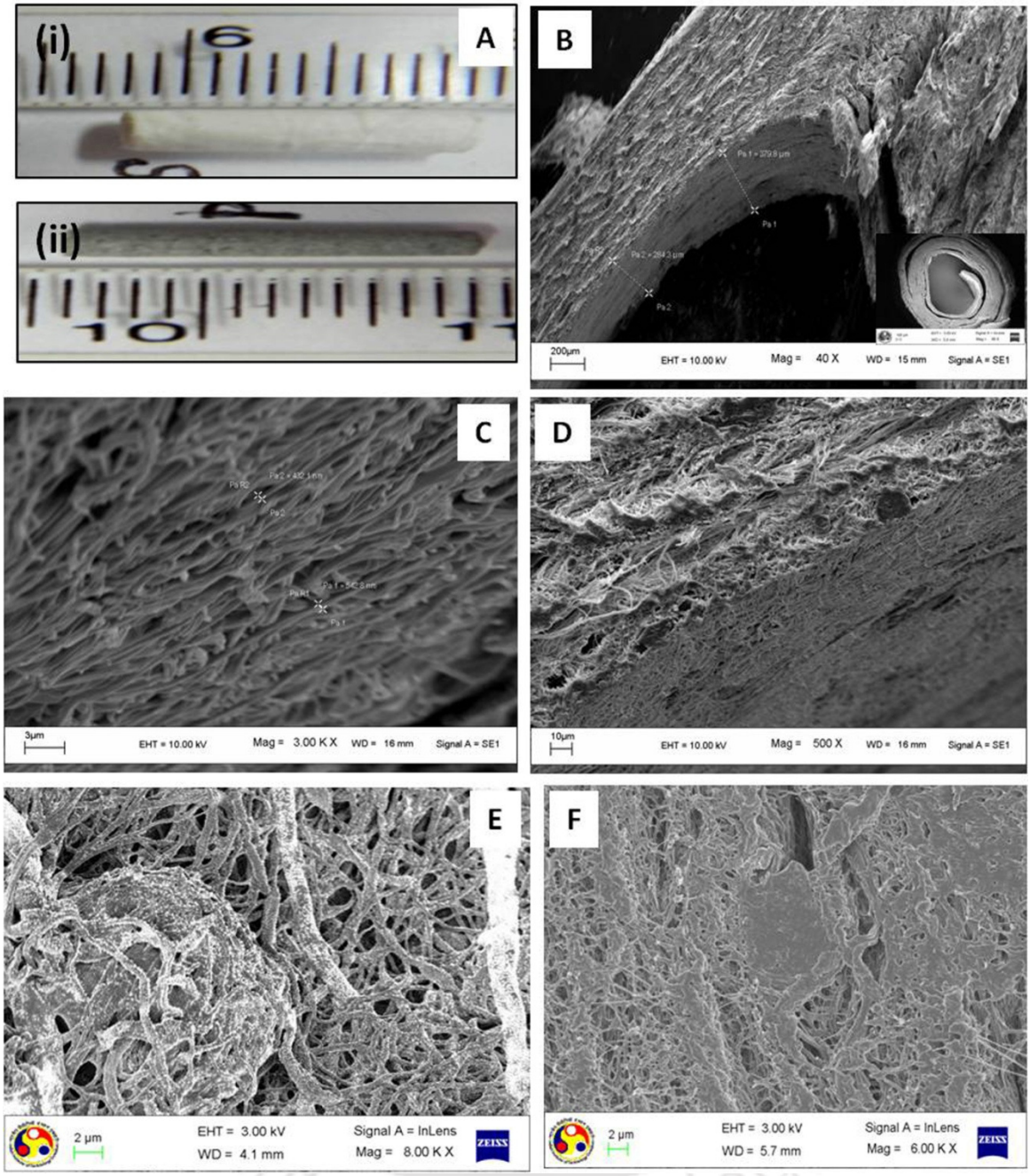

Fig 4.6: Morphology of nerve conduit and cellular growth on conduits. **A)** Digital image of silk fibroin (i) and silk fibroin-polyaniline nerve conduit (ii). **B-D**) FESEM images of a nerve conduit illustrating the stacking of multiple layers of nanofibers, inset shows cross section of a conduit **E**) Schwann cell adhesion and proliferation on PASF nerve conduit, **F**) Schwann cell adhesion and proliferation on SF nerve conduit.

The nerve conduction velocity (NCV) of a normal sciatic nerve was found to be around 58m/sec while animals with PASF conduits had NCV of 40m/sec and 43m/sec after 6 and 12 months respectively. Schwann cell seeded PASF conduits exhibited NCV of 45m/sec and 50m/sec after 6 and 12 months respectively. NCV of

animals implanted with SF conduits were found to be 20m/sec and 41m/sec after a period of 6 and 12 months respectively. Animals with Schwann cell seeded SF conduits had NCV of 25m/sec and 46m/sec after 6 and 12 months respectively (Table 4.1).

Animals implanted with PASF nanocomposite conduits exhibited motor unit potential (MUP) of 112μV and 122μV as recorded from the gastrocnemius muscle of theanimals after 6 and 12 months respectively. Cell seeded PASF group exhibited MUP of 114μV and 124μV after 6 and 12 months respectively. In comparison, animals having SF conduits had a MUP of 75μV after 6 months and 82μV after 12 months of implantation. Cell seeded SF conduits exhibited MUP of 89μV and 105μV after 6 and 12months respectively. The MUP of a normal rat's gastrocnemius muscle was found to be 163μV while immediately post implantation (0 hour) a MUP of 27μV was recorded **(Table 4.1).**

The control group of untreated animals exhibited similar electrophysiological parameters over a period of one year. No action potential could be recorded in nerve conduction studies and minute MUP of around 30μV was generated around the gastrocnemius region (**Fig 4.11B,C**).

The sciatic function index (SFI) of animals implanted with PASF nanocomposite conduits was found to be -61 and -51 after 6 and 12 months respectively. Schwann cell pre-seeded PASF conduits exhibited SFI of -58 and -47 after 6 and 12 months respectively. SF conduits exhibited SFI of -79 and -72 after 6 and 12 months post implantation respectively. SFI of animals with Schwann cell preseeded SF conduits were found to be -79 and -70 after 6 and 12 months post implantation respectively. In comparison animals of control group exhibited SFI of -100 upto 12 months. (**Fig 4.12**).

4.3.8 *Morphological analysis of regenerated sciatic nerve*

The untreated animals with sciatic nerve transection (control group) did not exhibit any tissue regeneration and both the proximal and distal stumps were found to have receded thereby lengthening the nerve gap (**Fig 4.11A**). In treated groups the implanted conduits were observed to be stable with no dislocation or deformation when the surgical area was reopened after 6 and 12 months. Further the

surrounding tissue also appeared to be morphologically normal in all the experimental groups. Histological analysis of the regenerated nerve indicated cellular recruitment inside the PASF nanocomposite conduits (both with and without cell groups) (**Fig 4.13**). TEM analysis confirmed the deposition of myelin sheath visualised as black layering over axons in the regenerated tissue from inside the nanocomposite conduits (**Fig 4.14 B-D**). In contrast, animals implanted with SF conduits showed less cellular migration inside the nerve gap. Some amount cellular infiltration was evident inside the cell seeded SF from histological analysis but TEM studies revealed fragmented myelination of the regenerating axons among the animals having SF conduits (both with and without cells) (**Fig 4.13 and Fig 4.14 E-H**).

GROUPS	Nerve Conduction Velocity (m/sec)		Compound Muscle Action Potential (mV)		Motor Unit Potential (μV)	
	Recorded Value	Percentage recovery relative to normal	Recorded Value	Percentage recovery relative to normal	Recorded Value	Percentage recovery relative to normal
NORMAL	58±2	*100%*	16±1.5	*100%*	163±3.6	*100%*
PASF-6 months	40±2.2	*68.96%*	4.8±1.2	*30%*	112±2.9	*68.71%*
PASF-12 months	43 ± 2.1	*74.13%*	12±1.8	*75%*	122±4.2	*74.84%*
Cell seeded PASF-6months	45±1.8	*77.5%*	5.7±1.1	*35.62%*	114±2.1	*72.15%*
Cell seeded PASF-12 months	50 ± 2.2	***86.2%***	12.8 ± 1.3	***80.00%***	124±2.5	***76.07%***
SF-6 months	20±1.3	*34.48%*	3.4±0.4	*21.25%*	75±4.2	*46.01%*
SF-12 months	41 ± 1.7	*70.6%*	5.5±0.6	*34.38%*	82±3.8	*50.3%*
Cell seeded SF - 6months	25±1.1	*43.1%*	4.2±1.3	*26.25%*	89±4.1	*54.6%*
Cell seeded SF-12 months	46 ± 2.1	*79.3%*	11±1.6	*68.75%*	105±4.8	*64.41%*

Table 4.1: ***Electrophysiological parameters obtained in different groups***

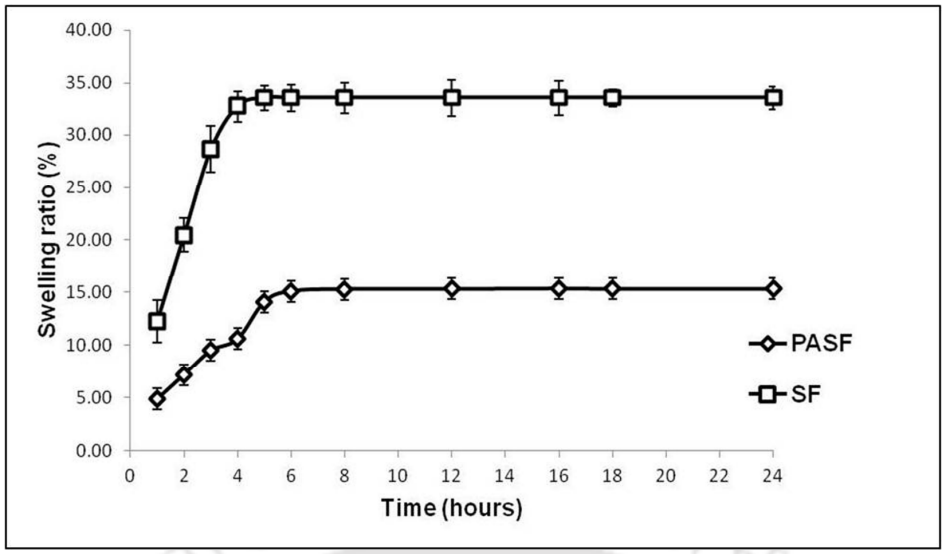

Fig 4.7: **Dynamic swelling ratio of PASF and SF conduits over 24 hours**.

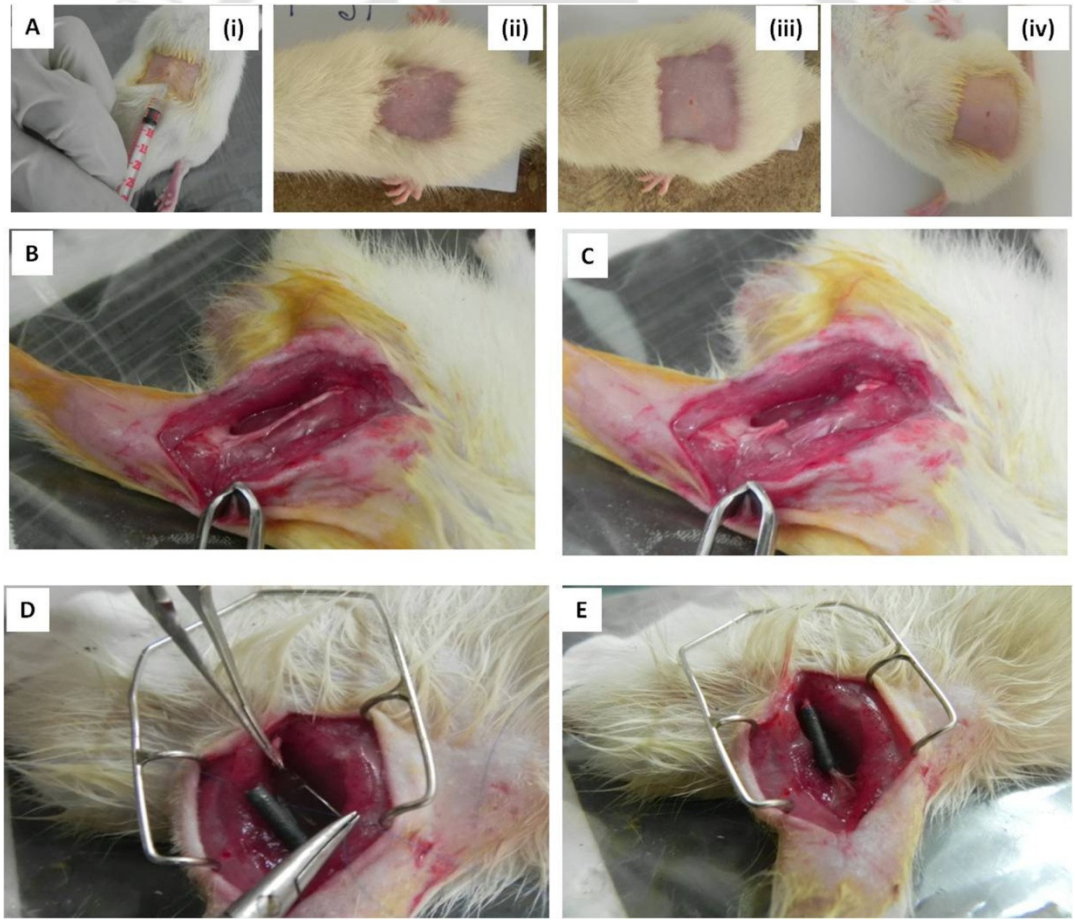

Fig 4.8: Intracutaneous skin irritation test and surgical implantation of conduit. A) (i) Intra-cutaneuous skin irritation test by administration of compounds thorough intradermal injection, Nature of skin 72 hours after administration of (ii) Saline extract of PASF conduits, (iii) Saline extract of SF conduits and (iv) Normal saline. **B-E**) Surgical procedure followed for implantation of conduit

4.4 Discussions

Fabrication of polyaniline blended poly(L-lactic acid-co-3-caprolactone) (P(LLACL)) – silk fibroin (SF) composite electrospun nanofibrous mesh has been previously reported to facilitate neuronal cell proliferation (Zhang J *et al*, 2014). The study was conducted with commercially available high molecular weight polyaniline (15kDa) and limited to exploring the compatibility of polyaniline based nanofibers with neuronal PC12 cells (Zhang J *et al*, 2014). However the safety and efficacy of polyaniline based nerve conduits in promoting functional regeneration of nerves remain unaddressed by the preliminary *in vitro* studies. Hence we focused our work on synthesising low molecular weight polyaniline oligomers to blend with silk fibroin and fabricate tubular nerve conduits for long duration *in vivo* studies.

In the present study, polyaniline powder was synthesised following previously reported literature (Ai *et al*, 2010; Jiang *et al*, 2009). The amphiphilic aniline monomer in the presence of strong acid releases anilinium cations and forms micelles which act as template for the polymerization reaction. The polyaniline powder was observed to undergo aggregation and was amorphous in nature which could be due to the high monomer to APS ratio **(**Abdolahi *et al*, 2012) (**Fig 4.1A**).

The biocompatibility of synthetic conducting polymers has always remained a major concern limiting their widespread use in biomedical applications. Extensive in vivo biocompatibility studies found that polyaniline did not induce any skin irritation or sensitization in humans and guinea pigs respectively **(**Humpolicek *et al*, 2012**).** However polyaniline did exhibit concentration dependent cytotoxicity when added in very high concentration in the range of 2- 100mg/ml **(**Humpolicek *et al*, 2012). Further the cytotoxic effects of conducting polymers like polyaniline/polypyrrole have been reported to vary widely between cell lines (Kucekova *et al*, 2014,; Vaitkuviene *et al*, 2013). In the present study we found the synthesised amorphous polyaniline powder to be non-toxic to rat Schwann cells (SCTM41) at lower concentration of 100µg/ml as well as at the highest concentration of 1000µg/ml when cellular viability was observed to be 80% of the control (**Fig 4.1B**). Live-dead assay with acridine orange (green fluorescence) and ethidium bromide (red fluorescence) was performed wherein the live cells preferentially take up acridine orange staining

green. Normal cellular morphology and abundant live cells were observed upto PA treatment concentration of 1000µg/ml through live-dead staining assay (**Fig 4.1C-H**).

The molecular weight distribution of a polymer is essential for analysing its physical, chemical and biological properties. The molecular weight of synthesised polyaniline has been previously studied using chromatographic techniques (Kolla *et al*, 2005). However, solubility of the sample in an organic solvent is an essential prerequisite to obtain accurate results by chromatography. Polyaniline has been reported to be almost insoluble in any solvent and only exists in a dispersion state when mixed with organic solvents (Wessling, 2000). Hence, for obtaining accurate molecular weight distribution of polyaniline, we performed Matrix-assisted laser desorption/ionization (MALDI). Both solvent-less and solvent based MALDI were carried out to study the role of solvents in isolating higher molecular weight oligomers of polyaniline. Polyaniline primarily produces three types of oligomers based on the presence/absence of terminal amine (-NH_2) which differ by a m/z value of 16. (**Fig 4.9**) (Dolan *et al*, 2014). Further, the addition of one phenyl group (-C_6H_4NH-) or 1-mer to the oligomer chain led to an increase of m/z value by 91 (Dolan *et al*, 2014).

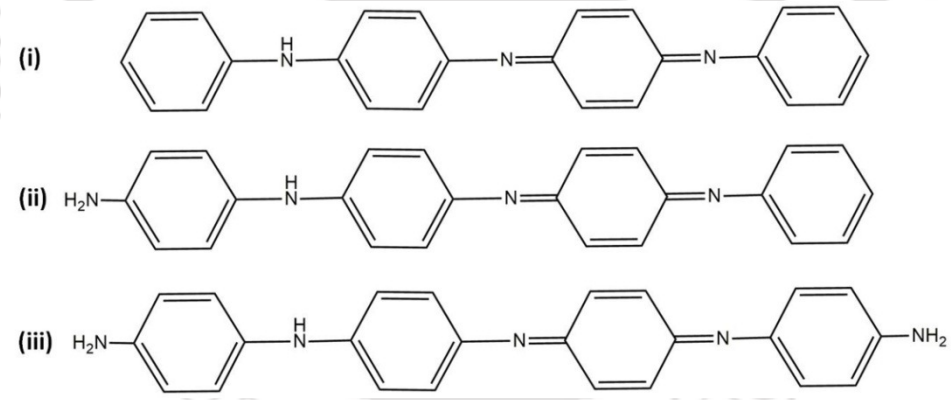

Fig 4.9: ***Representative structures of different types of aniline oligomers***. (i) Aniline oligomers terminated by phenyl group on both ends (lowest molecular weight species), (ii) Oligomers having an amine in one terminal and equal number of six-carbon rings and nitrogen atoms, (iii) Oligomers having amine group in both terminals.

Solvent based MALDI of polyaniline using acetonitrile and THF as solvent produced prominent peaks corresponding to 6-mer (m/z =542,558,574), 7-mer (m/z=634,650,666) and low intensity peaks for 8-mer (m/z=725,741). Polyaniline mixed in THF produces an additional peak for 8-mer around m/z = 757

corresponding to the structure depicted in **Fig 4.2(A-B)**. Solvent based MALDI analysis of polyaniline could detect oligomers upto a maximum of 8 repeat units since only very low molecular weight portions are sparingly soluble in organic solvents like acetonitrile and THF (**Fig 4.2A-B**).

In order to detect higher molecular weight oligomers we performed solvent less MALDI. The peaks for the oligomers in this case were observed to be of much higher intensity as compared to solvent based MALDI and polymers with upto 12 repeat units were detected (**Fig 4.2C-D**). The results provide strong indication that solvent less MALDI is an ideal method to study molecular mass spectrometry of insoluble polymers like polyaniline and can also detect higher oligomers more efficiently as compared to conventional solvent based techniques.

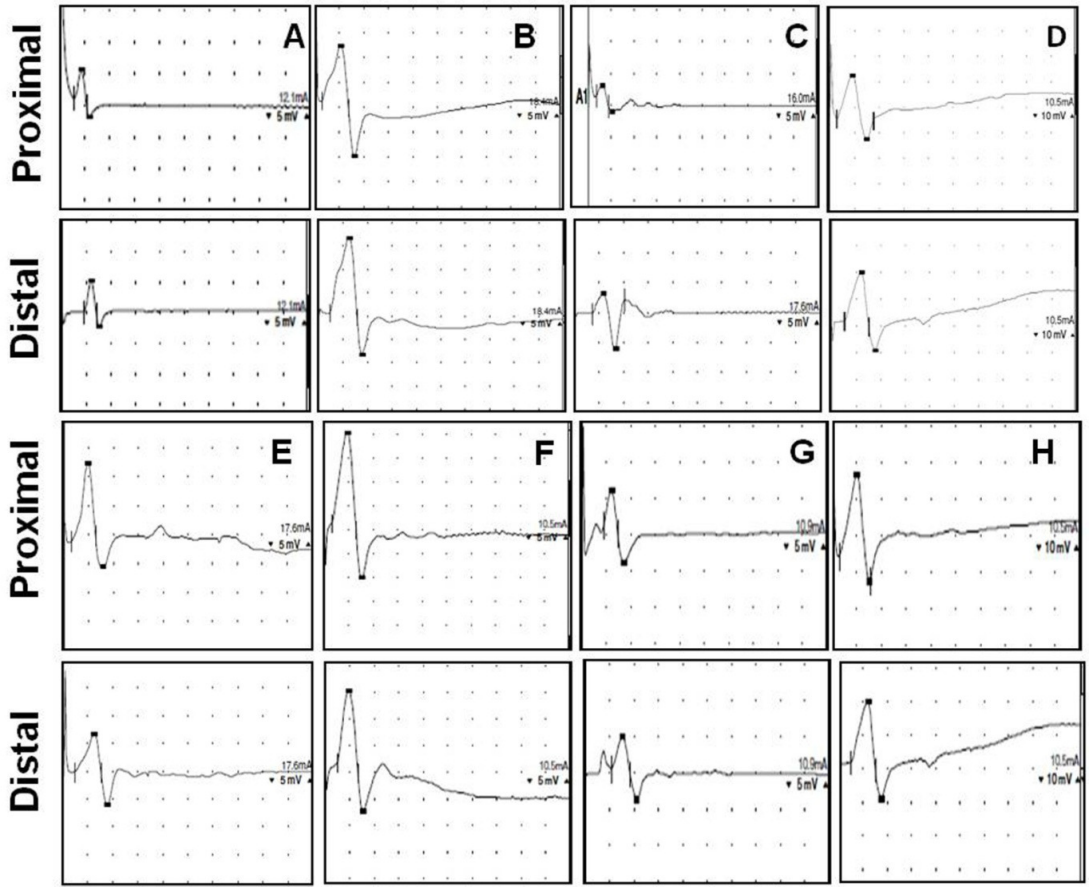

Fig 4.10: Wave pattern of compound muscle action potential. Action potential recorded after stimulating at the proximal and distal ends of implanted conduit **A**) PASF group after 6 months, **B**) PASF group after 12 months, **C**) SF group after 6 months, **D**) SF group after 12 months, **E**) Cell seeded PASF conduits after 6 months, **F**) Cell seeded PASF conduits after 12 months, **G**) Cell seeded SF conduits after 6 months and **H**) Cell seeded SF conduits after 12 months.

In the present study, aggregates of low molecular weight polyaniline were blended with silk fibroin protein in formic acid to form composite nanofibers through electrospinning. However, since PA is insoluble in formic acid and exists in a dispersed state it was observed through electron microscopy that the polyaniline aggregates were broken down to nano dimensions during electrospinning thereby forming a uniform covering of polyaniline nanoparticles (average size 40-60nm) over the silk nanofibers (**Fig 4.3B-C**). Consequently, the average diameter of PASF nanofibers (350-450nm) were found to be larger than pristine SF fibers (150-250nm) (**Fig 4.3D**).

Polyaniline based composite scaffolds have been previously demonstrated to support adhesion and differentiation of neuronal cells **(**Guarino *et al*, 2013**).** In our study, both PASF and SF nanofibers were found to support adhesion of Schwann cells (**Fig 4.3E-F**). The nanofibrous scaffolds (both PASF and SF) by virtue of their higher surface area were able to support growth and proliferation of cells for a longer time as compared to the control cell culture surface (**Fig 4.3G**).

The resistance of silk fibroin was observed to decrease by 12 folds upon addition of polyaniline powder in a very low concentration (1% of silk fibroin). Further decrease in resistance could be achieved by increasing the concentration of polyaniline in the polymer blend (data not shown), however, the propensity of PA powder to produce cytotoxic effect at higher concentration lead to its restricted use in the present study in order to balance between electrical conductivity and biocompatibility.

The electrospun mats (SF and PASF) were characterised by FTIR and XRD analysis and compared with polyaniline powder to confirm the formation of composite nanofibers (**Fig 4.4A-D**). The PASF nanocomposite mat exhibited a FTIR peak around 1614 cm^{-1} which correlates to 1668 cm^{-1} absorbance peak in SF for amide I and 1635 cm^{-1}peak present in PA powder corresponding to quinone ring C=N stretching vibration (Zhang *et al*, 2011; Kim *et al*, 2003). The lower frequency 1541 cm^{-1} peak of PASF nanocomposite can be attributed to 1579 cm^{-1} benzenoid diamine ring stretching of PA as well as amide II region (1514 cm^{-1}) of SF nanofibers (**38,39**). Similarly the peak at 1246 cm^{-1} for PASF nanofibers can be ascribed to the amide III structure of SF at 1240 cm^{-1} and the characteristic C-N stretching of PA (Zhang *et al*, 2011; Kim *et al*, 2003**).** A small peak was observed around 1146 cm^{-1} in SF

electrospun mat corresponding to aliphatic amine whereas a broad peak around 1119 cm^{-1} was exhibited by PASF nanocomposite scaffolds. However no similar peak was found in the polyaniline powder which comprises entirely of aromatic amines. A series of small peaks observed at 931 cm^{-1},777 cm^{-1}, 725 cm^{-1},644 cm^{-1}, 517 cm^{-1} in PA powder can be ascribed to out-of plane deformation of C-H (Zhang *et al*, 2011; Abdolahi *et al*, 2012**).** These were observed to be merged together forming a broad peak around 690 cm^{-1} in PASF nanocomposite mat.

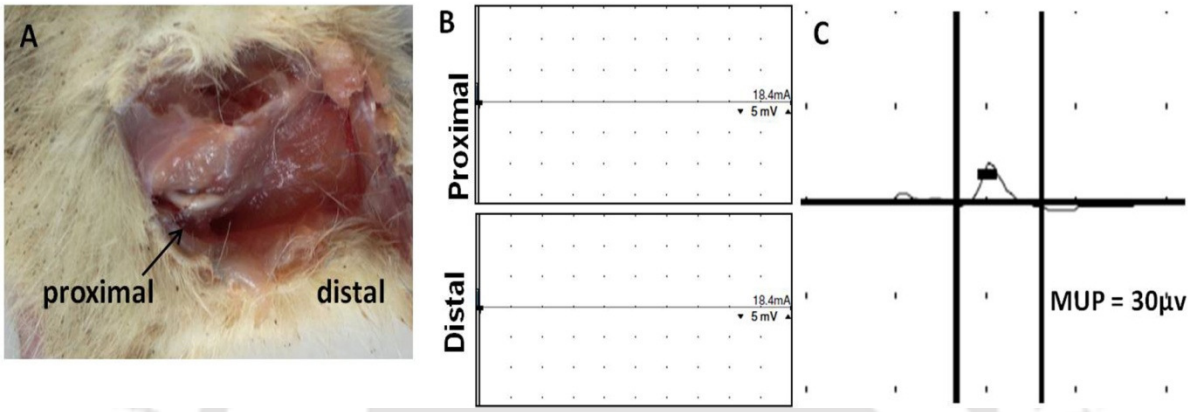

Fig 4.11: Morphological and electrophysiological assessment in control group. A) No tissue regeneration was observed in the nerve gap region after 12 months, **B**) No action potential could be detected by nerve conduction studies, **C**) MUP recorded in the gastrocnemius region.

The crystalline form of polyaniline has been reported to exhibit three characteristic XRD peaks at 2θ=15°, 20° and 25° corresponding to (011), (020) and (200) crystal planes with the one at 25° being the dominant peak (Abdolahi *et al*, 2012; Lee *et al*, 2006). However, we observed only a small and broad peak at 2θ=24° for the synthesised PA powder (**Fig 4.4D**). It indicates the low crystallinity and comparatively higher amorphous nature of the synthesised PA powder which is due to the high monomer (aniline) to APS ratio used during synthesis. The XRD pattern of SF electrospun nanofibrous mat exhibited a broad peak around 2θ=21° characteristic of amorphous silk fibroin protein in β-sheet configuration (**Fig 4.4C**) (Wang *et al*, 2014). The PASF nanocomposite sheet showed two peaks around 2θ=20.65° and 2θ=24.8° indicating the formation of a composite comprising amorphous silk fibroin and polyaniline (**Fig 4.4B**).

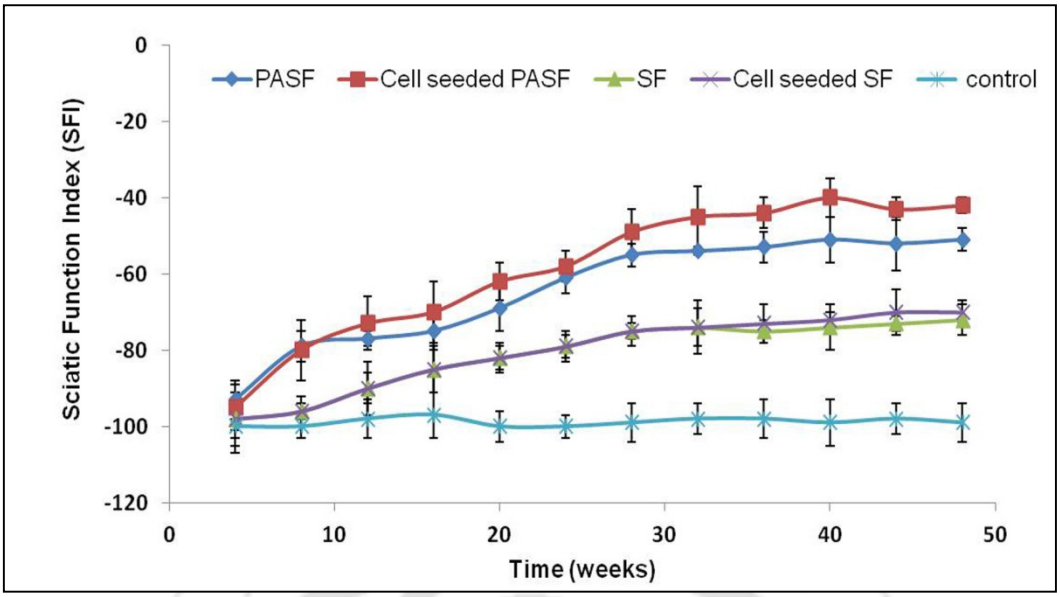

Fig 4.12: Sciatic Function Index (SFI) calculated through walking track analysis.

Polyaniline generally exhibits three major weight losses by TGA around 100C, 200^{0}C and 500^{0}C corresponding to water loss, loss of acid molecules and decomposition of polymer respectively (Wei Y *et al*, 1989). In the present study, PA was thoroughly dried and hence limited weight loss around 100^{o}C was observed. A major weight loss occurred between 205^{0}C-352^{0}C which can be attributed to the loss of hydrochloric acid molecules used as dopant. The polymer was found to steadily decompose to below 45% of its initial weight by 700^{0}C (**Fig 4.5**). Silk fibroin nanofibers showed a major weight loss around 245^{o}C due to thermal degradation of the protein and continued till 464^{o}C before becoming stable upto 700^{0}C (**Fig 4.5**) (Wei K *et al*, *Membranes*, 2011). PASF composite nanofibers exhibited thermal properties similar to that of pure silk fibroin since PA concentration was restricted to only 1% of the composite. The sharp weight loss around 246^{o}C points to the degradation of silk fibroin. The composite continued to degrade with increase in temperature and less than 45% of initial weight remained upto 700^{0}C (**Fig 4.5**).

The electrospun sheets (both SF and PASF) were peeled off and rolled over a needle of appropriate diameter. Such sheet rolling method enables fabrication of multiple nerve conduits with varying dimensions (wall thickness, diameter and length) from a single electrospun sheet. Multiple rotations of the electrospun sheet created a lamellar architecture of the nerve conduit which mimics the layer by layer deposition of myelin by Schwann cells over axons (**Fig 4.6A-D**). Consequently,

Schwann cells when cultured over the conduits (both SF and PASF) were found to adhere and proliferate in the form of clusters (**Fig 4.6E-F**). The fabricated nerve conduits exhibited no evident signs of cytotoxicity when cultured with Schwann cells over a period of 10 days. Additionally, such stacking and rolling of multiple layers of densely arranged nanofibers contributed to the overall low porosity and swelling tendency of the conduits (**Fig 4.7**).

The size of polyaniline particles have been found to influence the cytotoxicity and particularly its nanoform has been reported to be highly toxic at concentrations above 10µg/ml causing cell death, increase cellular reactive oxygen species and disturbed mitochondrial membrane potential **(**Li *et al*, 2014). Since the PASF nanocomposite fibers comprised of polyaniline nanoparticles it was essential to confirm their biocompatibility through intracutaneous skin irritation and toxicity studies. However no adverse immunogeneic or toxic response was noted among the animals (both PASF and SF groups) which may be attributed to the strong interaction between PA nanoparticles and SF protein which prevents any washout of nanoparticles into the saline extract (**Fig 4.8A**).

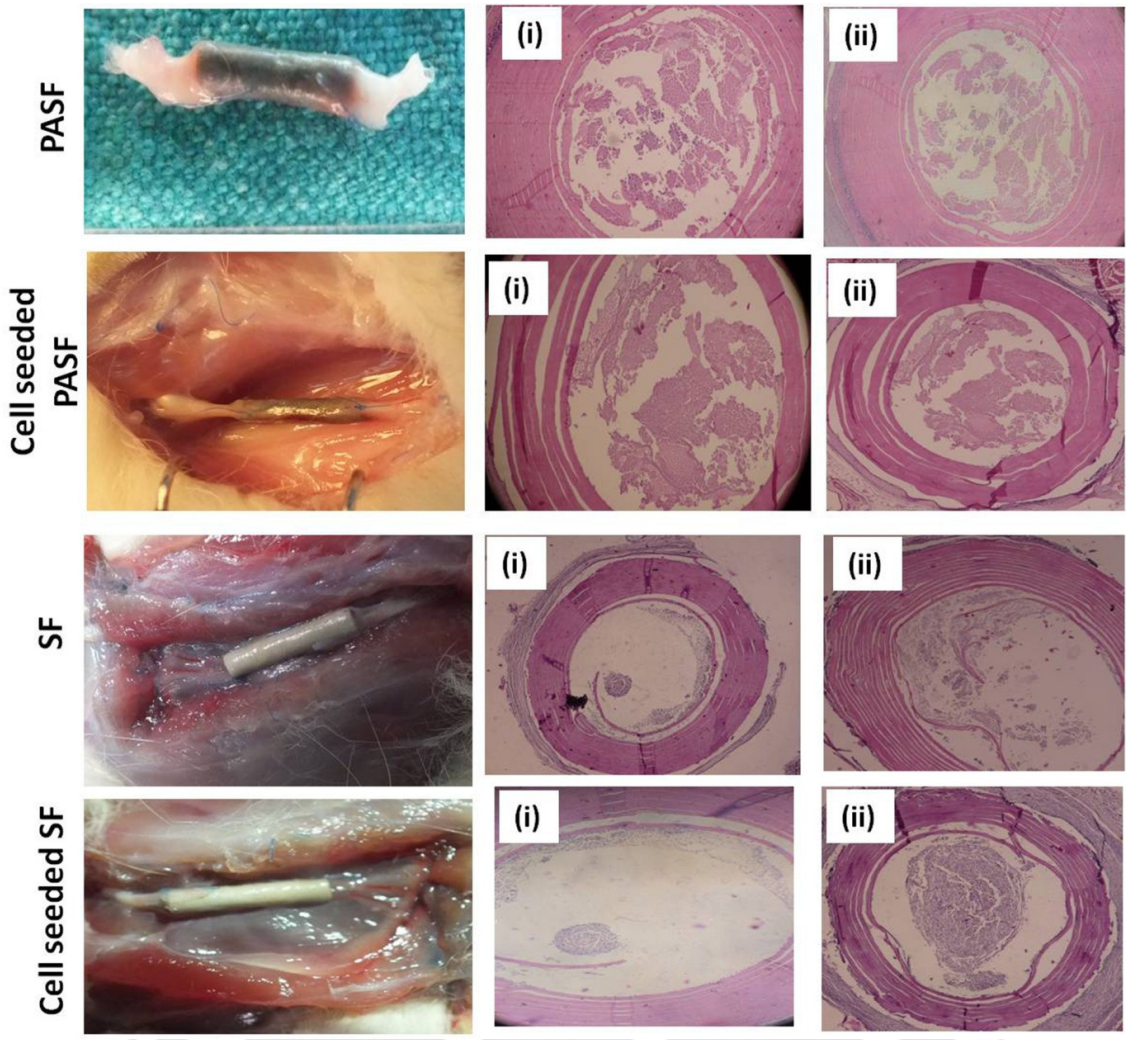

Fig 4.13: Gross and histological examination. Nerve conduits were harvested for gross observation and histological examination by hematoxylin-eosin staining after (**i**) 6months and (**ii**) 12 months of implantation.

The electrophysiological studies carried out to evaluate functional regeneration of the sciatic nerve can be broadly divided into a) nerve conduction velocity and muscle action potential measurements and b) motor unit potential recorded from the surrounding gastrocnemius muscle. The compound muscle action potential (CMAP) waveforms for all the experimental groups are depicted in **Fig 4.10** whereas the quantitative analysis of CMAP and NCV are represented in **Table 4.1.** The animals implanted with PASF conduits (both with and without cells) showed appreciable improvement in wave pattern with enhanced amplitude and higher area under the curve with time from 6 months to 12 months. A similar trend was also observed with animals having SF conduits (both with and without cells) after 6 and 12 months. However, the nanocomposite group with PASF conduits (both with and without cells)

clearly outperformed the animals with plain SF conduits (both with and without cells) with higher NCV and CMAP values after 12 months indicating better functional regeneration of the transacted nerve. The animals implanted with Schwann cell seeded PASF conduits exhibited recovery as high as 86.2% of NCV and 80.0% of CMAP as compared to normal rat thereby suggesting the positive role of Schwann cell pre-seeding in enhancing nerve regeneration outcomes. The animals that were left untreated (control group) did not exhibit any action potential even after applying stimulation up to 18.4mA at the proximal and distal end of the nerve gap over a period of 12 months indicating the absence of regenerated neural tissue across the gap (**Fig 4.11B**).

Nerve conduction studies and CMAP analysis form only a part of complete peripheral neurophysiological examination and are generally accompanied by monitoring motor unit potentials (MUP) recorded from the surrounding muscle area through needle EMG. A motor unit is the basic functional element of skeletal muscle comprising of the anterior horn cell, its axon and all the muscle fibers it innervates including the neuromuscular junctions. The action potential generated when a motor unit fires upon voluntary contraction of muscle is recorded as MUP. Since sciatic nerve is the major mixed nerve innervating the gastrocnemius region we conducted MUP measurements through needle EMG to evaluate the neuromuscular regeneration in the region. MUP recorded immediately post surgery exhibited minute potential of 27μV which could be attributed to smaller nerves other than the sciatic nerve which also innervate the gastrocnemius muscle fibers. The animals implanted with PASF conduits pre-seeded with Schwann cells exhibited highest MUP after 12 months corresponding to 76.07% of MUP of normal rat (**Table 4.1**). The result indicates enhanced re-innervations of the gastrocnemius muscle fibers with regenerated axons. MUP recorded from the untreated animals (control group) exhibited minute potential of 30μV which could be attributed to smaller nerves other than the sciatic nerve which also innervate the gastrocnemius muscle fibers (**Fig 4.11C**).

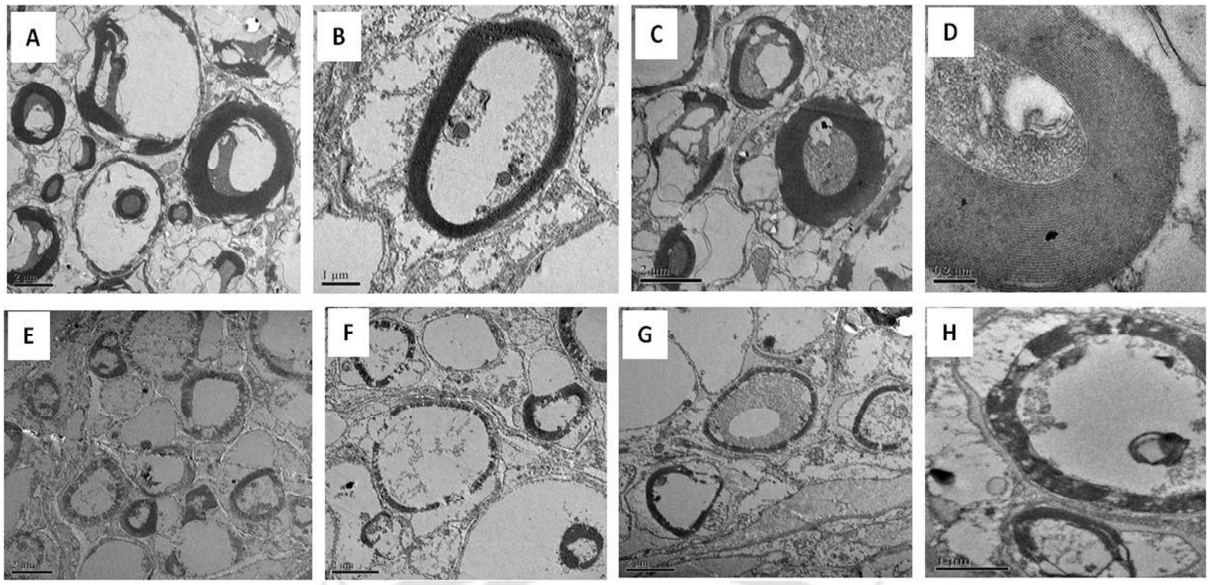

Fig 4.14: **Ultra structure of regenerated tissue under TEM**. **A)** Normal sciatic nerve, **B**) Regenerated tissue through PASF conduits 1year post implantation, **C**) Regenerated tissue through Schwann cell seeded PASF conduits 1year post implantation, **D**) Higher magnification image of myelin sheath in a single axon of cell seeded PASF conduits 1year post implantation, **E**-**F**) Regenerated tissue through SF conduits 1year post implantation, **G**-**H**) Regenerated tissue through cell seeded SF conduits 1year post implantation.

Although several advanced electrophysiological and behavioural tests are available to conduct peripheral neurophysiological examination, walking track analysis of rats by calculating Sciatic Function Index (SFI) is still one of the most preferred non-invasive ways to objectively assess recovery of motor function in peripheral nerve injury models (Varejão *et al*, 2001). A SFI score of -100 indicates complete inability to walk and severely damaged gait whereas a normal walking pattern gives a SFI score of 0. The untreated animals (with a nerve gap and without any nerve conduit) exhibited constant SFI of around -100 for 12 months (**Fig 4.12**). Sequential improvement of SFI was observed in all experimental groups with a saturation point after 32 weeks **(Fig 4.12).** Animals having SF conduits with and without cells showed SFI improvement upto a maximum of -70 and -72 respectively. In comparison Schwann cell seeded PASF conduits exhibited best gait pattern with a SFI of -41 which was much improved than the animals with PASF conduit having SFI of -51.

The conduits were harvested from the animals 6 and 12 months post implantation and the tissue within the nerve gap was histo-morphometricaly analysed for evaluating the extent of neuro-regeneration through the conduits (**Fig 4.13**). Low

amount of cellular growth was observed across the lumen of SF and cell seeded SF conduits after 6 months. However, after 12 months, accumulation of inflammatory cells inside the conduit was observed in SF and SF cell groups. Culture of Schwann cells over the nanocomposite PASF conduits evidently led to higher amount of normal neuronal cells inside the lumen facilitating regeneration of nervous tissue across the gap. The structural stability of the nerve conduits even after 12 months implantation can be attributed to the stacking of multiple layers of nanofibers leading to minimal swelling ratio of the conduits. In case of animals where no conduit was implanted (control group) the nerve gap increased considerably on both ends and no signs of neural regeneration was observed even after 12 months (**Fig 4.11A**). Although some portion of the proximal end remained the distal nerve stump was found to have completely degenerated. This could be due to long duration Wallerian degeneration occurring in neurotmesis grade nerve injury which causes the nerve stumps to degenerate and recede from the distal end.

The process of myelination is an important indicator of accurate neuron-glia interaction which is essential for complete neural regeneration. In the peripheral nervous system myelin is deposited around an axon by rotating Schwann cells in a layer by layer fashion (Garbay *et al*, 2000). The high lipid to protein ratio (75% lipid and 25% protein) of the myelin sheath confers it with electrically insulating property required for maintaining proper saltatory conduction of nerve impulse (Garbay *et al*, 2000). This high lipid content is exploited to stain the myelin sheath with lipid binding dyes like osmium tetra oxide, toluidene blue etc. The black coating observed around axons after osmium tetraoxide staining of the samples under TEM indicates deposition of myelin by Schwann cells (**Fig 4.14**). A closer look at the ultrastructure of the tissue harvested from the lumen of cell seeded PASF conduits revealed thick deposition of myelin in a lamellar fashion indicating proper myelination of the regenerating axons (**Fig 4.14 C-D**). In comparison, the thin, discontinuous and granular type deposition of myelin observed in the regenerating tissue of SF conduits (with and without cells) (**Fig 4.14 4.E-H**) points to incomplete and improper myelination which explains the low NCV, CMAP and MUP values observed in animals belonging to SF groups (with and without cells).

Although conductive polymer based scaffolds have been extensively researched for potential use as nerve conduits, their *in vivo* studies for evaluating nerve

regeneration in animal models have been very limited (Ahn *et al*, 2015; George *et al*, 2009**,** Mottaghitalab *et al*, 2013; Yu *et al*, 2014). Further these *in vivo* studies have been for a short duration (maximum 16 weeks) and monitored neuro-regeneration primarily based on histopathological/immuno-histochemical outcomes without complete electrophysiological analyses. In the present study, we observe the effects of synthetic conducting polymer like polyaniline in vivo over a long duration (1 year) and evaluate functional nerve regeneration through several electrophysiological tests like NCV, CMAP and MUP including walking track analysis. The animals implanted with Schwann cell pre-seeded nanocomposite PASF conduits exhibited excellent NCV and CMAP patterns along with high MUP values which are better than previous reports of nerve regeneration using similar electrically conducting nerve conduits (Ahn *et al*, 2015;; Mottaghitalab *et al*, 2013). These electrophysiological results along with thick myelination in a lamellar fashion strongly indicate superior functional and morphological regeneration of nerves in the PASF group as compared to previously reported conducting polymer based nerve conduits.

4.5 Conclusions

The present study demonstrates the fabrication of polyaniline-silk nanocomposite based tubular conduits by single nozzle electrospinning and subsequent rolling of the electrospun sheet. The extensive *in vitro* and *in vivo* toxicity studies prove the biocompatibility of polyaniline. Further the fact that the polyaniline-silk fibroin nanocomposite nerve conduits did not elicit any immune response or graft rejection over a period of one year upon implantation establishes the safety of polyaniline based scaffolds for biomedical applications. The study also demonstrates the efficacy of pre-seeding nerve conduits with Schwann cells in enhancing neural regeneration outcomes. The excellent electrophysiological parameters obtained after 12 months of implantation of polyaniline based nerve conduit along with cellular recruitment and thick lamellar deposition of myelin over regenerating axons should encourage further *in vivo* studies using conducting polymers for developing biocompatible electrically conductive nerve conduits.

Chapter 5

Summary and Future prospects

5.1 Summary

The present study demonstrates the utility of nanocomposite based scaffolds as potential biomaterials for fabricating nerve conduits. Although silk fibroin is one of the most used biomaterial as an implant (sutures), its highly insulating properties render it unsuitable for fabricating scaffolds for mimicking the electrically conductive tissues of the body like nerve and cardiac muscles. We hereby demonstrate how silk based nanocomposites consisting of metallic nanoparticles and conducting polymer enhances functional and morphological regeneration of nerve in a rat sciatic nerve injury model. The novel sheet rolling method utilised for fabricating conduits from nanofibers enables multiple conduit development of varied dimensions from a single electrospun sheet. Pre-seeding the conduits with Schwann cells also enhanced and accelerated neural regeneration through the nerve gap as evident from the extensive electrophysiological and histological studies. Further the long duration studies undertaken by us establish the safety and neuro-regenerative potential of such nanocomposite conduits.

5.1.1 Silk-Gold nanocomposite based scaffolds for neural tissue engineering

We report a novel silk-gold nanocomposite based nerve conduit successfully tested in a neurotmesis grade sciatic nerve injury model in rats over a period of eighteen months. The conduit was fabricated by adsorbing gold nanoparticles onto silk fibers and transforming them into a nanocomposite sheet by electrospinning which is finally given a tubular structure by rolling on a stainless steel mandrel of chosen diameter. The conduits were found to promote adhesion and proliferation of Schwann cells in vitro and did not elicit any toxic or immunogenic responses in vivo. We also report for the first time, the monitoring of muscular regeneration post nerve conduit implantation by recording motor unit potentials (MUPs) through needle electromyogram. Pre-seeding the conduits with Schwann cells enhanced myelination on the regenerated tissue. Histo-morphometric and electrophysiological studies proved that the nanocomposite based conduits pre-seeded with Schwann cells performed best in terms of structural and functional regeneration of severed sciatic nerves. The near normal values of nerve conduction velocity (50m/sec), compound muscle action potential (29.7mV) and motor unit potential (133μV) exhibited by the

animals implanted with Schwann cell loaded nerve conduits in the present study are superior to those observed in previous reports with synthetic materials as well as collagen based nerve conduits. Animals in this group were also able to perform complex locomotory activities like stretching and jumping with excellent sciatic function index (SFI) and led a normal life.

5.1.2 **Silk-Polyaniline nanocomposite based scaffolds for neural tissue engineering**

The present study describes the fabrication of polyaniline-silk fibroin nanocomposite based nerve conduits and its subsequent implantation in a rat sciatic nerve injury model for peripheral nerve regeneration. This is the first *in vivo* study of polyaniline based nerve conduit describing the safety and efficacy of the conduits in treating peripheral nerve injuries. The nanocomposite was synthesised by single nozzle electrospinning of a mixture of silk fibroin protein and polyaniline wherein the silk nanofibers were observed to be uniformly coated with polyaniline nanoparticles. Tubular shaped nerve conduits were subsequently formed by multiple rolling of the electrospun sheet over a stainless steel mandrel. The conduits were characterised *in vitro* for its physico-chemical properties as well as its compatibility with rat Schwann cells. Upon implantation in a 10mm sciatic nerve injury model, the conduits were evaluated for their neuro-regenerative potential through extensive electrophysiological studies and monitoring of gait pattern over a course of 12 months. Gross examination, histological and ultra-structure analyses of the conduits and the regenerated nerve were also performed to evaluate morphological regeneration of transected nerve. Polyaniline-silk fibroin nanocomposite conduits pre-seeded with Schwann cell (Cell seeded PASF) exhibited excellent nerve conduction velocity i.e NCV (43m/sec), compound muscle action potential i.e CMAP (12.8mV), motor unit potential i.e MUP (124μV), growth of healthy tissue along the nerve gap and thick myelination of regenerating axons 12 months after implantation indicating enhanced neuro-regeneration. The excellent functional recovery achieved by animals implanted with Cell seeded PASF conduits (86.2% NCV; 80.0% CMAP; 76.07% MUP) are superior to outcomes achieved previously with similar electrically conductive conduits. We believe that the present study would encourage further research in developing electrically active neural implants using synthetic conducting polymers and the *in vivo* applications of the same.

5.2 Future Prospects

Our attempts to develop novel bio-mimetic scaffolds for fabrication of artificial nerve conduits resulted in excellent functional and morphological regeneration of nerves upon implantation in rat sciatic nerve injury model. At this stage we believe that the technological know-how obtained from the extensive in vitro and in vivo studies can be exploited to develop advanced scaffolds for use in various biomedical applications as summarized below.

1) The rapid and facile method described in the present study for incorporation of gold nanoparticles into silk fibers can be used for conjugating metallic nanoparticles to biopolymers. The nanoparticles can be easily conjugated with a variety of biomolecules (growth factors, proteins) or drugs to provide multiple functionalities to the scaffold.
2) The sheet rolling method described in the study may be taken as a principle for developing automated techniques for high throughput production of customised nerve conduits.
3) At present there are limited reports of in vivo studies using conducting polymers in neural tissue engineering. Our work establishes the safety and efficacy of a conducting polymer like polyaniline as a scaffold material when used in a controlled manner. Other conducting polymers can also be explored for *in vivo* applications in neural tissue engineering.
4) Although rat sciatic nerve injury model is the most used platform for studying nerve regeneration, similar studies need to be implemented in a larger animal model like pigs which exhibit closer neurophysiology to humans.
5) Pre-clinical research on nerve conduits involves creating a nerve gap and immediately implanting a conduit between the proximal and distal stumps. However, in an actual clinical c, patients are often diagnosed with nerve injury at least a few months after the actual trauma. Hence simulating such a condition by delaying the implantation of conduit upon creation of nerve gap would render much more clinical relevance to the research in future.

6) The results obtained from the extensive long duration in vivo experiments establishes the safety and efficacy of the fabricated nerve conduits in

promoting nerve regeneration. We strongly believe that these conduits should be taken up for clinical trials looking at the urgent need for such neural implants in our country.

Bibliography

1. A Phase I Study of Convection-Enhanced Delivery of Liposomal-Irinotecan Using Real-Time Imaging With Gadolinium In Patients With Recurrent High Grade Glioma, ClinicalTrials.gov Identifier: NCT02022644.
2. Abdolahi A, Hamzah E, Ibrahim Z, Hashim S, Synthesis of Uniform Polyaniline Nanofibers through Interfacial Polymerization, Materials 2012;5;1487-1494.
3. Adams AM, Arruda EM, Larkin LM. Use of adipose-derived stem cells to fabricate scaffoldless tissue-engineered neural conduits in vitro. Neuroscience. 2012,10; 201:349-56.
4. Ahmadi N, Razavi S, Kazemi M, Oryan S. Stability of neural differentiation in human adipose derived stem cells by two induction protocols. Tissue Cell. 2012, 44,2:87-94.
5. Ahmed MR, Vairamuthu S, Shafiuzama M, Basha SH, Jayakumar R. Microwave irradiated collagen tubes as a better matrix for peripheral nerve regeneration. Brain Res. 2005, 1046, (1-2):55-67.
6. Ahmed MR, Venkateshwarlu U, Jayakumar R. Multilayered peptide incorporated collagen tubules for peripheral nerve repair, *Biomaterials*, 2004,25,13:2585–2594,
7. Ahn HS, Hwang JY, Kim MS, Lee JY, Kim JW, Kim HS, Shin US, Knowles JC, Kim HW, Hyun JK., Carbon-nanotube-interfaced glass fiber scaffold for regeneration of transected sciatic nerve. Acta Biomater. 2015;13;324-34.
8. Ai L, Jiang J, Zhang R, Uniform polyaniline microspheres: A novel adsorbent for dye removal from aqueous solution, Synthetic Metals 2010;160;762–767.
9. Alluin O, Wittmann C, Marqueste T, Chabas JF, Garcia S, Lavaut MN, Guinard D, Feron F, Decherchi P. Functional recovery after peripheral nerve injury and implantation of a collagen guide. Biomaterials, 2009,30,3:363–373.
10. Altman AM, Yan Y, Matthias N, Bai X, Rios C, Mathur AB, Song YH, Alt EU. IFATS collection: Human adipose-derived stem cells seeded on a silk fibroin-chitosan scaffold enhance wound repair in a murine soft tissue injury model. Stem Cells. 2009; 27,1:250-8.
11. Amado S, Simões MJ, Armada da Silva PAS, Luís AL, Shirosaki Y, Lopes MA, et al. Useof hybrid chitosan membranes and N1E-115 cells for promoting nerve regener-ation in an axonotmesis rat model. Biomaterials,2008;29:4409–19.
12. An JH , Kim TH, Oh BK, Choi JW. Detection of dopamine in dopaminergic cell using nanoparticles-based barcode DNA analysis. J Nanosci Nanotechnol. 2012,12,1:764-8.
13. An JH , Oh BK, Choi JW. Detection of tyrosine hydroxylase in dopaminergic neuron cell using gold nanoparticles-based barcode DNA. J Biomed Nanotechnol. 2013,9,4:639-43.

14. Araya E, Olmedo I, Bastus NG, Guerrero S, Puntes VF, Giralt E, Kogan MJ, Gold Nanoparticles and Microwave Irradiation Inhibit Beta-Amyloid Amyloidogenesis, Nanoscale Res Lett. 2008,3,11: 435–443.
15. Archibald S, Krarup C, Shefner J, Li S, Madison R. A collagen-based nerve guide conduit for peripheral nerve repair: an electrophysiological study of nerve regeneration in rodents and nonhuman primates. Journal of Comparative Neurology 1991;306:685–96.
16. Archibald SJ, Shefner J, Krarup C, Madison RD. Monkey median nerve repaired by nerve graft or collagen nerve guide tube. Journal of Neuroscience 1995;15:4109–23.
17. Arizono, M., Bannai, H. and Mikoshiba, K. Imaging mGluR5 Dynamics in Astrocytes Using Quantum Dots.Current Protocols in Neuroscience, 2014, 66:2.21.1–2.21.18.
18. Arslantunali D, Dursun T, Yucel D, Hasirci N, Hasirci V, Medical Devices: Evidence and Research, 2014,7:405–424.
19. Ashley WW, Weatherly T, Park TS, Collagen nerve guides for surgical repair of brachial plexus birth injury. Journal of Neurosurgery, 2006,105:452–6.
20. Asplund M, Thaning E, Lundberg J, Sandberg-Nordqvist AC, Kostyszyn B, Inganäs O, von Holst H. Toxicity evaluation of PEDOT/biomolecular composites intended for neural communication electrodes. Biomed Mater. 2009,4,4:045009.
21. Atala A. Tissue engineering of human bladder. Br Med Bull. 2011, 97:81-104.
22. Aznar-Cervantes S, Roca MI, Martinez JG, Meseguer-Olmo L, Cenis JL, Moraleda JM, Otero TF. Fabrication of conductive electrospun silk fibroin scaffolds by coating with polypyrrole for biomedical applications. Bioelectrochemistry. 2012, 85:36-43.
23. Balint R, Cassidy NJ, Cartmell SH. Conductive polymers: towards a smart biomaterial for tissue engineering. Acta Biomater, 2014,10,6:2341-53.
24. Baptista AF, Gomes JR, Oliveira JT, Santos SM, Vannier-Santos MA, Martinez AM.High- and low-frequency transcutaneous electrical nerve stimulation delay sciatic nerve regeneration after crush lesion in the mouse. J Peripher Nerv Syst, 2008,13:71–80.
25. Bartolomei JC, Greer CA. Olfactory ensheathing cells: bridging the gap in spinal cord injury. Neurosurgery, 2000,47: 1057–69.
26. Batrakova EV, Li S, Reynolds AD, Mosley RL, Bronich TK, Kabanov AV, Gendelman HE. A macrophage-nanozyme delivery system for Parkinson's disease. Bioconjug Chem. 2007,18,5:1498-506.
27. Battiston B, Geuna S, Ferrero M, Tos P. Nerve repair by means of tubulization: literature review and personal clinical experience comparing biological and synthetic conduits for sensory nerve repair. Microsurgery 2005,25:258–67.

28. Beesabathuni SN, Stockham JG., Kim JH, Lee HB, Chung JH, Shen AQ, Fabrication of conducting polyaniline microspheres using droplet microfluidics. RSC Adv 2013; 3;24423-24429.
29. Behr B, Schnabel R, Mirastschijski U, Ibrahim B, Angenstein F, Schneider W. Magnetic resonance imaging monitoring of peripheral nerve regeneration followingneurotmesis at 4.7 Tesla. Plast Reconstr Surg, 2009,123:1778–88.
30. Belkas, SJ, Shoichet, SM, Midha, R. Peripheral nerve regeneration through guidance tubes. Neurol.Res, 2004, 26, 151–160.
31. Bellamkonda, RV, Peripheral nerve regeneration: an opinion on channels, scaffolds and anisotropy. Biomaterials, 2006, 27:3515–3518.
32. Bender MD, Bennett JM, Waddell RL, Doctor JS, Marra KG. Multi-channeled biodegradable polymer/CultiSpher composite nerve guides. Biomaterials. 2004,25,7-8:1269-78.
33. Benfenati, V.; Stahl, K.; Gomis-Perez, C.; Toffanin, S.; Sagnella, A.; Torp, R.; Kaplan, D. L.; Ruani, G.; Omenetto, F. G.; Zamboni, R.; Muccini, M. Biofunctional Silk/Neuron Interfaces. Adv. Funct. Mater. 2012, 22, 1871–1884.
34. Berrocal, Y. A.; Almeida, V. W.; Gupta, R.; Levi, A. D. Transplantation of Schwann cells in a collagen tube for the repair of large, segmental peripheral nerve defects in rats. J. Neurosurg. 2013, 119, 720-32.
35. Bertleff MJOE, Meek MF, Nicolai J-PA. A prospective clinical evaluation of biodegradable neurolac nerve guides for sensory nerve repair in the hand. The Journal of Hand Surgery 2005,30:513–8.
36. Bettinger CJ, Bruggeman JP, Misra A, Borenstein JT, Langer R. Biocompatibility of biodegradable semiconducting melanin films for nerve tissue engineering. Biomaterials. 2009; 30, 17:3050-7.
37. Bhadra S, Khastgir D, Singha NK., Lee JH, Progress in preparation, processing and applications of polyaniline, Progress in Polymer Science 2009;34;783–810.
38. Bhang SH, Jeong SI, Lee TJ, Jun I, Lee YB, Kim BS, Shin H. Electroactive electrospun polyaniline/poly [(L-lactide)-co-(ε-caprolactone)] fibers for control of neural cell function. Macromol Biosci 2012;12;402-11.
39. Bian YZ, Wang Y, Aibaidoula G, Chen GQ, Wu Q. Evaluation of poly(3-hydroxybutyrate-co-3-hydroxyhexanoate) conduits for peripheral nerve regeneration. Biomaterials. 2009;30,2:217-25.
40. Bidez PR, Li S, Macdiarmid AG, Venancio EC, Wei Y, Lelkes PI. Polyaniline, an electroactive polymer, supports adhesion and proliferation of cardiac myoblasts. J Biomater Sci Polym Ed. 2006,17,1-2:199-212.

41. Bini TB, Gao S, Ta TC, Wang S, Lim A, Hai LB, Ramakrishna S, Electrospun poly(L-lactide-co-glycolide) biodegradable polymer nanofibre tubes for peripheral nerve regeneration. Nanotechnology, 2004,15,11:1459.
42. Bini TB, Shujun G, Shu W. Poly(l-lactide-co-glycolide) biodegradable microfibers and electrospun nanofibers for nerve tissue engineering: an in vitro study. *J Mat Sci.* 2006;41,19:6453.
43. Bittner GD, Keating CP., Kane JR, Rapid, effective and long-lasting behavioral recovery produced by microsutures, methylene blue, and polyethylene glycol after completely cutting rat sciatic nerves, Journal of Neuroscience Research, 2012, 90,5:967–980.
44. Bittner GD, Schallert T, Peduzzi JD, Degeneration trophic interactions, and repair of severed axons: a reconsideration of some common assumptions, Neuroscientist, 2000,6, 2:88–109.
45. Blesch A, Lu P, Tuszynski MH. Neurotrophic factors, gene therapy, and neural stem cells for spinal cord repair. Brain Res. Bull,2002,57:833–38.
46. Blesch A, Tuszynski MH. GDNF gene delivery to injured adult CNS motor neurons promotes axonal growth, expression of the trophic neuropeptide CGRP, and cellular protection. J Comp Neurol. 2001;436,4:399-410.
47. Blesch A, Tuszynski MH.. GDNF gene delivery to injured adult CNS motor neurons promotes axonal growth, expression of the trophic neuropeptide CGRP, and cellular protection. J. Comp. Neurol. 2001 436:399–410.
48. Bobo RH, Laske DW, Akbasak A, Morrison PF, Dedrick RL, Oldfield EH. Convection-enhanced delivery of macromolecules in the brain. Proc Natl Acad Sci U S A. 1994, 91,6:2076-80.
49. Boeckstyns ME, Sørensen AI, Viñeta JF, Rosén B, Navarro X, Archibald SJ, Valss-Solé J, Moldovan M, Krarup C, Collagen conduit versus microsurgical neurorrhaphy: 2-year follow-up of a prospective, blinded clinical and electrophysiological multicenter randomized, controlled trial. J. Hand Surg. Am. 2013, 38:2405-11.
50. Boehler RM, Graham JG, Shea LD. Tissue engineering tools for modulation of the immune response. *Biotech.*2011;51,4:239-40-244.
51. Borgens RB. Electrically mediate dregeneration and guidance of adult mammalian spinal axons into polymeric channels.*Neuroscience,* 1999, 91**:** 251–264.
52. Bostman OM, Pihlajamaki HK. Adverse tissue reactions to bioabsorbable fixation devices. Clinical Orthopaedics and Related Research 2000,216–27.
53. Bozkurt A, Brook GA, Moellers S, Lassner F, Sellhaus B, Weis J, Woeltje M, Tank J, Beckmann C, Fuchs P, Damink LO, Schügner F, Heschel I, Pallua N. *In vitro*

assessment of axonal growth using dorsal root ganglia explants in a novel three-dimensional collagen matrix. Tissue Engineering, 2007, 13,12:2971–2979.

54. Bozkurt A, Deumens R, Beckmann C, Olde Damink L, Schügner F, Heschel I, Sellhaus B, Weis J, Jahnen-Dechent W, Brook GA, Pallua N. *In vitro* cell alignment obtained with a Schwann cell enriched microstructured nerve guide with longitudinal guidance channels. Biomaterials, 2009, 30,2:169–179.
55. Bozkurt A, Deumens R, Scheffel J, O'Dey DM, Weis J, Joosten EA, et al. CatWalk gaitanalysis in assessment of functional recovery after sciatic nerve injury. J NeurosciMethods 2008a,173:91–8.
56. Bozkurt A, Tholl S, Wehner S, Tank J, Cortese M, O'Dey D, et al. Evaluation of functional nerve recovery with Visual-SSI – a novel computerized approach for the assess-ment of the static sciatic index (SSI). J Neurosci Methods 2008b, 170:117–22.
57. Bradbury EJ, Khemani S, Von R, King, Priestley JV, McMahon SB. NT-3 promotes growth of lesioned adult rat sensory axons ascending in the dorsal columns of the spinal cord. Eur J Neurosci. 1999; 11,11:3873-83.
58. Braun S, Croizat B, Lagrange MC, Warter JM, Poindron P. Neurotrophins increase motoneurons' ability to innervate skeletal muscle fibers in rat spinal cord--human muscle cocultures..J Neurol Sci. 1996; 136,1-2:17-23.
59. Bray LJ, George KA, Ainscough SL, Hutmacher DW, Chirila TV, Harkin DG. Human corneal epithelial equivalents constructed on Bombyx mori silk fibroin membranes. Biomaterials. 2011, 32,22:5086-91.
60. Bray LJ, George KA, Hutmacher DW, Chirila TV, Harkin DG. A dual-layer silk fibroin scaffold for reconstructing the human corneal limbus. Biomaterials. 2012, 33,13:3529-38.
61. Britt JM., Kane JR., Spaeth CS, Polyethylene glycol rapidly restores axonal integrity and improves the rate of motor behavior recovery after sciatic nerve crush injury, Journal of Neurophysiology, 2010, 104,2:695–703.
62. Broadhead KW, Biran R, Tresco PA. Hollow fiber membrane diffusive permeability regulates encapsulated cell line biomass, proliferation, and small molecule release. Biomaterials, 2002, 23, 24:4689–4699.
63. Buj-Bello A, Buchman VL, Horton A, Rosenthal A, Davies AM. GDNF is an age-specific survival factor for sensory and autonomic neurons. Neuron. 1995,15,4:821-8.
64. Bushnell BD, McWilliams AD, Whitener GB, Messer TM. Early clinical experience with collagen nerve tubes in digital nerve repair. The Journal of Hand Surgery, 2008, 33:1081–7.

65. Cai J, Peng X, Nelson KD, Eberhart R, Smith GM. Permeable guidance channels containing microfilament scaffolds enhance axon growth and maturation. Journal of Biomedical Materials Research Part A, 2005,75,2:374–386.
66. Cai L, Wang S. Poly (ε-caprolactone) acrylates synthesized using a facile method for fabricating networks to achieve controllable physicochemical properties and tunable cell responses. Polymer, 2010, 51,1:164–177.
67. Carlsen BT, Bishop AT, Shin AY, Late reconstruction for brachial plexus injury, Neurosurgery Clinics of North America, 2009, 20,1:51–64.
68. Casanas J, Serra J, Orduna M, Garcıa-Portabella M, Mir X. Repair of digital sensory nerves of the hand using polyglycolic acid conduits. Journal of Hand Surgery-British and European Volume,2000;25:44.
69. Chamberlain LJ., Yannas IV., Hsu HP, Spector M. Connective tissue response to tubular implants for peripheral nerve regeneration: the role of myofibroblasts. Journal of Comparative Neurology, 2000,417,4:415–430.
70. Chang CJ, Hsu SH. The effect of high outflow permeability in asymmetric poly(dl-lactic acid-co-glycolic acid) conduits for peripheral nerve regeneration. Biomaterials. 2006; 27,7:1035-42.
71. Chang G, Kim HJ, Kaplan D, Vunjak-Novakovic G, Kandel RA. Porous silk scaffolds can be used for tissue engineering annulus fibrosus. Eur Spine J. 2007, 16(11):1848-57.
72. Chang G, Kim HJ, Vunjak-Novakovic G, Kaplan DL, Kandel R. Enhancing annulus fibrosus tissue formation in porous silk scaffolds. J Biomed Mater Res A. 2010, 92,1:43-51.
73. Chang JY, Ho TY, Lee HC, Lai YL, Lu MC, Yao CH, Chen YS. Highly permeable genipin-cross-linked gelatin conduits enhance peripheral nerve regeneration. Artificial Organs, 2009, 33,12:1075–1085,.
74. Chang JY, Lin JH, Yao CH, Chen JH, Lai TY, Chen YS. *In vivo* evaluation of a biodegradable EDC/NHScross-linked gelatin peripheral nerve guide conduit material. Macromolecular Bioscience, 2007,7,4:500–507.
75. Chen CS, Soni S, Le C, Biasca M, Farr E, Chen EY, Chin WC. Human stem cell neuronal differentiation on silk-carbon nanotube composite. Nanoscale Res Lett. 2012, 14;7,1:126.
76. Chen L, Qin J, Cheng C, Niu S, Liu Y, Shi S, et al. Spatiotemporal expression of SSeCKSin injured rat sciatic nerve. Anat Rec 2008,291:527–37.
77. Chen M, Dong M, Havelund R, Regina VR, Meyer RL, Besenbacher F, Kingshott P Thermo-Responsive Core-Sheath Electrospun Nanofibers from Poly(N-isopropylacrylamide)/Polycaprolactone Blends. Chem. Mater 2010;22;4214–4221.

78. Chen MB, Zhang F, Lineaweaver WC. Luminal fillers in nerve conduits for peripheral nerve repair. Annals of Plastic Surgery, 2006, 57,4:462–471.
79. Chen RN, Ho HO, Tsai YT, et al. Process development of an acel¬lular dermal matrix (ADM) for biomedical applications. Biomaterials. 2004;25(13):2679–2686.
80. Chen YS, Chang JY, Cheng CY, Tsai FJ, Yao CH, Liu BS. An *in vivo* evaluation of a biodegradable genipincross-linked gelatin peripheral nerve guide conduit material, Biomaterials, 2005,26,18,3911–3918..
81. Chen, XM; Yang, YM; Wu, J; Zhao, YH; Ding, F; Gu, XS. Biocompatibility studies of silk fibroin-based artificial nerve grafts in vitro and in vivo. Progress in Natural Science. 2007, 17:1029-1034.
82. Chertok B, Moffat BA, David AE, Yu F, Bergemann C, Ross BD, Yang VC. Iron oxide nanoparticles as a drug delivery vehicle for MRI monitored magnetic targeting of brain tumors, Biomaterials. 2008,29,4:487-96.
83. Chew SY, Mi R, Hoke A, Leong KW. Aligned Protein-Polymer Composite Fibers Enhance Nerve Regeneration: A Potential Tissue-Engineering Platform. Adv Funct Mater. 2007,17,8:1288-1296.
84. Chiono V, Tonda-Turo C, Ciardelli G. Artificial scaffolds for peripheral nerve reconstruction. International Review of Neurobiology, 2009, 87:173–198.
85. Chiono V, Vozzi G, Vozzi F, Salvadori C, Dini F, Carlucci F, Arispici M, Burchielli S, Di Scipio F, Geuna S, Fornaro M, Tos P, Nicolino S, Audisio C, Perroteau I, Chiaravalloti A, Domenici C, Giusti P, Ciardelli G. Melt-extruded guides for peripheral nerve regeneration. Part I: poly(epsilon-caprolactone). Biomed Microdevices. 2009; 11,5:1037-50.
86. Chirila T, Barnard Z, Zainuddin, Harkin DG, Schwab IR, Hirst L. Bombyx mori silk fibroin membranes as potential substrata for epithelial constructs used in the management of ocular surface disorders. Tissue Eng Part A. 2008, 14,7:1203-11.
87. Chiu DT, Strauch B. A prospective clinical evaluation of autogenous vein grafts usedas a nerve conduit for distal sensory nerve defects of 3 cm or less. Plast ReconstrSurg, 1990, 86:928–34.
88. Cho EC, Zhang Y, Cai X, Moran CM., Wang LV., Xia Y, A Quantitative Analysis of the Fate of Au Nanocages after Uptake by U87-MG Tumor Cells under Both in vitro and in vivo Conditions Angew Chem Int Ed Engl., 2013,52,4: 1152–1155.
89. Choi I, Lee LP. Rapid detection of Aβ aggregation and inhibition by dual functions of gold nanoplasmic particles: catalytic activator and optical reporter. ACS Nano. 2013,7,7:6268-77.

90. Choi JS, Jun YW, Yeon SI, Kim HC, Shin JS, Cheon J. Biocompatible heterostructured nanoparticles for multimodal biological detection. J Am Chem Soc. 2006 ;128,50:15982-3.
91. Christopherson GT, Song H, Mao HQ The influence of fiber diameter of electrospun substrates on neural stem cell differentiation and proliferation. Biomaterials. 2009,30,4:556-64.
92. Ciardelli G, Chiono V. Materials for peripheral nerve regeneration. *Macromolecular Bioscience*, 2006, 6, 1:13–26.
93. Clements, IP., Kim, YT., English, AW, Lu, X.,Chung, A, Bellamkonda, RV, Thin-film enhanced nerve guidance channels for peripheral nerve repair. Biomaterials, 2009,30:3834–3846.
94. Cohen-Karni T, Jeong KJ, Tsui JH, Reznor G, Mustata M, Wanunu M, Graham A, Marks C, Bell DC, Langer R, Kohane DS, Nanocomposite gold-silk nanofibers. Nano Lett. 2012,12:5403-6.
95. Cordeiro PG, Seckel BR, Lipton SA, D'Amore PA, Wagner J, Madison R. Acidic fibroblast growth factor enhances peripheral nerve regeneration in vivo. Plast Reconstr Surg. 1989, 83,6:1013-9.
96. Correia C, Bhumiratana S, Yan LP, Oliveira AL, Gimble JM, Rockwood D, Kaplan DL, Sousa RA, Reis RL, Vunjak-Novakovic G. Development of silk-based scaffolds for tissue engineering of bone from human adipose-derived stem cells. Acta Biomater. 2012, 8,7:2483-92.
97. Costa LM, Simões MJ, Maurício AC, Varejão AS. Methods and protocols in peripheralnerve regeneration experimental research: Part IV. Kinematic gait analy-sis to quantify peripheral nerve regeneration in the rat. Int Rev Neurobiol,2009, 87:127–39.
98. Crawley WA, Dellon AL. Inferior alveolar nerve reconstruction with a polyglycolic acid bioabsorbable nerve conduit. Plastic and Reconstructive Surgery,1992,90:300–2.
99. Cui Z, Lockman PR, Atwood CS, Hsu CH, Gupte A, Allen DD, Mumper RJ. Novel D-penicillamine carrying nanoparticles for metal chelation therapy in Alzheimer's and other CNS diseases. Eur J Pharm Biopharm. 2005; 59,2:263-72.
100. Cunha C, Panseri S, Antonini S. Emerging nanotechnology approaches in tissue engineering for peripheral nerve regeneration. Nanomedicine 2011, 7: 50-9.
101. da Silva CF, Madison R, Dikkes P, Chiu TH, Sidman RL. An in vivo model to quantify motor and sensory peripheral nerve regeneration using bioresorbable nerve guide tubes. Brain Res. 1985,342,2:307-15.

102. Dadon-Nachum M, Melamed E, Offen D. Stem cells treatment for sciatic nerve injury. Expert Opin Biol Ther,2011,11:1591–7.
103. Dahl SL, Koh J, Prabhakar V, et al. Decellularized native and engineered arterial scaffolds for transplantation. Cell Transplant. 2003;12:659–666.
104. Dal Pra I, Chiarini A, Boschi A, Freddi G, Armato U. Novel dermo-epidermal equivalents on silk fibroin-based formic acid-crosslinked three-dimensional nonwoven devices with prospective applications in human tissue engineering/regeneration/repair. Int J Mol Med. 2006, 18,2:241-7.
105. Dalton PD, Flynn L., Shoichet M. S. Manufacture of poly(2-hydroxyethyl methacrylate-co-methyl methacrylate) hydrogel tubes for use as nerve guidance channels. Biomaterials, 2002,23, 18:3843–3851,.
106. Daly W, Yao L., Zeugolis D, Windebank A., Pandit A, A biomaterials approach to peripheral nerve regeneration: bridging the peripheral nerve gap and enhancing functional recovery, J. R. Soc. Interface, 2012,9:202–221.
107. Daly, W. T.; Knight, A. M.; Wang, H.; de Boer, R.; Giusti, G.; Dadsetan, M.; Spinner, R. J.; Yaszemski, M. J.; Windebank, A. J. Comparison and characterization of multiple biomaterial conduits for peripheral nerve repair. Biomaterials. 2013, 34, 8630-9.
108. Danielsen N, Pettmann B, Vahlsing HL, Manthorpe M, Varon S. Fibroblast growth factor effects on peripheral nerve regeneration in a silicone chamber model. J Neurosci Res. 1988;20(3):320-30.
109. D'Arrigo JS, Simon RH, Ho SY. Lipid-coated uniform microbubbles for earlier sonographic detection of brain tumors. J Neuroimaging. 1991,1,3:134-9.
110. Das M, Patil S, Bhargava N, Kang JF, Riedel LM, Seal S, Hickman JJ. Auto-catalytic ceria nanoparticles offer neuroprotection to adult rat spinal cord neurons. Biomaterials. 2007, 28,10:1918-25.
111. Das S, Sharma M, Saharia D, Sarma KK, Sarma MG, Borthakur BB, Bora U. In vivo studies of Silk based Gold Nano-Composite Conduits for Functional Peripheral Nerve Regeneration. Biomaterials, 2015, 62:66-75.
112. Das, R. K.; Borthakur, B. B.; Bora, U. Green synthesis of gold nanoparticles using ethanolic leaf extract of Centella asiatica. Materials Letters, 2010, 64:1445–47
113. Das, S, Sharma, M, Saharia, D, Sarma, K.K, Sarma, M.G., Borthakur, B.B., Bora, U. Data in support of In vivo studies of Silk based Gold Nano-Composite Conduits for Functional Peripheral Nerve Regeneration, Data in Brief, 2015 (Accepted).
114. De Filippo RE, Yoo JJ, Atala A. Urethral replacement using cell seeded tubularized collagen matrices. J Urol. 2002;168:1789–1792.

115. De Giglio E, Trapani A, Cafagna D, Sabbatini L, Cometa S. Dopamine-loaded chitosan nanoparticles: formulation and analytical characterization. Anal Bioanal Chem. 2011; 400, 7:1997-2002.
116. De Leon M, Welcher AA, Suter U, Shooter EM. Identification of transcriptionally regulated genes after sciatic nerve injury. J Neurosci Res 1991,29:437–48.
117. De Medinaceli L, Freed WJ, Wyatt RJ. An index of the functional condition of ratsciatic nerve based on measurements made from walking tracks. Exp Neurol,1982,77:634–43.
118. Dellon AL, Mackinnon SE. Sciatic nerve regeneration in the rat. Validity of walk-ing track assessment in the presence of chronic contractures. Microsurgery,1989,10:220–5.
119. Dellon AL, Maloney CT. Salvage of sensation in a hallux-to-thumb transfer by nerve tube reconstruction. The Journal of Hand Surgery 2006,31:1495–8.
120. Derby A, Engleman VW, Frierdich GE, Neises G, Rapp SR, Roufa DG. Nerve growth factor facilitates regeneration across nerve gaps: morphological and behavioral studies in rat sciatic nerve. Exp Neurol, 1993,119,2:176-91.
121. Deumens, R., Bozkurt, A., Meek, MF, Marcus, MA.E., Joosten, E. A. J., Weis, J, Brook, GA, Repairing injured peripheral nerves: bridging thegap. Prog. Neurobiol. 2010, 92, 245–276.
122. Dinis, T.; Vidal, G.; Marin, F.; Kaplan, D.; Eglès, C. Silk nerve: bioactive implant for peripheral nerve regeneration. Comput. Methods Biomech. Biomed. Engin. 2013, 16, 253-54.
123. Dodakundi C, Doi K., Hattori Y, Outcome of surgical reconstruction after traumatic total brachial plexus palsy, Journal of Bone and Joint Surgery, 2013, 95,16:1505–1512.
124. Dodla MC, Bellamkonda RV. Differences between the effect of anisotropic andisotropic laminin and nerve growth factor presenting scaffolds on nerve regen-eration across long peripheral nerve gaps. Biomaterials,2008,29:33–46.
125. Dolan AR, Wood TD, Analysis of polyaniline oligomers by laser desorption ionization and solventless MALDI, J. Am. Soc. Mass Spectrom. 2004,15:893–899.
126. Donoghoe N, Rosson GD, Dellon AL. Reconstruction of the human median nerve in the forearm with the neurotube (TM). Microsurgery 2007,27:595–600.
127. Ducic I, Maloney CT, Dellon AL. Reconstruction of the spinal accessory nerve with autograft or neurotube? Two case reports. Journal of Reconstructive Microsurgery 2005;21:29–33.

128. Ellis-Behnke RG, Liang YX, You SW, Tay DK, Zhang S, So KF, Schneider GE. Nano neuro knitting: peptide nanofiber scaffold for brain repair and axon regeneration with functional return of vision. Proc Natl Acad Sci USA. 2006, 103, 13: 5054-9.
129. Enochs WS , Harsh G, Hochberg F, Weissleder R. Improved delineation of human brain tumors on MR images using a long-circulating, superparamagnetic iron oxide agent**.** J Magn Reson Imaging. 1999,9,2:228-32.
130. Enomoto S, Sumi M, Kajimoto K, Nakazawa Y, Takahashi R, Takabayashi C, Asakura T, Sata M. Long-term patency of small-diameter vascular graft made from fibroin, a silk-based biodegradable material. J Vasc Surg. 2010, 51,1:155-64.
131. Eser F, Aktekin LA, Bodur H, Atan C. Etiological factors of traumatic peripheral nerve injuries. Neurol India. 2009,57,4:434-7.
132. European Medicines Agency, Assessment report on Centella asiatica (L.) Urban, herba by Committee on Herbal Medicinal Products (HMPC), EMA/HMPC/291177/2009.
133. Evans GR. Peripheral nerve injury: a review and approach to tissue engineered constructs. Anatomical Record,2001,263:396–404.
134. Exploratory Study to Detect Volatile Biomarkers of Idiopathic Parkinson's Disease and Parkinsonism From Exhaled Breath Using a Nanomedical Artificial Olfactory System, Rambam Health Care Campus and Technion, Israel Institute of Technology, ClinicalTrials.gov Identifier:NCT01246336.
135. Fabbro, A.; Prato, M.; Ballerini, L. Carbon nanotubes in neuroregeneration and repair. Adv. Drug Deliv. Rev. 2013, 65, 2034-44.
136. Fakih M, Vincent M. Adverse events associated with anti-EGFR therapies for the treatment of metastatic colorectal cancer. Curr Oncol. 2010, 17, Suppl 1:S18-30.
137. Farole A, Jamal BT. A Bioabsorbable collagen nerve cuff (NeuraGen) for repair of lingual and inferior alveolar nerve injuries: a case series. Journal of Oral and Maxillofacial Surgery 2008,66:2058–62.
138. Figueiró F, Bernardi A, Frozza RL, Terroso T, Zanotto-Filho A, Jandrey EH, Moreira JC, Salbego CG, Edelweiss MI, Pohlmann AR, Guterres SS, Battastini AM. Resveratrol-loaded lipid-core nanocapsules treatment reduces in vitro and in vivo glioma growth. J Biomed Nanotechnol. 2013;9,3:516-26.
139. Fine EG, Decosterd I, Papaloïzos M, Zurn AD, Aebischer P. GDNF and NGF released by synthetic guidance channels support sciatic nerve regeneration across a long gap. Eur J Neurosci. 2002;15,4:589-601.
140. Fleming CE, Saraiva MJ, Sousa MM. Transthyretin enhances nerve regeneration. JNeurochem, 2007,103:831–9.

141. Franzen R, Schoenen J, Leprince P, Joosten E, Moonen G, et al.. Effects of macrophage transplantation in the injured adult rat spinal cord: a combined immunocytochemical and biochemical study. J. Neurosci. Res. 1998, 51:316– 27.
142. Freeman JA, Manis PB, Snipes GJ, Mayes BN, Samson PC, Wikswo JP Jr, Freeman DB. Steady growth cone currents revealed by a novel circularly vibrating probe: a possible mechanism underlying neurite growth. J Neurosci Res, 1985, 13, 1-2:257-83.
143. Freier T, Montenegro R, Koh HS, Shoichet MS. Chitin-based tubes for tissue engineering in the nervous system. Biomaterials, 2005,26,22:4624–4632,.
144. Freytes DO, Badylak SF, Webster TJ, et al. Biaxial strength of multilaminated extracellular matrix scaffolds. Biomaterials. 2004;25:2353–2361.
145. Friesel RE, Maciag T. Molecular mechanisms of angiogenesis: fibroblast growth factor signal transduction. FASEB J. 1995;9,10:919-25.
146. Fuchs S, Jiang X, Schmidt H, Dohle E, Ghanaati S, Orth C, Hofmann A, Motta A, Migliaresi C, Kirkpatrick CJ. Dynamic processes involved in the pre-vascularization of silk fibroin constructs for bone regeneration using outgrowth endothelial cells. Biomaterials. 2009, 30,7:1329-38.
147. Gámez E, Goto Y, Nagata K, Iwaki T, Sasaki T, Matsuda T. Photofabricated gelatin-based nerve conduits: nerve tissue regeneration potentials. *Cell Transplantation*, 2004,13,5:549–564.
148. Gao H, Yang Z, Cao S, Xiong Y, Zhang S, Pang Z, Jiang X,Tumor cells and neovasculature dual targeting delivery for glioblastoma treatment. Biomaterials. 2014,35,7:2374-82.
149. Gao X, Chen J, Chen J, Wu B, Chen H, Jiang X, Quantum dots bearing lectin-functionalized nanoparticles as a platform for in vivo brain imaging. Bioconjug Chem. 2008,19,11:2189-95.
150. Gao Y, Li J, Yang X., Xiang Q, Wang K., Electrochemiluminescence Biosensor Based on PEDOT-PSS- Graphene Functionalized ITO Electrode. Electroanalysis 2014;26;382–388.
151. Garbay B, Heape AM, Sargueil F, Cassagne C, Myelin synthesis in the peripheral nervous system. Prog Neurobiol 2000; 61;267-304.
152. Gelain F, Bottai D, Vescovi A, Zhang S. Designer self-assembling peptide nanofiber scaffolds for adult mouse neural stem cell 3-dimensional cultures. PLoS One,2006;1:e119.
153. Georganopoulou DG, Chang L, Nam JM, Thaxton CS, Mufson EJ, Klein WL, Mirkin CA, Nanoparticle-based detection in cerebral spinal fluid of a soluble pathogenic biomarker for Alzheimer's disease. Proc Natl Acad Sci U S A. 2005,102,7:2273-6.

154. George PM, Lyckman AW, Lavan DA, Hegde A, Leung Y, Avasare R, Testa C, Alexander PM, Langer R, Sur M. Fabrication and biocompatibility of polypyrrole implants suitable for neural prosthetics. Biomaterials 2005;26;3511-9.
155. George PM, Saigal R, Lawlor MW, Moore MJ, Lavan DA, Marini RP, Selig M, Makhni M, Burdick JA, Langer R, Kohane DS. Three-dimensional conductive constructs for nerve regeneration. J Biomed Mater Res A. 2009;91,2:519-27.
156. Geuna S, Raimondo S, Ronchi G, Di Scipio F, Tos P, Czaja K, et al. Histology of theperipheral nerve and changes occurring during nerve regeneration. Int Rev Neurobiol, 2009,87:27–46.
157. Ghasemi-Mobarakeh L, Prabhakaran MP, Morshed M, Nasr-Esfahani MH, Baharvand H, Kiani S, Al-Deyab SS, Ramakrishna S. Application of conductive polymers, scaffolds and electrical stimulation for nerve tissue engineering. J Tissue Eng Regen Med. 2011, 5, 4:e17-35.
158. Ghasemi-Mobarakeh L, Prabhakaran MP, Morshed M, Nasr-Esfahani MH, Ramakrishna S. Electrical stimulation of nerve cells using conductive nanofibrous scaffolds for nerve tissue engineering. Tissue Eng Part A. 2009; 15,11:3605-19.
159. Gigo-Benato D, Russo TL, Geuna S, Domingues NR, Salvini TF, Parizotto NA. Electrical stimulation impairs early functional recovery and accentuates skeletalmuscle atrophy after sciatic nerve crush injury in rats. Muscle Nerve, 2010,41:685–93.
160. Gil ES (a), Park SH, Marchant J, Omenetto F, Kaplan DL. Response of human corneal fibroblasts on silk film surface patterns. Macromol Biosci. 2010, 10,6:664-73.
161. Gil ES (b), Mandal BB, Park SH, Marchant JK, Omenetto FG, Kaplan DL. Helicoidal multi-lamellar features of RGD-functionalized silk biomaterials for corneal tissue engineering. Biomaterials. 2010, 31,34:8953-63.
162. Gilbert TW, Sellaro TL, Badylak SF. Decellularization of tissues and organs. Biomaterials. 2006;27(19):3675–3683.
163. Gomez P III, Gil ES, Lovett ML, Rockwood DN, Di Vizio D, Kaplan DL, Adam RM, Estrada CR Jr, Mauney JR. The effect of manipulation of silk scaffold fabrication parameters on matrix performance in a murine model of bladder augmentation. Biomaterials. 2011, 32,30:7562-70.
164. Gorell JM., Ordidge RJ., Brown GG., Deniau JC., Buderer NM., Helpern JA., Increased iron-related MRI contrast in the substantia-nigra in Parkinson's disease, Neurology 1995,45:1138–1143.
165. Goyal RN, Singh SP, Simultaneous voltammetric determination of dopamine and adenosine using a single walled carbon nanotube – Modified glassy carbon electrode, Carbon 2008,46:1556-1562.

166. Gravel C, Götz R, Lorrain A, Sendtner M. Adenoviral gene transfer of ciliary neurotrophic factor and brain-derived neurotrophic factor leads to long-term survival of axotomized motor neurons. Nat Med. 1997, 3,7:765-70.
167. Green RA, Lovell NH, Poole-Warren LA. Cell attachment functionality of bioactive conducting polymers for neural interfaces. Biomaterials, 2009, 30**:** 3637–3644.
168. Griffin JW, Hogan MV, Chhabra AB, Deal DN. Peripheral nerve repair and reconstruc-tion. J Bone Joint Surg Am 2013,95,2144–51.
169. Grinsell D, Keating CP, Peripheral Nerve Reconstruction after Injury: A Review of Clinical and Experimental Therapies, 2014.
170. Guarino V, Alvarez-Perez MA, Borriello A, Napolitano T, Ambrosio L, Conductive PANi/PEGDA macroporous hydrogels for nerve regeneration. Adv Healthc Mater 2013;2;218-27.
171. Guimarda NK, Gomezb N, Schmidt CE. Conducting polymers in biomedical engineering. Progr Polym Sci, 2007, 32**:** 876–921.
172. Gulati AK. Evaluation of acellular and cellular nerve grafts in repair of rat peripheral nerve. J Neurosurg. 1988;68:117–123.
173. Gunatillake P, Mayadunne R, Adhikari R. Recent developments in biodegradable synthetic polymers. Biotechnology Annual Review,2006,12:301–47.
174. Guo J, Gao X, Su L, Xia H, Gu G, Pang Z, Jiang X, Yao L, Chen J, Chen H. Aptamer-functionalized PEG-PLGA nanoparticles for enhanced anti-glioma drug delivery. Biomaterials. 2011,32,31:8010-20.
175. Guo J, Su H, Zeng Y, Liang YX, Wong WM, Ellis-Behnke RG, So KF, Wu W. Reknitting the injured spinal cord by self-assembling peptide nanofiber scaffold. Nanomedicine. 2007, 3, 4:311-21.
176. Gupta R, Channual JC. Spatiotemporal pattern of macrophage recruitment afterchronic nerve compression injury. J Neurotrauma, 2006,23:216–26.
177. Hadlock T, Sundback C, Hunter D, Cheney M, Vacanti JP. A polymer foam conduit seeded with Schwann cells promotes guided peripheral nerve regeneration. Tissue Eng. 2000,6,2:119-27.
178. Hadlock TA, Sundback CA, Hunter DA, Vacanti JP, Cheney ML. A new artificial nerve graft containing rolled Schwann cell monolayers. Microsurgery 2001, 21:96–101.
179. Haes AJ., Hall WP, Chang L, Klein WL., Van Duyne RP., A Localized Surface Plasmon Resonance Biosensor: First Steps toward an Assay for Alzheimer's Disease; Nano Lett., 2004,4,6:
180. Hainfeld JF , Slatkin DN, Focella TM, Smilowitz HM , Gold nanoparticles: a new X-ray contrast agent. Br J Radiol. 2006,79,939:248-53.

181. Hainfeld JF , Slatkin DN, Smilowitz HM. The use of gold nanoparticles to enhance radiotherapy in mice. Phys Med Biol. 2004,49,1):N309-15.
182. Hainfeld JF, Smilowitz HM, O'Connor MJ, Dilmanian FA, Slatkin DN. Gold nanoparticle imaging and radiotherapy of brain tumors in mice. Nanomedicine (Lond). 2013,8,10:1601-9.
183. Harkin DG, George KA, Madden PW, Schwab IR, Hutmacher DW, Chirila TV. Silk fibroin in ocular tissue reconstruction. Biomaterials. 2011, 32,10:2445-58.
184. Harley BA., Spilker MH, Wu JW, Asano K, Hsu HP, Spector M, Yannas IV. Optimal degradation rate for collagen chambers used for regeneration of peripheral nerves over long gaps. Cells Tissues Organs, 2004, 176, 1-3:153–165.
185. Harrison BS, Anthony AT. Carbon nanotube applications for tissue engineering. Anat Rec, 2007, 28**:** 344–353.
186. Heath CA, Rutkowski GE, The development of bioartificial nerve grafts for peripheral-nerve regeneration, TIBTECH, 1998, 16.
187. Henderson CE, Camu W, Mettling C, Gouin A, Poulsen K, Karihaloo M, Rullamas J, Evans T, McMahon SB, Armanini MP, et al. Neurotrophins promote motor neuron survival and are present in embryonic limb bud. Nature. 1993,363,6426:266-70.
188. Henderson CE, Phillips HS, Pollock RA, Davies AM, Lemeulle C, Armanini M, Simmons L, Moffet B, Vandlen RA, Simpson LC corrected to Simmons L, Koliatsos VE, Rosenthal A, et al. GDNF: a potent survival factor for motoneurons present in peripheral nerve and muscle. Science. 1994;266,5187:1062-4.
189. Henry FP, Goyal NA., David WS, Improving electrophysiologic and histologic outcomes by photochemically sealing amnion to the peripheral nerve repair site, Surgery,2009, 145, 3: 313–321.
190. Heumann R, Lindholm D, Bandtlow C, Meyer M, Radeke MJ, et al.. Differential regulation of mRNA encoding nerve growth factor and its receptor in rat sciatic nerve during development, degeneration, and regeneration: role of macrophages. *Proc. Natl. Acad. Sci. USA* 1987,84:8735–39
191. Higa K, Takeshima N, Moro F, Kawakita T, Kawashima M, Demura M, Shimazaki J, Asakura T, Tsubota K, Shimmura S. Porous Silk Fibroin Film as a Transparent Carrier for Cultivated Corneal Epithelial Sheets. J Biomater Sci Polym Ed. 2010,22,17.
192. Hill, R. M. Electrical Conduction in Ultra Thin Metal Films. I. Theoretical Proc. R. Soc. Lond. A. 1969, 309, 377-95.
193. Hoffman-Kim, D, Mitchel, JA, Bellamkonda, RV, Topography, cell response, and nerve regeneration, Annu. Rev. Biomed. Eng. 2010, 12:203–231.

194. Hofmann S, Hagenmüller H, Koch AM, Müller R, Vunjak-Novakovic G, Kaplan DL, Merkle HP, Meinel L. Control of in vitro tissue-engineered bone-like structures using human mesenchymal stem cells and porous silk scaffolds. Biomaterials. 2007; 28,6:1152-62.
195. Holland EC. Glioblastoma multiforme: the terminator. Proc Natl Acad Sci U S A. 2000; 97,12:6242-4.
196. Hollowell JP, Villadiego A, Rich KM. Sciatic nerve regeneration across gaps within silicone chambers: long-term effects of NGF and consideration of axonal branching. Exp Neurol. 1990; 110,1:45-51.
197. Holmes TC, de Lacalle S, Su X, Liu G, Rich A, Zhang S. Extensive neurite outgrowth and active synapse formation on self-assembling peptide scaffolds. Proc Natl Acad Sci U S A. 2000, 97,12:6728-33.
198. Horner PJ, Power AE, Kempermann G, Kuhn HG, Palmer TD, et al.. Proliferation and differentiation of progenitor cells throughout the intact adult rat spinal cord. J. Neurosci.,2000; 20:2218–28.
199. Hu J, Chen B, Guo F, Du J, Gu P, Lin X, Yang W, Zhang H, Lu M, Huang Y, Xu G. Injectable silk fibroin/polyurethane composite hydrogel for nucleus pulposus replacement J Mater Sci Mater Med. 2012,23,3:711-22.
200. Hu K, Shi Y, Jiang W, Han J, Huang S, Jiang X. Lactoferrin conjugated PEG-PLGA nanoparticles for brain delivery: preparation, characterization and efficacy in Parkinson's disease. Int J Pharm. 2011,415,1-2:273-83.
201. Hu X, Huang J, Ye Z, Xia L, Li M, Lv B, Shen X, Luo Z. A novel scaffold with longitudinally oriented microchannels promotes peripheral nerve regeneration. Tissue Engineering Part A, 2009, 15, 11:3297–3308.
202. Hu, AJ; Zuo, BQ; Zhang, F; Lan, Q; Zhang, HX. Electrospun silk fibroin nanofibers promote Schwann cell adhesion, growth and proliferation. Neural Regeneration Research. 2012, 7:1171-1178.
203. Huang F, Sun L, Zheng J. In vitro and in vivo characterization of a silk fibroin-coated polyester vascular prosthesis. Artif Organs. 2008, 32,12:932-41.
204. Huang J, Hu X, Lu L, Ye Z, Zhang Q, Luo Z. Electrical regulation of Schwann cells using conductive polypyrrole/chitosan polymers. J Biomed Mater Res A 2010; 93;164-74.
205. Huang L, Hu J, Lang L, Wang X, Zhang P, Jing X, Wang X, Chen X, Lelkes PI, Macdiarmid AG, Wei Y. Synthesis and characterization of electroactive and biodegradable ABA block copolymer of polylactide and aniline pentamer Biomaterials. 2007; 28,10:1741-51.

206. Huang R, Ke W, Liu Y, Wu D, Feng L, Jiang C, Pei Y. Gene therapy using lactoferrin-modified nanoparticles in a rotenone-induced chronic Parkinson model. J Neurol Sci. 2010, 15, 290,1-2:123-30.

207. Huang R, Ma H, Guo Y, Liu S, Kuang Y, Shao K, Li J, Liu Y, Han L, Huang S, An S, Ye L, Lou J, Jiang C. Angiopep-conjugated nanoparticles for targeted long-term gene therapy of Parkinson's disease. Pharm Res, 2013,30,10:2549-59.

208. Huang W, Begum R, Barber T, Ibba V, Tee NC, Hussain M, Arastoo M, Yang Q, Robson LG, Lesage S, Gheysens T, Skaer NJ, Knight DP, Priestley JV. Regenerative potential of silk conduits in repair of peripheral nerve injury in adult rats. Biomaterials. 2012, 33,1:59-71.

209. Hudson TW, Liu SY, Schmidt CE. Engineering an improved acel¬lular nerve graft via optimized chemical processing. Tissue Eng. 2004;10:1346–1358.

210. Humpolicek P, Kasparkova V, Saha P, Stejskal J, Biocompatibility of polyaniline, Synthetic Metals 2012;162;722– 727.

211. Hussain MA, Kabir MA, Sood AK. On the cytotoxicity of carbon nanotubes. CurrSci, 2009, 96**:** 664–673.

212. Hyde AJ, Wippler C, Molecular weight of silk fibroin. J. Polym. Sci 1962;58;1083–1088.

213. Ikeda K, Okada T, Sawada S, Akiyoshi K, Matsuzaki K. Inhibition of the formation of amyloid beta-protein fibrils using biocompatible nanogels as artificial chaperones. FEBS Lett. 2006,580,28-29:6587-95.

214. Ikegawa Y, Sato S, Lim G, Hur W, Tanaka K, Komori M, Takenaka S, Taira T. Amelioration of the progression of an atopic dermatitis-like skin lesion by silk peptide and identification of functional peptides. Biosci Biotechnol Biochem. 2012, 76,3:473-7.

215. Inpanya P, Faikrua A, Ounaroon A, Sittichokechaiwut A, Viyoch J. Effects of the blended fibroin/aloe gel film on wound healing in streptozotocin-induced diabetic rats. Biomed Mater. 2012, 7,3:035008.

216. Jackson H , Muhammad O, Daneshvar H, Nelms J, Popescu A, Vogelbaum MA, Bruchez M, Toms SA. Quantum dots are phagocytized by macrophages and colocalize with experimental gliomas. Neurosurgery. 2007, 60,3:524-9

217. Jansen K, van der Werff JF, van Wachem PB, Nicolai JP, de Leij LF, van Luyn MJ. A hyaluronan-based nerve guide: *in vitro* cytotoxicity, subcutaneous tissue reactions, and degradation in the rat. Biomaterials, 2004, 25, 3:483–489.

218. Jenq CB, Coggeshall RE. Nerve regeneration through holey silicone tubes. Brain Research, 1985,361,1-2:233–241.

219. Jeong L, Yeo IS, Kim HN, Yoon YI, Jang da H, Jung SY, Min BM, Park WH. Plasma-treated silk fibroin nanofibers for skin regeneration. Int J Biol Macromol. 2009, 44,3:222-8.
220. Jiang J, Yan CS, Liu W, Facile template-free route to poly(N-methylaniline) microspheres in aqueous solution, Materials Letters 2009;63;2188–2190.
221. Jiang W, Xie H, Ghoorah D, Shang Y, Shi H, Liu F, Yang X, Xu H. Conjugation of functionalized SPIONs with transferrin for targeting and imaging brain glial tumors in rat model. PLoS One. 2012;7,5:e37376.
222. Jiang X, Lim SH, Mao H-Q, Chew SY. Current applications and future perspectives of artificial nerve conduits. Experimental Neurology,2010, 223:86–101.
223. Jiang X, Mi R, Hoke A, Chew SY. Nanofibrous nerve conduit-enhanced peripheral nerve regeneration. J Tissue Eng Regen Med. 2014, 8,5:377-85.
224. Jiang X, Zhao J, Wang S, Sun X, Zhang X, Chen J, Kaplan DL, Zhang Z. Mandibular repair in rats with premineralized silk scaffolds and BMP-2-modified bMSCs. Biomaterials. 2009,30,27:4522-32.
225. Johnson EO, Soucacos PN. Nerve repair: experimental and clinical evaluation of biodegradable artificial nerve guides. Injury,2008,39:30–6.
226. Johnson TS., O'Neill AC, Motarjem PM, Photochemical tissue bonding: a promising technique for peripheral nerve repair, Journal of Surgical Research, 2007,143,2:224–229.
227. Jones GL, Motta A, Marshall MJ, El Haj AJ, Cartmell SH. Osteoblast: osteoclast co-cultures on silk fibroin, chitosan and PLLA films. Biomaterials. 2009, 30,29:5376-84.
228. Jordan PH, Pikoulis M. Operative treatment for chronic pancreatitis pain. Journal of the American College of Surgeons 2001,192:498–509.
229. Josephson L, Tung CH, Moore A, Weissleder R. High-efficiency intracellular magnetic labeling with novel superparamagnetic-Tat peptide conjugates. Bioconjug Chem. 1999,10,2:186-91.
230. Kabalka GW, Davis MA, Holmberg E, Maruyama K, Huang L. Gadolinium-labeled liposomes containing amphiphilic Gd-DTPA derivatives of varying chain length: targeted MRI contrast enhancement agents for the liver. Magn Reson Imaging. 1991,9,3:373-7.
231. Kalbermatten DF, Kingham PJ, Mahay D, Mantovani C, Pettersson J, Raffoul W, Balcin H, Pierer G, Terenghi G. Fibrin matrix for suspension of regenerative cells in an artificial nerve conduit. J Plast Reconstr Aesthet Surg. 2008, 61, 6:669-75.
232. Kalyani AJ, Piper D, Mujtaba T, Lucero MT, Rao MS. Spinal cord neuronal precursors generate multiple neuronal phenotypes in culture. J. Neurosci. 1998,18:7856–68.

233. Katayama Y, Montenegro R, Freier T, Midha R, Belkas JS, Shoichet MS. Coil-reinforced hydrogel tubes promote nerve regeneration equivalent to that of nerve autografts, Biomaterials, 2006,27,3:505–518.
234. Kehoe, S.; Zhang, X. F.; Boyd, D. FDA approved guidance conduits and wraps for peripheral nerve injury: a review of materials and efficacy. Injury. 2012, 43, 553-72.
235. Keirstead HS. Stem cell transplantation into the central nervous system and the control of differentiation. J. Neurosci. Res. 2001,63:233–36.
236. Khuong HT, Midha R, Advances in nerve repair, Current neurology and neuroscience reports, 2013,13,1:322.
237. Kievit FM, Veiseh O, Fang C, Bhattarai N, Lee D, Ellenbogen RG, Zhang M. Chlorotoxin labeled magnetic nanovectors for targeted gene delivery to glioma. ACS Nano. 2010,4,8:4587-94..
238. Kilic A, Ojo B, Rajfer RA, Konopka G, Hagg D, Jang E, et al. Effect of white adipose tissueflap and insulin-like growth factor-1 on nerve regeneration in rats. Microsurgery,2013,33:367–75.
239. Kim DW, Hwang HS, Kim DS, Sheen SH, Heo DH, Hwang G, Kang SH, Kweon H, Jo YY, Kang SW, Lee KG, Park KW, Han KH, Park J, Eum WS, Cho YJ, Choi HC, Choi SY. Effect of silk fibroin peptide derived from silkworm Bombyx mori on the anti-inflammatory effect of Tat-SOD in a mice edema model. BMB Rep. 2011, 44,12:787-92.
240. Kim HJ, Kim UJ, Kim HS, Li C, Wada M, Leisk GG, Kaplan DL. Bone tissue engineering with premineralized silk scaffolds. Bone. 2008, 42,6:1226-34.
241. Kim HJ, Kim UJ, Leisk GG, Bayan C, Georgakoudi I, Kaplan DL. Bone regeneration on macroporous aqueous-derived silk 3-D scaffolds. Macromol Biosci. 2007, 7,5:643-55.
242. Kim HJ, Kim UJ, Vunjak-Novakovic G, Min BH, Kaplan DL. Influence of macroporous protein scaffolds on bone tissue engineering from bone marrow stem cells. Biomaterials. 2005; 26,21:4442-52.
243. Kim SG , Harel N, Jin T, Kim T, Lee P, Zhao F**.** Cerebral blood volume MRI with intravascular superparamagnetic iron oxide nanoparticles. NMR Biomed. 2013,26,8:949-62.
244. Kim SH, Young Sik NAM, Lee TS, Park WH, Silk Fibroin Nanofiber, Electrospinning, Properties, and Structure. Polymer Journal 2003;35;185-190.
245. Kim YT, Haftel VK, Kumar S, Bellamkonda RV. The role of aligned polymer fiber-based constructs in the bridging of long peripheral nerve gaps. Biomaterials. 2008,29,21:3117-27.

246. Kim, HL; Yoo, H; Park, HJ; Kim, YG; Lee, D; Kang, YS; Khang, G. Effect of PLGA/Silk Fibroin Hybrid Film on Attachment and Proliferation of Schwann Cells. Polymer-Korea, 2011,35:7-12.
247. Kim, UJ, Park J.; Kim, HJ.; Wada, M.; Kaplan, DL. Three-dimensional aqueous-derived biomaterial scaffolds from silk fibroin. Biomaterials, 2005, 26, 2775–85.
248. Kimura K, Yanagida Y, Haruyama T, Kobatake E, Aizawa M. Electrically induced neurite outgrowth of PC12 cells on the electrode surface. Med Biol Eng Comput. 1998; 36,4:493-8.
249. Kimura K, Yanagida Y, Haruyama T, Kobatake E, Aizawa M. Gene expression in the electrically stimulated differentiation of PC12 cells. J Biotechnol. 1998, 30, 63, 1:55-65.
250. Kircher MF, Mahmood U, King RS, Weissleder R, Josephson L. A multimodal nanoparticle for preoperative magnetic resonance imaging and intraoperative optical brain tumor delineation. Cancer Res. 2003, 63,23:8122-5.
251. Kirker-Head C, Karageorgiou V, Hofmann S, Fajardo R, Betz O, Merkle HP, Hilbe M, von Rechenberg B, McCool J, Abrahamsen L, Nazarian A, Cory E, Curtis M, Kaplan D, Meinel L. BMP-silk composite matrices heal critically sized femoral defects. Bone. 2007; 41,2:247-55.
252. Kitchen S. Electrotherapy: Evidence based Practice. Churchill Livingstone:Edinburgh, 2002.
253. Kocsis JD, Akiyama Y, Lankford KL, Radtke C.. Cell transplantation of peripheral-myelin-forming cells to repair the injured spinal cord. J. Rehabil. Res. Dev. 2002,39:287–98.
254. Kokai LE, Ghaznavi AM, Marra KG. Incorporation of double-walled microspheres into polymer nerve guides for the sustained delivery of glial cell line-derived neurotrophic factor. Biomaterials. 2010,31,8:2313-22.
255. Kokai LE, Lin Y-C, Oyster NM, Marra KG. Diffusion of soluble factors through degradable polymer nerve guides: controlling manufacturing parameters. Acta Biomaterialia,2009,5:2540–50.
256. Kolla HS, Surwade SP, Zhang X, Macdiarmid AG, Manohar SK. Absolute molecular weight of polyaniline. J Am Chem Soc 2005;127;16770-1.
257. Konofaos P, ver Halen JP, Nerve repair by means of tubulization: past, present, future," Journal of Reconstructive Microsurgery, 2013,29,3:149–164.
258. Koprivica V, Cho KS, Park JB, Yiu G, Atwal J, Gore B, Kim JA, Lin E, Tessier-Lavigne M, Chen DF, He Z. EGFR activation mediates inhibition of axon regeneration by myelin and chondroitin sulfate proteoglycans. Science, 2005, 310,5745:106-10.

259. Kotwal A, Schmid CE. Electrical stimulation alters protein adsorption and nerve cell interactions with electrically conducting biomaterials. Biomaterials, 2001, 22:1055–1064.

260. Kramer M, Chaudhuri JB, Ellis MJ. Promotion of neurite outgrowth in corporation poly-l-lysine into aligned PLGA nanofibers scafolds. *Europ Cell Mater* . 2011;22:53.

261. Krisljak E, Stajcic Z. Evidence that ampicillin and streptomycin can suppress autotomic behaviour in rats. Acta Vet,2004,54:145–52.

262. Kroehne V, Heschel I, Schügner F, Lasrich D, Bartsch JW, Jockusch H. Use of a novel collagen matrix with oriented pore structure for muscle cell differentiation in cell culture and in grafts. Journal of Cellular and Molecular Medicine, 2008,12,5A:1640–1648.

263. Kucekova Z, Humpolicek P, Kasparkova V, Perecko T, Lehocký M, Hauerlandová I, Sáha P, Stejskal J, Colloidal polyaniline dispersions: antibacterial activity, cytotoxicity and neutrophil oxidative burst, Colloids Surf B Biointerfaces 2014; 116;411-7.

264. Kundu B, Kundu SC. Silk sericin/polyacrylamide in situ forming hydrogels for dermal reconstruction. Biomaterials. 2012, 33,30:7456-67.

265. Laroas G, Battiston G, Sard A, Ferrero M, Dellon A. Digital nerve reconstruction with the bioabsorbable neurotube. Rivista Italiana Di Chirurgia Plastica Clinical and Experimental Plastic Surgery 2003,35:125–8.

266. Lawrence BD, Marchant JK, Pindrus MA, Omenetto FG, Kaplan DL. Silk film biomaterials for cornea tissue engineering. Biomaterials. 2009, 30,7:1299-308.

267. Le´on MJD. Electrospinning nanofibers of polyaniline and polyaniline/polystyrene and polyethylene oxide blends. In Proceedings of the National Conference on Undergraduate Research, Lexington, KY,USA, 2001.

268. Leach JB, Schmidt CE. Characterization of protein release from photo-crosslinkable hyaluronic acidpolyethylene glycol hydrogel tissue engineering scaffolds. Biomaterials, 2005, 26, 2,125–135.

269. Lee JH , Kang DY, Lee T, Kim SU, Oh BK, Choil JW. Signal enhancement of surface plasmon resonance based immunosensor using gold nanoparticle-antibody complex for beta-amyloid (1-40) detection. J Nanosci Nanotechnol. 2009,9,12:7155-60.

270. Lee JY, Bashur CA, Goldstein AS, Schmidt CE. Polypyrrole-coated electrospun PLGA nanofibers for neural tissue applications. Biomaterials. 2009,30,26:4325-35.

271. Lee K, Cho S, Park SH, Heeger AJ, Lee CW, Lee SH, Metallic transport in polyaniline. Nature 2006;441;65-8.

272. Lee SK, Wolfe SW, Nerve transfers for the upper extremity: new horizons in nerve reconstruction, Journal of the American Academy of Orthopaedic Surgeons, 2012,20,8:506–517.

273. Lee SK., Wolfe SW., Peripheral nerve injury and repair, Journal of the American Academy of Orthopaedic Surgeons, 2000,8,4:243–252.
274. Levison SW, Ducceschi MH, Young GM, Wood TL. Acute exposure to CNTF in vivo induces multiple components of reactive gliosis. Exp Neurol. 1996,141,2:256-68.
275. Li C, Vepari C, Jin HJ, Kim HJ, Kaplan DL. Electrospun silk-BMP-2 scaffolds for bone tissue engineering. Biomaterials. 2006; 27,16:3115-24.
276. Li GN, Hoffman-Kim D. Tissue engineered platforms of axon guidance. Tissue Eng B, 2008,14**:** 33–51.
277. Li H, Li L, Qian Y, Cai K, Lu Y, Zhong L, Liu W, Yang L. Preparation and cytocompatibility study of poly (epsilon-caprolactone)/silk sericin nanofibrous scaffolds. Sheng Wu Yi Xue Gong Cheng Xue Za Zhi. 2011, 28,2:305-9.
278. Li M, Guo Y, Wei Y, MacDiarmid AG, Lelkes PI. Electrospinning polyaniline-contained gelatin nanofibers for tissue engineering applications. Biomaterials*,* 2006,27**:** 2705–2715.
279. Li S, Wu H, Hu XD, Tu CQ, Pei FX, Wang GL, Lin W, Fan HS. Preparation of electrospun PLGA-silk fibroin nanofibers-based nerve conduits and evaluation in vivo. Artif Cells Blood Substit Immobil Biotechnol. 2012,40,1-2:171-8.
280. Li ST, Archibald SJ, Krarup C, Madison RD. Peripheral nerve repair with collagen conduits. Clinical Materials, 1992, 9, 3-4,195–200.
281. Li ST, Archibald SJ, Krarup C, Madison RD. The development of collagen nerve conduits that promote peripheral-nerve regeneration. Biotechnology and Polymers, 1991:281–93.
282. Li ST, Yuen D. Implant devices for nerve repair. US Patent no. 6,716,225. Edited by USPTO. Franklin Lakes, NJ, USA: Collagen Matrix, Inc.; 2004.
283. Li YS, Chen BF, Li XJ, Zhang WK, Tang HB, Cytotoxicity of polyaniline nanomaterial on rat celiac macrophages in vitro. PLoS One 2014;9;e107361.
284. Liao CD, Zhang F, Guo RM, Zhong XM, Zhu J, Wen XH, et al. Peripheral nerve repair:monitoring by using gadofluorine M-enhanced MR imaging with chitosan nerveconduits with cultured mesenchymal stem cells in rat model of neurotmesis.Radiology,2012,262:161–71.
285. Liao YH , Chang YJ, Yoshiike Y, Chang YC, Chen YR. Negatively charged gold nanoparticles inhibit Alzheimer's amyloid-fibrillization, induce fibril dissociation, and mitigate neurotoxicity. Small. 2012,8,23:3631-9.
286. Lin K., Yang D, Chu I, DuraSeal as a ligature in the anastomosis of rat sciatic nerve gap injury, Journal of Surgical Research, 2010, 161,1:101–110.
287. Lin P, Chan WC, Badylak SF, et al. Assessing porcine liver-derived biomatrix for hepatic tissue engineering. Tissue Eng. 2004;10:1046–1053.

288. Lin YC, Ramadan M, Hronik-Tupaj M, Kaplan DL, Philips BJ, Sivak W, Rubin JP, Marra KG. Spatially controlled delivery of neurotrophic factors in silk fibroin-based nerve conduits for peripheral nerve repair. Ann Plast Surg. 2011, 67,2:147-55.

289. Liu BS. Fabrication and evaluation of a biodegradable proanthocyanidin-crosslinked gelatin conduit in peripheral nerve repair. Journal of Biomedical Materials Research Part A, 2008,87,4:1092–1102.

290. Liu CX, Liao YF, Li HL, Zheng SB. Cytocompatibility of silk fibroin film with rabbit urinary bladder transitional epithelial cells in vitro. Nan Fang Yi Ke Da Xue Xue Bao. 2008, 28,2:216-8.

291. Liu CX, Lin YY, Li HL, Zheng SB. Application of silk fibroin film for repairing rabbit urethral defect. Nan Fang Yi Ke Da Xue Xue Bao. 2007, 27,2:184-7.

292. Liu D, Chen W, Tian Y, He S, Zheng W, Sun J, Wang Z, Jiang X. A highly sensitive gold-nanoparticle-based assay for acetylcholinesterase in cerebrospinal fluid of transgenic mice with Alzheimer's disease. Adv Healthc Mater. 2012,1,1:90-5.

293. Liu H (a), Li X, Niu X, Zhou G, Li P, Fan Y. Improved hemocompatibility and endothelialization of vascular grafts by covalent immobilization of sulfated silk fibroin on poly(lactic-co-glycolic acid) scaffolds. Biomacromolecules. 2011,12,8:2914-24.

294. Liu H (b), Li X, Zhou G, Fan H, Fan Y. Electrospun sulfated silk fibroin nanofibrous scaffolds for vascular tissue engineering. Biomaterials. 2011;32,15:3784-93.

295. Liu HL, Hua MY, Yang HW, Huang CY, Chu PC, Wu JS, Tseng IC, Wang JJ, Yen TC, Chen PY, Wei KC. Magnetic resonance monitoring of focused ultrasound/magnetic nanoparticle targeting delivery of therapeutic agents to the brain. Proc Natl Acad Sci U S A. 2010,107,34:15205-10.

296. Liu Y, Lu W. Recent advances in brain tumor-targeted nano-drug delivery systems. Expert Opin Drug Deliv. 2012; 9,6:671-86.

297. Lohmeyer JA, Siemers F, Machens HG, Mailander P. The clinical use of artificial nerve conduits for digital nerve repair: a prospective cohort study and literature review. Journal of Reconstructive Microsurgery,2009,25:55–61.

298. Long L, Huang Y, Wu H, Luan W, Zhang Q, Wen H, et al. Dynamic change of Prohibitin2expression in rat sciatic nerve after crush. Cell Mol Neurobiol 2013,33:689–98.

299. Lou D, Sun B, Wei H, Deng X, Chen H, Xu D, et al. Spatiotemporal expression of testicu-lar protein kinase 1 after rat sciatic nerve injury. J Mol Neurosci 2012,47:180–91.

300. Lovat V, Pantarotto D, Lagostena L, Cacciari B, Grandolfo M, Righi M, Spalluto G, Prato M, Ballerini L. Carbon nanotube substrates boost neuronal electrical signaling. Nano Lett. 2005; 5, 6:1107-10.

301. Lovett M, Cannizzaro C, Daheron L, Messmer B, Vunjak-Novakovic G, Kaplan DL. Silk fibroin microtubes for blood vessel engineering. Biomaterials. 2007, 28,35:5271-9.

302. Lovett M, Eng G, Kluge JA, Cannizzaro C, Vunjak-Novakovic G, Kaplan DL. Tubular silk scaffolds for small diameter vascular grafts. Organogenesis. 2010, 6,4:217-24.

303. Lovett ML, Cannizzaro CM, Vunjak-Novakovic G, Kaplan DL. Gel spinning of silk tubes for tissue engineering. Biomaterials. 2008, 29,35:4650-7.

304. Lu J, Ashwell K.. Olfactory ensheathing cells: their potential use for repairing the injured spinal cord. Spine,2002,27:887–92.

305. Lu MC, Hsiang SW, Lai TY, Yao CH, Lin LY, Chen YS., Influence of cross-linking degree of a biodegradable genipin-cross-linked gelatin guide on peripheral nerve regeneration. Journal of Biomaterials Science, Polymer Edition, 2007,18,7:843–863.

306. Lu MC, Huang YT, Lin JH, Yao CH, Lou CW, Tsai CC, Chen YS. Evaluation of a multi-layer microbraided polylactic acid fiber-reinforced conduit for peripheral nerve regeneration. J Mater Sci Mater Med. 2009; 20, 5:1175-80.

307. Lu Q, Hu K, Feng QL, Cui F. Growth of fibroblast and vascular smooth muscle cells in fibroin/collagen scaffold. Materials Science and Engineering C 2009,29: 2239–2245.

308. Lu Y, Chi FL, Zhao X, Shao ZZ, Cao ZB. Experimental study on facial nerve regeneration by porous silk fibroin conduit. Zhonghua Er Bi Yan Hou Tou Jing Wai Ke Za Zhi. 2006, 41,8:603-6.

309. Luangbudnark W, Viyoch J, Laupattarakasem W, Surakunprapha P, Laupattarakasem P. Properties and biocompatibility of chitosan and silk fibroin blend films for application in skin tissue engineering. Scientific WorldJournal. 2012:697201.

310. Luis AL, Rodrigues JM, Amado S, Veloso AP, Armada-Da-silva PAS, Raimondo S,et al. PLGA 90/10 and caprolactone biodegradable nerve guides for the reconstruction of the rat sciatic nerve. Microsurgery, 2007,27:125–37.

311. Lundborg G, Dahlin L, Dohi D, Kanje M, Terada N. A new type of 'bioartificial' nerve graft for bridging extended defects in nerves. Journal of Hand Surgery, 1997, 22, 3: 299–303.

312. Luo SC, Mohamed Ali E, Tansil NC, Yu HH, Gao S, Kantchev EA, Ying JY. Poly(3,4-ethylenedioxythiophene) (PEDOT) nanobiointerfaces: thin, ultrasmooth, and functionalized PEDOT films with in vitro and in vivo biocompatibility. Langmuir. 2008,5;24,15:8071-7.

313. Luppi B, Bigucci F, Corace G, Delucca A, Cerchiara T, Sorrenti M, Catenacci L, Di Pietra AM, Zecchi V. Albumin nanoparticles carrying cyclodextrins for nasal delivery of the anti-Alzheimer drug tacrine. Eur J Pharm Sci. 2011,44,4:559-65.

314. Ma ML, Cao CB, Li JH, Zhu HS. Novel prosthesis using silk fibroin for small caliber vascular. ASBM6: Advanced Biomaterials VI Book Series: Key Engineering Materials. 2005; 288-289: 461-464.
315. MacDiarmid AG, Epstein AJ.; The concept of secondary doping as applied to polyaniline. Synthetic Metals, 1994,65**:** 103–116.
316. Mackinnon SE, Dellon AL. Clinical nerve reconstruction with a bioabsorbable polyglycolic acid tube. Plastic and Reconstructive Surgery 1990,85:419–24.
317. Mackinnon SE, Dellon AL., Nerve repair and nerve grafts, Surgery of the Peripheral Nerve, 1988, S. E. Mackinnon, Ed. Thieme, New York, NY, USA.
318. Madden PW, Lai JN, George KA, Giovenco T, Harkin DG, Chirila TV. Human corneal endothelial cell growth on a silk fibroin membrane. Biomaterials. 2011, 32,17:4076-84.
319. Madduri S, Papaloïzos M, Gander B. Trophically and topographically functionalized silk fibroin nerve conduits for guided peripheral nerve regeneration. Biomaterials. 2010, 31,8:2323-34.
320. Madduri, S.; Papaloïzos, M.; Gander, B. Trophically and topographically functionalized silk fibroin nerve conduits for guided peripheral nerve regeneration. Biomaterials 2010, 31, 2323-334.
321. Mamot C, Nguyen JB, Pourdehnad M, Hadaczek P, Saito R, Bringas JR, Drummond DC, Hong K, Kirpotin DB, McKnight T, Berger MS, Park JW, Bankiewicz KS. Extensive distribution of liposomes in rodent brains and brain tumors following convection-enhanced delivery. J Neurooncol. 2004,68,1:1-9.
322. Mandal BB (a), Park SH, Gil ES, Kaplan DL. Stem cell-based meniscus tissue engineering. Tissue Eng Part A. 2011,17,21-22:2749-61.
323. Mandal BB (b), Park SH, Gil ES, Kaplan DL. Multilayered silk scaffolds for meniscus tissue engineering. Biomaterials. 2011, 32,2:639-51.
324. Mandal BB, Kundu SC. Non-mulberry silk gland fibroin protein 3-D scaffold for enhanced differentiation of human mesenchymal stem cells into osteocytes. Acta Biomater. 2009; 5,7:2579-90.
325. Manninger SP, Muldoon LL, Nesbit G, Murillo T, Jacobs PM, Neuwelt EA. An exploratory study of ferumoxtran-10 nanoparticles as a blood-brain barrier imaging agent targeting phagocytic cells in CNS inflammatory lesions. AJNR Am J Neuroradiol. 2005, 26,9:2290-300.
326. Manoli T, Schulz L, Stahl S, Jaminet P, Schaller HE. Evaluation of sensory recovery afterreconstruction of digital nerves of the hand using muscle-in-vein conduits incomparison to nerve suture or nerve autografting. Microsurgery 2015 [in press]

327. Marcoccio I, Vigasio A. Muscle-in-vein nerve guide for secondary reconstruction indigital nerve lesions. J Hand Surg Am 2010,35:1418–26.
328. Mardor Y, Roth Y, Lidar Z, Jonas T, Pfeffer R, Maier SE, Faibel M, Nass D, Hadani M, Orenstein A, Cohen JS, Ram Z. Monitoring response to convection-enhanced taxol delivery in brain tumor patients using diffusion-weighted magnetic resonance imaging. Cancer Res, 2001, 61, 13:4971-3.
329. Marelli B, Alessandrino A, Farè S, Freddi G, Mantovani D, Tanzi MC. Compliant electrospun silk fibroin tubes for small vessel bypass grafting. Acta Biomater. 2010, 6,10:4019-26.
330. Marelli B, Ghezzi CE, Alessandrino A, Barralet JE, Freddi G, Nazhat SN. Silk fibroin derived polypeptide-induced biomineralization of collagen. Biomaterials. 2012 33,1:102-8.
331. Marolt D, Augst A, Freed LE, Vepari C, Fajardo R, Patel N, Gray M, Farley M, Kaplan D, Vunjak-Novakovic G. Bone and cartilage tissue constructs grown using human bone marrow stromal cells, silk scaffolds and rotating bioreactors. Biomaterials. 2006; 27,36:6138-49.
332. Martino G, Pluchino S. The therapeutic potential of neural stem cells, Nat Rev Neurosci. 2006,7,5:395-406.
333. Matheson CR, Carnahan J, Urich JL, Bocangel D, Zhang TJ, Yan Q. Glial cell line-derived neurotrophic factor (GDNF) is a neurotrophic factor for sensory neurons: comparison with the effects of the neurotrophins. J Neurobiol. 1997,32,1:22-32.
334. Mathew A, Fukuda T, Nagaoka Y, Hasumura T, Morimoto H, Yoshida Y, Maekawa T, Venugopal K, Kumar DS. Curcumin loaded-PLGA nanoparticles conjugated with Tet-1 peptide for potential use in Alzheimer's disease. PLoS One. 2012; 7,3:e32616.
335. Matsumoto, K., Ohnishi, K., Kiyotani, T., Sekine, T, Ueda, H., Nakamura, T, Endo, K, Shimizu, Y. Peripheral nerve regeneration across an 80-mm gap bridged by a polyglycolic acid (PGA)-collagen tube filled with laminin-coated collagen fibers: a histological and electrophysiological evaluation of regenerated nerves. Brain Res. 2000, 868:315–328.
336. Mauney JR, Cannon GM, Lovett ML, Gong EM, Di Vizio D, Gomez P 3rd, Kaplan DL, Adam RM, Estrada CR Jr. Evaluation of gel spun silk-based biomaterials in a murine model of bladder augmentation. Biomaterials. 2011, 32,3:808-18.
337. McClure, MJ; Sell, SA; Ayres, CE; Simpson, DG; Bowlin, GL. Electrospinning-aligned and random polydioxanonepolycaprolactone- silk fibroin-blended scaffolds: geometry for a vascular matrix. Biomedical Materials, 2009, 4,5: 055010.

338. Meek MF, Coert JH. US Food and Drug Administration/Conformit Europe approved absorbable nerve conduits for clinical repair of peripheral and cranial nerves. Annals of Plastic Surgery,2008; 60:466–72.
339. Meek MF, Dunnen WFAD. Porosity of the wall of a Neurolac nerve conduit hampers nerve regeneration. Microsurgery,2009, 29:473–8.
340. Meek MF, Nicolai JP, Robinson PH. Secondary digital nerve repair in the foot with resorbable p(DLLA-epsilon-CL) nerve conduits. Journal of Reconstruction Microsurgery,2006,22:149–51.
341. Meek MF. More than just sunshine with implantation of resorbable (p(DLLA-e-CL)) biomaterials. Bio-Medical Materials and Engineering, 2007,17:329–34.
342. Meinel L (a), Betz O, Fajardo R, Hofmann S, Nazarian A, Cory E, Hilbe M, McCool J, Langer R, Vunjak-Novakovic G, Merkle HP, Rechenberg B, Kaplan DL, Kirker-Head C. Silk based biomaterials to heal critical sized femur defects. Bone. 2006; 39,4:922-31.
343. Meinel L (b), Hofmann S, Betz O, Fajardo R, Merkle HP, Langer R, Evans CH, Vunjak-Novakovic G, Kaplan DL. Osteogenesis by human mesenchymal stem cells cultured on silk biomaterials: comparison of adenovirus mediated gene transfer and protein delivery of BMP-2. Biomaterials. 2006; 27,28:4993-5002.
344. Meinel L, Fajardo R, Hofmann S, Langer R, Chen J, Snyder B, Vunjak-Novakovic G, Kaplan D. Silk implants for the healing of critical size bone defects. Bone. 2005; 37,5:688-98.
345. Meiners, S., Ahmed, I., Ponery, A. S., Amor, N., Harris, S. L., Ayres, V., Fan, Y., Chen, Q., Delgado-Rivera, R. and Babu, A. N., Engineering electrospun nanofibrillar surfaces for spinal cord repair: a discussion. Polym. Int., 2007,56:1340–1348.
346. Menei P, Montero-Menei C, Whittemore SR, Bunge RP, Bunge MB.. Schwann cells genetically modified to secrete human BDNF promote enhanced axonal regrowth across transected adult rat spinal cord. Eur. J. Neurosci. 1998 10:607– 21.
347. Miao D, Jiang M, Liu Z, Gu G, Hu Q, Kang T, Song Q, Yao L, Li W, Gao X, Sun M, Chen J. Co-administration of dual-targeting nanoparticles with penetration enhancement peptide for antiglioblastoma therapy. Mol Pharm. 2014,11,1:90-101.
348. Miladi I, Alric C, Dufort S, Mowat P, Dutour A, Mandon C, Laurent G, Bräuer-Krisch E, Herath N, Coll JL, Dutreix M, Lux F, Bazzi R, Billotey C, Janier M, Perriat P, Le Duc G, Roux S, Tillement O. The in vivo radiosensitizing effect of gold nanoparticles based MRI contrast agents. Small. 2014,10,6:1116-24.
349. Min S, Gao X, Liu L, Tian L, Zhu L, Zhang H, Yao J. Fabrication and characterization of porous tubular silk fibroin scaffolds. J Biomater Sci Polym Ed. 2009, 20,13:1961-74.

350. Mittal G, Carswell H, Brett R, Currie S, Kumar MN. Development and evaluation of polymer nanoparticles for oral delivery of estradiol to rat brain in a model of Alzheimer's pathology. J Control Release. 2011,150,2:220-8.
351. Miyamoto K, Sasaki M, Minamisawa Y, Kurahashi Y, Kano H, Ishikawa S. Evaluation of *in vivo* biocompatibility and biodegradation of photo-crosslinked hyaluronate hydrogels (HADgels). Journal of Biomedical Materials Research Part A, 2004,70,4: 550–559,.
352. Morgan AW, Roskov KE, Lin-Gibson S, Kaplan DL, Becker ML, Simon CG Jr. Characterization and optimization of RGD-containing silk blends to support osteoblastic differentiation. Biomaterials. 2008; 29,16:2556-63.
353. Mosahebi A., Woodward B., Wiberg M., Martin R, Terenghi, G, Retroviral labeling of Schwann cells: in vitro characterization and in vivo transplantation to improve peripheral nerve regeneration. Glia, 2001, 34: 8–17.
354. Mosmann, T, Rapid colorimetric assay for cellular growth and survival: application to proliferation and cytotoxicity assays. J Immunol Methods 1983;65;55-63.
355. Mosmann, T., Rapid colorimetric assay for cellular growth and survival: application to proliferation and cytotoxicity assays. J Immunol Methods, 1983, 65: 55-63.
356. Mottaghitalab F, Farokhi M, Zaminy A, Kokabi M, Soleimani M, Mirahmadi F, Shokrgozar MA, Sadeghizadeh M, A biosynthetic nerve guide conduit based on silk/SWNT/fibronectin nanocomposite for peripheral nerve regeneration. PLoS One 2013;30;e74417.
357. Mukhatyar, V., Karumbaiah, L., Yeh, J, Bellamkonda, R., Tissue engineering strategies designed to realize the endogenous regenerative potential of peripheral nerves. Adv. Mat. 2009, 21:4670–4679.
358. Murakami Y, Furukawa S, Nitta A, Furukawa Y.. Accumulation of nerve growth factor protein at both rostral and caudal stumps in the transected rat spinal cord. *J. Neurol. Sci.* 2002,198:63–69
359. Nair LS, Laurencin CT. Biodegradable polymers as biomaterials. Progress in Polymer Science,2007,32,762–98.
360. Nakahara Y, Gage FH, Tuszynski MH. Grafts of fibroblasts genetically modified to secrete NGF, BDNF, NT-3, or basic FGF elicit differential responses in the adult spinal cord. Cell Transplant. 1996,5,2:191-204.
361. Nakahara Y, Gage FH, Tuszynski MH.. Grafts of fibroblasts genetically modified to secrete NGF, BDNF, NT-3, or basic FGF elicit differential responses in the adult spinal cord. Cell Transpl. 1996 5:191– 204.
362. Nakamura T, Inada Y, Fukuda S, Yoshitani M, Nakada A, Itoi S, Kanemaru S, Endo K, Shimizu Y. Experimental study on the regeneration of peripheral nerve gaps

through a polyglycolic acid-collagen (PGA-collagen) tube. Brain Res. 2004; 1027,1-2:18-29.

363. Nakazawa Y, Sato M, Takahashi R, Aytemiz D, Takabayashi C, Tamura T, Enomoto S, Sata M, Asakura. Development of Small-Diameter Vascular Grafts Based on Silk Fibroin Fibers from Bombyx mori for Vascular Regeneration. J Biomater Sci Polym Ed. 2010, 22,1-3: 195-206.
364. Nalwa HS. Handbook of Organic Conductive Molecules and Polymers. Wiley:New York. 1997.
365. National Toxicology Program. NTP Toxicology and Carcinogenesis Studies of Tetrakis(hydroxymethyl)phosphonium sulfate (THPS) (CAS No. 55566-30-8) and Tetrakis(hydroxymethyl)phosphonium chloride (THPC) (CAS No. 124-64-1) in F344/N Rats and B6C3F1 Mice (Gavage Studies). Natl Toxicol Program Tech Rep Ser. 1987, 296:1-290.
366. Navarro X, Udina E. Methods and protocols in peripheral nerve regeneration experimental research: Part III. Electrophysiological evaluation. Int Rev Neurobiol,2009,87:105–26.
367. Navissano M, Malan F, Carnino R, Battiston B. Neurotube for facial nerve repair. Microsurgery 2005;25:268–71.
368. Nayak S, Talukdar S, Kundu SC. Potential of 2D crosslinked sericin membranes with improved biostability for skin tissue engineering. Cell Tissue Res. 2012, 347,3:783-94.
369. Neely A, Perry C, Varisli B, Singh AK, Arbneshi T, Senapati D, Kalluri JR, Ray PC. Ultrasensitive and highly selective detection of Alzheimer's disease biomarker using two-photon Rayleigh scattering properties of gold nanoparticle. ACS Nano. 2009; 3,9:2834-40.
370. Nerem RM, Seliktar D. Vascular tissue engineering. Annu Rev Biomed Eng. 2001, 3:225-43.
371. Neuwelt EA , Várallyay P, Bagó AG, Muldoon LL, Nesbit G, Nixon R. Imaging of iron oxide nanoparticles by MR and light microscopy in patients with malignant brain tumours. Neuropathol Appl Neurobiol. 2004,30,5:456-71.
372. Newman JP, Verity AN, Hawatmeh S, Fee WE Jr, Terris DJ. Ciliary neurotrophic factors enhances peripheral nerve regeneration. Arch Otolaryngol Head Neck Surg. 1996;122,4:399-403.
373. Nijhuis TH, Bodar CW, van Neck JW, Walbeehm ET, Siemionow M, Madajka M, et al.Natural conduits for bridging a 15-mm nerve defect: comparison of the veinsupported by muscle and bone marrow stromal cells with a nerve autograft. JPlast Reconstr Aesthet Surg 2013,66:251–9.

374. Nisbet DR., Crompton KE, Horne MK., Finkelstein DI, Forsythe JS. Neural tissue engineering of the CNS using hydrogels. *Journal of Biomedical Materials Research Part B*, 2008, 87, 1:251–263.

375. O'Neill AC., Randolph MA, Bujold KE., Kochevar IE., Redmond RW., Winograd JM., Photochemical sealing improves outcome following peripheral neurorrhaphy, Journal of Surgical Research, 2009,151,1:33–39,.

376. O'Neill AC., Randolph MA, Bujold KE., Kochevar IE., Redmond RW., Winograd JM, Preparation and integration of human amnion nerve conduits using a light-activated technique, Plastic and Reconstructive Surgery, 2009,124,2:428–437.

377. Oh SH, Kim JH, Song KS, Jeon BH, Yoon JH, Seo TB, Namgung U, Lee IW, Lee JH. Peripheral nerve regeneration within an asymmetrically porous PLGA/Pluronic F127 nerve guide conduit. Biomaterials. 2008,29,11:1601-9.

378. Okabayashi R, Nakamura M, Okabayashi T, Tanaka Y, Nagai A, Yamashita K. Efficacy of polarized hydroxyapatite and silk fibroin composite dressing gel on epidermal recovery from full-thickness skin wounds. J Biomed Mater Res B Appl Biomater. 2009; 90,2:641-6.

379. Okamoto H, Hata K, Kagami H, Okada K, Ito Y, Narita Y, Hirata H, Sekiya I, Otsuka T, Ueda M. Recovery process of sciatic nerve defect with novel bioabsorbable collagen tubes packed with collagen filaments in dogs. Journal of Biomedical Materials Research Part A, 2010, 92, 3:859–868.

380. Orbay H, Uysal AC, Hyakusoku H, Mizuno H. Differentiated and undifferentiated adipose-derived stem cells improve function in rats with peripheral nerve gaps. J Plast Reconstr Aesthet Surg. 2011,1.

381. Oudega M, Hagg T. Nerve growth factor promotes regeneration of sensory axons into adult rat spinal cord. Exp Neurol. 1996;140,2:218-29.

382. Oudega M, Hagg T. Neurotrophins promote regeneration of sensory axons in the adult rat spinal cord. Brain Res. 1999;818,2:431-8.

383. Oyesiku NM, Wigston DJ. Ciliary neurotrophic factor stimulates neurite outgrowth from spinal cord neurons. J Comp Neurol. 1996,364,1:68-77.

384. Panseri S, Cunha C, Lowery J, Del Carro U, Taraballi F, Amadio S, Vescovi A, Gelain F. Electrospun micro- and nanofiber tubes for functional nervous regeneration in sciatic nerve transections. BMC Biotechnol. 2008 Apr 11;8:39.

385. Park SH (a), Gil ES, Mandal BB, Cho H, Kluge JA, Min BH, Kaplan DL. Annulus fibrosus tissue engineering using lamellar silk scaffolds. J Tissue Eng Regen Med. 2012,6,s3:s24-s33.

386. Park SH (b), Gil ES, Cho H, Mandal BB, Tien LW, Min BH, Kaplan DL. Intervertebral disc tissue engineering using biphasic silk composite scaffolds. Tissue Eng Part A. 2012, 18,5-6:447-58.
387. Passariello R, Pavone P, Patrizio G, Di Renzi P, Mastantuono M, Giuliani S. Liposomes loaded with nonionic contrast media. Hepatosplenic computed tomographic enhancement. Invest Radiol. 1990,25,Suppl 1:S92-4.
388. Patel N, PO MM.; Orientation of neurite growth by extracellar electric fields. J Neurosci,1982,2**:** 483–496.
389. Patra C, Talukdar S, Novoyatleva T, Velagala SR, Mühlfeld C, Kundu B, Kundu SC, Engel FB. Silk protein fibroin from Antheraea mylitta for cardiac tissue engineering. Biomaterials. 2012, 33,9:2673-80.
390. Peramo A, Urbanchek MG, Spanninga SA, Povlich LK, Cederna P, Martin DC, In situ polymerization of a conductive polymer in acellular muscle tissue constructs. Tissue Eng Part A 2008;14;423-32.
391. Pereira JH, Bowden REM, Gattuso JM, Norris RW. Comparison of results of repair ofdigital nerves by denatured muscle grafts and end-to-end sutures. J Hand Surg,1991,16:519–23.
392. Pettersson, J., Kalbermatten, D., Mcgrath, A, Novikova, LN, Biodegradable fibrin conduit promotes long-term regeneration after peripheral nerve injury in adult rats. J. Plast. Reconstr. Aesthet. Surg, 2010, 63:1893–1899.
393. Pettikiriarachchi J, Parish C, Shoichet M. Biomaterials for Brain Tissue Engineering. *Aust J Chem.* 2010; 63:1143-1154.
394. Peyman GA, Koziol J, Kaiserman R. Iris tissue reaction to dacron and silk in primates: evaluation for intraocular lens fixation. Ophthalmic Surg. 1979, 10,1:69-75.
395. Pfister B. J., Gordon T., Loverde J. R., Kochar A. S., Mackinnon S. E., Cullen D.K, Biomedical engineering strategies for peripheral nerve repair: surgical applications, state of the art, and future challenges, Critical Reviews in Biomedical Engineering, 2011, 39, 2:81–124.
396. Pfister LA., Papaloızos M, Merkle HP, Gander B. Hydrogel nerve conduits produced from alginate/chitosan complexes. Journal of Biomedical Materials Research Part A, 2007,80,4:932–937.
397. Piantino J, Burdick JA, Goldberg D, Langer R, Benowitz LI. An injectable, biodegradable hydrogel for trophic factor delivery enhances axonal rewiring and improves performance after spinal cord injury. Exp Neurol, 2006, 201, 2:359-67.
398. Pillay S, Pillay V, Choonara YE, Naidoo D, Khan RA, du Toit LC, Ndesendo VM, Modi G, Danckwerts MP, Iyuke SE. Design, biometric simulation and optimization of

a nano-enabled scaffold device for enhanced delivery of dopamine to the brain. Int J Pharm. 2009,382,1-2:277-90.

399. Piotrowicz A, Shoichet MS. Nerve guidance channels as drug delivery vehicles," *Biomaterials*, 2006,27, 9:2018–2027.
400. Popescu MA, Toms SA. In vivo optical imaging using quantum dots for the management of brain tumors. Expert Rev Mol Diagn. 2006; 6,6:879-90.
401. Pöselt E, Schmidtke C, Fischer S, Peldschus K, Salamon J, Kloust H, Tran H, Pietsch A, Heine M, Adam G, Schumacher U, Wagener C, Förster S, Weller H. Tailor-made quantum dot and iron oxide based contrast agents for in vitro and in vivo tumor imaging, ACS Nano. 2012,6,4:3346-55.
402. Prabhakaran MP, Ghasemi-Mobarakeh L, Jin G, Ramakrishna S, Electrospun conducting polymer nanofibers and electrical stimulation of nerve stem cells. J Biosci Bioeng 2011;112;501-7.
403. Prabhakaran MP, Venugopal JR, Ramakrishna S. Mesenchymal stem cell differentiation to neuronal cells on electrospun nanofibrous substrates for nerve tissue engineering. Biomaterials. 2009; 30,28:4996-5003.
404. Priestley JV, Ramer MS, King VR, McMahon SB, Brown RA. Stimulating regeneration in the damaged spinal cord. J Physiol Paris. 2002,96(1-2):123-33.
405. Qian Y, Shen Y, Lu Z, Fan Z, Liu T, Zhang J, Zhang F. Biocompatibility of silk fibroin nanofibers scaffold with olfactory ensheathing cells. Zhongguo Xiu Fu Chong Jian Wai Ke Za Zhi. 2009, 23, 11:1365-70.
406. Qu, J.; Wang, D.; Wang, H.; Dong, Y.; Zhang, F.; Zuo, B.; Zhang, H. Electrospun silk fibroin nanofibers in different diameters support neurite outgrowth and promote astrocyte migration. J. Biomed. Mater. Res. A. 2013, 101, 2667-78.
407. Rabchevsky AG, Streit WJ. Grafting of cultured microglial cells into the lesioned spinal cord of adult rats enhances neurite outgrowth. J. Neurosci. Res 1997,47:34–48.
408. Ramer MS, Priestley JV, McMahon SB. Functional regeneration of sensory axons into the adult spinal cord. Nature. 2000,403,6767:312-6.
409. Ramón-Cueto A, Cordero MI, Santos-Benito FF, Avila J. Functional recovery of paraplegic rats and motor axon regeneration in their spinal cords by olfactory ensheathing glia, Neuron,2000,25,2:425-35.
410. Ramon-Cueto A, Plant GW, Avila J, Bunge MB.. Long-distance axonal regeneration in the transected adult rat spinal cord is promoted by olfactory ensheathing glia transplants. J. Neurosci. 1998,18:3803–15.

411. Rao, JW; Quan, DP; Peng, LM; Xie, GY; Xu, YB. The fabrication and characterization of linearly oriented lamellar-like multiple-channel silk fibroin nerve conduits. Biomedical Engineering-Applications Basis Communications. 2011, 23: 403-417.
412. Reddy KR, Sin BC, Yoo CH, Sohn D, Lee Y, Coating of multiwalled carbon nanotubes with polymer nanospheres through microemulsion polymerization, J Colloid Interface Sci 2009;340;160-5.
413. Ribble D., Goldstein NB., Norris D.A., Shellman YG., A simple technique for quantifying apoptosis in 96-well plates. BMC Biotechnol., 2005,5:12.
414. Rich KM, Alexander TD, Pryor JC, Hollowell JP. Nerve growth factor enhances regeneration through silicone chambers. Exp Neurol. 1989; 105,2:162-70.
415. Richardson-Burns SM, Hendricks JL, Foster B, Povlich LK, Kim DH, Martin DC. Polymerization of the conducting polymer poly(3,4-ethylenedioxythiophene) (PEDOT) around living neural cells. Biomaterials. 2007; 28, 8:1539-52.
416. Robinson R, Viviano SR, Criscione JM, Williams CA, Jun L, Tsai JC, Lavik EB. Nanospheres delivering the EGFR TKI AG1478 promote optic nerve regeneration: the role of size for intraocular drug delivery. ACS Nano. 2011,5,6:4392-400.
417. Rockwood DN, Preda RC, Yücel T, Wang X, Lovett ML, Kaplan DL, Materials fabrication from Bombyx mori silk fibroin. Nat. Protoc 2011;6;1612-31.
418. Roh DH, Kang SY, Kim JY, Kwon YB, Young Kweon H, Lee KG, Park YH, Baek RM, Heo CY, Choe J, Lee JH. Wound healing effect of silk fibroin/alginate-blended sponge in full thickness skin defect of rat. J Mater Sci Mater Med. 2006; 17,6:547-52.
419. Roman JA, Niedzielko TL, Haddon RC, Parpura V, Floyd CL. Single-walled carbon nanotubes chemically functionalized with polyethylene glycol promote tissue repair in a rat model of spinal cord injury. J Neurotrauma, 2011, 28,11:2349-62.
420. Romero MI, Rangappa N, Garry MG, Smith GM. Functional regeneration of chronically injured sensory afferents into adult spinal cord after neurotrophin gene therapy. J Neurosci. 2001,21,21:8408-16.
421. Rosson GD, Williams EH, Dellon AL. Motor nerve regeneration across a conduit. Microsurgery,2009,29:107–14.
422. Rosson GD, Williams EH, Dellon AL. Motor nerve regeneration across a conduit. Microsurgery 2009,29:107–14.
423. Rozenberg OA, Hanson KP, Alijakparov MT, Davidenkova EF, Zerbin EA. Diagnostic possibilities of the contrast medium verografin in liposomes (animal experiments Radiol Diagn (Berl). 1985, 26,2:285-92.
424. Runge MB, Dadsetan M, Baltrusaitis J, Knight AM, Ruesink T, Lazcano EA, Lu L, Windebank AJ, Yaszemski MJ. The development of electrically conductive

polycaprolactone fumaratepolypyrrole composite materials for nerve regeneration, Biomaterials, 2010, 31, 23:5916–5926.

425. Rupp A, Schmahl W, Lederer W, Matiasek K. Strain differences in the branching ofthe sciatic nerve in rats. Anat Histol Embryol 2007b; 36:202–8.
426. Saito R, Bringas JR, McKnight TR, Wendland MF, Mamot C, Drummond DC, Kirpotin DB, Park JW, Berger MS, Bankiewicz KS. Distribution of liposomes into brain and rat brain tumor models by convection-enhanced delivery monitored with magnetic resonance imaging. Cancer Res. 2004,64,7:2572-9.
427. Saito R, Krauze MT, Bringas JR, Noble C, McKnight TR, Jackson P, Wendland MF, Mamot C, Drummond DC, Kirpotin DB, Hong K, Berger MS, Park JW, Bankiewicz KS. Gadolinium-loaded liposomes allow for real-time magnetic resonance imaging of convection-enhanced delivery in the primate brain. Exp Neurol. 2005,196,2:381-9.
428. Saitow C, Kaplan DL, Castellot JJ Jr. Heparin stimulates elastogenesis: application to silk-based vascular grafts. Matrix Biol. 2011; 30,5-6:346-55.
429. Sakai Y, Matsuyama Y, Takahashi K, Sato T, Hattori T, Nakashima S, Ishiguro N. New artificial nerve conduits made with photo-crosslinked hyaluronic acid for peripheral nerve regeneration. Bio-Medical Materials and Engineering, 2007, 17, 3,:191–197.
430. Sakono M, Zako T, Maeda M. Naked-eye detection of amyloid aggregates using gold nanoparticles modified with amyloid beta antibody. Anal Sci. 2012,28,1:73.
431. Sameem M, Wood TJ, Bain JR, Asystematic review on the use of fibrin glue for peripheral nerve repair," Plastic and Reconstructive Surgery,2011,127,6:2381–2390.
432. Sanchez JG, Tsuchii A, Tokiwa Y. Degradation of polycaprolactone at 50 degrees C by a thermotolerant Aspergillus sp. Biotechnology Letters,2000,22:849–53.
433. Sanders EH, Kloefkorn R, Bowlin GL, Simpson DG, Wnek GE, Two-phase electrospinning from a single electrified jet: microencapsulation of aqueous reservoirs in poly (ethylene-co-vinyl acetate) fibers. Macromolecules 2003;36;3803–3805.
434. Sanghvi AB, Miller KP, Belcher AM, Schmidt CE. Biomaterials functionalization using a novel peptide that selectively binds to a conducting polymer. Nat Mater. 2005,4,6:496-502.
435. Schmalbruch H. Fiber composition of the rat sciatic nerve. Anat Rec 1986, 215:71–81.
436. Schmidt CE, Leach JB. Neural tissue engineering: strategies for repair and regeneration. Annual Review of Biomedical Engineering, 2003, 5:293–347.
437. Schmidt CE, Leach JB. Neural Tissue Engineering: Strategies for Repair and Regeneration. Annu. Rev. Biomed. Eng. 2003. 5:293–347.

438. Schneider A, Wang XY, Kaplan DL, Garlick JA, Egles C. Biofunctionalized electrospun silk mats as a topical bioactive dressing for accelerated wound healing. Acta Biomater. 2009; 5,7:2570-8.
439. Schültke E, Menk R, Pinzer B3, Astolfo A, Stampanoni M, Arfelli F, Harsan LA, Nikkhah G, Single-cell resolution in high-resolution synchrotron X-ray CT imaging with gold nanoparticles. J Synchrotron Radiat. 2014,21,Pt 1:242-50.
440. Schwendener, R.A. Liposomes as carriers for paramagnetic gadolinium chelates as organ specific contrast agents for magnetic resonance imaging, IMRIL J. Liposome Res., 1994,4:837-855.
441. Seal BL, Otero TC, Panitch A. Polymeric biomaterials for tissue and organ regeneration. Materials Science & Engineering R-Reports,2001,34:147–230.
442. Seddon H. J., The use of autogenous grafts for the repair of large gaps in peripheral nerves,The British Journal of Surgery,1947,35,138:151–167.
443. See EY, Toh SL, Goh JC. Simulated intervertebral disc-like assembly using bone marrow-derived mesenchymal stem cell sheets and silk scaffolds for annulus fibrosus regeneration. J Tissue Eng Regen Med. 2012; 6,7:528-35.
444. Sendtner M, Kreutzberg GW, Thoenen H. Ciliary neurotrophic factor prevents the degeneration of motor neurons after axotomy. Nature. 1990,345,6274:440-1.
445. Sexton KW., Pollins AC., Cardwell NL, Hydrophilic polymers enhance early functional outcomes after nerve autografting, Journal of Surgical Research, 2012, 177,2:392–400.
446. Shadforth AM, George KA, Kwan AS, Chirila TV, Harkin DG. The cultivation of human retinal pigment epithelial cells on Bombyx mori silk fibroin. Biomaterials. 2012, 33,16:4110-7.
447. Shen Y, Qian Y, Zhang H, Zuo B, Lu Z, Fan Z, Zhang P, Zhang F, Zhou C. Guidance of olfactory ensheathing cell growth and migration on electrospun silk fibroin scaffolds. Cell Transplant. 2010, 19,2:147-57.
448. Shi G, Rouabhia M, Wang Z, Dao LH, Zhang Z. A novel electrically conductive and biodegradable composite made of polypyrrole nanoparticles and polylactide. Biomaterials. 2004; 25,13:2477-88.
449. Shimamura T. Growth promotion of urothelial cells by a silk suture in the bladder walls of rats. Acta Pathol Jpn. 1987, 37,2:273-80.
450. Shin RH, Friedrich PF, Crum BA, Bishop AT, Shin AY. Treatment of a segmental nerve defect in the rat with use of bioabsorbable synthetic nerve conduits: a comparison of commercially available conduits. Journal of Bone and Joint Surgery-American Volume, 2009,91:2194–204.

451. Shoichet MS, Tate CC, Baumann MD, LaPlaca MC. Strategies for Regeneration and Repair in the Injured Central Nervous System. In: Reichert WM, editor. Indwelling Neural Implants: Strategies for Contending with the In Vivo Environment. Boca Raton (FL): CRC Press; 2008.
452. Siegel SG, Patton B, English AW. Ciliary neurotrophic factor is required for motoneuron sprouting. Exp Neurol. 2000; 166,2:205-12.
453. Siemionow M, Brzezicki G. Current techniques and concepts in peripheral nerverepair. Int Rev Neurobiol,2009,87:141–72.
454. Simon RH , Ho SY, D'Arrigo J, Wakefield A, Hamilton SG. Lipid-coated ultrastable microbubbles as a contrast agent in neurosonography. Invest Radiol. 1990,25,12:1300-4.
455. Simon RH, Ho SY, Perkins CR, D'Arrigo JS. Quantitative assessment of tumor-enhancement by ultrastable lipid-coated microbubbles as a sonographic contrast agent. Invest Radiol. 1992, 27, 1:29-34.
456. Sisken BF, Kanje M, Lundborg G, Herbst E, Kurtz W. Stimulation of rat sciatic nerve regeneration with pulsed electromagnetic fields. Brain Res. 1989, 485, 2:309-16.
457. Skaat H, Corem-Slakmon E, Grinberg I, Last D, Goez D, Mardor Y, Margel S. Antibody-conjugated, dual-modal, near-infrared fluorescent iron oxide nanoparticles for antiamyloidgenic activity and specific detection of amyloid-β fibrils. Int J Nanomedicine. 2013;8: 4063-76.
458. Skotheim TA, Reynolds JR. Handbook of Conducting Polymers, 3rd edn. CRC Press: Gainesville. 2007.
459. Soffer L, Wang X, Zhang X, Kluge J, Dorfmann L, Kaplan DL, Leisk G. Silk-based electrospun tubular scaffolds for tissue-engineered vascular grafts. J Biomater Sci Polym Ed. 2008,19,5:653-64.
460. Son YJ, Trachtenberg JT, Thompson WJ. Schwann cells induce and guide sprouting and reinnervation of neuromuscular junctions. Trends Neurosci 1996. 19:280– 85.
461. Sta M, Cappaert NL, Ramekers D, Baas F, Wadman WJ. The functional and morpho-logical characteristics of sciatic nerve degeneration and regeneration after crushinjury in rats. J Neurosci Methods, 2014,222:189–98.
462. Stammen JA, Williams S, Ku DN, Guldberg RE. Mechanical properties of a novel PVA hydrogel in shear and unconfined compression. Biomaterials,2001,22:799–806.
463. Stang F, Keilhoff G, Fansa H. Biocompatibility of different nerve tubes. Materials,2009;2:1480–507.
464. Stegemann JP, Kaszuba SN, Rowe SL. Review: advances in vascular tissue engineering using protein-based biomaterials. Tissue Eng. 2007, 13,11:2601-13.

465. Sterne GD, Brown RA, Green CJ, Terenghi G. Neurotrophin-3 delivered locally via fibronectin mats enhances peripheral nerve regeneration. Eur J Neurosci. 1997; 9, 7:1388-96.
466. Subramanian A, Krishnan UM, Sethuraman S. Development of biomaterial scaffold for nerve tissue engineering: Biomaterial mediated neural regeneration. J Biomed Sci. 2009;16:108.
467. Sugihara A, Sugiura K, Morita H, Ninagawa T, Tubouchi K, Tobe R, Izumiya M, Horio T, Abraham NG, Ikehara S. Promotive effects of a silk film on epidermal recovery from full-thickness skin wounds. Proc Soc Exp Biol Med. 2000; 225,1:58-64.
468. Sun C, Veiseh O, Gunn J, Fang C, Hansen S, Lee D, Sze R, Ellenbogen RG, Olson J, Zhang M. In vivo MRI detection of gliomas by chlorotoxin-conjugated superparamagnetic nanoprobes. Small, 2008,4,3:372-9.
469. Sun M, Gao Y, Guo C, Cao F, Song Z, Xi Y, Yu A, Li A, Zhai G, Enhancement of transport of curcumin to brain in mice by poly(n-butyl cyano-acrylate) nanoparticle. J Nanopart Res,2010,12:3111–3122.
470. Sunderland S., The function of nerve fibers whose structure has been disorganized, Anatomical Record, 1951,109,3:503–513.
471. Tabesh H, Amoabediny G, Nik NS, Heydari M, Yosefifard M, Siadat SOR, et al. The role of biodegradable engineered scaffolds seeded with Schwann cells for spinal cord regeneration. Neurochemistry International,2009,54:73–83.
472. Tang S, Zhu J, Xu Y, Xiang AP, Jiang MH, Quan D, The effects of gradients of nerve growth factor immobilized PCLA scaffolds on neurite outgrowth in vitro and peripheral nerve regeneration in rats. Biomaterials 2013;34;7086-7096.
473. Tang X, Xue C, Wang Y, Ding F, Yang Y, Gu X. Bridging peripheral nerve defects with a tissue engineered nerve graft composed of an in vitro cultured nerve equivalent and a silk fibroin-based scaffold. Biomaterials. 2012, 33, 15:3860-7.
474. Tang, B.; Tao, J.; Xua, S.; Wang, J.; Hurren, C.; Xu, W.; Sun, L.; Wang, X. Using hydroxy carboxylate to synthesize gold nanoparticles in heating and photochemical reactions and their application in textile colouration. Chemical Engineering J. 2011, 172, 601–7.
475. Taras JS, Nanavati V, Steelman P. Nerve conduits. Journal of Hand Therapy 2005;18:191–7.
476. Taras JS, Nanavati V, Steelman P. Nerve conduits. Journal of Hand Therapy,2005,18:191–7.
477. Temple CLF, Ross DC., Dunning CE, Johnson J.A., Resistance to disruption and gapping of peripheral nerve repairs: an in vitro biomechanical assessment of techniques, Journal of Reconstructive Microsurgery, 2004, 20, 8: 645–650.

478. Teng YD, Lavik EB, Qu X, Park KI, Ourednik J, Zurakowski D, Langer R, Snyder EY. Functional recovery following traumatic spinal cord injury mediated by a unique polymer scaffold seeded with neural stem cells. Proc Natl Acad Sci USA, 2002, 99,5:3024-9.
479. Thanos PK, Okajima S, Terzis JK. Ultrastructure and cellular biology of nerve regeneration. J. Reconstr. Microsurg. 1998, 14:423–36.
480. Theil EC., Ferritin: structure, gene regulation, and cellular function in animals, plants and microorganisms, Ann. Rev. Biochem. 1987, 56:289–315.
481. Thompson BC, Richardson RT, Moulton SE, Evans AJ, O'Leary S, Clark GM, Wallace GG, Conducting polymers, dual neurotrophins and pulsed electrical stimulation--dramatic effects on neurite outgrowth. J Control Release 2010;25;161-7.
482. Tierney CM, Haugh MG, Liedl J, Mulcahy F, Hayes B, O'Brien FJ. The effects of collagen concentration and crosslink density on the biological, structural and mechanical properties of collagen-GAG scaffolds for bone tissue engineering. *J Mech Behav Biomed Mater.* 2009;2(2):202-9.
483. Timnak A, Gharebaghi FY, Shariati RP, Bahrami SH, Javadian S, Emami Sh H, et al. Fabrication of nano-structured electrospun collagen scaffold intended for nerve tissue engineering. J Mater Sci Mater Med. 2011; 22,6:1555-67.
484. Tokuraku K, Marquardt M, Ikezu T. Real-time imaging and quantification of amyloid-beta peptide aggregates by novel quantum-dot nanoprobes. PLoS One. 2009,4,12:e8492.
485. Torchilin VP, Surface-modified liposomes in gamma- and MR-imaging, Advanced Drug Delivery Reviews 1997,24,2–3:301–313.
486. Torchilin VP. Liposomes as delivery agents for medical imaging. Mol Med Today, 1996, 2,6:242-9.
487. Tos P, Battiston B, Ciclamini D, Geuna S, Artiaco S. Primary repair of crush nerveinjuries by means of biological tubulization with muscle-vein-combined grafts.Microsurgery, 2012, 32:358–63.
488. Toth C, Martinez JA, Liu WQ, Diggle J, Guo GF, Ramji N, et al. Local erythro-poietin signaling enhances regeneration in peripheral axons. Neuroscience2008,154:767–83.
489. Triulzi RC, Dai Q, Zou J, Leblanc RM, Gu Q, Orbulescu J, Huo Q. Photothermal ablation of amyloid aggregates by gold nanoparticles. Colloids Surf B Biointerfaces. 2008,63,2:200-8.
490. Tsai EC, Dalton PD, Shoichet MS, Tator CH. Matrix inclusion within synthetic hydrogel guidance channels improves specific supraspinal and local axonal

regeneration after complete spinal cord transection. Biomaterials, 2006, 27, 3,519–533.

491. Tse R, Ko JH, Nerve glue for upper extremity reconstruction, Hand Clinics, 2012, 28,4: 529–540.
492. Tsukada S, Nakashima H, Torimitsu K, Conductive polymer combined silk fiber bundle for bioelectrical signal recording. PLoS One 2012;7;e33689.
493. Turski P , Kalinke T, Strother L, Perman W, Scott G, Kornguth S. Magnetic resonance imaging of rabbit brain after intracarotid injection of large multivesicular liposomes containing paramagnetic metals and DTPA. Magn Reson Med,1988,7,2:184-96.
494. Tuszynski MH, Gabriel K, Gage FH, Suhr S, Meyer S, et al.. Nerve growth factor delivery by gene transfer induces differential outgrowth of sensory, motor, and noradrenergic neurites after adult spinal cord injury. *Exp. Neurol.* 1996,137:157–73.
495. Tuszynski MH, Weidner N, McCormack M, Miller I, Powell H, et al.. Grafts of genetically modified Schwann cells to the spinal cord: survival, axon growth, and myelination. Cell Transplant. 1998; 7:187–96.
496. Tysseling-Mattiace VM1, Sahni V, Niece KL, Birch D, Czeisler C, Fehlings MG, Stupp SI, Kessler JA. Self-assembling nanofibers inhibit glial scar formation and promote axon elongation after spinal cord injury. J Neurosci. 2008, 28, 14:3814-23.
497. Udina E, Verdu´ E, Navarro X. Effects of the immunophilin ligand FK506 on nerve regeneration in collagen guides seeded with Schwann cells in rats. Neuroscience Letters,2004,357:99–102.
498. Unger RE, Ghanaati S, Orth C, Sartoris A, Barbeck M, Halstenberg S, Motta A, Migliaresi C, Kirkpatrick CJ. The rapid anastomosis between prevascularized networks on silk fibroin scaffolds generated in vitro with cocultures of human microvascular endothelial and osteoblast cells and the host vasculature. Biomaterials. 2010, 31,27:6959-67.
499. Unger RE, Peters K, Wolf M, Motta A, Migliaresi C, Kirkpatrick CJ. Endothelialization of a non-woven silk fibroin net for use in tissue engineering: growth and gene regulation of human endothelial cells. Biomaterials. 2004, 25,21:5137-46.
500. Utley DS, Lewin SL, Cheng ET, Verity AN, Sierra D, Terris DJ. Brain-derived neurotrophic factor and collagen tubulization enhance functional recovery after peripheral nerve transection and repair. Arch Otolaryngol Head Neck Surg. 1996;122,4:407-13.
501. Vaitkuviene A, Kaseta V, Voronovic J, Ramanauskaite G, Biziuleviciene G, Ramanaviciene A, Ramanavicius A, Evaluation of cytotoxicity of polypyrrole

nanoparticles synthesized by oxidative polymerization, J Hazard Mater 2013;250-25;167-74.

502. Valentini RF, Vargo TG, Gardella JA Jr, Aebischer P. Electrically charged polymeric substrates enhance nerve fibre outgrowth *in vivo*. Biomaterials, 1992, 13**:**183–190.
503. Varallyay P, Nesbit G, Muldoon LL, Nixon RR, Delashaw J, Cohen JI, Petrillo A, Rink D, Neuwelt EAComparison of two superparamagnetic viral-sized iron oxide particles ferumoxides and ferumoxtran-10 with a gadolinium chelate in imaging intracranial tumors. AJNR Am J Neuroradiol. 2002;23,4:510-9.
504. Varejão AS, Meek MF, Ferreira AJ, Patrício JA, Cabrita AM, Functional evaluation of peripheral nerve regeneration in the rat: walking track analysis. J Neurosci Methods 2001;108;1-9.
505. Varejão AS, Meek MF, Ferreira AJ, Patrício JA, Cabrita AM. Functional evaluationof peripheral nerve regeneration in the rat: walking track analysis. J NeurosciMethods 2001,15,108:1–9.
506. Varejão AS, Melo-Pinto P, Meek MF, Filipe VM, Bulas-Cruz J. Methods for the exper-imental functional assessment of rat sciatic nerve regeneration. Neurol Res, 2004a, 26:186–94.
507. Varejão ASP, Cabrita AM, Meek MF, Bulas-Cruz J, Melo-Pinto P, Raimondo S, et al.Functional and morphological assessment of a standardized rat sciatic nervecrush injury with a non-serrated clamp. J Neurotrauma, 2004 b,21:1652–70.
508. Vasita R, Katti DS. Nanofibers and their applications in tissue engineering. *Int J Nanomed* 2006;**1**(1):15-30.
509. Veiseh O, Sun C, Gunn J, Kohler N, Gabikian P, Lee D, Bhattarai N, Ellenbogen R, Sze R, Hallahan A, Olson J, Zhang M. Optical and MRI multifunctional nanoprobe for targeting gliomas. Nano Lett. 2005,5,6:1003-8.
510. Verdu E, Navarro X, Gudino-Cabrera G, Rodriguez FJ, Ceballos D.. Olfactory bulb ensheathing cells enhance peripheral nerve regeneration. Neuroreport 1999,10:1097–101.
511. Vindigni V, Cortivo R, Iacobellis L, Abatangelo G, Zavan B. Hyaluronan benzyl ester as a scaffold for tissue engineering. Int J Mol Sci. 2009;10,7:2972-85.
512. Vleggeert-Lankamp CL, de Ruiter GC, Wolfs JF, Pêgo AP, van den Berg RJ, Feirabend HK, Malessy MJ, Lakke EA. Pores in synthetic nerve conduits are beneficial to regeneration. J Biomed Mater Res A. 2007,80,4:965-82.
513. Wang A, Ao Q, Wei Y, Gong K, Liu X, Zhao N, Gong Y, Zhang X. Physical properties and biocompatibility of a porous chitosan-based fiber-reinforced conduit for nerve regeneration. Biotechnology Letters,2007,29,11:1697–1702.

514. Wang C, Liu D, Wang Z. Gold nanoparticle based dot-blot immunoassay for sensitively detecting Alzheimer's disease related β-amyloid peptide. Chem Commun (Camb). 2012,48,67:8392-4.
515. Wang CH, Dong YQ, Sengothi K, Tan KL, Kang ET. *In vivo* tissue response to polyaniline. Synthetic Metals, 1999, 102**:** 1313–1314.
516. Wang CY, Zhang KH, Fan CY, Mo XM, Ruan HJ, Li FF. Aligned natural-synthetic polyblend nanofibers for peripheral nerve regeneration. Acta Biomater. 2011, 7,2:634-43.
517. Wang CZ, Chen YJ, Wang YH, Yeh ML, Huang MH, Ho ML, et al. Low-level laserirradiation improves functional recovery and nerve regeneration in sciatic nervecrush rat injury model. Plos One, 2014, 9,8:e103348.
518. Wang DY, Huang YY. Fabricate coaxial stacked nerve conduits through soft lithography and molding processes. Journal of Biomedical Materials Research Part A, 2008, 85, 2:434–438.
519. Wang G, Hu X, Lin W, Dong C, Wu H. Electrospun PLGA-silk fibroin-collagen nanofibrous scaffolds for nerve tissue engineering. In Vitro Cell Dev Biol Anim. 2011,47,3:234-40.
520. Wang HY, Zhang YQ, Processing and characterisation of a novel electropolymerized silk fibroin hydrogel membrane. Sci Rep 2014;4;6182.
521. Wang J, Ye R, Wei Y, Wang H, Xu X, Zhang F, Qu J, Zuo B, Zhang H. The effects of electrospun TSF nanofiber diameter and alignment on neuronal differentiation of human embryonic stem cells. J Biomed Mater Res A. 2012, 100,3:632-45.
522. Wang S, Cai L, Polymers for Fabricating Nerve Conduits, International Journal of Polymer Science, 2010,138686:20
523. Wang S, Wan A, Xu X, Gao S, Mao H, Leong K, et al. A new nerve guide conduit material composed of a biodegradable poly(phosphoester). Biomaterials 2001;22:1157–69.
524. Wang S, Yaszemski MJ, Knight AM, Gruetzmacher JA, Windebank AJ, Lu L.. Photo-crosslinked poly(*ε*-caprolactone fumarate) networks for guided peripheral nerve regeneration: material properties and preliminary biological evaluations. Acta Biomaterialia,2009,5,5:1531–1542.
525. Wang S., Kempen DHR., de Ruiter GCW, Cai L, Spinner RJ, Windebank AJ, Yaszemski M J, Lu L. Molecularly Engineered Biodegradable Polymer Networks with a Wide Range of Stiffness for Bone and Peripheral Nerve Regeneration. Adv. Funct. Mater, 2015, 25: 2715–2724.

526. Wang S., Yaszemski MJ., Gruetzmacher JA., Lu L. Photo-crosslinked poly(ε-caprolactone fumarate) networks:roles of crystallinity and crosslinking density in determining mechanical properties. Polymer, 2008.49, 26:5692–5699.
527. Wang SD, Zhang YZ, Yin GB, Wang HW, Dong ZH. Fabrication of a composite vascular scaffold using electrospinning technology. Materials Science and Engineering C 2010,30: 670–676.
528. Wang W, Itoh S, Matsuda A, Aizawa T, Demura M, Ichinose S, Shinomiya K, Tanaka J. Enhanced nerve regeneration through a bilayered chitosan tube: the effect of introduction of glycine spacer into the CYIGSR sequence. Journal of Biomedical Materials Research Part A, 2008, 85,4:919–928.
529. Wang X, Gu X, Yuan C, Chen S, Zhang P, Zhang T, Yao J, Chen F, Chen G. Evaluation of biocompatibility of polypyrrole *in vitro* and *in vivo*. J Biomed Mater Res A 2004, 68A:411–422.
530. Wang X., Hu W., Cao Y., Yao J., Wu J, Gu X. Dog sciatic nerve regeneration across a 30-mm defect bridged by a chitosan/PGA artificial nerve graft. Brain, 2005, 128, 8:1897–1910.
531. Wang X., Zhang J., Chen H., Wang Q. Preparation and characterization of collagen-based composite conduit for peripheral nerve regeneration. Journal of Applied Polymer Science, 2009, 112, 6,3652–3662.
532. Wang Z, Zhang Y, Zhang J, Huang L, Liu J, Li Y, Zhang G, Kundu SC, Wang L, Exploring natural silk protein sericin for regenerative medicine: an injectable, photoluminescent, cell-adhesive 3D hydrogel. Sci Rep 2014;20;7064.
533. Wang, H. B.; Mullins, M. E.; Cregg, J. M.; McCarthy, C. W.; Gilbert, R. J. Varying the diameter of aligned electrospun fibers alters neurite outgrowth and Schwann cell migration. Acta Biomater. 2010, 6, 2970-978.
534. Wang, SD; Zhang, YZ; Yin, GB; Wang, HW; Dong, ZH. Electrospun Polylactide/Silk Fibroin-Gelatin Composite Tubular Scaffolds for Small-Diameter Tissue Engineering Blood Vessels. Journal of Applied Polymer Science. 2009, 113: 2675-2682.
535. Wang, Z., Zhang, Y, Zhang, J, Huang, L, Liu, J, Li, Y, Zhang, G, Kundu, SC., Wang, L, Exploring natural silk protein sericin for regenerative medicine: an injectable, photoluminescent, cell-adhesive 3D hydrogel. Sci Rep, 2014, 20,4,7064.
536. Wangensteen KJ, Kalliainen LK. Collagen tube conduits in peripheral nerve repair: a retrospective analysis. Hand (NY) 2009.
537. Weber RA, Breidenbach WC, Brown RE, Jabaley ME, Mass DP. A randomized prospective study of polyglycolic acid conduits for digital nerve reconstruction in humans. Plastic and Reconstructive Surgery,2000, 106:1036–45.

538. Webster TJ, Waid MC, McKenzie JL, Price RL, Ejiofo JU. Nano-biotechnology: carbon nanofibers as improved neural and orthopaedic implants. Nanotechnology, 2004, 15**:** 48–54.

539. Wei K, Kim BS, Kim IS, Fabrication and biocompatibility of electrospun silk biocomposites, Membranes (Basel). 2011,1:275–298.

540. Wei K, Li Y, Kim KO, Nakagawa Y, Kim BS, Abe K, Chen GQ, Kim IS. Fabrication of nano-hydroxyapatite on electrospun silk fibroin nanofiber and their effects in osteoblastic behavior. J Biomed Mater Res A. 2011; 97,3:272-80.

541. Wei Y, Gong K, Zheng Z, Wang A, Ao Q, Gong Y, Zhang X. Chitosan/silk fibroin-based tissue-engineered graft seeded with adipose-derived stem cells enhances nerve regeneration in a rat model. J Mater Sci Mater Med. 2011, 22,8:1947-64.

542. Wei Y, Hsueh KF, Thermal analysis of chemically synthesized polyaniline and effects of thermal aging on conductivity, J. Polym. Sci. Part A Polym. Chem. 1989,27:4351–4363.

543. Wei, M., Kang, B., Sung, C, Mead, J, Core-Sheath Structure in Electrospun Nanofibers from Polymer Blends. Macromol. Mater. Eng 2006, 291: 1307–1314.

544. Wen X, Tresco PA. Effect of filament diameter and extracellular matrix molecule precoating on neurite outgrowth and Schwann cell behavior on multifilament entubulation bridging device *in vitro*. Journal of Biomedical Materials Research Part A, 2006, 76, 3:626–637.

545. Wen X, Tresco PA. Fabrication and characterization of permeable degradable poly(DL-lactide-co-glycolide) (PLGA) hollow fiber phase inversion membranes for use as nerve tract guidance channels. Biomaterials. 2006,27,20:3800-9.

546. Wessling B, Handbook of Nanostructured Materials and Nanotechnology, Elsevier, 2000.

547. Widmer MS, Gupta PK, Lu L, Meszlenyi RK, Evans GR, Brandt K, Savel T, Gurlek A, Patrick CW Jr, Mikos AG. Manufacture of porous biodegradable polymer conduits by an extrusion process for guided tissue regeneration. Biomaterials. 1998,19,21:1945-55.

548. Willerth SM, Sakiyama-Elbert SE. Approaches to neural tissue engineering using scaffolds for drug delivery. Adv Drug Deliv Rev. 2007;59,4-5:325-38.

549. Williams DF, Definitions in Biomaterials, Proceedings of a Consensus Conference of the European Society for Biomaterials. Amsterdam: Elsevier, 2004.

550. Williams HB, A clinical pilot study to assess functional return following continuous muscle stimulation after nerve injury and repair in the upper extremity using a completely implantable electrical system, Microsurgery, 1996a, 17,11:597–605,.

551. Williams HB., The value of continuous electrical muscle stimulation using a completely implantable system in the preservation of muscle function following motor nerve injury and repair: an experimental study, Microsurgery, 1996 b, 17, 11, pp. 589–96.
552. Williams LR. Exogenous fibrin matrix precursors stimulate the temporal progress of nerve regeneration within a silicone chamber. Neurochemical Research, 1987,12,10:851–860.
553. Williams RL, Doherty PJ. A preliminary assessment of poly(pyrrole) in nerve guide studies, Journal of Materials Science: Materials in Medicine 1994;5;429-433.
554. Williams, LR, Longo, FM, Powell, HC, Lundborg, G. Varon, S. Spatial-temporal progress of peripheral nerve regeneration within a silicone chamber: parameters for a bioassay. J. Comp. Neurol. 1983, 218, 460–470.
555. Winter CG, Saotome Y, Levison SW, Hirsh D. A role for ciliary neurotrophic factor as an inducer of reactive gliosis, the glial response to central nervous system injury. Proc Natl Acad Sci U S A. 1995,92,13:5865-9.
556. Winter, J, Schmidt, C. Biomimetic strategies and applications in the nervous system. In Biomimetic materials and design (eds A. K. Dillow, A. M. Lowman), 2002, 375–415. Boca Raton, FL: CRC Press.
557. Wittmer CR, Claudepierre T, Reber M, Wiedemann P, Garlick JA, Kaplan D, Egles C. Multifunctionalized electrospun silk fibers promote axon regeneration in central nervous system. Adv Funct Mater. 2011, 21,22:4202.
558. Wolford LM, Stevao EL. Considerations in nerve repair. Proceedings (Baylor University Medical Center) 2003,16:152–6.
559. Wong JY, Langer R, Ingberi DE. Electrically conducting polymers can noninvasively control the shape and growth of mammalian cells. *Proc Natl Acad Sci USA,* 1994, 91**:** 3201–3204.
560. Wood M, Willits RK. Short-duration DC electrical stimulation increases chick embryo DRG neurite outgrowth. Bioelectromagnetics, 2006, 27**:** 328–331.
561. Woodruff MA, Hutmacher DW. The return of a forgotten polymer – polycaprolactone in the 21st century. Progress in Polymer Science, 2010; 35:1195–310.
562. Woods T, Gratzer PF. Effectiveness of three extraction techniques in the development of a decellularized bone–anterior cruciate ligament–bone graft. Biomaterials. 2005;26:7339–7349.
563. Wright MC, Mi R, Connor E, Reed N, Vyas A, Alspalter M, et al. Novel roles forosteopontin and clusterin in peripheral motor and sensory axon regeneration. JNeurosci,2014,34:1689–700.

564. Xia Y, Lu Y. Fabrication and properties of conductive conjugated polymers/silk fibroin composite fibers. Composites Science and Technology. 2008, 68:1471–1479.
565. Xiao L, Zhao D, Chan WH, Choi MM, Li HW. Inhibition of beta 1-40 amyloid fibrillation with N-acetyl-L-cysteine capped quantum dots. Biomaterials. 2010, 31,1:91-8.
566. Xie F, Qing FL., Gu B, Liu K, Guo XS. In vitro and in vivo evaluation of a biodegradable chitosan-PLA composite peripheral nerve guide conduit material. Microsurgery, 2008, 28,6:471–479,.
567. Xie J, Wang CH. Electrospun micro- and nanofibers for sustained delivery of paclitaxel to treat C6 glioma in vitro. Pharm Res. 2006, 23, 8:1817-26.
568. Xin H, Sha X, Jiang X, Zhang W, Chen L, Fang X. Anti-glioblastoma efficacy and safety of paclitaxel-loading Angiopep-conjugated dual targeting PEG-PCL nanoparticles. Biomaterials. 2012; 33,32:8167-76.
569. Xu X., Zhuang X., Chen X., Wang X., Yang L, Jing X, Preparation of Core-Sheath Composite Nanofibers by Emulsion Electrospinning. Macromol. Rapid Commun 2006;27;1637–1642.
570. Yamasaki T, Fujiwara H, Oda R, Mikami Y, Ikeda T, Nagae M, et al. In vivo evaluation of rabbit sciatic nerve regeneration with diffusion tensor imaging (DTI): correlations with histology and behavior. Magn Reson Imaging 2015; 33:95–101.
571. Yan H, Zhang F, Chen MB, Lineaweaver WC. Conduit luminal additives for peripheral nerve repair. International Review of Neurobiology, 2009,87:199–225.
572. Yan LP, Oliveira JM, Oliveira AL, Caridade SG, Mano JF, Reis RL. Macro/microporous silk fibroin scaffolds with potential for articular cartilage and meniscus tissue engineering applications. Acta Biomater. 2012, 8,1:289-301.
573. Yan Q, Elliott J, Snider WD. Brain-derived neurotrophic factor rescues spinal motor neurons from axotomy-induced cell death. Nature. 1992,360,6406:753-5.
574. Yang F, Murugan R, Wang S, Ramakrishna S. Electrospinning of nano/micro scale poly(L-lactic acid) aligned fibers and their potential in neural tissue engineering. Biomaterials. 2005; 26,15:2603-10.
575. Yang JA, Johnson BJ, Wu S, Woods WS, George JM, Murphy CJ. Study of wild-type α-synuclein binding and orientation on gold nanoparticles Langmuir, 2013, 29,14:4603-15.
576. Yang JA, Lin W, Woods WS, George JM, Murphy CJ. α-Synuclein's adsorption, conformation, and orientation on cationic gold nanoparticle surfaces seeds global conformation change. J Phys Chem B. 2014, 118,13:3559-71.
577. Yang MC, Chi NH, Chou NK, Huang YY, Chung TW, Chang YL, Liu HC, Shieh MJ, Wang SS. The influence of rat mesenchymal stem cell CD44 surface markers on cell

growth, fibronectin expression, and cardiomyogenic differentiation on silk fibroin - Hyaluronic acid cardiac patches. Biomaterials. 2010, 31,5:854-62.

578. Yang MC, Wang SS, Chou NK, Chi NH, Huang YY, Chang YL, Shieh MJ, Chung TW. The cardiomyogenic differentiation of rat mesenchymal stem cells on silk fibroin-polysaccharide cardiac patches in vitro. Biomaterials. 2009, 30,22:3757-65.
579. Yang Y, Chen X, Ding F, Zhang P, Liu J, Gu X. Biocompatibility evaluation of silk fibroin with peripheral nerve tissues and cells in vitro. Biomaterials. 2007, 28,9:1643-52.
580. Yang Y, Ding F, Wu J, Hu W, Liu W, Liu J, Gu X. Development and evaluation of silk fibroin-based nerve grafts used for peripheral nerve regeneration. Biomaterials. 2007, 28,36:5526-35.
581. Yang Y, Yuan X, Ding F, Yao D, Gu Y, Liu J, Gu X. Repair of rat sciatic nerve gap by a silk fibroin-based scaffold added with bone marrow mesenchymal stem cells. Tissue Eng Part A. 2011, 17,17-18:2231-44.
582. Yang Y, Zhao Y, Gu Y, Yan X, Liu J, Ding F, Gu X. Degradation behaviors of nerve guidance conduits made up of silk fibroin in vitro and in vivo. Polymer Degradation and Stability. 2009, 94:2213–2220.
583. Yao L, de Ruiter GC, Wang H, Knight AM, Spinner RJ, Yaszemski MJ, Windebank AJ, Pandit A. Controlling dispersion of axonal regeneration using a multichannel collagen nerve conduit. Biomaterials, 2010, 31,22:5789–5797.
584. Yin D., Wang X., Yan Y, Zhang R. Preliminary studies on peripheral nerve regeneration using a new polyurethane conduit. Journal of Bioactive and Compatible Polymers, 2007,22, 2:143–159.
585. Yin Q, Kemp GJ, Frostick SP.. Neurotrophins, neurones and peripheral nerve regeneration. *J. Hand Surg. [Br.]* 1998,23:433–37
586. Yiu G, He Z. Glial inhibition of CNS axon regeneration. Nat Rev Neurosci. 2006,7,8:617-27.
587. Yoo CR, Yeo IS, Park KE, Park JH, Lee SJ, Park WH, Min BM. Effect of chitin/silk fibroin nanofibrous bicomponent structures on interaction with human epidermal keratinocytes. Int J Biol Macromol. 2008, 42,4:324-34.
588. Yoo JJ, Meng J, Oberpenning F, et al. Bladder augmentation using allogenic bladder submucosa seeded with cells. Urology. 1998;51:221–225.
589. Youn J, Won N, Kim S, Choi JH, Near-Infrared Quantum Dots Imaging in the Mouse Brain, Biomedical Optics, St. Petersburg, Florida United States, March 16-19, 2008, BIOMED Poster Session I (BSuE), http://dx.doi.org/10.1364/BIOMED.2008.BSuE2
590. Young RC, Wiberg M, Terenghi G. Poly-3-hydroxybutyrate (PHB): a resorbable conduit for long-gap repair in peripheral nerves. Br J Plast Surg. 2002; 55,3:235-40.

591. Yu W, Jiang X, Cai M, Zhao W, Ye D, Zhou Y, Zhu C, Zhang X, Lu X, Zhang Z, A novel electrospun nerve conduit enhanced by carbon nanotubes for peripheral nerve regeneration. Nanotechnology 2014;25;165102.
592. Yu, W.; Zhao, W.; Zhu, C.; Zhang, X.; Ye, D.; Zhang, W.; Zhou, Y.; Jiang, X.; Zhang, Z. Sciatic nerve regeneration in rats by a promising electrospun collagen/poly(ε-caprolactone) nerve conduit with tailored degradation rate. BMC Neurosci. 2011, 12, 68.
593. Yucel D, Kose GT, Hasirci V. Polyester based nerve guidance conduit design. Biomaterials. 2010; 31, 7:1596-603.
594. Yue HY, Huang S, Chang J, Heo C, Yao F, Adhikari S, Gunes F, Liu LC, Lee TH, Oh ES, Li B, Zhang JJ, Huy TQ, Luan NV, Lee YH. ZnO nanowire arrays on 3D hierachical graphene foam: biomarker detection of Parkinson's disease. ACS Nano. 2014,8,2:1639-46.
595. Yue K, Guduru R, Hong J, Liang P, Nair M, Khizroev S. Magneto-electric nano-particles for non-invasive brain stimulation. PLoS One. 2012,7,9:e44040.
596. Yuen D, Jenssen J, Rodriguez G. A semipermeable, kink resistant type I collagen-based nerve guide for PNS repair. Transactions of the Society for Biomaterials,2003:228.
597. Yukawa H, Tsukamoto R, Kano A, Okamoto Y, Tokeshi M, et al. Quantum Dots Conjugated with Transferrin for Brain Tumor Cell Imaging. J Cell Sci Ther,2013,4: 150. doi: 10.4172/2157-7013.1000150
598. Zhang B, Sun X, Mei H, Wang Y, Liao Z, Chen J, Zhang Q, Hu Y, Pang Z, Jiang X. LDLR-mediated peptide-22-conjugated nanoparticles for dual-targeting therapy of brain glioma. Biomaterials. 2013,34,36:9171-82.
599. Zhang C, Wan X, Zheng X, Shao X, Liu Q, Zhang Q, Qian Y. Dual-functional nanoparticles targeting amyloid plaques in the brains of Alzheimer's disease mice. Biomaterials. 2014; 35,1:456-65.
600. Zhang J, Qiu K, Sun B, Fang J, Zhang K, El-Hamshary H, Al-Deyabd S, Mo X, The aligned core–sheath nanofibers with electrical conductivity for neural tissue engineering, J. Mater. Chem. B 2014;2;7945-7954.
601. Zhang K, Wang H, Huang C, Su Y, Mo X, Ikada Y. Fabrication of silk fibroin blended P(LLA-CL) nanofibrous scaffolds for tissue engineering. J Biomed Mater Res A. 2010, 93,3:984-93.
602. Zhang L, Waterhouse GIN, Zhang L, Coaxially Aligned Polyaniline Nanofibers Doped with 3-Thiopheneacetic Acid through Interfacial Polymerization. Journal of Nanomaterials 2011;7;1-7.

603. Zhang Q, Yan Y, Li S, Feng T. The synthesis and characterization of a novel biodegradable and electroactive polyphosphazene for nerve regeneration. *Mater Sci Eng C,* 2010, 30**:** 160–166.

604. Zhang Q, Zhao Y, Yan S, Yang Y, Zhao H, Li M, Lu S, Kaplan DL. Preparation of uniaxial multichannel silk fibroin scaffolds for guiding primary neurons. Acta Biomater. 2012, 8,7:2628-38.

605. Zhang S. Fabrication of novel biomaterials through molecular self-assembly. Nat Biotechnol, 2003, 21, 10:1171-8.

606. Zhang X, Baughman CB, Kaplan DL. In vitro evaluation of electrospun silk fibroin scaffolds for vascular cell growth. Biomaterials. 2008, 29,14:2217-27.

607. Zhang X, Wang X, Keshav V, Wang X, Johanas JT, Leisk GG, Kaplan DL. Dynamic culture conditions to generate silk-based tissue-engineered vascular grafts. Biomaterials. 2009, 30,19:3213-23.

608. Zhang Y, Zhou P, Pan LF, Xie SZ, Sun M, Li WT. Growth of Human Smooth Muscle Cells on the Silk Fibroin Modified-Polyhydroxyalkanoate Scaffold. Acta Chim. Sinica. 2007,65,24:2935-2940.

609. Zhao, HJ. Prediction of Mechanical Properties of Braided Silk Fibroin Tubes for Small Diameter Vascular Scaffolds: A Preliminary Study. International Journal Of Nonlinear Sciences And Numerical Simulation. 2010, 11 S: 317-319.

610. Zhou J, Cao C, Ma X, Lin J. Electrospinning of silk fibroin and collagen for vascular tissue engineering Int J Biol Macromol. 2010,47,4:514-9.

611. Zou XH, Zhi YL, Chen X, Jin HM, Wang LL, Jiang YZ, Yin Z, Ouyang HW. Mesenchymal stem cell seeded knitted silk sling for the treatment of stress urinary incontinence. Biomaterials. 2010, 31,18:4872-9.

List of Publications

Book contents Chapter contents

Search this book

Front matter
Copyright
Contributor contact details
Woodhead Publishing Series in Biomat...
Foreword
Part I: Fundamentals, processing and types of silk biomaterials
1 - Introduction to silk biomaterials
2 - Applications of silk biomaterials in tissue engineering and regenerative medicine
3 - Processing of *Bombyx mori* silk f...
4 - Silk nanostructures based on nat...
5 - Electrospun silk sericin nanofiber...
6 - Silk fibroin microfiber and nanofi...
7 - Silk powder for regenerative me...
Part II: Properties and behaviour of sil...
Part III: Tissue engineering, regenerati...
Index

Silk Biomaterials for Tissue Engineering and Regenerative Medicine

2014, Pages 41–77

2 – Applications of silk biomaterials in tissue engineering and regenerative medicine

S. Das, U. Bora

B.B. Borthakur

Show more

doi:10.1533/9780857097064.1.41

Abstract:

The historical roots of the use of silk in medicine can be traced to its application long ago as surgical sutures. In the last decade, extensive biological, mechanical and physico-chemical studies have projected silk fiber as an exciting biomaterial for fabricating scaffolds. This chapter discusses in detail the application of silk based scaffolds in engineering hard and soft neotissue as well as organ-specific tissue. The chapter concludes by identifying the potential obstacles holding back the clinical translation of silk based tissue engineered products and the aspects of silk technology worth exploring in future.

Key words

silk; biomaterial; neotissue; tissue engineering; scaffold; fibroin; sericin

Biomaterials 62 (2015) 66–75

Contents lists available at ScienceDirect

Biomaterials

journal homepage: www.elsevier.com/locate/biomaterials

In vivo studies of silk based gold nano-composite conduits for functional peripheral nerve regeneration

Suradip Das [a], Manav Sharma [a], Dhiren Saharia [b], Kushal Konwar Sarma [c], Monalisa Goswami Sarma [d], Bibhuti Bhusan Borthakur [e, f], Utpal Bora [a, f, *]

[a] Department of Biosciences and Bioengineering, Indian Institute of Technology Guwahati, Guwahati 781039, Assam, India
[b] Saharia's Path Lab & Blood Bank, Guwahati 781005, Assam, India
[c] Department of Surgery and Radiology, College of Veterinary Sciences, Khanapara, Guwahati 781022, Assam, India
[d] Nemcare Hospital, Guwahati 781005, Assam, India
[e] Department of Surgical Oncology, Dr. B. Borooah Cancer Institute, Gopinathnagar, Guwahati 781016, Assam, India
[f] Mugagen Laboratories Private Limited, Technology Incubation Centre, Indian Institute of Technology Guwahati, Guwahati 781039, Assam, India

ARTICLE INFO

Article history:
Received 15 February 2015
Received in revised form
19 April 2015
Accepted 30 April 2015
Available online 27 May 2015

Keywords:
Nanocomposite
Nerve conduit
Gold nanoparticle
Silk fibroin
Peripheral nerve
Regeneration

ABSTRACT

We report a novel silk-gold nanocomposite based nerve conduit successfully tested in a neurotmesis grade sciatic nerve injury model in rats over a period of eighteen months. The conduit was fabricated by adsorbing gold nanoparticles onto silk fibres and transforming them into a nanocomposite sheet by electrospinning which is finally given a tubular structure by rolling on a stainless steel mandrel of chosen diameter. The conduits were found to promote adhesion and proliferation of Schwann cells in vitro and did not elicit any toxic or immunogenic responses *in vivo*. We also report for the first time, the monitoring of muscular regeneration post nerve conduit implantation by recording motor unit potentials (MUPs) through needle electromyogram. Pre-seeding the conduits with Schwann cells enhanced myelination of the regenerated tissue. Histo-morphometric and electrophysiological studies proved that the nanocomposite based conduits pre-seeded with Schwann cells performed best in terms of structural and functional regeneration of severed sciatic nerves. The near normal values of nerve conduction velocity (50 m/sec), compound muscle action potential (29.7 mV) and motor unit potential (133 μV) exhibited by the animals implanted with Schwann cell loaded nerve conduits in the present study are superior to those observed in previous reports with synthetic materials as well as collagen based nerve conduits. Animals in this group were also able to perform complex locomotory activities like stretching and jumping with excellent sciatic function index (SFI) and led a normal life.

1. Introduction

Damage of peripheral nerve results from traumatic injuries caused by accidents, physical conflict as well as during surgical intervention. Peripheral nerve injuries are primarily characterised by flaccid atrophy of surrounding muscles leading to partial or complete paralysis. Seddon had classified neurotmesis as the most severe form of peripheral nerve injury where the nerve is completely severed with limited chance of axon re-growth making surgical intervention essential. Neurotmesis grade injuries with a gap larger than 5 mm rarely show complete axonal reconnection and functional regeneration [1]. Surgical intervention in large nerve gaps generally involves grafting a part of nerve harvested from a healthy area into the damaged area. Although autografts remain the clinical gold standard for repairing large nerve gaps, the technique is largely fraught with donor site morbidity in the secondary surgical site and inefficient functional regeneration. While many studies have shown autografts to be superior to the available conduits there have been reports indicating an increased growth of nociceptive fibres along autografts which result in high autotomy among animals [2,3]. An alternative approach to nerve autograft is entubulation of nerve gaps using nerve conduits or nerve guides made of synthetic or natural polymers.

In the present study, silk fibroin nanofibers mats have been used to fabricate functional nerve conduits, exploiting the

* Corresponding author. Department of Biosciences and Bioengineering, Indian Institute of Technology Guwahati, Guwahati 781039, Assam, India.
E-mail addresses: ubora@iitg.ernet.in, ubora@rediffmail.com (U. Bora).

http://dx.doi.org/10.1016/j.biomaterials.2015.04.047
0142-9612/
TH-1468_10610612

biocompatibility and bio-mimetic properties of silk fibroin protein. Silk fibroin films functionalized with nerve growth factor (NGF) promotes neurite outgrowth and modulates functional properties of dorsal root ganglion (DRG) neurons [4]. Functionalization of silk fibroin based nerve guidance conduits with NGF and glial-derived nerve factor (GDNF) has been reported to enhance functional recovery of injured peripheral nerves [5,6]. Moreover, the incorporation of electrospun silk fibroin nanofibers within the lumen of the conduit was found to provide topographical guidance to the regenerating axons by directing neurite outgrowth and Schwann cell migration [7–9].

Electrically active silk scaffolds based on carbon nanotube (CNT) have been explored to facilitate signal transmission across a nerve gap through the conduit. Such conduits can easily interface with neuronal circuits, synapses and facilitate conduction of nerve impulse thereby promoting neural regeneration [9]. Silk-single walled carbon nanotubes (SWCNT) based composite conduit was also found to promote neural regeneration when implanted across a 10 mm sciatic nerve injury model [10]. The present study demonstrates the fabrication of nanocomposite comprising of gold nanoparticle-silk fibroin nanofiber (GNP-SF) which appreciably decreases the resistance of an electrically insulating material like silk thereby making the scaffold more suitable for neural tissue engineering applications.

2. Materials and methods

2.1. Fabrication and characterization of nanocomposite mat

Bombyx mori silk cocoons were purchased from local market in Guwahati, Assam. Degumming of cocoons was done by standard protocol reported earlier [11]. The degummed silk fibroin fibres were rinsed thoroughly with distilled water and dried at 50 °C overnight. Gold nanoparticles (GNP) were synthesized following a method reported earlier by our laboratory and were stored at 4 °C [12]. Degummed silk fibroin fibres (1 g) were kept submerged in the GNP solution (100 ml) and stirred at room temperature for 10 min until most of the particles were adsorbed onto the silk fibroin fibres. Both the pristine silk fibroin and the GNP incorporated silk fibres were dissolved in a chaotropic solvent (e.g Lithium bromide) and subsequently dialysed against distilled water and finally freeze dried as per standard procedures [13]. The freeze dried powder of pristine and GNP incorporated silk fibroin protein were separately dissolved in formic acid (98% pure) at a concentration of 100 mg of protein/ml along with 1 mg/ml of polyethylene oxide (PEO). The mixture was electrospun using an electrospinning machine (Make – Physics Equipment Company; Model – ESPIN-NANO) to form silk fibroin nanofibrous scaffold (SF) and gold nanoparticle-silk fibroin nanocomposite (GNP-SF) following standard procedures [11].

The uptake of GNPs by the degummed silk fibres was monitored by UV–Visible Spectrometer. The GNP incorporated silk fibres as well as the pristine degummed silk fibres were visualised under transmission electron microscope (TEM). The electrospun nanocomposite mat was dried overnight and scraped before X-Ray Diffraction studies. The mats were further viewed under Field Emission Electron Microscope (FESEM) to study the architecture of the nanofibers. Energy dispersive X-ray analysis (EDAX) was also performed on multiple locations over the nanocomposite mat to check for the presence of gold (Au). For electrical conductivity measurements the electrospun mats were placed on aluminium coated corning glass and adhered with silver paste [23].

2.2. Fabrication of nerve conduit and pre-seeding with Schwann cells

Immediately after electrospinning, the nanofibrous mat (made either of GNP-SF or SF) was slowly peeled off the aluminium sheet and rolled onto a stainless steel needle and pressed together so that each layer adhere to one another (Fig. 1D). The rolled conduits were sterilized by treatment with methanol followed by UV exposure. All fabricated conduits were washed with sterile phosphate buffered saline (PBS), pH = 7.4 to remove residues of methanol. Conduits were then conditioned by keeping in Dulbecco's Modified Eagle's Medium (DMEM) with 10% Foetal Bovine Serum (FBS) in CO_2 incubator for 24 h. Conduits were washed again with sterile PBS following UV sterilisation before implantation in rat.

For preparation of cell loaded conduit the same was seeded with SCTM 41 (rat Schwann cell) and incubated for five days with regular replacement of media. These conduits were also washed 3–4 times with sterile PBS before implantation.

2.3. Surgical implantation of nerve conduits

Clinically healthy sub-adult (12weeks) Sprague Dawley rats with average body weight of 250 g considered for the study were procured from authorized supplier and were housed under good managerial condition under veterinary supervision following CPCSEA, India and Institutional Animal Ethical Committee (IAEC) guidelines at College of Veterinary Sciences, AAU, Khanapara, Assam (approved vide CPCSEA, India letter no: 770/ac/CPCSEA/FVSc/AAU/IAEC/11-12/116 dated 27.03.2012). An outline of the surgical procedure performed is depicted in the data article [23].

All animals were anaesthetized using Ketamine (50–100 mg/kg bwt, i/p) and Xylazine (5 mg/kg bwt, i/p) after Atropine (0.05 mg/kg bwt, i/p) as pre-anaesthetics. The region below the hip joint was prepared for surgery and an incision was made on the right leg covering the upper thigh and lower gluteal region to expose the sciatic nerve. 10 mm length of sciatic nerve was transected out before it branches to fibular, tibial and sural nerve. The nerve gap was left untreated in the control group. In other groups conduit was sutured to both proximal and distal end of the nerve stumps by 7-0 polypropylene suture (Ethicon). Surgical wound was closed with 6-0 black braided silk suture (Ethicon). Post operatively antibiotic and NSAID were followed for seven days with regular dressing and antiseptic spray. Suture was removed on tenth day. The implantation of all the conduits was evaluated by magnetic resonance imaging (MRI) of the operated leg one week after implantation [23]. The details of all the groups maintained are delineated in Table 1.

2.4. Functional analysis of regenerated sciatic nerve

The functional regeneration of sciatic nerve was monitored by electrophysiological studies and walking track analysis. The electrophysiological studies were conducted using an electromyogram (EMG) machine (Make – Nicolet Model- Viking Quest). Animals were chemically restrained using sedative dose of Xylazine (1 mg/kg body wt) and Ketamine (100 mg/kg body wt) and placed on ventral recumbency over a wooden table. Area concerned was shaved and disinfected before recording. Grounding electrode was attached to the base of tail as shown in the data article [23].

For recording nerve conduction velocity (NCV) and compound muscle action potential (CMAP), percutaneous stimulation of sciatic nerve with bipolar electrode was done first at the proximal end of the implanted conduit at the level of hip joint and second distal stimulation point was at level of popliteal fossa. Distance between the two points was measured for calculating NCV.

Motor unit potentials (MUPs) were recorded by inserting a

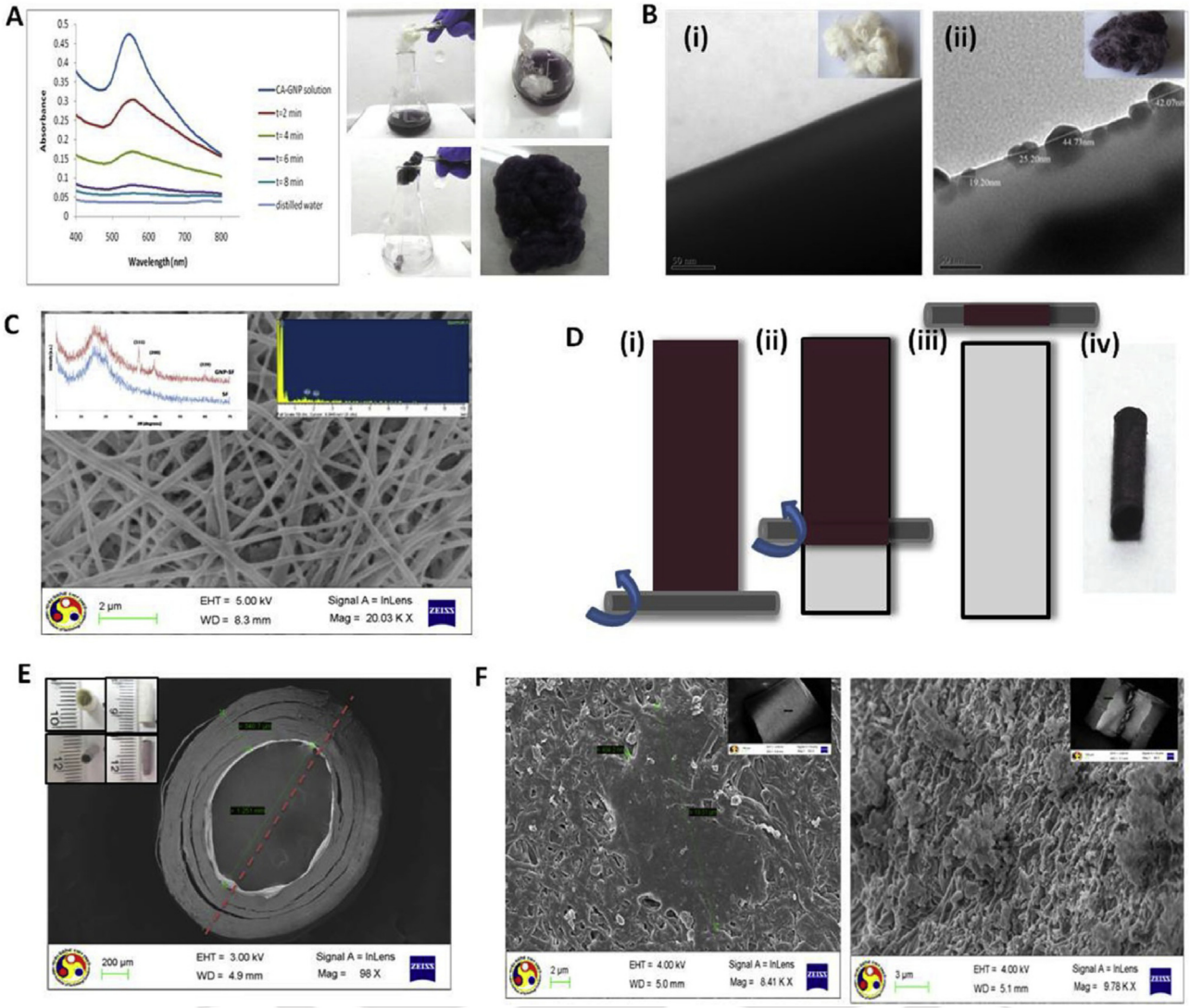

Fig. 1. Fabrication and characterization of pre-seeded nanocomposite conduits. A, Adsorption of gold nanoparticles by degummed silk fibroin fibres and subsequent colouration of silk fibres with concomitant decrease in intensity of 540 nm peak as recorded by UV-VIS spectrometer. B, TEM micrographs of (i) pristine degummed silk fibres and (ii) gold nanoparticle-silk fibroin composite. C, FESEM image of gold nanoparticle-silk fibroin nanocomposite nanofibers without gold sputter coating of the sample. Scale bar 2 μm. The nanocomposite formation was confirmed by XRD and EDAX analysis (inset). D, Fabrication of nerve conduits by novel sheet rolling method. The electrospun sheet was peeled off and rolled on a stainless steel mandrel of specific dimensions (i–iii) to form a nerve conduit (iv). E, Cross-sectional view of a typical nerve conduit as observed under FESEM. Scale bar 200 μm. Digital photographs of silk fibroin (white) and gold nanoparticle-silk fibroin nanocomposite nerve conduit (purple) prepared for implantation in rat (inset). F, Culturing Schwann cells (SCTM41) on nerve conduits with the gross pictures of conduit portions in the inset. Cells were found to adhere and proliferate on the outer (left) as well as on the inner surface (right) of the nerve conduits. (For interpretation of the references to colour in this figure legend, the reader is referred to the web version of this article.)

bipolar needle electrode into the gastrocnemius muscle. Sensory stimulus was provided by interdigital pinch.

For walking track analysis a blank white paper was placed on a walking track of 16 inch length and 3 inch breadth for obtaining the foot prints. The hind limbs of the animals were painted with methylene blue and they were allowed to walk through the track. Subsequently Sciatic Functional Index (SFI) was calculated using the following formula.

$$SFI = -38.3\left(\frac{EPL - NPL}{NPL}\right) + 109.5\left(\frac{ETS - NTS}{NTS}\right) + 13.3\left(\frac{EITS - NITS}{NITS}\right) - 8.8$$

where,

Table 1
Outline of animal groups maintained.

Groups	Name	Number of animals	Description
1	Control	8	10 mm nerve gap was created and left without treatment.
2	SF	8	10 mm nerve gap was created and gap was filled up with SF Plain conduit.
3	SF cell	8	10 mm nerve gap was created and gap was filled up with SF conduit seeded with Rat Schwann Cell.
4	GNP-SF	8	10 mm nerve gap was created and gap was filled up with GNP Plain conduit.
5	GNP-SF cell	8	10 mm nerve gap was created and gap was filled up with GNP conduit seeded with Rat Schwann Cell.

EPL – Experimental print length
NPL – Normal print length
ETS –Experimental toe spread
NTS – Normal toe spread
EITS – Experimental inter toe spread
NITS – Normal inter toe spread

2.5. Morphological analysis of regenerated sciatic nerve

Samples for histological analysis were collected in 10% neutral buffer formalin (Make-Sigma Aldrich) at an interval of nine and eighteen months after surgery by euthanizing the animal with intravenous over dose of Thiopentone sodium. Conduit was isolated and processed for Haematoxylin & Eosin (H&E) staining and cross sectional images were taken at 400× magnification. For TEM studies, cross-sections of the regenerated nerve after 18 months were stained with osmium tetra-oxide and processed by standard protocol.

3. Results

3.1. Fabrication and characterization of nanocomposite mat

The rapid discolouration of the gold nanoparticle (GNP) solution was found to be accompanied by purple colouration of the degummed silk fibroin fibres with a concomitant decrease in peak intensity at 540 nm of visible spectra (Fig. 1A). We observed that the GNPs were impregnated along the surface as well as inside the silk fibroin fibres (Fig. 1B). The electrospun silk fibroin nanofibers had diameters in the range of 100 nm–200 nm and pores of size 1000–1300 nm whereas diameters of the nanocomposite nanofibers were mostly in the range of 200 nm–300 nm with pores predominantly in the range of 700–1000 nm as evident from FESEM analysis [23]. Elemental analysis by EDAX revealed the presence of gold (Au) upto a concentration of 1.71% by weight of the nanocomposite mat (Fig. 1C). XRD analysis of the electrospun nanocomposite scaffolds showed sharp peaks around $2\theta = 38.5$, 44.5 and 64.95° and a broader peak around $2\theta = 21°$ (Fig. 1C). The I–V characteristic obtained for GNP-SF nanofibers was found to be mostly ohmic. Electrical resistance of the nanocomposite scaffolds, calculated from the slope of the I–V curve was found to be $0.48 \times 10^9\Omega$ for GNP-SF nanofibers [23] as compared to $12 \times 10^9\Omega$ (graph not shown) for silk fibroin nanofibers.

3.2. Morphology of nerve conduits and Schwann cell adhesion and proliferation

FESEM images showed that the fabricated conduits had an internal diameter of 1.25 mm and a wall thickness of 0.34 mm with a lamellar architecture comprising multiple layers of nanofibers (Fig. 1E). Electron microscopic observations of conduits cultured with rat Schwann cell line (SCTM41) showed adherence of cells, formation of cell clusters and growth of cells in three dimensions on both inner and outer surface of GNP-SF as well as SF conduits (Fig. 1F).

3.3. Surgical implantation of nerve conduits

The dimensions of the conduits were found to be suitable for implantation in a rat sciatic nerve. The texture and strength of the conduits were also appropriate and could withstand the implantation and suturing process without any deformation. The MRI image of the thigh region post implantation reveals accurate implantation of the conduits and no deformation or delocalisation of the conduits from their implanted position was observed [23].

3.4. Functional analysis of regenerated sciatic nerve

A normal nerve was found to exhibit NCV of 59 m/sec, CMAP of 17.5 mV, MUP of 152 μV and an ideal SFI of 0. The results of electrophysiological studies and walking track analysis are presented in Figs. 2 and 3. Immediately post implantation of the conduits a minute MUP of 32 μV was observed in all the groups. At 9 months after implantation the animals with nanocomposite conduits without Schwann cells (GNP-SF) exhibited NCV of 54 m/sec, CMAP of 3.4 mV, MUP of 105 μV and SFI of −55. Animals having pre-seeded nanocomposite conduits with Schwann cells (GNP-SF cell) after 9 months showed NCV of 58 m/sec, CMAP of 7.8 mV, MUP of 112 μV and SFI of −47. The silk fibroin conduits without Schwann cells (SF) exhibited NCV of 22 m/sec, CMAP of 4.3 mV, MUP of 85 μV and SFI of −75 after 9 months. Pre-seeded silk fibroin conduits with Schwann cells (SF cell) after 9 months showed NCV of 29 m/sec, CMAP of 4.4 mV, MUP of 105 μV and SFI of −73.

After 18 months, the animals implanted with GNP-SF conduits exhibited NCV of 42 m/sec, CMAP of 16.5 mV, MUP of 116 μV and SFI of −43.4. Animals with GNP-SF cell conduits showed NCV of 50 m/sec, CMAP of 29.7 mV, MUP of 133 μV and SFI of −38.4 after 18 months. Implantation of SF conduits led to a NCV of 50 m/sec, CMAP of 6 mV, MUP of 87 μV and SFI of −70 after 18 months. Animals implanted with SF cell nerve conduits exhibited NCV of 50 m/sec, CMAP of 10 mV, MUP of 123 μV and SFI of −64 after 18 months. The control group showed a more or less constant SFI of around −100 throughout their life span.

The locomotory activities of the animals implanted with nanocomposite conduits after 10 months are presented in Fig. 4A–D.

3.5. Morphological analysis of regenerated sciatic nerve

All the conduits were found to be structurally intact up to 18 months maintaining adherence to micro-sutured proximal and distal nerve ends. In the animals implanted with GNP-SF and GNP-SF cell conduits, growth of nerve along the nerve gap was complete 18 months post implantation and the regenerated nerve appeared morphologically normal (Fig. 4E and F). However, even after 18 months in the animals with silk fibroin conduits (both SF and SF cell) the gap along the conduit was found to be filled with tissue which appeared to be fibrous in nature (Fig. 4G and H). Histological analysis of the regenerated tissue in the nanocomposite group by H&E staining revealed large recruitment of Schwann cells inside the lumen and as well as within the interlayer gaps of the conduits (Fig. 5A and B). Upon closer observation Schwann cells were found to be aligned in characteristic wave like fashion in the GNP-SF cell group. Fewer Schwann cells and more inflammatory cells were found inside the silk fibroin conduits (Fig. 5C and D). TEM analysis of the regenerated sections after 18 months showed presence of many myelinated fibres with thick myelin deposition in the nanocomposite group. However, few myelinated axons with fragmented myelin sheath was observed within the silk fibroin conduits (Fig. 6).

4. Discussions

Fabrication of Gold-Silk nanocomposite fibres have been previously performed using a co-electrospinning technique wherein a mixture of silk fibroin solution and colloidal gold nanoparticles were electrospun to incorporate nanoparticles on and within the nanofibers [14]. However, the need for multiple reduction steps employing strong alkaline reagents like tetrakis (hydroxymethyl) phosphonium chloride (THPC) and potassium carbonate (K_2CO_3) with proven neural toxicity limits the prospect for clinical

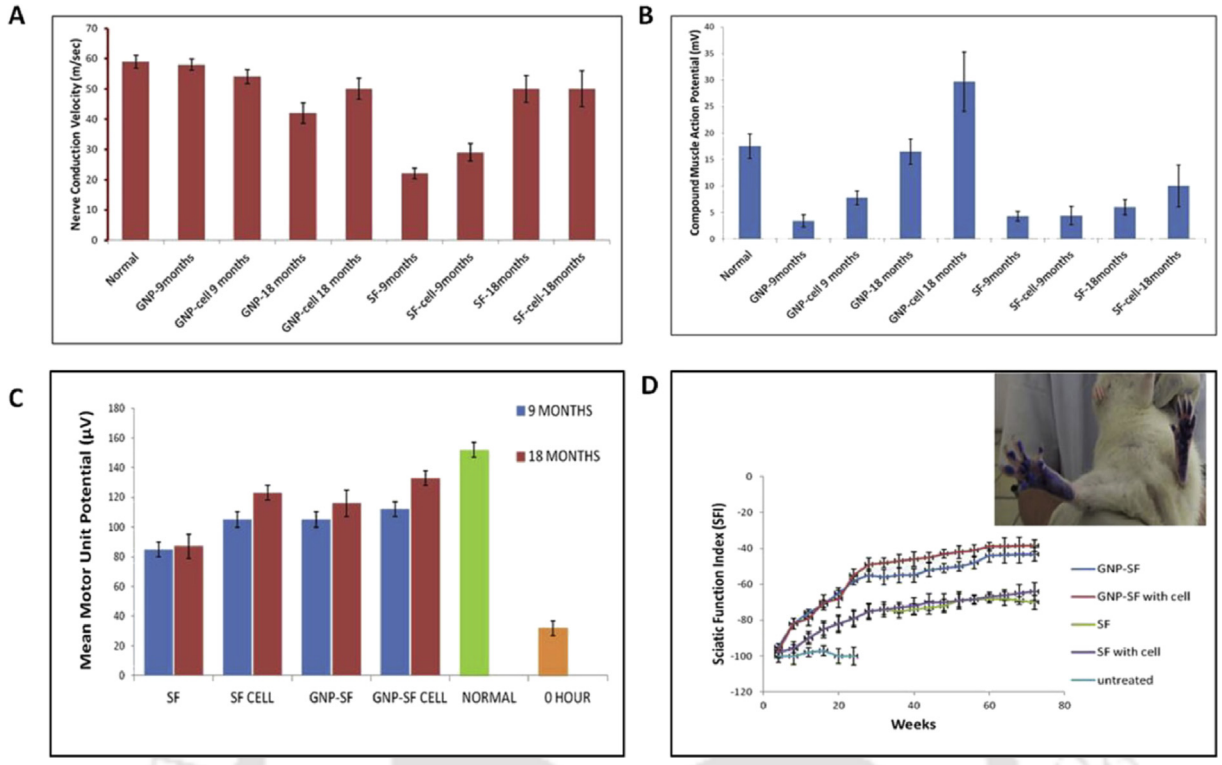

Fig. 2. Functional analysis of regenerated nerve. A, Nerve conduction velocity (NCV) recorded after 9 months and 18 months (n = 8). B, Compound muscle action potential (CMAP) values recorded after 9 months and 18 months (n = 8). C, Mean Motor unit potential (MUP) recorded from the gastrocnemius muscle after 9 months and 18 months. D, Sciatic function index (SFI) calculated by walking track analysis at 2 week interval for 18 months (n = 8). The hind limbs of the animals were stained with methylene blue for obtaining footprints (inset).

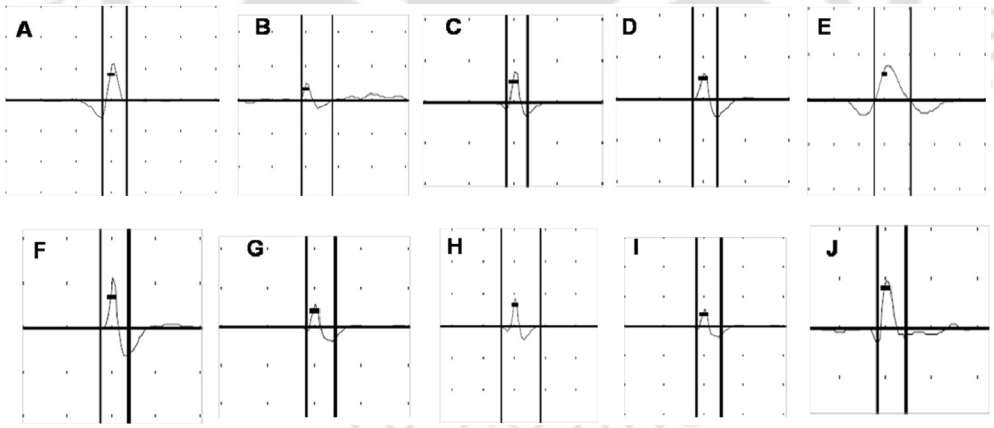

Fig. 3. Motor unit potential wave patterns. A, A representative image of MUP pattern of normal rat, B, MUP recorded immediately after nerve transection (0 h group), C, GNP-SF conduit group after 9 months, D, GNP-SF conduit group after 18 months, E, GNP-SF cell conduit group after 9 months, F, GNP-SF cell conduit group after 18 months, G, SF conduit group after 9 months, H, SF conduit group after 18 months, I, SF cell conduit group after 9 months, J, SF-cell conduit group after 18 months.

deployment of grafts fabricated by such methods [15].

In the present study, gold nanoparticles (GNP s) were formed by reduction with ethanolic extract of *Centella asiatica* (CA), an herb reported to facilitate neuro-regeneration and wound healing [16]. The CA extract mediated synthesis of GNP and particle characterization have been standardised earlier in our laboratory [12]. In this current work we found these GNPs to be non-toxic to rat Schwann cell line SCTM41 [23]. GNPs produced using synthetic reducing agents like malate, citrate and tartarate exhibit a net negative surface charge and have been studied as potential dyes for colouration of silk due to LSPR properties of plasmonic nanoparticles. One possible mechanism that was postulated for the rapid incorporation of GNPs on and within silk fibres was the electrostatic attraction between negatively charged GNPs and amine groups present on the fibroin protein which gets protonated in the acidic environment of the reaction [17]. In the present study, a similar phenomenon could have led to the purple colouration of silk fibres upon treatment with GNP solution due to the presence of free −COOH groups in CA extract [12]. Further, the highly acidic (pH 2.0) nature of the GNP solution could have facilitated the protonation of amine groups present on silk fibroin protein.

The gold nanoparticle incorporated silk fibroin fibres and the

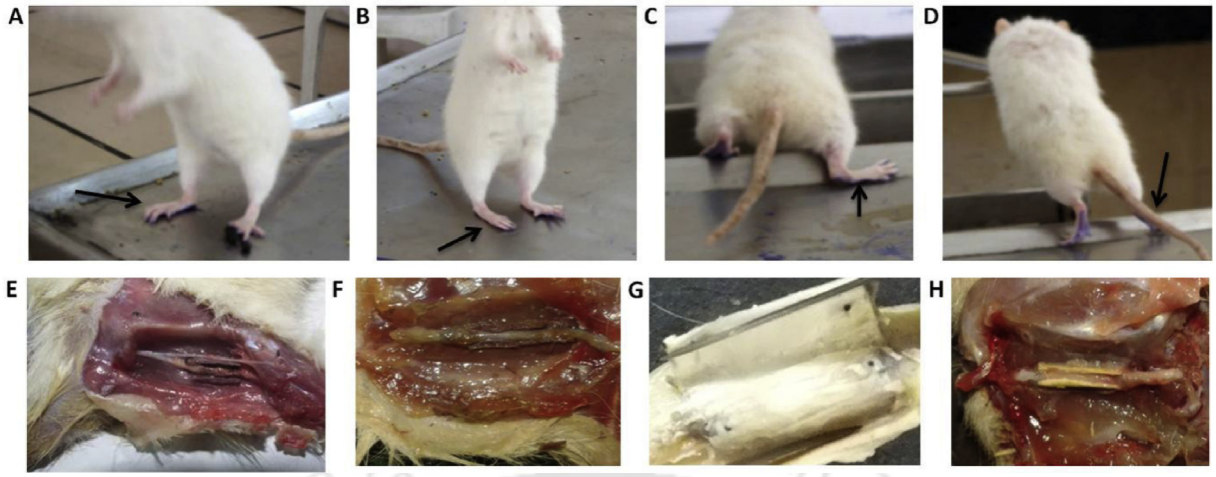

Fig. 4. Gait analysis and neural regeneration. A–D, The animals implanted with GNP-SF cell conduits exhibited improved gait and could stand, stretch and jump by the end of 10 months. Black arrows indicate the operated leg. E–H, The implanted conduits were slit open after 18 months to monitor tissue regeneration. Growth of tissue was observed in GNP-SF (E), GNP-SF cell (F), SF (G) and SF cell (H) groups.

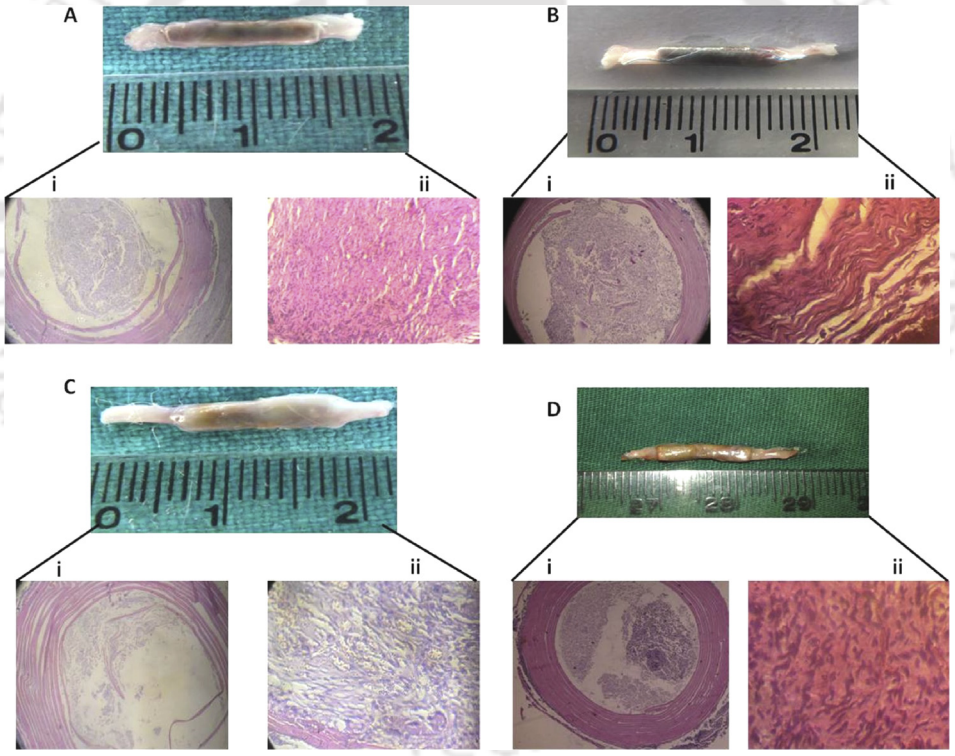

Fig. 5. Gross examination and histology of harvested conduits. A, GNP-SF conduit harvested and stained with haematoxylin-eosin (H&E) after 9 months (i) and 18 months (ii). B, GNP-SF conduits with cell (GNP-SF cell) harvested after 9 months (i) and 18 months (ii) and stained with H&E exhibiting characteristic wave like organisation of Schwann cells and nervous tissue. C, SF conduit and D, SF conduit with cell (SF-cell) harvested and histological analysis by H&E staining after 9 months (i) and 18 months (ii).

pristine degummed silk fibres were processed and electrospun following standard procedures to convert them into nano-dimension [11]. The hence formed silk fibroin nanofibers (SF) could not be visualised under scanning electron microscope (SEM) without gold coating. However, we found that no sputter coating with gold was necessary to observe the gold nanoparticle-silk fibroin nanocomposite (GNP-SF) nanofibers under electron microscope (Fig. 1C). This is due to the improved electrical conductivity of GNP-SF nanofibers arising from the presence of GNPs on silk nanofibers. The formation of the nanocomposite (GNP-SF) was confirmed through XRD analysis by the presence of characteristic sharp peaks for crystalline GNP corresponding to (111), (200), (220) fcc structure of gold. The broad peak around $2\theta = 21^{\circ}$ corresponds to amorphous silk fibroin protein (Fig. 1C inset). The ohmic nature of the I–V characteristics obtained for GNP-SF nanofibers was indicative of the electronic tunnelling/hopping effect as reported previously for similar ultrathin films [18]. The 25 fold decrease in resistance of silk nanofibers upon incorporation of GNPs indicates the enhanced electronic conduction through the silk-gold nanocomposite scaffold. Further the GNP-SF and SF scaffolds were also

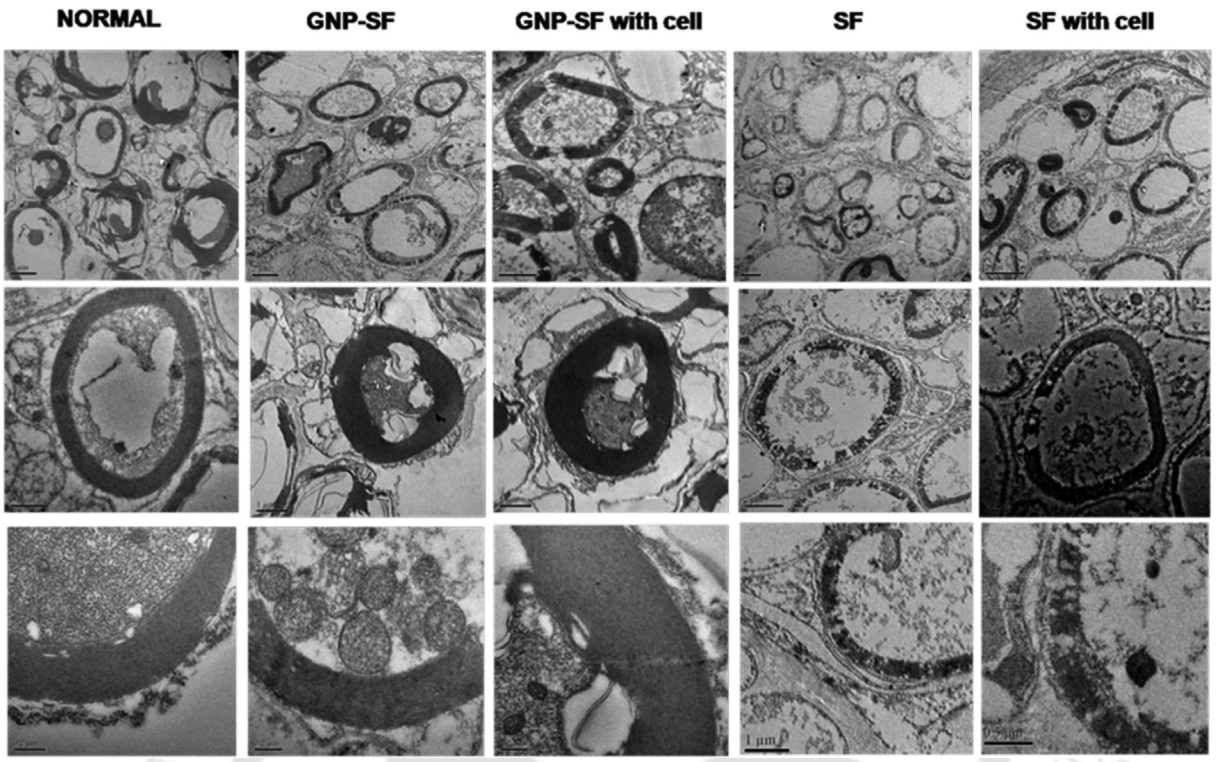

Fig. 6. Ultra structure of regenerated tissue. Normal, Ultra structure of a normal sciatic nerve as observed under TEM. Closer look at each axon reveals the myelin sheath encapsulation stained black due to osmium tetra-oxide treatment. The myelin sheath is seen being deposited in a lamellar fashion over the axon. GNP-SF and GNP-SF cell, Many axons with thick deposition of myelin were observed in both groups after 18 months. A closer look revealed lamellar architecture of the myelin sheath similar to the normal nerve. SF and SF cell, Few myelinated axons were observed after 18 months. Higher magnification images reveal discontinuous deposition of myelin over the axons and absence of lamellar architecture of myelin sheath.

found to promote Schwann cell adhesion and proliferation [23]. The nano-architecture of the electrospun scaffolds provided higher surface area to volume ratio for cellular attachment as compared to a single well of 12 well-culture plates having similar diameter.

Most of the fabrication methods used for developing nerve conduits like electrospinning, injection moulding, solvent casting etc predominantly rely on a mould like a teflon mandrel of specific dimension to provide the scaffold a conduit shaped architecture. Hence conduits with one particular dimension can only be made at a time. In the present study we have used a novel sheet rolling method to fabricate multiple conduits with varied length and diameters from a single electrospun sheet. Another advantage of the fabrication method is that the wall thickness of the conduits can be manipulated simply by the number of rotations of the electrospun sheet around the axis. Such layer by layer stacking of densely packed nanofibers lead to low porosity and limited swelling of the nerve conduits [23].

For our experiments we fabricated conduits by rotating the electrospun sheets on 16 gauge sterile needles with multiple rotations. The dimensions of the conduits were chosen after thorough standardization to match the dimensions of a rat sciatic nerve. The conduits were treated with methanol upon fabrication to induce β-sheet formation. This also served as a measure for sterilizing the implants. The conduits were further UV-sterilized prior to seeding with rat Schwann cell line (SCTM41) to ensure minimum possibility of contamination to cells or infection *in vivo*. The three dimensional environment of the lamellar conduits was found to mimic the native architecture of the nerve and promote Schwann cell growth in the form of clusters (Fig. 1F).

Regeneration of nerves following neurotmesis grade injury (complete axonal loss and conduction failure) is a highly complex, time consuming process often shackled with very low success rate inspite of surgical intervention. Most studies reported till date has been on an average for 3–4 months duration which is a short duration in terms of nerve regeneration and healing process. Only a handful of studies have been reported with post surgical observation time of 1 year or more [19]. Although the nerve is found to grow along the conduit filling the gap within 3–4 months of implantation, the innervations of muscles to restore strength and sensory function takes a much longer time.

One of the major goals of this study was to observe the long term effect of a metal-polymer nanocomposite based neural implant fabricated with GNPs and a non-absorbable natural polymer like silk on the structural and functional regeneration of nerve tissue as well as its impact on surrounding muscles. No signs of erythema or oedema were observed upon intra-cutaneous irritation and toxicity tests of the conduits, thereby establishing the non-immunogenicity of the nanocomposite material inside the body [23]. Further the fact that all the animals survived their normal life span before being sacrificed indicates the biocompatibility and safety of the silk-gold nanocomposite conduits.

A nerve injury is immediately followed by a series of degenerative processes called Wallerian degeneration leading to physical fragmentation of axon and disintegration of myelin sheath and ultimately loss of nerve conduction. Nerve conduction velocity (NCV) measurements along the nerve gap and the compound muscle action potential (CMAP) in the region of conduit implantation provide information about the extent of remyelination and conduction of nerve impulse through the grafted nerve conduit.

Electrophysiological measurements among all the groups immediately (within 1 h) after surgery revealed minute generation of action potential in the distal region while no signal could be

recorded by stimulating from the proximal side of the nerve gap (data not shown). This was particularly necessary to ascertain whether using an electrically conductive conduit with metallic nanoparticles can lead to conduction artefacts in nerve conduction studies. We found the NCVs of the group implanted with GNP-SF conduits (with and without cells) to be close to the normal values after a period of 18 months (Fig. 2A). They also exhibited near normal CMAP values which are possible only if the regenerating axons have been remyelinated. Rats implanted with GNP-SF conduits containing pre-seeded Schwann cells were found to have higher CMAP values than normal rats which may be due to high amount of myelin deposition by the Schwann cells (Fig. 2B). The data also indicated that there was no conduction block along the conduit. Rats implanted with SF conduits (with and without Schwann cells) exhibited increase in conduction velocities over a period of 18 months (Fig. 2A). However the low CMAP values exhibited by these groups can be attributed to the loss of myelin sheath and incomplete neural regeneration due to persistent axonal damage (Fig. 2B).

Neurotmesis grade nerve injuries are associated with complete loss of a nerve which leads to severe degeneration and atrophy of muscles innervated by the damaged nerve. Motor Unit Potential (MUP) evaluates the integrity of the motor unit comprising of the motor neuron, motor axon and the muscle which the particular nerve innervates. Both nerve conduction (NCV and CMAP) and electromyogram (MUP) are performed in clinical cases of nerve injuries, neurodegenerative diseases and neuropathies. However for evaluating nerve regeneration through a tissue engineered conduit only nerve conduction parameters have been measured so far. Hence to evaluate complete structural and functional regeneration of nerve and re-innervation of damaged muscle, it is essential to study the MUP patterns in neural tissue engineering applications. The MUP wave patterns observed for all the groups are presented in Fig. 3. MUPs recorded immediately after surgical transection of nerve (0 h group) and implantation of conduit exhibit very low amplitude of 32 μV trailed by fibrillation (Figs. 2C and 3A) suggesting complete loss of sciatic nerve activity. The minute MUP recorded in the region are due to the action potential of other minor nerves that innervate the gastrocnemius muscle. The GNP-SF group were observed to have similar MUP wave pattern with slight increase in amplitude after 18 months as compared to 9months (Figs. 2C, 3C and D). The GNP-SF conduits seeded with Schwann cells however exhibited marked improvement in MUP wave pattern with decrease of duration, area and increased amplitude after 18 months. The mean MUP amplitude of the GNP-SF cell group was found to be 133 μV which is almost comparable to normal control group value of 152 μV (Figs. 2C, 3E and F). The animals implanted with SF conduits were found to have identical MUP pattern and amplitude with no appreciable improvement over the duration of the study (Figs. 2C, 3G and H). SF conduits seeded with Schwann cells did reveal enhanced MUP amplitude after 18 months as compared to the 9 month old MUP but fibrillation patterns similar to 0 h group was also evident (Figs. 2C, 3I and J). Hence electrophysiological studies over 18 months suggested that near normal functional regeneration of nerve as well as re-innervations of surrounding muscles was achieved in the GNP-SF conduit group containing pre-seeded Schwann cells.

The sciatic nerve is one of the major nerves supplying to the muscles of hind limbs and is particularly responsible for proprioception in the feet as well as locomotion. The ability of the animals to regain locomotor activities following surgical implantation of conduits was studied by walking track analysis on the operated leg by sciatic function index (SFI) measurement (Fig. 2D). The rats implanted with GNP-SF conduits seeded with Schwann cells (GNP-SF cell) performed better than the GNP-SF, SF and SF-cell groups with SFI values approaching normal level after 18 months. We noted that none of the animals in the negative control group survived more than 6 months and exhibited SFI values close to −100 indicating complete neuromuscular degeneration. In all the other groups the SFI values were observed to rise sharply in the initial 12–16 weeks thereby gradually saturating over a period of 36–40 weeks.

Collagen remains the most preferred biopolymer for fabricating nerve conduits which is reflected in numerous collagen based conduits that have been approved by the US FDA in the recent past [20]. The described nanocomposite conduits upon implantation exhibited high degree of functional neuro-muscular regeneration that is superior to even collagen based implants [21]. In a comparative study of 4 synthetic conduits the maximum CMAP amplitude reported was around 1 mV with poly-caprolactone fumarate (PCLF) and PLGA conduits in comparison to autografts showing amplitude of 2.5 mV [2]. However, normal nerves show CMAP amplitude of 15–20 mV. Although most studies keep autograft as the control we have compared our results with a normal nerve thereby setting a higher standard. In the present study, the animals with nanocomposite conduits seeded with Schwann cells exhibit near normal values of CMAP, NCV and motor unit potentials after 18 months which conclusively proves that these conduits significantly enhance neural regeneration to a far more extent than previously reported.

In addition to electrophysiological tests, the rats were regularly monitored for signs of pain, discomfort and incidental abnormalities. The initial implantation of nerve conduit was done on three month old animals and thereafter monitored over a period of 18 months. The rats were found to lead a normal life span (except the control group which did not survive more than 6 months). No behavioural or clinical anomalies (like autotomy) were noted in any of the groups. The animals with GNP-SF conduits pre-seeded with Schwann cells displayed near-normal locomotor activities. Although the digits of the operated leg (right leg) remained flexed, the rats were able to stand, stretch and jump at will by the end of 10 months (Fig. 4A–D). Such activities put strain on the toe and thigh of the animals and could not be possible without functional regeneration of the sciatic nerve and regaining of strength in the gastrocnemius region.

To physically examine nerve growth by histo-morphometric analysis, the conduits were harvested along with the proximal and distal sections of the sciatic nerve 9 and 18 months post implantation. All the conduits were found to be structurally intact up to 18 months maintaining adherence to micro-sutured proximal and distal nerve ends. This could be attributed to the minimal swelling tendency of the conduits which helped it to retain its structural integrity over 18 months *in vivo*. In the groups implanted with GNP-SF and GNP-SF cell conduits, growth of nerve along the nerve gap was complete 18 months post implantation and the regenerated nerve appeared morphologically normal (Fig. 4E and F). However, in the silk fibroin group (SF and SF cell) after 18 months, the gap along the conduit was found to be filled with tissue which appeared to be fibrous in nature (Fig. 4G and H). The nanocomposite conduits (GNP-SF and GNP-SF cell) were found to be encapsulated by fascia and fibrous tissue. No signs of inflammation were visible and both the proximal and distal ends appeared normal (Fig. 5A and B). In histological studies the conduits lamellar architecture appeared to be intact with cellular proliferation along the lumen as well as the interlayer gaps of the conduits (Fig. 5A i and B i). A closer look at the regenerated nerve tissue of GNP-SF group after 18 months indicated recruitment of large amount of Schwann cells (Fig. 5A ii) whereas the Schwann cells were observed to be aligned in characteristic wave like fashion in the GNP-SF cell group (Fig. 5B ii). Upon gross examination, the silk fibroin conduits

(SF and SF-cell) appeared to be associated with inflammation at the distal end (Fig. 5C and D). Histology of the SF conduits after 9 months showed little recruitment of neuronal cells with most of the lumen empty (Fig. 5C i). Further, 18 months post surgery also cellular proliferation inside conduit remained minimal (Fig. 5C ii). The SF conduits seeded with Schwann cells (SF-cell) did have more cells inside the lumen after 9 months as compared to SF group (Fig. 5D i). However over 18 months it was found that the cells were mostly inflammatory in nature indicating possible neuroma formation (Fig. 5D ii).

In order to evaluate the degree of myelination, the regenerated nerve tissue was observed under transmission electron microscope following lipid specific osmium tetraoxide staining (Fig. 6). The animals implanted with gold nanoparticle containing conduits (GNP-SF and GNP-SF cell) exhibited neural ultra-structure similar to that of a normal nerve. Thick coating of myelin sheath along with characteristic lamellar structure was evident in the GNP-SF and GNP-SF cell groups indicating sufficient deposition of myelin in aligned fashion by Schwann cells. On the contrary, the animals with silk fibroin conduits (SF and SF cell) displayed fewer myelinated axons along with incomplete deposition of myelin in a more granular fashion rather than the desired lamellar organization. Although SF cell group exhibited more number of myelinated axons as compared to SF, there was no significant improvement in the myelin architecture.

The pre-seeding of Schwann cells forms an inner and outer sheet of cells on the conduit. When the conduit is sutured to the two ends of the nerve stump the Schwann cell sheath inside the conduit serves as natural guidance for the migration of endothelial cells and fibroblasts from the proximal and distal nerve stumps. This helps in formation of a biological tissue cable augmenting axonal regeneration and myelination [22]. The porous nature of the conduit facilitates the transport of nutrients as well as growth factors and signalling molecules released by the outer layer of Schwann cells into the interior. Overall this enhances neuro-regeneration across the nerve gap as compared to animals implanted with un-seeded conduits.

5. Conclusions

A major accomplishment of the present study is the fabrication of a metal-biopolymer based nano-composite for deployment as a nerve conduit. Here, we have demonstrated in principle how the nanocomposite nerve conduits exhibited improved structural and functional neuro-muscular regeneration as compared to silk fibroin and control group. Pre-seeding the nerve conduits with Schwann cells was found to enhance its neuro-regenerative potential. The GNP-SF cell group exhibited increased CMAP, better MUP patterns and improved SFI values over 18 months. Histological and TEM analysis of regenerated nerve harvested from GNP-SF cell group revealed increased recruitment of Schwann cells leading to better myelination of axons in a lamellar fashion.

We also report here for the first time the utility of motor unit potentials (MUP) recorded from surrounding gastrocnemius muscle in studying nerve regeneration through an implanted conduit. The MUP patterns obtained through electromyogram along with nerve conduction studies helped us to accurately analyse nerve continuity across the gap as well as re-innervation of surrounding muscles which is of direct clinical relevance.

The novel sheet rolling approach adopted in the present study for fabrication of multidimensional conduits from a single electrospun sheet can be scaled up through automation in future. Such a process would aid in fabricating conduits which can fit nerves of varied dimension in the human body.

The present study convincingly demonstrates that neural implants comprising of gold nanoparticles are safe, stable and remain functional *in vivo* for a long duration. The presence of GNPs in the conduits neither elicited any inflammatory response in the host nor in situ at the site of implantation. This may be attributed to the fact that such particles were synthesised using biological agents like herbal extracts. Further the strong interaction between the nanoparticles and nanofibers kept the GNPs embedded in the nanofibers limiting their migration into the surrounding tissue as evident from by the retention of colour of the GNP-SF nerve conduits after 18 months of implantation. Such well characterised materials would be able to withstand the complex and lengthy process of neuromuscular regeneration and prove to be ideal for clinical translation.

Further the formation of nanoparticle-nanofiber nanocomposite also opens up new opportunities for fabricating advanced scaffolds. Such nanocomposites would enable chemical modifications of biomaterial and can potentially act as platforms for delivery of nerve growth factors providing chemical cues for cellular proliferation and directing neurite outgrowth. The method demonstrated herein can potentially be used as a platform to fabricate smart materials having applications not only in tissue engineering but also in optoelectronics, sensing technologies and development of e-textiles. Research on extending the applicability of the method to different polymers using a variety of nanoparticles as well as attempts to better understand the possible mechanism behind such nanocomposite formation are presently underway in our laboratory.

Author contributions

Bora U, conceptualised the doping of silk with nanoparticles, subsequent fabrication of nerve conduits and was responsible for overall study design, analysis of results and drafting of manuscript. Das S, implemented the above concept, developed and characterized the conduits, carried out cell culture experiments as well as *in vivo* electrophysiological studies, analysed the data and drafted the manuscript. Sharma M, carried out the surgical experiments, developed the sciatic injury model and was responsible for overall animal care and maintenance. Saharia D, carried out the histopathological studies. Sarma K.K, designed the animal experimentation and surgical procedures followed herein. Sarma M.G, was involved in interpretation of electrophysiological studies. Borthakur B.B, was involved in interpretation of electrophysiological studies as well as conducting the MRI experiment.

Conflict of interest

A portion of the work reported in the present article has been used to file an Indian patent application vide application number 1131/KOL/2013 dated 01.10.2013.

Acknowledgements

We would like to thank Dr Elizabeth Muir, University of Cambridge for providing the rat schwann cell line (SCTM41) for our experimental purpose. We further thank and acknowledge Central Silk Board, Bengaluru, Govt of India (Sanction order no:CSB-31/2/PROJECT/2010-11-RCS dated 26.05.2011) and Department of Biotechnology, New Delhi, Govt of India (Sanction order no:-BT/PR14042/MED/30/338/2010 dated 04.01.2011) for providing partial funding support for this work. SD would like to thank IIT Guwahati and Ministry of Human Resource Development (MHRD), Govt of India.

References

[1] C. Cunha, S. Panseri, S. Antonini, Emerging nanotechnology approaches in tissue engineering for peripheral nerve regeneration, Nanomedicine 7 (2011) 50–59.

[2] W.T. Daly, A.M. Knight, H. Wang, R. de Boer, G. Giusti, M. Dadsetan, R.J. Spinner, M.J. Yaszemski, A.J. Windebank, Comparison and characterization of multiple biomaterial conduits for peripheral nerve repair, Biomaterials 34 (2013) 8630–8639.

[3] Y.A. Berrocal, V.W. Almeida, R. Gupta, A.D. Levi, Transplantation of Schwann cells in a collagen tube for the repair of large, segmental peripheral nerve defects in rats, J. Neurosurg. 119 (2013) 720–732.

[4] V. Benfenati, K. Stahl, C. Gomis-Perez, S. Toffanin, A. Sagnella, R. Torp, D.L. Kaplan, G. Ruani, F.G. Omenetto, R. Zamboni, M. Muccini, Biofunctional silk/neuron interfaces, Adv. Funct. Mater. 22 (2012) 1871–1884.

[5] S. Madduri, M. Papaloïzos, B. Gander, Trophically and topographically functionalized silk fibroin nerve conduits for guided peripheral nerve regeneration, Biomaterials 31 (2010) 2323–2334.

[6] T. Dinis, G. Vidal, F. Marin, D. Kaplan, C. Eglès, Silk nerve: bioactive implant for peripheral nerve regeneration, Comput. Methods Biomech. Biomed. Eng. 16 (2013) 253–254.

[7] H.B. Wang, M.E. Mullins, J.M. Cregg, C.W. McCarthy, R.J. Gilbert, Varying the diameter of aligned electrospun fibers alters neurite outgrowth and Schwann cell migration, Acta Biomater. 6 (2010) 2970–2978.

[8] J. Qu, D. Wang, H. Wang, Y. Dong, F. Zhang, B. Zuo, H. Zhang, Electrospun silk fibroin nanofibers in different diameters support neurite outgrowth and promote astrocyte migration, J. Biomed. Mater. Res. A 101 (2013) 2667–2678.

[9] A. Fabbro, M. Prato, L. Ballerini, Carbon nanotubes in neuroregeneration and repair, Adv. Drug Deliv. Rev. 65 (2013) 2034–2044.

[10] F. Mottaghitalab, M. Farokhi, A. Zaminy, M. Kokabi, M. Soleimani, F. Mirahmadi, M.A. Shokrgozar, M. Sadeghizadeh, A biosynthetic nerve guide conduit based on silk/SWNT/fibronectin nanocomposite for peripheral nerve regeneration, PLoS One 8 (2013) 74417.

[11] D.N. Rockwood, R.C. Preda, T. Yücel, X. Wang, M.L. Lovett, D.L. Kaplan, Materials fabrication from *Bombyx mori* silk fibroin, Nat. Protoc. 6 (2011) 1612–1631.

[12] R.K. Das, B.B. Borthakur, U. Bora, Green synthesis of gold nanoparticles using ethanolic leaf extract of Centella asiatica, Mater. Lett. 64 (2010) 1445–1447.

[13] U.J. Kim, J. Park, H.J. Kim, M. Wada, D.L. Kaplan, Three-dimensional aqueous-derived biomaterial scaffolds from silk fibroin, Biomaterials 26 (2005) 2775–2785.

[14] T. Cohen-Karni, K.J. Jeong, J.H. Tsui, G. Reznor, M. Mustata, M. Wanunu, A. Graham, C. Marks, D.C. Bell, R. Langer, D.S. Kohane, Nanocomposite gold-silk nanofibers, Nano Lett. 12 (2012) 5403–5406.

[15] National Toxicology Program, NTP Toxicology and Carcinogenesis Studies of Tetrakis(hydroxymethyl)phosphonium sulfate (THPS) (CAS No. 55566-30-8) and Tetrakis(hydroxymethyl)phosphonium chloride (THPC) (CAS No. 124-64-1) in F344/N Rats and B6C3F1 Mice (Gavage Studies), Natl. Toxicol. Progr. Tech. Rep. Ser. 296 (1987) 1–290.

[16] Assessment Report on *Centella asiatica* (L.) Urban, Herba by Committee on Herbal Medicinal Products (HMPC), European Medicines Agency, EMA/HMPC/291177/2009.

[17] B. Tang, J. Tao, S. Xua, J. Wang, C. Hurren, W. Xu, L. Sun, X. Wang, Using hydroxy carboxylate to synthesize gold nanoparticles in heating and photochemical reactions and their application in textile colouration, Chem. Eng. J. 172 (2011) 601–607.

[18] R.M. Hill, Electrical conduction in ultra thin metal films. I, Theor. Proc. R. Soc. Lond. A 309 (1969) 377–395.

[19] M.E. Boeckstyns, A.I. Sørensen, J.F. Viñeta, B. Rosén, X. Navarro, S.J. Archibald, J. Valss-Solé, M. Moldovan, C. Krarup, Collagen conduit versus microsurgical neurorrhaphy: 2-year follow-up of a prospective, blinded clinical and electrophysiological multicenter randomized, controlled trial, J. Hand Surg. Am. 38 (2013) 2405–2411.

[20] S. Kehoe, X.F. Zhang, D. Boyd, FDA approved guidance conduits and wraps for peripheral nerve injury: a review of materials and efficacy, Injury 43 (2012) 553–572.

[21] W. Yu, W. Zhao, C. Zhu, X. Zhang, D. Ye, W. Zhang, Y. Zhou, X. Jiang, Z. Zhang, Sciatic nerve regeneration in rats by a promising electrospun collagen/poly(ε-caprolactone) nerve conduit with tailored degradation rate, BMC Neurosci. 12 (2011) 68.

[22] W. Daly, L. Yao, D. Zeugolis, A. Windebank, A. Pandit, A biomaterials approach to peripheral nerve regeneration: bridging the peripheral nerve gap and enhancing functional recovery, J. R. Soc. Interface 67 (2012) 202–221.

[23] S. Das, M. Sharma, D. Saharia, K.K. Sarma, M.G. Sarma, B.B. Borthakur, U. Bora. Data in Support of in vivo Studies of Silk Based Gold Nano-composite Conduits for Functional Peripheral Nerve Regeneration, Data in Brief, (article in press).

Data in Brief 4 (2015) 315–321

Contents lists available at ScienceDirect

Data in Brief

journal homepage: www.elsevier.com/locate/dib

Data Article

Data in support of in vivo studies of silk based gold nano-composite conduits for functional peripheral nerve regeneration

Suradip Das [a], Manav Sharma [a], Dhiren Saharia [b], Kushal Konwar Sarma [c], Monalisa Goswami Sarma [d], Bibhuti Bhusan Borthakur [e,f], Utpal Bora [a,f,*]

[a] Department of Biosciences and Bioengineering, Indian Institute of Technology Guwahati, Guwahati 781039, Assam, India
[b] Saharia's Path Lab & Blood Bank, Guwahati 781005, Assam, India
[c] Department of Surgery and Radiology, College of Veterinary Sciences, Khanapara, Guwahati 781022, Assam, India
[d] Nemcare Hospital, Guwahati 781005, Assam, India
[e] Department of Surgical Oncology, Dr. B. Borooah Cancer Institute, Gopinathnagar, Guwahati 781016, Assam, India
[f] Mugagen Laboratories Private Limited, Technology Incubation Centre, Indian Institute of Technology Guwahati, Guwahati 781039, Assam, India

ARTICLE INFO

Article history:
Received 15 May 2015
Received in revised form
23 May 2015
Accepted 29 May 2015
Available online 16 June 2015

ABSTRACT

In the present data article we report the in vitro and in vivo biocompatibility of fabricated nerve conduits described in Das et al. [1]. Green synthesised gold nanoparticles (GNPs) were evaluated for their cytotoxicity in rat Schwann cells (SCTM41). We also describe herein the adhesion and proliferation of Schwann cells over the nanofibrous scaffolds. Methods describing surgical implantation of conduits in a rat sciatic nerve injury model, confirming its accurate implantation as well as the porosity and swelling tendency of the nerve conduits are illustrated in the various figures and graphs.

DOI of original article: http://dx.doi.org/10.1016/j.biomaterials.2015.04.047
* Corresponding author at: Department of Biosciences and Bioengineering, Indian Institute of Technology Guwahati, Guwahati 781039, Assam, India.
E-mail addresses: ubora@iitg.ernet.in, drutpalbora@gmail.com (U. Bora).

http://dx.doi.org/10.1016/j.dib.2015.05.020

Specifications table

Subject area	Biology, Chemistry
More specific subject area	Nerve regeneration, nerve conduit
Type of data	Image (MRI, microscopy), graph, figure
How data was acquired	• Cytotoxicity values were acquired through UV–vis multiwell plate reader (Make-TECAN). • Live–dead staining results were acquired through inverted fluorescence microscope (Make-ProSciTech), • Images of nanofibers and cell-loaded nanofibers were acquired through FESEM (Make-ZEISS, Model-Sigma), • MRI images taken using 1.5T MRI machine ((Make-Philips Model-Achieva). • Electrical resistance of scaffolds were measured through Sub-femto-ampmeter (Make-Keithley).
Data format	Raw data (digital photographs), Analyzed (Image J software, NIH, USA)
Experimental factors	• Nanofibers and nerve conduits were sterilised by methanol and UV prior to cell culture and in vivo intra-dermal test respectively. • Nanofibers with cells were fixed with 4% paraformaldehyde prior to FESEM.
Experimental features	• MTT assay, live–dead staining. • FESEM of nanofibers and cell growth over nanofibrous scaffolds. • Electrical conductivity of nanofibrous scaffolds. • Intracutaneous irritation and toxicity study of nerve conduits as per ASTM STP 1452. • Surgical method of implantation of nerve conduits. • Magnetic resonance Imaging of implanted nerve conduits. • Porosity and swelling characteristics of nerve conduits.
Data source location	N/A
Data accessibility	All the data are embedded in the article.

Value of the data

- In vitro and in vivo toxicity study of green synthesised gold nanoparticles and nanocomposite based nerve conduits respectively provides an insight into the potential safety of using nanoparticle based neural implants.
- Method for culturing and monitoring cellular proliferation over nanofibrous scaffolds.
- Data for porosity and swelling ratio of the conduits can be compared to other three dimensional scaffolds.

1. Data, experimental design, materials and methods

Green synthesised gold nanoparticles (GNPs) were evaluated for their cytotoxicity in rat Schwann cells (SCTM41). We also describe herein the adhesion and proliferation of Schwann cells over the nanofibrous scaffolds. Data supporting methods to surgically implant conduits in a rat sciatic nerve injury model, confirming its accurate implantation as well as the porosity and swelling tendency of the nerve conduits are illustrated in the various figures and graphs.

1.1. Cytotoxicity of synthesized GNPs

Cytotoxic effect of *Centella asiatica* mediated synthesized gold nanoparticles (GNP) was assessed by MTT assay on rat schwann cell line (SCTM41) following standard assay procedures [2]. Briefly, the nano-particle solution was lyophilized to get GNP as powder form. A stock solution (10 mg/ml) was prepared in Dulbecco's modified eagle's medium (DMEM) without serum. This solution was used to make further working concentrations (5 μg/100 μl to 500 μg/100 μl) of GNP

against which MTT assay was done. The cells were cultured in 96 well cell culture plates and incubated with various concentrations of GNP (5 μg/100 μl to 500 μg/100 μl) in serum free DMEM for 24 h in a CO_2 incubator (Make – Healforce) under 37 °C and relative humidity 90%. This was followed by addition of DMSO and recording absorbance at 570 nm using a UV–vis multiwell plate reader (Make-TECAN).

The gold nanoparticles synthesised using ethanolic extract of *C. asiatica* were found to be non-toxic to SCTM41 rat schwann cells up to a concentration of 500 μg/ml (Fig. 1A). Live dead assay with Acridine orange and Ethidium bromide conducted with GNP concentration of 5 μg/ml (Fig. 1B-i), 50 μg/ml (Fig. 1B-ii) and 500 μg/ml (Fig. 1B-iii) revealed normal cellular morphology up to the highest concentration of 500 μg/ml. The live cells preferentially take up Acridine orange (green) whereas Ethidium bromide (red) stains the nuclei of dead cells [3].

1.2. Electrical resistance of scaffolds

A piece of corning glass was first coated with aluminium using a suitable masking agent to generate a 2 mm thick uncoated strip in the middle. In order to study the electrical resistance, a 1 cm × 1 cm portion of the electrospun silk fibroin (SF) and gold nanoparticle-silk fibroin nanocomposite (GNP-SF) sheet was placed over the uncoated strip with its edges fixed on the aluminum coated section by silver paste. An *I–V* graph was generated for GNP-SF sample (Fig. 2) and the resistance of the materials was calculated.

1.3. Architecture of nanofibers and culture of Schwann cells over nanofibrous scaffolds

FESEM analysis of the electrospun mats (both GNP-SF and SF) showed the nanofibers were distributed in a mesh like architecture (Fig. 3A and B). Pore size distribution and fiber diameter of the nanofibers were studied using Image J. The nanocomposite nanofibers were observed to have a larger diameter of 200–300 nm and smaller pore size distribution in the range of 700–1000 nm as compared to silk fibroin nanofibers (Fig. 3C and D). Pristine silk fibroin and GNP incorporated silk fibroin nanofibers were collected in cover slip separately for 2D culture of cells. Cover slips were treated with methanol and UV ray for conversion to β sheet and sterilization. They were then washed 3–4 times with sterile phosphate buffer saline (PBS) and incubated with DMEM containing 10% FBS for 24 h in CO_2 incubator for conditioning. SCTM41 cells (rat Schwann cell) were seeded over cover slips and incubated for 10 days. On fifth day cover slips were processed for FESEM analysis to monitor cell

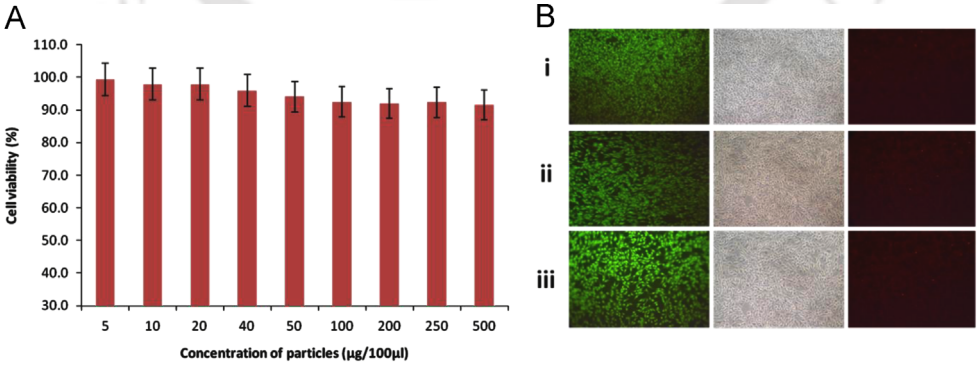

Fig. 1. Cytotoxicity of GNPs. (A) MTT assay of GNPs on rat Schwann cell line SCTM41. Each concentration was done in triplicate to generate standard deviation. (B) Live–dead staining assay with Acridine orange (AO) and Ethidium bromide (EtBr).The assay was done by treating the cells with GNP concentration of 5 μg/100 μl (i), 50 μg/100 μl (ii) and 500 μg/100 μl (iii). The live cells are stained green from AO while the dead cells stain red with EtBr.

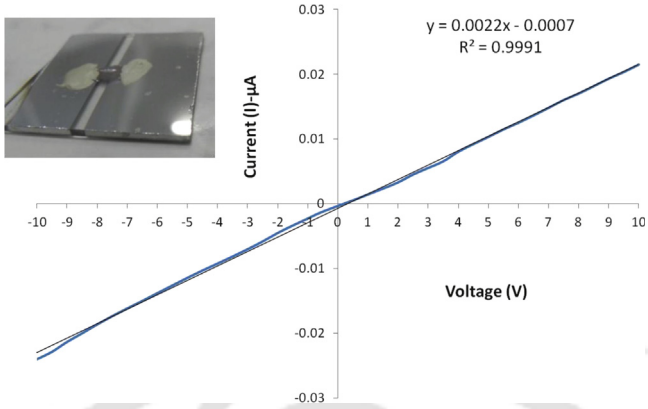

Fig. 2. Electrical property of GNP-SF nanocomposite scaffold. The figure shows the ohmic nature of the *I–V* characteristic of the GNP-SF nanocomposite scaffold with the experimental setup in inset.

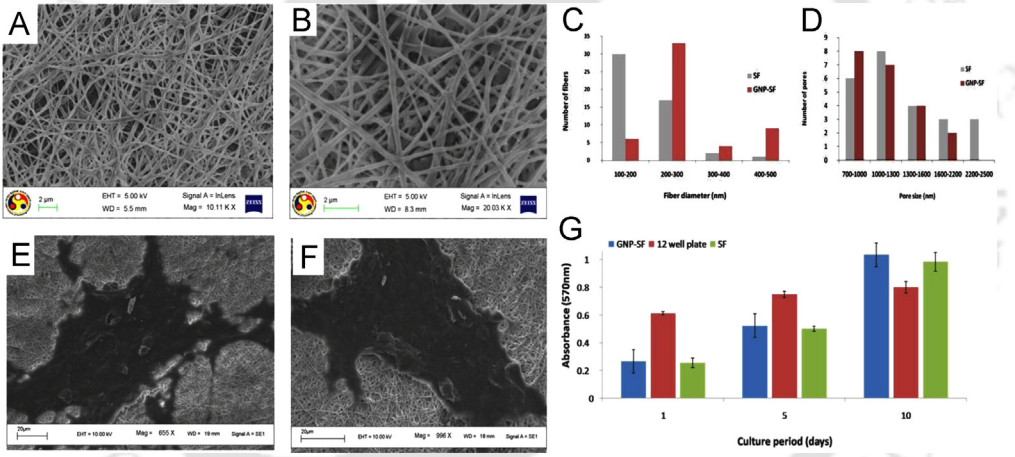

Fig. 3. Architecture of nanofibers and culture of Schwann cells over nanofibrous scaffolds. (A) FESEM image of SF nanofibrous scaffold and (B) nanocomposite (GNP-SF) nanofibrous scaffold. (C) Size distribution of nanofibers calculated using Image J (NIH, USA), (D) pore size distribution of the nanofibrous scaffolds calculated using Image J (NIH, USA), (E) FESEM image of SF nanofibrous scaffold after 5 days of culturing Schwann cells (SCTM41) and (F) FESEM image of GNP-SF nanocomposite nanofibrous scaffold after 5 days of culturing Schwann cells (SCTM41). (G) Cell proliferation study by MTT assay by culturing Schwann cells for 10 days over GNP-SF and SF scaffolds keeping one well of 12-well culture plate as control.

adhesion. Cellular proliferation was also quantitatively studied over the cover slips by MTT analysis at 0, 5th and 10th day.

The cells were found to adhere and grow over the surface of electrospun nanofibers (Fig. 3A, B, E and F). MTT assay of cells growing over the scaffolds exhibited subsequent increment of absorbance with time over a period of 10 days as compared to a more saturated growth in control group of 12 well tissue culture plate (Fig. 3G). These results indicate enhanced cellular proliferation over porous nano-scaffolds with higher surface area to volume ratio than conventional tissue culture plates with similar dimensions. However, no appreciable difference was observed in rate of proliferation between GNP-SF and SF scaffolds.

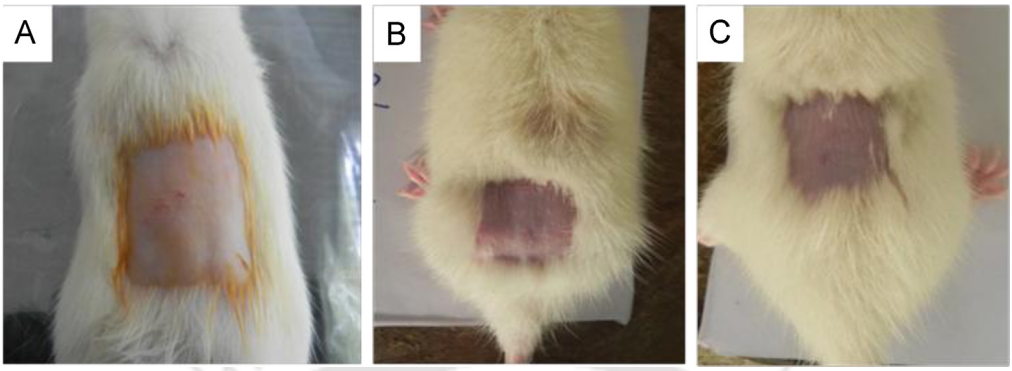

Fig. 4. In vivo intracutaneous irritation test. The animals observed after 72 h of injecting saline extract of (A) GNP-SF conduit and (B) SF conduit. (C) In the control group only saline was injected.

1.4. *In vivo intradermal test*

Intra-cutaneous irritation and toxicity studies were performed on Sprague Dawley rats ($n=9$) following standard procedures as described in ASTM standard protocol for "Standards Used in Meeting Requirements for a Model Pre-Market Approval (PMA) of a Neural Guidance Conduit" (ASTM STP 1452). Briefly, 24 h saline extract of the silk fibroin ($n=3$) and GNP-incorporated silk fibroin conduit ($n=3$) were taken and injected intradermally. Normal saline was injected in the control group ($n=3$) (Fig. 4C). The animals were observed for 72 h.

The 24 h saline extract of the GNP-SF (Fig. 4A) and SF conduits (Fig. 4B) did not produce any abnormal clinical symptoms, oedema or erythema in the animals. The site of administration of the extract did not exhibit any abnormality as compared to the control saline group up to 72 h from the time of intra-dermal injection.

1.5. *Surgical implantation and electrophysiological study*

A 10 mm gap was created in the sciatic nerve and the conduits were implanted and secured to the proximal and distal ends of the nerve by suture (Fig. 5A–B). For the electrophysiological study of measuring nerve conduction velocity (NCV) and compound muscle action potential (CMAP) the proximal and distal ends of the conduit were sequentially stimulated while the recording electrode was fixed near the ankle region of the animal (Fig. 5C)

1.6. *Magnetic resonance imaging (MRI)*

The animals were subjected to MRI imaging using a 1.5T MRI machine (Make-Philips Model-Achieva) and a 40 mm diameter coil one week post implantation. The conduit was found to be accurately placed in the sciatic nerve (Fig. 6).

1.7. *Porosity and swelling ratio of nerve conduits*

The porosity of the conduits was determined by a previously described ethanol displacement method [4]. Briefly, the dimensions of the conduits ($n=4$) were precisely measured using a vernier caliper and the volume (V) calculated according to the following formula:

$$V = \pi\left(R^2 - r^2\right)h,$$

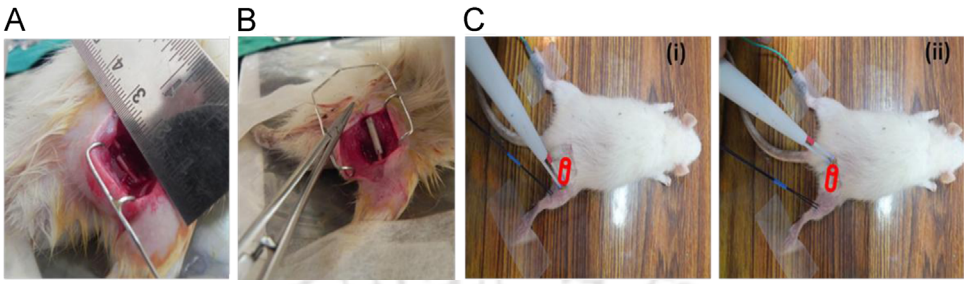

Fig. 5. Surgical implantation and electrophysiological study. (A) Rat sciatic injury model having a 10 mm gap was created. (B) The fabricated nerve conduits were implanted within the gap and sutured to the proximal and distal ends of the nerve stump. (C) Experimental setup for conducting NCV and CMAP studies with the nerve stimulator (white) and recording electrode (black). The nerve stimulator is placed once at the distal end (i) and again at the proximal end (ii) of the implanted conduit (apparent position shown in red) to record NCV through the conduit. The recording electrode is kept fixed near the ankle of the animal.

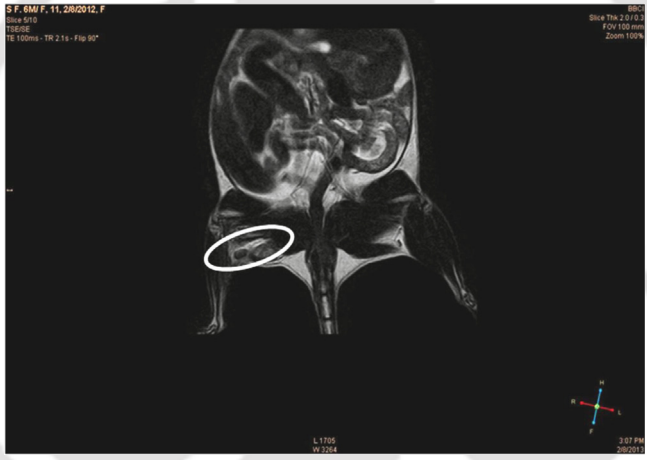

Fig. 6. Magnetic resonance imaging of animals. The implanted conduit could be visualized (encircled area) by MRI after a week of implantation.

where R was the outer radius of the conduit, r was the inner radius of the conduit and h was the length of the conduit. The conduits were then weighed in dry condition (M_o) and immersed in ethanol for 24 h before being weighed again to get M_t. The porosity of the conduit was calculated according to the following formula:

$$Porosity\ (\%) = \frac{(M_t) - (M_o)}{V \times \rho} \times 100$$

where ρ is the density of ethanol (0.79 g/cc). Both SF and GNP-SF conduits were found to have low porosity. The porosity of SF nerve conduit was found to be 15.6% (± 0.3) while GNP-SF conduits exhibited minute porosity of 5.37% (± 0.08).

The dynamic swelling ratio of the nerve conduits was measured according to a previously described method [5]. The conduits were immersed in phosphate buffered saline (pH 7.4) and the swelling ratio was calculated periodically every hour according to the following formula:

$$\text{Swelling ratio}\ (\%) = \frac{(W_s - W_d)}{W_d} \times 100$$

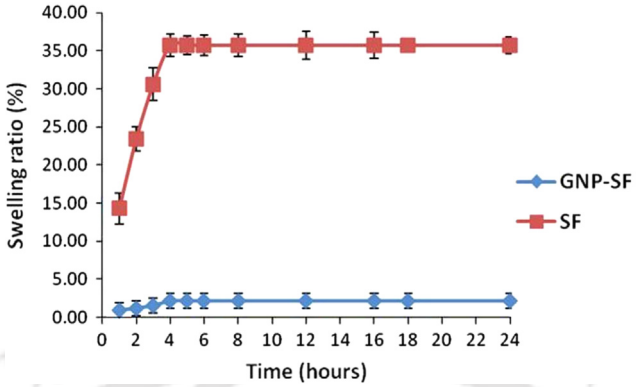

Fig. 7. Swelling ratio of conduits. The dynamic swelling ratio of the conduits were calculated periodically every hour upto 24 h.

where W_s is weight of the conduit in swollen state and W_d is the dry weight. The SF conduits saturated at a swelling ratio of 35.7% while GNP-SF conduits showed a maximum swelling of only 2.1% (Fig. 7).

The low porosity and minimum swelling tendency of both GNP-SF and SF conduits can be attributed to the stacking of multiple layers of nanofibers during conduit fabrication [1].

Acknowledgements

We would like to thank Dr Elizabeth Muir, University of Cambridge for providing the rat schwann cell line (SCTM41) for our experimental purpose. We further thank and acknowledge Central Silk Board, Bengaluru, Govt of India and Department of Biotechnology, New Delhi, Govt of India for providing partial funding support for this work. SD would like to thank IIT Guwahati and Ministry of Human Resource Development (MHRD), Govt of India.

References

[1] S. Das, M. Sharma, D. Saharia, K.K. Sarma, M.G. Sarma, B.B. Borthakur, U. Bora, In vivo studies of silk based gold nano-composite conduits for functional peripheral nerve regeneration, Biomaterials 62 (2015) 66–75.
[2] T. Mosmann, Rapid colorimetric assay for cellular growth and survival: application to proliferation and cytotoxicity assays, J. Immunol. Methods 65 (1983) 55–63.
[3] D. Ribble, N.B. Goldstein, D.A. Norris, Y.G. Shellman, A simple technique for quantifying apoptosis in 96-well plates, BMC Biotechnol. 5 (2005) 12.
[4] S. Tang, J. Zhu, Y. Xu, A.P. Xiang, M.H. Jiang, D. Quan, The effects of gradients of nerve growth factor immobilized PCLA scaffolds on neurite outgrowth in vitro and peripheral nerve regeneration in rats, Biomaterials 34 (29) (2013) 7086–7096.
[5] Z. Wang, Y. Zhang, J. Zhang, L. Huang, J. Liu, Y. Li, G. Zhang, S.C. Kundu, L. Wang, Exploring natural silk protein sericin for regenerative medicine: an injectable, photoluminescent, cell-adhesive 3D hydrogel, Sci. Rep. 20 (4) (2014) 7064.

Copyright Permissions

SPRINGER LICENSE
TERMS AND CONDITIONS

Jul 01, 2015

This is a License Agreement between Suradip Das ("You") and Springer ("Springer") provided by Copyright Clearance Center ("CCC"). The license consists of your order details, the terms and conditions provided by Springer, and the payment terms and conditions.

All payments must be made in full to CCC. For payment instructions, please see information listed at the bottom of this form.

License Number	3660181463226
License date	Jul 01, 2015
Licensed content publisher	Springer
Licensed content publication	Hand
Licensed content title	Overcoming short gaps in peripheral nerve repair: conduits and human acellular nerve allograft
Licensed content author	Jonathan Isaacs
Licensed content date	Jan 1, 2014
Volume number	9
Issue number	2
Type of Use	Thesis/Dissertation
Portion	Figures
Author of this Springer article	No
Order reference number	None
Original figure numbers	Fig 1, 2, 3
Title of your thesis / dissertation	Artificial Scaffolds for Neural Tissue Engineering
Expected completion date	Jul 2015
Estimated size(pages)	200
Total	0.00 USD
Terms and Conditions	

Introduction

The publisher for this copyrighted material is Springer Science + Business Media. By clicking "accept" in connection with completing this licensing transaction, you agree that the following terms and conditions apply to this transaction (along with the Billing and Payment terms and conditions established by Copyright Clearance Center, Inc. ("CCC"), at the time that you opened your Rightslink account and that are available at any time at http://myaccount.copyright.com).

Limited License

With reference to your request to reprint in your thesis material on which Springer Science and Business Media control the copyright, permission is granted, free of charge, for the use indicated in your enquiry.

Licenses are for one-time use only with a maximum distribution equal to the number that you identified in the licensing process.

ELSEVIER LICENSE
TERMS AND CONDITIONS

Jun 24, 2015

This is a License Agreement between Suradip Das ("You") and Elsevier ("Elsevier") provided by Copyright Clearance Center ("CCC"). The license consists of your order details, the terms and conditions provided by Elsevier, and the payment terms and conditions.

All payments must be made in full to CCC. For payment instructions, please see information listed at the bottom of this form.

Supplier	Elsevier Limited The Boulevard,Langford Lane Kidlington,Oxford,OX5 1GB,UK
Registered Company Number	1982084
Customer name	Suradip Das
Customer address	Department of Biotechnology Guwahati, Assam 781039
License number	3655691376176
License date	Jun 24, 2015
Licensed content publisher	Elsevier
Licensed content publication	Journal of Plastic, Reconstructive & Aesthetic Surgery
Licensed content title	Differentiated and undifferentiated adipose-derived stem cells improve function in rats with peripheral nerve gaps
Licensed content author	Hakan Orbay,Ahmet Cagri Uysal,Hiko Hyakusoku,Hiroshi Mizuno
Licensed content date	May 2012
Licensed content volume number	65
Licensed content issue number	5
Number of pages	8
Start Page	657
End Page	664
Type of Use	reuse in a thesis/dissertation
Intended publisher of new work	other
Portion	figures/tables/illustrations
Number of figures/tables /illustrations	3
Format	print
Are you the author of this Elsevier article?	No
Will you be translating?	No
Original figure numbers	Fig 1, Fig 4, Fig 5
Title of your thesis/dissertation	Artificial Scaffolds for Neural Tissue Engineering
Expected completion date	Jul 2015

ELSEVIER LICENSE
TERMS AND CONDITIONS

Jul 16, 2015

This is a License Agreement between Suradip Das ("You") and Elsevier ("Elsevier") provided by Copyright Clearance Center ("CCC"). The license consists of your order details, the terms and conditions provided by Elsevier, and the payment terms and conditions.

All payments must be made in full to CCC. For payment instructions, please see information listed at the bottom of this form.

Supplier	Elsevier Limited The Boulevard,Langford Lane Kidlington,Oxford,OX5 1GB,UK
Registered Company Number	1982084
Customer name	Suradip Das
Customer address	Department of Biotechnology Guwahati, Assam 781039
License number	3670700934845
License date	Jul 16, 2015
Licensed content publisher	Elsevier
Licensed content publication	Biomaterials
Licensed content title	In vivo studies of silk based gold nano-composite conduits for functional peripheral nerve regeneration
Licensed content author	Suradip Das,Manav Sharma,Dhiren Saharia,Kushal Konwar Sarma,Monalisa Goswami Sarma,Bibhuti Bhusan Borthakur,Utpal Bora
Licensed content date	September 2015
Licensed content volume number	62
Licensed content issue number	n/a
Number of pages	10
Start Page	66
End Page	75
Type of Use	reuse in a thesis/dissertation
Intended publisher of new work	other
Portion	full article
Format	print
Are you the author of this Elsevier article?	Yes
Will you be translating?	No
Title of your thesis/dissertation	Artificial Scaffolds for Neural Tissue Engineering
Expected completion date	Jul 2015
Estimated size (number of pages)	200

ELSEVIER LICENSE
TERMS AND CONDITIONS

Jun 24, 2015

This is a License Agreement between Suradip Das ("You") and Elsevier ("Elsevier") provided by Copyright Clearance Center ("CCC"). The license consists of your order details, the terms and conditions provided by Elsevier, and the payment terms and conditions.

All payments must be made in full to CCC. For payment instructions, please see information listed at the bottom of this form.

Supplier	Elsevier Limited The Boulevard,Langford Lane Kidlington,Oxford,OX5 1GB,UK
Registered Company Number	1982084
Customer name	Suradip Das
Customer address	Department of Biotechnology Guwahati, Assam 781039
License number	3655200290759
License date	Jun 24, 2015
Licensed content publisher	Elsevier
Licensed content publication	Biomaterials
Licensed content title	Functional recovery after peripheral nerve injury and implantation of a collagen guide
Licensed content author	Olivier Alluin,Catherine Wittmann,Tanguy Marqueste,Jean-François Chabas,Stéphane Garcia,Marie-Noëlle Lavaut,Didier Guinard,François Feron,Patrick Decherchi
Licensed content date	January 2009
Licensed content volume number	30
Licensed content issue number	3
Number of pages	11
Start Page	363
End Page	373
Type of Use	reuse in a thesis/dissertation
Intended publisher of new work	other
Portion	figures/tables/illustrations
Number of figures/tables /illustrations	3
Format	print
Are you the author of this Elsevier article?	No
Will you be translating?	No
Original figure numbers	Fig 1, Fig 2
Title of your thesis/dissertation	Artificial Scaffolds for Neural Tissue Engineering

JOHN WILEY AND SONS LICENSE TERMS AND CONDITIONS

Jun 24, 2015

This Agreement between Suradip Das ("You") and John Wiley and Sons ("John Wiley and Sons") consists of your license details and the terms and conditions provided by John Wiley and Sons and Copyright Clearance Center.

License Number	3655400680039
License date	Jun 24, 2015
Licensed Content Publisher	John Wiley and Sons
Licensed Content Publication	Journal of Tissue Engineering and Regenerative Medicine
Licensed Content Title	Application of conductive polymers, scaffolds and electrical stimulation for nerve tissue engineering
Licensed Content Author	Laleh Ghasemi-Mobarakeh,Molamma P Prabhakaran,Mohammad Morshed,Mohammad Hossein Nasr-Esfahani,Hossein Baharvand,Sahar Kiani,Salem S Al-Deyab,Seeram Ramakrishna
Licensed Content Date	Jan 10, 2011
Pages	1
Type of use	Dissertation/Thesis
Requestor type	University/Academic
Format	Print
Portion	Figure/table
Number of figures/tables	3
Original Wiley figure/table number(s)	Figure 2, Figure 3, Figure 4
Will you be translating?	No
Title of your thesis / dissertation	Artificial Scaffolds for Neural Tissue Engineering
Expected completion date	Jul 2015
Expected size (number of pages)	200
Requestor Location	Suradip Das Department of Biotechnology IIT Guwahati Guwahati- 781039 Guwahati, India 781039 Attn: Suradip Das
Billing Type	Invoice
Billing Address	Suradip Das Department of Biotechnology IIT Guwahati Guwahati- 781039 Guwahati, India 781039 Attn: Suradip Das
Total	0.00 USD
Terms and Conditions	

TERMS AND CONDITIONS

TH-1468_10610612

Creative Commons Attribution License (CC BY)

This article is available under the terms of the Creative Commons Attribution License (CC BY). You may copy and distribute the article, create extracts, abstracts and new works from the article, alter and revise the article, text or data mine the article and otherwise reuse the article commercially (including reuse and/or resale of the article) without permission from Elsevier. You must give appropriate credit to the original work, together with a link to the formal publication through the relevant DOI and a link to the Creative Commons user license above. You must indicate if any changes are made but not in any way that suggests the licensor endorses you or your use of the work.

Permission is not required for this type of reuse.

CLOSE WINDOW

ELSEVIER LICENSE
TERMS AND CONDITIONS

Jun 24, 2015

This is a License Agreement between Suradip Das ("You") and Elsevier ("Elsevier") provided by Copyright Clearance Center ("CCC"). The license consists of your order details, the terms and conditions provided by Elsevier, and the payment terms and conditions.

All payments must be made in full to CCC. For payment instructions, please see information listed at the bottom of this form.

Supplier	Elsevier Limited The Boulevard,Langford Lane Kidlington,Oxford,OX5 1GB,UK
Registered Company Number	1982084
Customer name	Suradip Das
Customer address	Department of Biotechnology Guwahati, Assam 781039
License number	3655371323944
License date	Jun 24, 2015
Licensed content publisher	Elsevier
Licensed content publication	Neuroscience
Licensed content title	Electrically mediated regeneration and guidance of adult mammalian spinal axons into polymeric channels
Licensed content author	R.B. Borgens
Licensed content date	June 1999
Licensed content volume number	91
Licensed content issue number	1
Number of pages	14
Start Page	251
End Page	264
Type of Use	reuse in a thesis/dissertation
Intended publisher of new work	other
Portion	figures/tables/illustrations
Number of figures/tables /illustrations	4
Format	print
Are you the author of this Elsevier article?	No
Will you be translating?	No
Original figure numbers	Fig 1, Fig 2, Fig 4, Fig 6
Title of your thesis/dissertation	Artificial Scaffolds for Neural Tissue Engineering
Expected completion date	Jul 2015

ELSEVIER LICENSE
TERMS AND CONDITIONS

Jul 06, 2015

This is a License Agreement between Suradip Das ("You") and Elsevier ("Elsevier") provided by Copyright Clearance Center ("CCC"). The license consists of your order details, the terms and conditions provided by Elsevier, and the payment terms and conditions.

All payments must be made in full to CCC. For payment instructions, please see information listed at the bottom of this form.

Supplier	Elsevier Limited The Boulevard,Langford Lane Kidlington,Oxford,OX5 1GB,UK
Registered Company Number	1982084
Customer name	Suradip Das
Customer address	Department of Biotechnology Guwahati, Assam 781039
License number	3663211450268
License date	Jul 06, 2015
Licensed content publisher	Elsevier
Licensed content publication	Injury
Licensed content title	FDA approved guidance conduits and wraps for peripheral nerve injury: A review of materials and efficacy
Licensed content author	S. Kehoe,X.F. Zhang,D. Boyd
Licensed content date	May 2012
Licensed content volume number	43
Licensed content issue number	5
Number of pages	20
Start Page	553
End Page	572
Type of Use	reuse in a thesis/dissertation
Intended publisher of new work	other
Portion	figures/tables/illustrations
Number of figures/tables /illustrations	5
Format	print
Are you the author of this Elsevier article?	No
Will you be translating?	No
Original figure numbers	Table 1,2,4,6,8
Title of your thesis/dissertation	Artificial Scaffolds for Neural Tissue Engineering
Expected completion date	Jul 2015

TH-1468_10610612

ELSEVIER LICENSE
TERMS AND CONDITIONS

Jun 24, 2015

This is a License Agreement between Suradip Das ("You") and Elsevier ("Elsevier") provided by Copyright Clearance Center ("CCC"). The license consists of your order details, the terms and conditions provided by Elsevier, and the payment terms and conditions.

All payments must be made in full to CCC. For payment instructions, please see information listed at the bottom of this form.

Supplier	Elsevier Limited The Boulevard,Langford Lane Kidlington,Oxford,OX5 1GB,UK
Registered Company Number	1982084
Customer name	Suradip Das
Customer address	Department of Biotechnology Guwahati, Assam 781039
License number	3655290501241
License date	Jun 24, 2015
Licensed content publisher	Elsevier
Licensed content publication	Biomaterials
Licensed content title	An in vivo evaluation of a biodegradable genipin-cross-linked gelatin peripheral nerve guide conduit material
Licensed content author	Yueh-Sheng Chen,Ju-Ying Chang,Chun-Yuan Cheng,Fuu-Jen Tsai,Chun-Hsu Yao,Bai-Shuan Liu
Licensed content date	June 2005
Licensed content volume number	26
Licensed content issue number	18
Number of pages	8
Start Page	3911
End Page	3918
Type of Use	reuse in a thesis/dissertation
Intended publisher of new work	other
Portion	figures/tables/illustrations
Number of figures/tables /illustrations	3
Format	print
Are you the author of this Elsevier article?	No
Will you be translating?	No
Original figure numbers	Fig 1, Fig 4, Fig 5
Title of your thesis/dissertation	Artificial Scaffolds for Neural Tissue Engineering

TH-1468_10610612

NATURE PUBLISHING GROUP LICENSE TERMS AND CONDITIONS

Jun 24, 2015

This is a License Agreement between Suradip Das ("You") and Nature Publishing Group ("Nature Publishing Group") provided by Copyright Clearance Center ("CCC"). The license consists of your order details, the terms and conditions provided by Nature Publishing Group, and the payment terms and conditions.

All payments must be made in full to CCC. For payment instructions, please see information listed at the bottom of this form.

License Number	3655161236026
License date	Jun 24, 2015
Licensed content publisher	Nature Publishing Group
Licensed content publication	Nature Reviews Neuroscience
Licensed content title	Glial inhibition of CNS axon regeneration
Licensed content author	Glenn YiuandZhigang He
Licensed content date	Aug 1, 2006
Volume number	7
Issue number	8
Type of Use	reuse in a dissertation / thesis
Requestor type	academic/educational
Format	print
Portion	figures/tables/illustrations
Number of figures/tables /illustrations	2
High-res required	no
Figures	Fig 1, Fig 3,
Author of this NPG article	no
Your reference number	None
Title of your thesis / dissertation	Artificial Scaffolds for Neural Tissue Engineering
Expected completion date	Jul 2015
Estimated size (number of pages)	200
Total	0.00 USD
Terms and Conditions	

Terms and Conditions for Permissions

Nature Publishing Group hereby grants you a non-exclusive license to reproduce this material for this purpose, and for no other use,subject to the conditions below:

1. NPG warrants that it has, to the best of its knowledge, the rights to license reuse of this material. However, you should ensure that the material you are requesting is original to Nature Publishing Group and does not carry the copyright of another entity (as credited in the published version). If the credit line on any part of the material you have requested indicates that it was reprinted or adapted by NPG with permission from another source,

ELSEVIER LICENSE
TERMS AND CONDITIONS

Jul 03, 2015

This is a License Agreement between Suradip Das ("You") and Elsevier ("Elsevier") provided by Copyright Clearance Center ("CCC"). The license consists of your order details, the terms and conditions provided by Elsevier, and the payment terms and conditions.

All payments must be made in full to CCC. For payment instructions, please see information listed at the bottom of this form.

Supplier	Elsevier Limited The Boulevard,Langford Lane Kidlington,Oxford,OX5 1GB,UK
Registered Company Number	1982084
Customer name	Suradip Das
Customer address	Department of Biotechnology Guwahati, Assam 781039
License number	3661351298154
License date	Jul 03, 2015
Licensed content publisher	Elsevier
Licensed content publication	Advanced Drug Delivery Reviews
Licensed content title	Modified natural nanoparticles as contrast agents for medical imaging
Licensed content author	P. Mukherjee,Peter A. Jarzyna,Willem J.M. Mulder,Zahi A. Fayad
Licensed content date	8 March 2010
Licensed content volume number	62
Licensed content issue number	3
Number of pages	10
Start Page	329
End Page	338
Type of Use	reuse in a thesis/dissertation
Portion	figures/tables/illustrations
Number of figures/tables /illustrations	1
Format	print
Are you the author of this Elsevier article?	No
Will you be translating?	No
Original figure numbers	Fig 1
Title of your thesis/dissertation	Artificial Scaffolds for Neural Tissue Engineering
Expected completion date	Jul 2015
Estimated size (number of pages)	200

TH-1468_10610612

ELSEVIER LICENSE
TERMS AND CONDITIONS

Jun 23, 2015

This is a License Agreement between Suradip Das ("You") and Elsevier ("Elsevier") provided by Copyright Clearance Center ("CCC"). The license consists of your order details, the terms and conditions provided by Elsevier, and the payment terms and conditions.

All payments must be made in full to CCC. For payment instructions, please see information listed at the bottom of this form.

Supplier	Elsevier Limited The Boulevard,Langford Lane Kidlington,Oxford,OX5 1GB,UK
Registered Company Number	1982084
Customer name	Suradip Das
Customer address	Department of Biotechnology Guwahati, Assam 781039
License number	3654651301892
License date	Jun 23, 2015
Licensed content publisher	Elsevier
Licensed content publication	Advanced Drug Delivery Reviews
Licensed content title	Modified natural nanoparticles as contrast agents for medical imaging
Licensed content author	P. Mukherjee,Peter A. Jarzyna,Willem J.M. Mulder,Zahi A. Fayad
Licensed content date	8 March 2010
Licensed content volume number	62
Licensed content issue number	3
Number of pages	10
Start Page	329
End Page	338
Type of Use	reuse in a thesis/dissertation
Intended publisher of new work	other
Portion	figures/tables/illustrations
Number of figures/tables /illustrations	2
Format	print
Are you the author of this Elsevier article?	No
Will you be translating?	No
Original figure numbers	Fig 1, Fig 3
Title of your thesis/dissertation	Artificial Scaffolds for Neural Tissue Engineering
Expected completion date	Jul 2015

TH-1468_10610612

Title: ZnO Nanowire Arrays on 3D Hierachical Graphene Foam: Biomarker Detection of Parkinson's Disease

Author: Hong Yan Yue, Shuo Huang, Jian Chang, et al

Publication: ACS Nano

Publisher: American Chemical Society

Date: Feb 1, 2014

PERMISSION/LICENSE IS GRANTED FOR YOUR ORDER AT NO CHARGE

This type of permission/license, instead of the standard Terms & Conditions, is sent to you because no fee is being charged for your order. Please note the following:

- Permission is granted for your request in both print and electronic formats, and translations.
- If figures and/or tables were requested, they may be adapted or used in part.
- Please print this page for your records and send a copy of it to your publisher/graduate school.
- Appropriate credit for the requested material should be given as follows: "Reprinted (adapted) with permission from (COMPLETE REFERENCE CITATION). Copyright (YEAR) American Chemical Society." Insert appropriate information in place of the capitalized words.
- One-time permission is granted only for the use specified in your request. No additional uses are granted (such as derivative works or other editions). For any other uses, please submit a new request.

If credit is given to another source for the material you requested, permission must be obtained from that source.

BACK CLOSE WINDOW

Title: Neural Tissue Engineering: Strategies for Repair and Regeneration

Author: Christine E. Schmidt, Jennie Baier Leach

Publication: Annual Review of Biomedical Engineering

Publisher: Annual Reviews

Date: Aug 1, 2003

Permission Not Required

Material may be republished in a thesis / dissertation without obtaining additional permission from Annual Reviews, providing that the author and the original source of publication are fully acknowledged.

BACK | CLOSE WINDOW

ELSEVIER LICENSE
TERMS AND CONDITIONS

Jun 24, 2015

This is a License Agreement between Suradip Das ("You") and Elsevier ("Elsevier") provided by Copyright Clearance Center ("CCC"). The license consists of your order details, the terms and conditions provided by Elsevier, and the payment terms and conditions.

All payments must be made in full to CCC. For payment instructions, please see information listed at the bottom of this form.

Supplier	Elsevier Limited The Boulevard,Langford Lane Kidlington,Oxford,OX5 1GB,UK
Registered Company Number	1982084
Customer name	Suradip Das
Customer address	Department of Biotechnology Guwahati, Assam 781039
License number	3655470954438
License date	Jun 24, 2015
Licensed content publisher	Elsevier
Licensed content publication	Neuron
Licensed content title	Functional Recovery of Paraplegic Rats and Motor Axon Regeneration in Their Spinal Cords by Olfactory Ensheathing Glia
Licensed content author	Almudena Ramón-Cueto,M.Isabel Cordero,Fernando F. Santos-Benito,Jesús Avila
Licensed content date	February 2000
Licensed content volume number	25
Licensed content issue number	2
Number of pages	11
Start Page	425
End Page	435
Type of Use	reuse in a thesis/dissertation
Intended publisher of new work	other
Portion	figures/tables/illustrations
Number of figures/tables /illustrations	2
Format	print
Are you the author of this Elsevier article?	No
Will you be translating?	No
Original figure numbers	Fig 1, Fig 2
Title of your thesis/dissertation	Artificial Scaffolds for Neural Tissue Engineering

TH-1468_10610612

ELSEVIER LICENSE
TERMS AND CONDITIONS

Jun 24, 2015

This is a License Agreement between Suradip Das ("You") and Elsevier ("Elsevier") provided by Copyright Clearance Center ("CCC"). The license consists of your order details, the terms and conditions provided by Elsevier, and the payment terms and conditions.

All payments must be made in full to CCC. For payment instructions, please see information listed at the bottom of this form.

Supplier	Elsevier Limited The Boulevard,Langford Lane Kidlington,Oxford,OX5 1GB,UK
Registered Company Number	1982084
Customer name	Suradip Das
Customer address	Department of Biotechnology Guwahati, Assam 781039
License number	3655351453800
License date	Jun 24, 2015
Licensed content publisher	Elsevier
Licensed content publication	Acta Biomaterialia
Licensed content title	Photo-crosslinked poly(ε-caprolactone fumarate) networks for guided peripheral nerve regeneration: Material properties and preliminary biological evaluations
Licensed content author	Shanfeng Wang,Michael J. Yaszemski,Andrew M. Knight,James A. Gruetzmacher,Anthony J. Windebank,Lichun Lu
Licensed content date	June 2009
Licensed content volume number	5
Licensed content issue number	5
Number of pages	12
Start Page	1531
End Page	1542
Type of Use	reuse in a thesis/dissertation
Intended publisher of new work	other
Portion	figures/tables/illustrations
Number of figures/tables /illustrations	3
Format	print
Are you the author of this Elsevier article?	No
Will you be translating?	No
Original figure numbers	Fig 7, Fig 8, Fig 9, Scheme 1
Title of your thesis/dissertation	Artificial Scaffolds for Neural Tissue Engineering

PNAS

About PNAS (/site/aboutpnas/index.xhtml#PNAS_Online)

Free Content (/site/aboutpnas/index.xhtml#free)

Special Features (/site/aboutpnas/special.xhtml)

Colloquium Papers (/site/aboutpnas/colloquia.xhtml)

Developing Countries With Free Access to PNAS Online (/site/aboutpnas/developingcountries.xhtml)

2015 Marketing Brochure (/site/misc/2015Brochure.pdf)

RSS Feeds (/site/aboutpnas/rss.xhtml)

About Direct Submission (/site/aboutpnas/submiss.xhtml)

Reprints (/site/aboutpnas/reprints.xhtml)

Rights and Permissions (/site/aboutpnas/rightperm.xhtml)

Author Rights and Permissions Frequently Asked Questions (/site/aboutpnas/rightpermfaq.xhtml)

Frequently Asked Questions (/site/aboutpnas/faq.xhtml)

PNAS Portals (/site/misc/pnas_portals.xhtml)

PNAS Mobile (/site/misc/pnas_mobile.xhtml)

Android App Permissions (/site/misc/androidfaq.xhtml)

PNAS Alerts (/site/misc/PNASalerts.xhtml)

Editorial Board (/site/misc/masthead.xhtml)

News & Multimedia (/multimedia)

Rights and Permissions

Beginning with articles submitted in Volume 106 (2009) the author(s) retains copyright to individual articles, and the National Academy of Sciences of the United States of America retains an exclusive license to publish these articles and holds copyright to the collective work. Volumes 90–105 (1993–2008) copyright © by the National Academy of Sciences. Volumes 1–89 (1915–1992), the author(s) retains copyright to individual articles, and the National Academy of Sciences holds copyright to the collective work.

The PNAS listing on the Sherpa RoMEO publisher copyright policies & self-archiving detail pages can be found here (http://www.sherpa.ac.uk/romeo/search.php?id=94&la=en&fIDnum=|).

Requests for Permission to Reprint

Requests for permission should be made in writing. For the fastest response time, please send your request via email to PNASPermissions@nas.edu (mailto:PNASPermissions@nas.edu). If necessary, requests may be faxed to 202-334-2739 or mailed to:

PNAS Permissions Editor
500 Fifth Street, NW
NAS 340
Washington, DC 20001 USA

Anyone may, without requesting permission, use original figures or tables published in PNAS for noncommercial and educational use (i.e., in a review article, in a book that is not for sale) provided that the original source and the applicable copyright notice are cited.

For permission to reprint material in volumes 1–89 (1915–1992), requests should be addressed to the original authors, who hold the copyright. The full journal reference must be cited.

For permission to reprint material in volumes 90–present (1993–present), requests must be sent via email, fax, or mail and include the following information about the original material:

1. Your full name, affiliation, and title
2. Your complete mailing address, phone number, fax number, and email address
3. PNAS volume number, issue number, and issue date
4. PNAS article title
5. PNAS authors' names
6. Page numbers of items to be reprinted
7. Figure/table number or portion of text to be reprinted

Also include the following information about the intended use of the material:

1. Title of work in which PNAS material will appear
2. Authors/editors of work
3. Publisher of work
4. Retail price of work
5. Number of copies of work to be produced
6. Intended audience
7. Whether work is for nonprofit or commercial use

PNAS authors need not obtain permission for the following cases: (1) to use their original figures or tables in their future works; (2) to make copies of their papers

(/content/current)

Current Issue (/content/current)

Email Alerts (/site/misc/PNASalerts.xhtml)

Subscribe (/site/subscriptions/index.xhtml)

RSS (/site/aboutpnas/rss.xhtml)

Don't Miss

Help PNAS celebrate 100 years of service to science and society. Visit the PNAS 100th Anniversary Portal (http://pnas100th.org) for commentaries, perspectives, special features and more celebrating this milestone.

Other PNAS Media

Image Gallery (/site/media/imagegallery.xhtml)

Video Library (/site/media/videolibrary.xhtml)

Follow Us on Twitter (https://twitter.com/PNASNews)

Find Us on Facebook (http://www.facebook.com/pages/PNAS/18262365099)

MOST READ **MOST CITED**

1. The genome of cultivated sweet potato contains Agrobacterium T-DNAs with expressed genes: An example of a naturally transgenic food crop (/cgi/content/short/112/18/5844?rss=1&ssource=mfr)
2. Core Concept: CRISPR gene editing (/cgi/content/short/112/20/6245?rss=1&ssource=mfr)
3. National hiring experiments reveal 2:1 faculty preference for women on STEM tenure track (/cgi/content/short/112/17/5360?rss=1&ssource=mfr)
4. News Feature: Microplastics present pollution puzzle (/cgi/content/short/112/18/5547?rss=1&ssource=mfr)

ELSEVIER LICENSE
TERMS AND CONDITIONS

Jun 24, 2015

This is a License Agreement between Suradip Das ("You") and Elsevier ("Elsevier") provided by Copyright Clearance Center ("CCC"). The license consists of your order details, the terms and conditions provided by Elsevier, and the payment terms and conditions.

All payments must be made in full to CCC. For payment instructions, please see information listed at the bottom of this form.

Supplier	Elsevier Limited The Boulevard,Langford Lane Kidlington,Oxford,OX5 1GB,UK
Registered Company Number	1982084
Customer name	Suradip Das
Customer address	Department of Biotechnology Guwahati, Assam 781039
License number	3655320591119
License date	Jun 24, 2015
Licensed content publisher	Elsevier
Licensed content publication	Biomaterials
Licensed content title	Coil-reinforced hydrogel tubes promote nerve regeneration equivalent to that of nerve autografts
Licensed content author	L. Lu,Rivelino Montenegro,Thomas Freier,Rajiv Midha,Jason S. Belkas,Molly S. Shoichet
Licensed content date	January 2006
Licensed content volume number	27
Licensed content issue number	3
Number of pages	14
Start Page	505
End Page	518
Type of Use	reuse in a thesis/dissertation
Intended publisher of new work	other
Portion	figures/tables/illustrations
Number of figures/tables /illustrations	2
Format	print
Are you the author of this Elsevier article?	No
Will you be translating?	No
Original figure numbers	Fig 1, Fig 6
Title of your thesis/dissertation	Artificial Scaffolds for Neural Tissue Engineering

TH-1468_10610612

ELSEVIER LICENSE
TERMS AND CONDITIONS

Jun 15, 2015

This is a License Agreement between Suradip Das ("You") and Elsevier ("Elsevier") provided by Copyright Clearance Center ("CCC"). The license consists of your order details, the terms and conditions provided by Elsevier, and the payment terms and conditions.

All payments must be made in full to CCC. For payment instructions, please see information listed at the bottom of this form.

Supplier	Elsevier Limited The Boulevard,Langford Lane Kidlington,Oxford,OX5 1GB,UK
Registered Company Number	1982084
Customer name	Suradip Das
Customer address	Department of Biotechnology Guwahati, Assam 781039
License number	3650060737475
License date	Jun 15, 2015
Licensed content publisher	Elsevier
Licensed content publication	Trends in Biotechnology
Licensed content title	The development of bioartificial nerve grafts for peripheral-nerve regeneration
Licensed content author	Carole A Heath,Gregory E Rutkowski
Licensed content date	1 April 1998
Licensed content volume number	16
Licensed content issue number	4
Number of pages	6
Start Page	163
End Page	168
Type of Use	reuse in a thesis/dissertation
Portion	figures/tables/illustrations
Number of figures/tables /illustrations	2
Format	print
Are you the author of this Elsevier article?	No
Will you be translating?	No
Original figure numbers	Fig 2, Table 1
Title of your thesis/dissertation	Artificial Scaffolds for Neural Tissue Engineering
Expected completion date	Jul 2015
Estimated size (number of pages)	200

TH-1468_10610612

ELSEVIER LICENSE
TERMS AND CONDITIONS

Jun 29, 2015

This is a License Agreement between Suradip Das ("You") and Elsevier ("Elsevier") provided by Copyright Clearance Center ("CCC"). The license consists of your order details, the terms and conditions provided by Elsevier, and the payment terms and conditions.

All payments must be made in full to CCC. For payment instructions, please see information listed at the bottom of this form.

Supplier	Elsevier Limited The Boulevard,Langford Lane Kidlington,Oxford,OX5 1GB,UK
Registered Company Number	1982084
Customer name	Suradip Das
Customer address	Department of Biotechnology Guwahati, Assam 781039
License number	3658400951218
License date	Jun 29, 2015
Licensed content publisher	Elsevier
Licensed content publication	Journal of Neuroscience Methods
Licensed content title	Sciatic nerve injury: A simple and subtle model for investigating many aspects of nervous system damage and recovery
Licensed content author	Luis E. Savastano,Sergio R. Laurito,Marcos R. Fitt,Jorge A. Rasmussen,Virginia Gonzalez Polo,Sean I. Patterson
Licensed content date	30 April 2014
Licensed content volume number	227
Licensed content issue number	n/a
Number of pages	15
Start Page	166
End Page	180
Type of Use	reuse in a thesis/dissertation
Intended publisher of new work	other
Portion	figures/tables/illustrations
Number of figures/tables /illustrations	2
Format	print
Are you the author of this Elsevier article?	No
Will you be translating?	No
Original figure numbers	Fig 1, Fig 3
Title of your thesis/dissertation	Artificial Scaffolds for Neural Tissue Engineering

TH-1468_10610612

ELSEVIER LICENSE
TERMS AND CONDITIONS

Jul 03, 2015

This is a License Agreement between Suradip Das ("You") and Elsevier ("Elsevier") provided by Copyright Clearance Center ("CCC"). The license consists of your order details, the terms and conditions provided by Elsevier, and the payment terms and conditions.

All payments must be made in full to CCC. For payment instructions, please see information listed at the bottom of this form.

Supplier	Elsevier Limited The Boulevard,Langford Lane Kidlington,Oxford,OX5 1GB,UK
Registered Company Number	1982084
Customer name	Suradip Das
Customer address	Department of Biotechnology Guwahati, Assam 781039
License number	3661301325543
License date	Jul 03, 2015
Licensed content publisher	Elsevier
Licensed content publication	Acta Biomaterialia
Licensed content title	Aligned natural–synthetic polyblend nanofibers for peripheral nerve regeneration
Licensed content author	Chun-Yang Wang,Kui-Hua Zhang,Cun-Yi Fan,Xiu-Mei Mo,Hong-Jiang Ruan,Feng-Feng Li
Licensed content date	February 2011
Licensed content volume number	7
Licensed content issue number	2
Number of pages	10
Start Page	634
End Page	643
Type of Use	reuse in a thesis/dissertation
Intended publisher of new work	other
Portion	figures/tables/illustrations
Number of figures/tables /illustrations	2
Format	print
Are you the author of this Elsevier article?	No
Will you be translating?	No
Original figure numbers	Fig 4, 10
Title of your thesis/dissertation	Artificial Scaffolds for Neural Tissue Engineering

TH-1468_10610612

Biography

Suradip Das was born and brought up in Kolkata, West Bengal. He completed his secondary (2004) and higher secondary education (2006) from South Point High School, Kolkata. He qualified West Bengal Joint Entrance Examination and completed his Bachelor of Technology in Biotechnology in 2010 from Heritage Institute of Technology, Kolkata under West Bengal University of Technology. In 2010, he qualified GATE examination in Biotechnology with an All India Rank of 137 and joined IIT Guwahati as a PhD scholar in the Department of Biosciences and Bioengineering under the supervision of Prof. Utpal Bora. His PhD work involves fabrication of artificial scaffolds for neural tissue engineering applications. He has been working on developing nerve conduits using silk based nanocomposites and evaluating their efficacy on promoting neural regeneration across a nerve gap in rat sciatic nerve injury models through extensive electrophysiological, histo-morphometric and walking pattern analysis. His work has been published in peer-reviewed journals and has been widely covered by the national and international media. He bagged the best oral presentation award in 2008 for presenting a project proposal at Genesis, a technological fest organised by IIT Kharagpur. He received the prestigious Indian Academy of Science fellowship in summer 2009 for working at CSIR-CFTRI, Mysore for three months under the guidance of Dr.V.Prakash, Former Director, CFTRI. He also received international travel awards from DBT, Govt of India and DST, Govt of India during 2014 for presenting a poster at the 16th Spinal research meeting held at London. At the time of compilation of thesis he had published 4 articles and 1 book chapter and a few more were in communication. He is a member of TERMIS and a nominated young member of the Indo-Italian Forum on Biomaterials and Tissue Engineering.